ELECTRICAL AND PHOTOACOUSTIC STUDIES ON PHASE TRANSITIONS IN CERTAIN AMMONIUM CONTAINING CRYSTALS

R. NAVIL KUMAR

THESIS SUBMITTED
IN PARTIAL FULFILMENT OF THE REQUIREMENTS
FOR THE DEGREE OF
DOCTOR OF PHILOSOPHY

DEPARTMENT OF PHYSICS
COCHIN UNIVERSITY OF SCIENCE AND TECHNOLOGY
COCHIN - 682 022

1989

DEDICATED TO

MY PARENTS, BROTHERS AND SISTERS

CERTIFICATE

Certified that the research work presented in this thesis is based on the original work done by Mr.R.Navil Kumar under my guidance in the Department of Physics, Cochin University of Science and Technology, and has not been included in any other thesis submitted previously for the award of any degree.

Cochin 682 022,
28 June 1989.

Prof.(Dr.) C.P.Girijavallabhan,
Supervising Teacher.

DECLARATION

Certified that the work presented in this thesis is based on the original work done by me under the guidance of Prof.(Dr.) C.P.Girijavallabhan in the Department of Physics, Cochin University of Science and Technology, and has not been included in any other thesis submitted previously for the award of any degree.

Cochin 682 022,
28 June 1989.

R.Navil Kumar.

PREFACE

During the last two decades there has been considerable interest in the development and characterisation of new materials suitable for a wide range of technological applications. Progress in the field of materials science has thus made it possible to identify and produce a variety of new substances suitable for evolving novel systems and a host of other devices. A greater understanding of the structue and properties of these materials has resulted essentially from the use of a number of sophisticated analytical techniques which give precise information regarding the behaviour of the materials under specific physical conditions. In this context, the study of properties like electrical conductivity, dielectric constant and ionic thermocurrent and photoacoustic response can yield valuable information on the nature and characteristics of the material under investigation. The phenomenon of phase transition exhibited by a large number of crystalline solids is one such aspect which is especially suitable for a detailed study using the above technique. The thesis attempts to summarise the work carried out in this direction by the author during the past few years in the Department of Physics of Cochin University of Science and Technology.

In the present thesis a series of exhaustive investigations have been carried out on a number of crystalline samples with special reference to the phase transitions exhibited by them. These include single crystals of pure, doped or deuterated specimens of certain ammonium containing crystals viz., $(NH_4)_3H(SO_4)2$, $(NH_4)_2HPO_4$, $(NH_4)_2Cr_2O_7$ and $NH_4H_2PO_4$. ac/dc electrical conductivity, dielectric constant, ionic thermocurrent as well as photoacoustic measurements have been carried out on most of them over a wide range of temperature. In addition investigations have been carried out in pure and doped single crystals of $NaClO_3$ and $NaNO_3$ using ionic thermocurrent measurements and these are presented here. Special attention has been paid to reveal the mechanism of electrical conduction in various phases of these crystals and to evaluate the different parameters involved in the conduction as well as phase transition process.

The thesis contains ten chapters which by and large are self contained with separate abstracts, conclusions and references. In the first chapter, a general introduction is given to provide an understanding of the importance of the study of phase transition in solids and many of its theoretical aspects. Special attention has

been paid to the study of this phenomenon in relation to the electrical and photoacoustic properties. This section also describes, the various techniques generally employed to elucidate the mechanisms of these phase transitions occurring in these materials. A brief theoretical background of the techniques employed for the present investigation is also presented in this section. In the last part of this chapter a brief discussion of the various applications of phase transition is also given.

Various experimental systems employed as well as fabricated specifically for the present investigation are described in chapter II. The experimental systems fabricated include, a pulling rate controller for Bridgman furnace, a thin film vacuum evaporation unit for electrode deposition, a metallic cell for temperature variation measurement of electrical properties and a low temperature cell for photoacoustic study of phase transitions.

The experimental investigations carried out in single crystals of pure and deuterated triammonium disulphate (TAHDS) using electrical conductivity and dielectric constant measurements are described in chapter III and in pure and doped diammonium hydrogen phosphate are

given in chapter IV. The mechanisms of electrical conduction processes and of the different phase transitions in these crystals are also discussed in these chapters.

Extensive study of thermally stimulated depolarization current (TSDC) measurements carried out in single crystals of pure and SO_4^{2-} doped specimens of $(NH_4)_2HPO_4$ in the temperature range 80K to 423K are presented in this chapter V. Detailed analysis of the TSDC spectra as a function of poling field, poling temperature, poling time, impurity concentration and effect of heating rate has been carried out and these investigations reveal the origin and nature of each of the peaks occurring in the TSDC spectra.

In the sixth chapter, the detailed investigations carried out in single crystals of pure and doped ammonium dichromate (AD) grown from solution using electrical conductivity, dielectric constant and ionic thermocurrent measurements have been presented. The photoacoustic studies of phase transitions in AD and ammoium dihydrogen phosphate (ADP) are presented in chapter VII. The power and versatility of this technique to characterise materials undergoing phase transitions are clearly demonstrated in this chapter.

The effect of various impurities like Ba^{2+}, Pb^{2+}, Sr^{2+} and Ca^{2+} ions on the ITC spectra of $NaClO_3$ crystals have been presented in chapter VIII. The activation energy values as well as the various relaxation parameters obtained from these measurements are also given here.

Chapter IX deals with the study of TSDC and thermally stimulated polarization (TSPC) measurements carried out in pure and doped single crystals of $NaNO_3$. The effect of various experimental parameters like poling field, poling temperature, concentration of impurities and effect of heating rate on the TSDC and TSPC spectra are discussed in detail. The role of phase transition on TSDC and TSPC of this material has been specially investigated. Accurate fixing of transition temperature has been achieved here for the first time in this material.

The last chapter presents the investigations carried out in doubly doped specimens of sodium nitrate crystals using ITC technique and the effect of various experimental parameters on the ITC spectra of $NaNO_3$. The experimental techniques employed here establish clearly the superiority and sensitivity of the present approach for detecting phase transitions occurring in crystalline solids.

Part of the investigations contained in this thesis has been presented in conferences or published/communicated in the form of following papers.

1. Study of high temperature phase transition in $(NH_4)_3H(SO_4)_2$ $(ND_4)_3D(SO_4)_2$ using dielectric measurements

   R.Navil Kumar and C.P.G.Vallabhan

   Proceedings of XV National Seminar on Crystallography, New Delhi. Paper No.C-19 (1983).

2. Effect of deuteration on the electrical conductivity of triammonium hydrogen disulphate

   R.Navil Kumar and C.P.G.Vallabhan

   Proceedings of the Solid State Physics Symposium, Nagpur. Vol.28A, 240 (1985).

3. Ionic thermocurrent studies in pure and doped $NaNO_3$ crystals

   A.G.Valyomana, R.Navil Kumar and C.P.G.Vallabhan

   Proceedings of the XVIII National Seminar on Crystallography, Jammu. Paper No.H-11 (1986).

4. Ionic thermocurrent studies in pure and doped $NaClO_3$ crystals

   R.Navil Kumar and C.P.G.Vallabhan

   Proceedings of the National Conference on Electrical and Optical Properties of Solids, Sagar. Paper No.OE.8 (1987).

5. Effect of heating rate on ionic thermocurrent spectrum of $NaClO_3$ crystals

   R.Navil Kumar and C.P.G.Vallabhan

   Proceedings of the XIX National Seminar on Crystallography, Kottayam. Paper No.D-10 (1987).

6. Observation of a high temperature space charge current peak in $NaNO_3$ using ITC technique

   P.S.Asoka Kumar, R.Navil Kumar and C.P.G.Vallabhan

   Proceedings of the XIX National Seminar on Crystallography, Kottayam. Paper No.D-14 (1987).

7. DC electrical conductivity, dielectric constant and phase transitions in $(NH_4)_2HPO_4$

   Elizebeth Thomas, R.Navil Kumar and C.P.G.Vallabhan

   Proceedings of the XIX National Seminar on Crystallography, Kottayam. Paper No.D-16 (1987).

8. DC electrical conductivity studies in pure,doped and deuterated potassium acid phalate

   Hazeena George, N.C.Santha Kumari, R.Navil Kumar and C.P.G.Vallabhan

   Proceedings of the XIX National Seminar on Crystallography, Kottayam. Paper No.D-15 (1987).

9. Effect of ionic radii on thermally stimulated depolarization currents in doped $NaClO_3$ crystals

   R.Navil Kumar and C.P.G.Vallabhan

   Proceedings of the Solid State Physics Symposium, Bhopal. Vol.31C (1988) 51.

10. Ionic thermocurrent study of Pb^{2+} doped $NaClO_3$ crystals

    R.Navil Kumar and C.P.G.Vallabhan

    Journal of Material Science Letters, 8 (1989) 453.

11. Electrical conductivity dielectric constant and phase transitions in pure and doped diammonium hydrogen phosphate

    R.Navil Kumar and C.P.G.Vallabhan

    J.Phys:Condensed Matter (in press).

12. Effect of deuteration on electrical conductivity, dielectric constant and phase transitions in $(NH_4)_3H(SO_4)_2$

    R.Navil Kumar and C.P.G.Vallabhan

    Physics Status Solidi(a) (To appear in Vol.112, 1989).

ACKNOWLEDGEMENTS

The investigations presented in this thesis have been carried out under the guidance and supervision of Dr.C.P.Girijavallabhan, Professor, Department of Physics, Cochin University of Science and Technology. I am extremely thankful to him for giving me the necessary advice to carry out the research work in the experimental field. It is with great pleasure I express my sincere gratitude for his able guidance and competent advice throughout the course of this work.

I am extremely thankful to Dr.K.Sathianandan, Dr.M.G.Krishna Pillai, former Heads of the Department and to Dr.K.Babu Joseph, Professor and Head of the Department who have shown keen interest in this work and provided all the necessary facilities for carrying out the same.

I am highly indebted to Prof.R.Gopalakrishna Pillai, Head, Department of Physics, S.N.M.College, Maliankara, for giving me constant encouragement and inspiration throughout the period of this work.

I would like to thank Dr.U.Syamaprasad, Scientist, Regional Research Laboratory, Bhubaneswar for his constant help in the beginning stages of this work.

The immense help and encouragement I have received from all the members of the faculty of the Department of Physics particularly from Dr.K.P.Vijayakumar and Dr.V.P.N. Nampoori are gratefully acknowledged.

The constant help and co-operation received from the technical, administrative and library staff are sincerely acknowledged. Special thanks go to the staff of the University Science Instrumentation Centre, especially to Shri K. Madhusoodanan, Scientific Officer, and Shri Muraleedharan for their timely help and advice in fabricating various parts of experimental systems.

I express my sincere thanks to all my colleagues, especially my co-workers Mrs.N.C.Santha Kumari, Mr.Edwin Xavier, Mr.Rajeev Kumar and Mr.M.K.Jayaraj of thin film division for their whole-hearted co-operation and immense help I received from them.

The junior as well as senior research fellowships awarded by the Cochin University of Science and Technology in the earlier stages and a senior research fellowship awarded by the STEC, Government of Kerala during the rest of the period are gratefully acknowledged.

Finally, I would like to thank Mr.Sasi for neatly typing the manuscript.

R.Navil Kumar.

CONTENTS

		Page
PREFACE	.. ..	i
ACKNOWLEDGEMENTS	.. ..	ix
Chapter I	INTRODUCTION	1
1.1	Importance of the study of phase transition ..	2
1.2	Thermodynamic aspects of phase transition..	4
1.3	Techniques employed in the study of phase transformation ..	11
1.4	Electrical conductivity of ionic solids ..	20
1.5	Dielectric methods ..	26
1.6	Ionic thermocurrent measurements ..	28
1.7	Theory of thermally stimulated polarization current (TSPC) ..	33
1.8	Applications of phase transition ..	35
1.9	References ..	38
Chapter II	EXPERIMENTAL TECHNIQUES AND METHODS OF MEASUREMENTS ..	50
2.1	Introduction ..	51
2.2	Methods used for crystal growth ..	52
2.3	Preparation of samples for electrical measurements ..	55
2.4	Vacuum system for the deposition of thin film electrodes ..	56
2.5	Metallic cell for electrical measurements..	56
2.6	Methods of measurement ..	61
2.7	Photoacoustic measurements ..	70
2.8	References ..	73

		Page
Chapter III	DC ELECTRICAL CONDUCTIVITY,DIELECTRIC CONSTANT AND PHASE TRANSITIONS IN PURE AND DEUTERATED $(NH_4)_3H(SO_4)_2$ ..	75
3.1	Introduction ..	76
3.2	Experimental details ..	78
3.3	Experimental Results ..	79
3.4	Discussion ..	84
3.5	Conclusions ..	89
3.6	References ..	92
Chapter IV	DC/AC ELECTRICAL CONDUCTIVITY,DIELECTRIC CONSTANT AND PHASE TRANSITIONS IN $(NH_4)_2HPO_4$ ..	95
4.1	Introduction ..	96
4.2	Experimental details ..	98
4.3	Experimental results ..	99
4.4	Discussion ..	107
4.5	Conclusions ..	119
4.6	References ..	120
Chapter V	THERMAL DEPOLARIZATION STUDIES OF PURE AND DOPED DIAMMONIUM HYDROGEN PHOSPHATE ..	123
5.1	Introduction ..	124
5.2	Experimental details ..	126
5.3	Experimental results ..	127
5.4	Discussion ..	143
5.5	Conclusions ..	148
5.6	References ..	150

		Page
Chapter VI	DC AND AC ELECTRICAL CONDUCTIVITY, DIELECTRIC CONSTANT, IONIC THERMO-CURRENT AND PHASE TRANSITIONS IN PURE AND DOPED $(NH_4)_2Cr_2O_7$ CRYSTALS ..	153
6.1	Introduction ..	154
6.2	Experimental details ..	157
6.3	Experimental results ..	158
6.4	Discussion ..	168
6.5	Conclusions ..	174
6.6	References ..	176
Chapter VII	PHTOACOUSTIC STUDIES ON PHASE TRANSITIONS IN $(NH_4)_2Cr_2O_7$ AND $NH_4H_2PO_4$ ..	179
7.1	Introduction ..	180
7.2	Experimental details ..	183
7.3	Experimental results ..	190
7.4	Discussion ..	198
7.5	Conclusions ..	201
7.6	References ..	202
Chapter VIII	IONIC THERMOCURRENT STUDIES IN PURE AND DOPED $NaClO_3$ CRYSTALS ..	205
8.1	Introduction ..	206
8.2	Experimental details ..	209
8.3	Experimental results ..	210
8.4	Discussion ..	229
8.5	Conclusions ..	233
8.6	References ..	236

			Page
Chapter IX	THERMALLY STIMULATED POLARIZATION AND DEPOLARIZATION CURRENT STUDIES IN PURE AND DOPED $NaNO_3$ CRYSTALS	..	239
9.1	Introduction	..	240
9.2	Experimental details	..	244
9.3	Experimental results	..	244
9.4	Discussion	..	262
9.5	Conclusions	..	268
9.6	References	..	271
Chapter X	IONIC THERMOCURRENT STUDIES OF DOUBLY DOPED $NaNO_3$ CRYSTALS	..	274
10.1	Introduction	..	275
10.2	Experimental details	..	277
10.3	Results of ITC measurements	..	277
10.4	Discussion	..	284
10.5	Conclusions	..	287
10.6	References	..	289

Chapter 1

INTRODUCTION

Abstract

This chapter presents an overview of ideas and concepts necessary for the exposition of the importance of the study of phase transitions in solids. It also describes a reasonably comprehensive theoretical basis of some of the thermodynamical aspects of phase transition process. The experimental techniques generally employed in the study of phase transitions and some of their theoretical aspects are also specified in this section. Special attention has been paid to the study of this phenomenon with respect to the electrical and photoacoustic properties. In the last part of this chapter, a concise review of the current status and some of the applications of the phase transition phenomena are described.

1.1 IMPORTANCE OF THE STUDY OF PHASE TRANSITION

During the last two decades, research activities in the field of phase transformations in solids have grown enormously because of its technological importance and interest from a fundamental standpoint. There is a consensus among researchers in the field that a more basic understanding of phase transformations is required to explain the properties of materials and to develop and select new materials. Phase transformations are also of fundamental interest because they are related to a variety of processes that lend to changes in phase, structure and features thus often creating new forms of matter with properties which usually differ from those of their constituents. A greater understanding of the structure and properties of these materials undergoing phase transitions has resulted essentially from the use of a number of sophisticated analytical techniques which give precise information regarding the behaviour of such materials under specific physical conditions. Thus the progress in material science as well as in various branches of studies on solid state has been greatly influenced by the introduction of new methods, techniques, and instruments some of which are highly advanced and sophisticated. Much of the modern methodology of mathematics, physics and chemistry has been

called upon to refine the investigation of matter in the crystalline state and solid state at large. This has been the case not only for the fundamental and scientific exploration of solid state, but also for the techniques used to measure properties and evaluate performance and for specific applications in actual use. As a result much greater variety of their functions under normal and extreme conditions has been studied and this has led to the development of a vast body of knowledge and especially of highly specialised methods and techniques.

This thesis aims to present a series of experimental investigations of phase transition in materials, studies particularly in certain ammonium containing crystals, viz., $(NH_4)_3H(SO_4)_2$, $(NH_4)_2HPO_4$, $(NH_4)_2Cr_2O_7$ and $NH_4H_2PO_4$ using electrical and photoacoustic techniques. The electrical studies include, measurement of dc/ac electrical conductivity dielectric constant, thermally stimulated polarization and depolarization current. The studies extended to doped and deuterated specimens of the crystals have revealed the mechanisms of phase transition and of the electrical charge transport processes. The thesis also describes the results of investigation carried out in pure as well as doped specimens of $NaClO_3$ and $NaNO_3$ using thermally stimulated polarization and thermally stimulated depolarization current measurements.

1.2 THERMODYNAMIC ASPECTS OF PHASE TRANSITIONS

The most fully developed theories of phase transformations are based on thermodynamics and in particular on statistical thermodynamics. An assembly of systems, for instance, of molecules or atoms of various kinds, can be physically and chemically either homogeneous or not homogeneous. A non-homogeneous assembly can be divided into a number of homogeneous parts called phases, each possessing its characteristic energy, temperature and entropy. The statistical nature of these quantities indicates that a rigorous definition of a phase and especially of phase boundary, on an atomic scale is difficult if not impossible. This will seriously limits our present understanding of the mechanism of many phase transformations in solids. In spite of this, thermodynamics provides a very convenient frame work for description of these phenomena. Gibb's who was the first to give a rather complete analysis of transformations on this basis, by considering the function.

$$G = U - TS + PV \tag{1.1}$$

where G is known as the Gibb's function [1]. An equilibrium between phase 1 and phase 2 at a given temperature T, and pressure P requires $G_1 - G_2 = 0$. Since the compressibility

of solids is relatively small, one can assume dV = 0 and then the equilibrium condition can be expressed as

$$dF = 0 \text{ where } F = U - TS \tag{1.2}$$

where F is the Helmholtz free energy. It should be kept in mind however, that for solids, the use of F instead of G in the equilibrium requirement is only an approximation. An estimation of the free energy of a solid as a function of temperature can be obtained in the following manner. From equation (1.2)

$$dF = -PdV - SdT \tag{1.3}$$

at constant pressure we have,

$$F = F_o - \int_o^T S.dT - P(V_T - V_o) \tag{1.4}$$

On the other hand

$$S = \int_o^T \frac{C_p}{T} dT \tag{1.5}$$

and thus

$$F = F_o - P(V_T - V_o) - \int_o^T \left(\int_o^{T''} \frac{C_p}{T'} dT' \right) dT'' \tag{1.6}$$

where V_T and V_o are molar volumes at pressure P and F_o is

the energy at absolute zero equal to the internal energy U_o at that temperature. Equation (1.5) gives the absolute value of S by assuming that S = 0 at T = 0 which is the Nernst heat postulate [2] or the third law of thermodynamics. For certain solids, this law appears not to be applicable because of orientation effects, order effects, isotopic composition etc. Such cases are metastable, which in proximity of absolute zero have no chance to reach true equilibrium because of vanishing mobility of atoms.

For solids, the second term in equation (1.6) is very small. Therefore,

$$F = A - \int_0^T \left(\int_0^{T''} \frac{C_p}{T'} dT' \right) dT'' \qquad (1.7)$$

where A is a constant. This formula is useful in discussing the influence of the lattice specific heat and of the electronic specific heat on phase transformations, such as $\alpha - \gamma$ transformation in iron [3] and it permits an understanding of the influence of alloying elements on this transformation [4]. It can be used also to compare the free energy of solid phases if the specific heats are known experimentally or theoretically. The latter possibility is useful if Debye specific heat theory is applicable. At

the transformation temperature we have a change in the total energy.

$$\Delta U = T\,\Delta S - P\,\Delta V \tag{1.8}$$

which gives for the change of enthalpy.

$$\Delta H = \Delta U + P\,\Delta V = T\,\Delta S \tag{1.9}$$

This relation enables one to obtain the entropy of transformation ΔS from the experimentally known heat of transformation at constant pressure, ΔH. Thus it is possible to find the transformation temperature provided we know the enthalpies and entropies of both phases as a function of temperature. We have further,

$$S = \left(\frac{\partial G}{\partial T}\right)_P \tag{1.10}$$

which gives,

$$G = H + T\left(\frac{\partial G}{\partial T}\right)_P \tag{1.11}$$

and

$$\Delta G = \Delta H + T\left(\frac{\partial \Delta G}{\partial T}\right)_P \tag{1.12}$$

is the Gibb's Helmholtz equation. The derivative in the equation (1.12) vanishes at absolute zero and thus $\Delta G(T)$ can be calculated from measured $\Delta H(T)$. Among the other thermodynamical formulas of importance for transformations, it is worth mentioning in particular

$$\left(\frac{\partial \alpha}{\partial P}\right)_T = -\left(\frac{\partial \beta}{\partial T}\right)_T \tag{1.13}$$

and the Maxwell relations,

$$\left(\frac{\partial S}{\partial V}\right)_T = \left(\frac{\partial P}{\partial T}\right)_V = \frac{\alpha}{\beta} \tag{1.14}$$

$$\left(\frac{\partial S}{\partial P}\right)_T = -\left(\frac{\partial V}{\partial T}\right)_V = -\alpha V \tag{1.15}$$

where

$$\alpha = \frac{1}{V}\left(\frac{\partial V}{\partial T}\right)_P \tag{1.16}$$

is the cubic thermal expansion coefficient and

$$\beta = -\frac{1}{V}\left(\frac{\partial V}{\partial P}\right)_T \tag{1.17}$$

is the isothermal compressibility. These equations are only applicable to single phases.

Differentiating the equation (1.15) one obtains,

$$\left(\frac{\partial C_p}{\partial p}\right)_T = -\alpha^2 TV - T\left(\frac{\partial \alpha}{\partial T}\right)_p V \tag{1.18}$$

in which for solids $\left(\frac{\partial \alpha}{\partial T}\right)_p$ is usually very small and thus approximately

$$\left(\frac{\partial C_p}{\partial V}\right)_T \simeq \left(\frac{\alpha^2 T}{\beta}\right) \tag{1.19}$$

here

$$C_p = T\left(\frac{\partial S}{\partial T}\right)_p = \left(\frac{\partial H}{\partial T}\right)_p \tag{1.20}$$

is the usual specific heat at constant pressure. From relation (1.14) one can deduce that at equilibrium between two phases 1 and 2,

$$\frac{dP}{dT} = \frac{S_1 - S_2}{V_1 - V_2} = \frac{H_1 - H_2}{T\,(V_1 - V_2)} \tag{1.21}$$

where the quantities S, V and H refer to one mole of a single component. This is the so called Clausius-Clapeyron relation which describes the effect of pressure on transitions.Equation

(1.21) is very useful for explaining transformations like melting, change of crystal structure etc.

An important consequence of the existence of relationships among the various thermodynamic quantities is the so called Gibb's phase rule.

$$C = F + P - 2 \qquad (1.22)$$

in which C is the number of independent components, F is the number of degrees of freedom, and P is the number of phases. Degrees of freedom are independently variable parameters such as temperature, pressure composition of phases etc. In applying this rule to transitions in solids, containing more than one species of atoms or molecules, it should be kept in mind that if the two phases have the same chemical composition then C is equal to unity. Such conditions occur for instance, at a congruent melting point or at the critical temperature of order-disorder transformations [5-9].

1.2.1 Transformations of higher order

According to Ehrenfest the order of transition can be defined as follows: "A transition is said to be n^{th} order if the derivatives lower than the n^{th} derivative of the function G are continuous at the transform-

ation temperature while the n^{th} derivative is discontinuous". Or in other words, a transition is a phase transformation only when it is of the first order. The applicability of Ehrenfest's criterion turned out to be limited not only because of experimental difficulties in establishing whether a certain quantity is continuous or not, but also because of the existence of various intermediate kinds of anomalies [10]. Figure 1.2a illustrates the various kinds of transitions reported [11]. The main difference between first order and anomalous first order transition is that in the latter category each phase anticipates the change with approaching transformation temperature or transition pressure. Instead of simple second-order transition as one observed usually a lambda transformation in which near the transformation point both faces show a pronounced continuous change in the various thermodynamic quantities. Since thermodynamics is unable to give an atomistic quantitative picture of second order transitions much effort has been diverted towards obtaining a solution using purely statistical methods.

1.3 Techniques employed in the study of phase transformation

Phase transformations in solids are often accompanied by interesting changes in their physical properties. Hence, measurement of such physical quantities as a function of

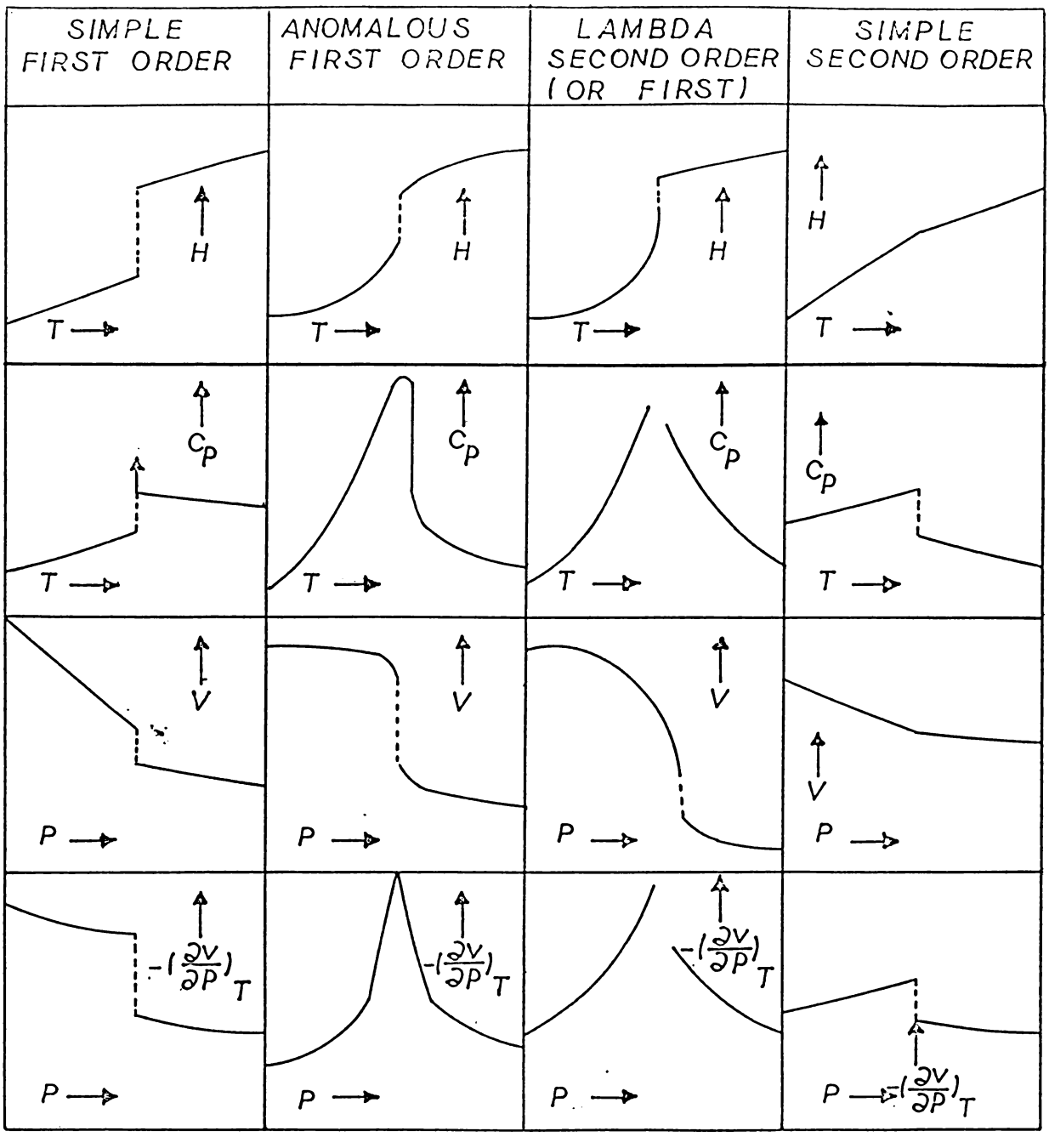

Figure 1.2a. Change in physical quantities at various kinds of transitions.

an external parameters like pressure or temperature is a direct way of investigating these phase transitions. Several techniques are employed to investigate phase transitions depending on the nature of the solid and properties of interest. Such studies are not only of academic value in understanding the structural and mechanistic aspects of phase transitions but are also of technological importance. The availability of modern experimental methods employing highly sophisticated electronic techniques has brought out a quite large number of new transitions as well as transitions which have not been observed in earlier measurements. A large number of techniques are already reported in the literature [12-23]. They include diffraction, thermal, optical, spectroscopic, magnetic, electrical, photoacoustic and ultrasonic measurements.

1.3.1 Diffraction techniques

X-ray diffraction can conveniently be used to study the structural features of solids undergoing phase transition. Diffraction gives information in fourier form, which can be analysed in terms of the average spacings of lines and planes, the symmetries of point groups, and the location of particular species of atoms, in the different phases of the transition process. In this respect, electron

diffraction techniques has certain special advantages, because of the wavelength of radiation used can be smaller than the distances to be resolved, and hence, it can be used for the study of super structures and small domains. Neutron diffraction studies are most useful in studying position of light atoms like hydrogen and in magnetic structure. The analysis of the powder neutron diffraction profiles [24] yields valuable structural informations.

1.3.2 Thermal measurements

Thermal measurements have been widely used to identify thermal and characteristic transitions. Differential thermal analysis (DTA), differential scanning calorimetry (DSC) and thermo gravimetric analysis (TGA) techniques provide valuable information regarding changes in various physical parameters associated with the phase transition. The heat capacity measurements using DSC and DTA technique give precise data on enthalpy changes and thermodynamic order of transition. The information on activation energies of transformation has also been obtained by fitting the DSC and DTA peak to first order kinetic equations [25,26]. Thermal hysteresis has also conveniently been studied by DTA and DSC. Being a dynamic technique DTA suffers from certain disadvantage compared to that of DSC. For example the heat capacity data

and ΔH values obtained by DTA are not reliable, whereas the values obtained from DSC being much more reliable than those of DTA.

1.3.3 Optical spectroscopic and related techniques

The field of phase transitions has experienced a period of extremely rapid growth since development of lasers in the early 1966's. Optical methods, particularly the light scattering has played an increasingly crucial role in the investigation of many types of phase transitions. The optical microscopic analysis is a valuable tool for studying phase transformations, particular with respect to the movement of boundaries, growth of nuclei and changes in grain size. Pressure transitions can also be studied by using an optical microscope and a diamond anvil press. The dislocations and structural aspects of solids can be conveniently studied using the electron microscope along with a variable temperature controlling facility which would undoubtedly be of great value, in this regard. Optical spectroscopy in the infrared visible and ultraviolet regions has been used extensively to study solids undergoing transitions. Laser Raman spectroscopy has been particularly exploited in recent years to investigate these transitions. In addition to neutron

scattering, Raman spectroscopy also yield direct information on soft modes in solids. X-ray and ultraviolet photoelectron investigations at the phase transitions points provide valuable information on the changes in electronic structure of the solids. Positron annihilation is a technique in which the phenomenon of e^+, e^- recombination with consequent emission of γ-rays is used to study phase transitions in solids. Since purity of the material plays a crucial role in phase transition characteristics, preparation, purification, and characterisation of materials undoubtedly form an important part of phase transition studies. It is therefore important that efforts are being made to use the purest material possible while studying phase transitions. In this regard all the well-known techniques for the analysis and characterisation of materials like mass spectroscopy, spectrography, atomic absorption spectrophotometry and electron microscopic analysis have to be employed.

1.3.4 Magnetic properties and resonance techniques

Magnetic measurements give direct information regarding electron correlations and ligand field potentials. The Weiss molecular field approach gives the basis for understanding the temperature variation of magnetic susceptibility and magnetisation. Measurement of magnetic susceptibility and magnetisation as a function of temperature along with

techniques like neutron diffraction, inelastic neutron scattering, and Mossbauer spectroscopy, provides information on magnetic moments, the nature of coupling and magnetic order in solids. NMR spectroscopy has been employed to study phase transitions of solids containing the appropriate nuclei, for example, V in VO_2 and V_2O_3 and Mn in $MnCr_2O_4$. Phase transitions in NaCN and NaHS have been studied by NMR spectroscopy. Studies of hindered rotation of CH_3 or NH_4 groups and phase transitions in hydrogen bonded ferroelectric like KH_2PO_4 are other important applications of NMR spectroscopy. ESR spectra of solids undergoing transitions have been reported in the literature. A useful application of ESR spectroscopy is to study a diamagnetic crystal doped with a paramagnetic ion, (eg., Mn in KNO_3) in the region of the phase transition. NQR spectroscopy has been employed to study phase transitions of halides (eg., $CsPbCl_3$), nitrates, and nitrites ($NaNO_3$ and $NaNO_2$). Other solids containing nuclei like halogen, nitrogen and others (Nb in $KNbO_3$) with quadrupole moments have been studied in detail. Excellent treatments on magnetism and chemical bond [27] and detailed studies of several magnetic transitions [28-53] on a variety of solids are available in the literature. In addition, ferromagnetic and antiferromagnetic resonance experiments also provide useful information on magnetically ordered solids.

1.3.5 Electrical measurements

The electrical properties like electrical conductivity, dielectric constant and thermoelectric power, hall effect, ionic thermocurrent measurements etc. have been used to characterise these materials and to study the phase transitions in them. The study of electrical conduction process in materials can yield a great deal of information on the formation and migration of charge carriers in them. Basically electrical conductivity in these materials is a defect controlled phenomenon and hence, detailed investigation of the electrical properties of these materials is one of the best available methods for the study of defects in them. Usually, these electrical properties are investigated as a function of temperature or as a function of pressure. Recently, the electrical conductivity (both dc and ac), dielectric constant and ionic thermocurrent measurements have become accepted as a very sensitive method for the study of phase transitions as well as for the study of defects in ammonium containing crystals [54-61]. Therefore a detailed theoretical background of these techniques are necessary here and this will be described in the latter sections.

1.3.6 Photoacoustic measurements

The photoacoustic (PA) technique has been recently accepted as an important spectroscopic technique for condensed

matter [22,23,62-67]. The basic principle for the detection of the PA effect is measurement of acoustic signal produced when a sample is placed in a sealed gas filled cell and illuminated by an audio frequency chopped light. The generation and propagation of acoustic waves in the sample depend critically on the thermoelastic and physical properties of the sample. By monitoring the PA signal amplitude and phase, it is possible to probe or measure such properties as acoustic velocities, elasticity, density, thickness, specific heat, material discontinuities, crystallinity, phase transition etc., since, the thermal properties of the sample like thermal conductivity, specific heat etc. are drastically changed at the point of phase transition, a corresponding variation in PA amplitude and phase will be detected. This is the reason why the PA effect can be used for the study of phase transitions [68-72]. A detailed theoretical description will be given in Chapter VII.

1.3.7 Ultrasonic measurements

Ultrasonic measurements is an important tool for the investigation of structural phase transitions in solids. It is possible to get information on nature of phase transition by the measurement of the elastic response of this method. This elastic constant measurements are a very sensitive tool

to locate transition points, to determine phase diagrams, and in certain special cases, to make statements about the order of phase transition. Furthermore, from the temperature variation of the elastic response functions the type of coupling between strain and order parameter can be deduced. Thus the coupling parameters and the characteristic variations of other important quantities can be derived. Also, the elastic measurements are used to test the aspects of the modern renormalisation theories such as the Crossover and Dimensional effects. Ultrasonics thus offers an attractive method for investigations in the field of phase transitions [73-75].

1.4 ELECTRICAL CONDUCTIVITY OF IONIC SOLIDS

The study of ionic solids, comparatively is a new field of materials science and technology. Most of the solid state devices developed in the last three decades are based essentially on the motion of the electrons. In fact, the ionic solids have received very little attention in the past, in spite of the fact that these solids are best understood by solid state physicists and chemists. However, in 1967 the situation suddenly changed with the discovery of fast sodium-ion conduction in β-alumina and silver ion conduction in MAg_4I_5 (M = K, Rb, NH_4) [76-77]. Since 1967 a large number

of such solids have been discovered and numerous applications have been found such as solid state batteries, fuel cells, memory devices, display panels etc. The possibility of the development of a high density solid state battery for vehicular traction and low density miniaturised batteries for device applications has been the most important factor responsible for the recent involvement of a large number of physicists, chemists, materials scientists and engineers. In this respect the role played by the superconducting materials is very important in the sense that, these materials are potentially important from the point of view of technical applications.

The foundations upon which our understanding of ionic conductivity are built were laid down before 1940 by the early work of Schottky [78], Wagner [79] and Mott and Littleton [80,81]. It was found that the transference of mass and charge occurring in alkali halide crystal is mainly by means of ionic processes. Later the subject of ionic conductivity was expounded at length by Lidiard [82-84], Fuller [85-90], Barr [91-92], Franklin [93] etc. In addition to these, some other notable works [94-110] can also be found in the literature.

1.4.1 Theory of ionic conductivity

Consider the case of ionic conductivity in NaCl type lattice in which ions are made to move under the

application of electric field E. The potential barrier seen by an interstitial ion jumping from one position to another is equivalent to the addition of a term - qEx to the potential energy term Δg, where q is the charge on the interstitial ion. Hence, the jump of the interstitial ion in the field direction is taking place with an increased probability

$$\omega' = \gamma_o \exp\left[-\frac{(\Delta g - \frac{1}{2}qaE)}{kT}\right] \tag{1.23}$$

where $x = \frac{a}{2}$ and a is the interionic distance, γ_o is the jump frequency, and a jump against the field takes place with reduced probability

$$\omega'' = \gamma_o \exp\left[-\frac{(\Delta g + \frac{1}{2}qaE)}{kT}\right] \tag{1.24}$$

The net number of ions moving per unit volume in the direction of the field

$$n' = n(\omega' - \omega'') \approx nwqaE/kT \tag{1.25}$$

assuming $qaE << kT$. Here n is the number of interstitial ions per unit volume. Therefore the current density

$$j = na^2q^2\omega E/kT$$

Hence ionic conductivity is given by

$$\sigma = j/E = \frac{na^2q^2\omega}{kT} = nq\mu \qquad (1.26)$$

where the mobility is given by

$$\mu = a^2q\omega/kT \qquad (1.27)$$

If the charge carrier can jump to more than one forward position (for NaCl lattice this number is 4).

$$\text{i.e., } \sigma = 4na^2q^2\omega/kT \qquad (1.28)$$

If 'x' is the mole fraction of defect concentration then n = Nx where N is the total number of ions per unit volume, then σ can be written as

$$\sigma = (4Na^2q^2/kT)x.\omega \qquad (1.29)$$

1.4.2 Pure crystal

Consider the case of Schottky defects. Let the mole fractions of positive and negative ion vacancies be respectively x_1 and x_2 and their respective numbers be n_+ and n_- given by

$$n_+ = n_- = N \exp(-g_s/kT)$$

$$x_1 x_2 = x_o^2 = \exp(-g_s/kT) = \exp(s_s/k)\exp(-h_s/kT) \qquad (1.30)$$

where g_s, s_s, and h_s are the Gibb's energy, entropy and enthalpy of formation respectively for a Schottky pair, N is the number of cation or anion sites. In the case of pure crystals, the charge neutrality condition is written as

$$x_1 = x_2 = x_o \qquad (1.31)$$

An expression similar to equation (1.30) can be written for the Frenkel defects, n_F as

$$n_F = (NN')^{\frac{1}{2}} \exp(-g_f/kT) \qquad (1.32)$$

where N' is the number of interstitial sites and g_F is the Gibb's energy for formation of Frenkel defects.

1.4.3 Doped crystal

If an ionic crystal is doped by an aliovalent impurity ion (e.g., Ca^{2+} in NaCl) additional cation vacancies

are produced to compensate for the charge difference. Suppose, the mole fraction of divalent cation impurity is c_1. The charge neutrality equation is

$$x_1 = x_2 + c_1 \tag{1.33}$$

From equations (1.33) and (1.30)

$$\begin{aligned} x_1 &= \tfrac{1}{2} c_1 \left\{ [1+(2x_o/c_1)^2]^{\frac{1}{2}} + 1 \right\} \\ x_2 &= \tfrac{1}{2} c_1 \left\{ [1+(2x_o/c_1)^2]^{\frac{1}{2}} - 1 \right\} \end{aligned} \tag{1.34}$$

for large dopant concentration, $c \gg x_o$

$$x_1 = c \quad \text{and}$$

$$x_2 = x_o^2/c$$

For small dopant concentration ($c \ll x_o$) the concentrations reduce to the pure crystal values as expected, that is $x_1 = x_2 = x_o$.

It is also possible to write a similar expression when the crystal is doped by a divalent anion impurity like

CO_3^{2-}, SO_4^{2-} etc. with a concentration c_2. The charge neutrality condition can be written as

$$x_1 + c_2 = x_2.$$

The values of x_1 and x_2 for this case are

$$\begin{aligned} x_1 &= \frac{1}{2} c_2 \left\{ [1+(2x_o/c_2)^2]^{\frac{1}{2}} - 1 \right\} \\ x_2 &= \frac{1}{2} c_2 \left\{ [1+(2x_o/c_2)^2]^{\frac{1}{2}} + 1 \right\} \end{aligned} \qquad (1.36)$$

1.5 DIELECTRIC METHODS

If an electric field is created in a dielectric material the dipole moments of separate kinetic elements or atomic groups will tend to orient in the field direction. If the external electric field is now removed then after a certain time the polarization of the sample will diminish to zero as a result of thermal motion of separate kinetic elements, and the system will return to its previous equilibrium (or quasi equilibrium) state. Such a process of transition to equilibrium is called dielectric relaxation. It is characterised by the relaxation time τ . On the other hand if an alternating voltage is applied to the dielectric, the dielectric properties of the material will obviously

depend on the relation between the frequency of the applied voltage ω and the dielectric relaxation time τ .

The dielectric properties of the specimen can be characterised by the complex dielectric constant (relative permittivity)

$$\varepsilon^* = \varepsilon' - i\varepsilon'' \tag{1.37}$$

where ε' - the real component of complex dielectric constant, and ε'' - the imaginary component of complex dielectric constant (also called the dielectric loss factor).

The ratio

$$\frac{\varepsilon''}{\varepsilon'} = \tan\delta \tag{1.38}$$

is the dielectric loss tangent. It characterises the phase shift between the alternating voltage applied to the capacitor between whose plates the sample is placed and the current passing through the capacitor.

If the dielectric relaxation can be described by a single relaxation time then,

$$\varepsilon' = \varepsilon_\infty + \frac{\varepsilon_o - \varepsilon_\infty}{1+\omega^2\tau^2} \tag{1.39}$$

$$\varepsilon'' = \frac{(\varepsilon_o - \varepsilon_\infty)\,\omega\tau}{1+\omega^2\tau^2} \qquad (1.40)$$

where ε_o dielectric constant at $\omega = 0$.

ε_∞ dielectric constant at $\omega = \infty$ and

$$\tan\delta = \frac{\omega\tau\,(\varepsilon_o - \varepsilon_\infty)}{\varepsilon_o + \omega^2\tau^2} \qquad (1.41)$$

If ε_o the static dielectric constant, ε_r the relative permittivity ω the angular frequency and $\tan\delta$ the loss tangent then, the σ_{ac} can be given by the equation

$$\sigma_{ac} = \varepsilon_o \varepsilon_r \omega \tan\delta \qquad (1.42)$$

1.6 IONIC THERMOCURRENT MEASUREMENTS

The ionic thermocurrent technique is a general method of investigating the electrical properties of high resistivity solids via the study of thermal relaxation effects. This method offers an attractive alternative to the conventional bridge methods or current-voltage-temperature measurements. The mathematics behind this is similar to that found in other nonisothermal techniques such as thermoluminescence, thermally stimulated electronic emission differential scanning calorimetry or thermo gravimetric

analysis. The first theoretical basis of the thermally stimulated depolarization current (TSDC) phenomenon was suggested by Bucci and Fieschi based on their work on point defect dipoles in ionic crystals [111] and, it still took several years before TSDC was recognised as a method for studying all the fundamental mechanisms of charge storage and release in nonmetallic solids.

Denoted as ionic thermocurrent or ionic thermoconductivity by Bucci and Fieschi, the TSDC procedure thereafter received a number of confusing names due to the fact that it was reinitiated and developed by several investigators using quite different starting points and who, most of the time were not aware of preceding work in the field. The complimentary names used for this phenomenon are:

1. Electret Thermal Analysis (ETA)
2. Thermally Stimulated Discharge (TSD)
3. Thermal Current Spectra (TCS)
4. Thermally Activated Depolarization (TAD)

In the following text we will make use of the term thermally stimulated depolarization current (TSDC) or ionic thermocurrent (ITC) which seems to be the most appropriate

and descriptive name to be given to this process by considering the actual phenomena observed.

1.6.1 The Bucci-Fieschi theory or theory of TSDC

The time and temperature dependence of the dipolar polarization is determined by the competition between the orienting action of the field and the randomising action of thermal motions. The build-up of polarization at a constant temperature T can be described by the equation

$$P(t) = P_o[1-\exp(-t/\tau)] \tag{1.43}$$

with respect to time. In equation (1.43), P_o is the maximum amount of polarization possible at temperature T_p and this for all but the lowest temperatures and very high fields has been shown by Langevin [121] to be

$$P_o = \frac{N_D \mu^2 E_p}{3kT_p} \tag{1.44}$$

where N_D is the concentration of defect dipoles, E_p is the polarizing field, μ is the dipolemoment and is independent of temperature. The term τ in equation (1.43) is the time taken to polarize the dipoles at temperature T. Equation (1.43) describes the build up of polarization from P(0) = 0

to $P(\infty) = P_o$. If the field is removed at $t = \infty$, then the polarization will decay according to

$$P(t) = P_o \exp(-t/\tau_R) \tag{1.45}$$

where τ_R is the relaxation time for the dipoles at temperature T. In a crystalline solid association of an impurity ion with a vacancy can form such dipole which undergo reorientation. By making use of the assumption that time taken to polarize the impurity-vacancy (I-V) dipoles at a given temperature is the same as the time taken for those dipoles to depolarize at the same temperature.

We may represent the temperature variation of τ by the Arrhenius type equation,

$$\tau(T) = \tau_o \exp(E/kT) \tag{1.46}$$

where τ_o is the characteristic frequency factor for a vacancy jump from one lattice site to another for reorientation of the impurity-vacancy (I-V) dipole and is independent of temperature. E is the activation energy. We can rewrite equation (1.45) to be

$$P(t) = P_o[\exp(-\int_o^t dt/\tau)]$$

$$= P_o[\exp(-\int_o^t \frac{\exp(-\frac{E}{kT})}{\tau_o} dt)] \tag{1.47}$$

The current density arising from this depolarization is

$$j_D(T) = -\frac{\partial P(t)}{\partial t} \tag{1.48}$$

To perform this differentiation we make use of the fact that in our experiment, the temperature is to be raised at a constant rate, according to the equation $T = T_o + \beta T$ giving $\beta = \frac{dT}{dt}$. Changing the variable from t to T in order to find the measured thermally stimulated depolarization current density $j_D(T)$ we get

$$j_D(T) = -\frac{P_o}{\tau_o} \exp -\left\{ \frac{E}{kT} + \frac{1}{\beta \tau_o} \int_{T_o}^{T} \exp\left(\frac{-E}{kT'}\right) dT' \right\} \tag{1.49}$$

Finally using equation (1.44) we may write

$$j_D(T) = -\frac{N_D \mu^2 E_p}{3kT_p} \exp -\left\{ \frac{E}{kT} + \frac{1}{\beta \tau_o} \int_{T_o}^{T} \exp\left(\frac{-E}{kT'}\right) dT' \right\} \tag{1.50}$$

Equation (1.50) can be seen to be equivalent to the Randall and Wilkins glow curve equation [122] for the case of monomolecular recombination.

Using Garlick and Gibson's [123] approximation which is based on the assumption that the integral term in equation (1.50) is negligible over the initial part of the

curve, we may write equation (1.50) in the form

$$\dot{\mathcal{J}}_D(T) = \text{Constant exp } (-E/kT) \tag{1.51}$$

So a plot of log $\dot{\mathcal{J}}_D(T)$ against T^{-1} for the initial part of the TSDC curve will give a straight line of slope -E/k. It can be seen that the value of E obtained by this method is independent of the polarizing field E_p.

The maximum of equation (1.50) is given by

$$\frac{\partial \mathcal{J}_D(T)}{\partial T} = 0 \text{ at } T = T_M$$

Using this equation, we get

$$\exp(E/kT_M) = \frac{k T_M^2}{\beta E \tau_0} \quad \text{or} \quad T_M = \left[\frac{\tau(T_M)\beta E}{k}\right]^{1/2} \tag{1.52}$$

Thus knowing T_M we cán find $\tau(T_M)$. This value along with E gives a value for τ_0 from equation (1.46).

1.7 THEORY OF THERMALLY STIMULATED POLARIZATION CURRENT (TSPC)

In a TSPC experiment the increase in polarization is monitored during a linear rise in temperature in the

presence of an applied field. Thus we may write,

$$P(t) = P_{\infty} \left[1-\exp - \int_{o}^{t} \frac{dt}{\tau(T)} \right] \qquad (1.53)$$

where P is the saturation polarization described by Langevin's function. By neglecting the T^{-1} dependence of P compared with exp(-E/kT) and of $\tau(T)$, we can arrive at the equation for the current density (TSPC) namely,

$$j_p(T) = \frac{P_{\infty}}{\tau_o} \exp - \left\{ \frac{E}{kT} + \frac{1}{\beta \tau_o} \int_{T_o}^{T} \exp \frac{-E}{kT'} dT' \right\} \qquad (1.54)$$

i.e., the same equation as (1.50) but of opposite sign.

In principle, both TSPC and TSDC techniques offer an important key to the comprehension of the fundamental mechanism of charge storage and release in dielectrics and semiconductors and is also considered as a very sensitive probe of kinetic transition and molecular relaxation process in polar materials. It has several basic advantages,compared with more conventional step response or loss measurements. It is inherently more sensitive, allowing us to detect dipole concentrations of less than 0.1 ppm [124] or carrier concentrations of about 10^8 to 10^9 cm^{-3} [125] and it is characterised by high resolving power, so as to resolve relaxation

process arising from set of dipoles with only slightly different energies [124].

1.8 APPLICATIONS OF PHASE TRANSITION

A large number of applications are already reported in the literature in which the phenomenon of phase transitions have been applied. According to Goodenough [126], applications of phase transitions may be classified into four groups:

(1) The formation and/or motion of mobile boundaries between two or more phases existing below a critical temperature T_c.

(2) Changes in physical properties as the temperature approaches T_c.

(3) Changes in properties at T_c and

(4) Metastable phase obtained by control of the kinetics of nucleation or diffusion required for the transformation of stable phases.

The properties related to the orientational order of molecules in the temperature range between T_c and melting

point have been widely used in type II superconductors. The superconductors are used for getting high magnetic fields at low temperatures. The properties exhibited by certain liquid crystals are widely used for optical display, detection of temperature uniformity and impurities. Certain crystals can act as thermal switches during a phase transition. Metal-insulator transition exhibited by certain oxides are of considerable interest from a technical standpoint. With the discovery of the high temperature superconductivity in ceramic materials, the phenomenon of phase transition have become an extremely important subject.

Two important properties which change near T_c are softening of an optical mode before a displacive transition, and temperature dependence of spontaneous magnetisation in ferromagnets below T_c. These properties are used in dielectric and pyromagnetic detectors. The applications of soft mode anomalies have been discussed by Fleury [127].

The properties exhibited at the first order phase transition can be used for switching semiconductor-metal transitions. This could be employed in circuit breakers voltage dividers or optical switches.

Ferroelectrics undergoing transitions are being widely used in practical applications. They are extensively used in high and ultra high capacitance capacitors, dynamic elements of memory and logical elements of electronic computers, electromechanical converters, capacitance analogues of thermistors and special thermistors with a positive temperature coefficient, high voltage, accumulators, electrets, radiation modulators and regulators of the quality of optical quantum generators, IR detectors, ferroelectric energy convertors, frequency multipliers etc. Ferroelectrics are also used in pulse generation circuits, devices for controlling luminescence of electroluminophores, voltage and current stabilizers etc. Recently substance with both ferroelectric and ferro or antiferro magnetic properties has been discovered so that we can expect a further widening of the field of application of ferroelectrics.

1.9 REFERENCES

[1] P.Ehrenfest, Proc.Amsterdam Acad. 36 (1963) 153.

[2] A.B.Pippard, "Elements of Classical Thermodynamics", Cambridge University Press, 1966.

[3] F.Seitz, "Modern Theory of Solids", McGraw-Hill, New York, 1940.

[4] R.Smoluchowski, Metal Progr. 41 (1942) 363.

[5] M.A.Krivoglaz and A.Smirnov, "Theory of Order-Disorder in Alloys", Macdonald, London, 1964.

[6] H.Yamouchi and D.de Fontaine, in "Order-Disorder Transformation in Alloys", H.Warlimont (Ed.), Springer-Verlag, Berlin, 1974, p.148.

[7] J.M.Cowley, J.Appl.Phys. 21 (1950) 24.

[8] H.Lipson, in "Progress in Metal Physics", B.Chalmers (Ed.), Vol.2, Pergamon Press, New York, 1957.

[9] B.H.Kear, T.Sims, N.S.Stoloff and J.H.Westbrook (Eds.), "Ordered Alloys, Structural Applications and Physical Metallurgy", Clautiors Publishing Division, Baton Range, 1979.

[10] E.Bauer, Changements de Phases,Soc.Chim.Phys. p.3, Paris, 1952.

[11] J.E.Mayer and S.F.Streeter, J.Chem.Phys. 7 (1939) 1019.

[12] Helen D.Megan, "Ferroelectricity in Crystals", Methuen and Co., London, 1957.

[13] C.N.R.Rao and M.Natarajan, "Crystal Structure Transformations in Binary Halides", NSRDS-NBS Monograph 41, Washington D.C., 1972.

[14] C.N.R.Rao and G.V.Subba Rao, "Transition Metal Oxides: Crystal Chemistry, Phase Transitions and Related Aspects", NSRDS-NBS Monograph 49, Washington D.C., 1974.

[15] C.N.R.Rao, B.Prakash and M.Natarajan, Crystal Structure Transformation in Inorganic Nitrites, Nitrates and Chromates", NSRDS-NBS Monograph 53, Washington D.C., 1975.

[16] C.N.R.Rao and B.Prakash, "Crystal Structure Transformations in Inorganic Sulphates, Phosphates, Perchlorates and Chromates", NSRDS-NBS Monograph 56, Washington D.C., 1975.

[17] C.N.R.Rao and K.P.R.Pisharody, "Progress in Solid State Chemistry", Pergamon Press, Oxford, Vol.10, 1975.

[18] J.B.Goodenough and J.M.Longo, "Crystallographic and Magnetic Properties of Perovskite and Perovskite related Compounds", Landolt-Bornstein, New Series Group III, Vol.4a, Springer-Verlag, Berlin, 1970.

[19] E.P.Papadakis, "Physical Acoustics", W.P.Mason and R.N.Thruston (Ed.), Vol.12, Academic Press, New York, 1976.

[20] R.Truell, C.Elbaum and B.B.Chick, "Ultrasonic Methods in Solid State Physics", Academic Press, New York, 1969.

[21] E.R.Fuller, A.V.Granato, J.Holder and E.R.Naimon, "Methods of Experimental Physics", R.V.Coleman (Ed.), Vol.11, Academic Press, New York, 1974.

[22] Yoh-han-Pao, "Optoacoustic Spectroscopy and Detection", Academic Press, New York, 1977.

[23] A.Rosencwaig, "Photoacoustics and Photoacoustic Spectroscopy", John Wiley, New York, 1980.

[24] H.M.Hietveld, J.Appl.Cryst. 2 (1969) 65.

[25] K.J.Rao and C.N.R.Rao, J.Mater.Sci. 1 (1966) 238.

[26] M.Natarajan, A.R.Das and C.N.R.Rao, Trans.Faraday Soc. 65 (1969) 3081.

[27] J.B.Goodenough, "Magnetism and Chemical Bond", John Wiley, New York, 1963.

[28] E.Barthelemy, O.Gorochov and Mckinzie, Mat.Res.Bull. 8 (1973) 1401.

[29] K.Dwight, N.Menyuk and J.A.Kafalas, Phys.Rev.B. 2 (1970) 3630.

[30] B.Van Laar, Phys.Rev. 156 (1967) 654.

[31] D.K.Dwight, R.W.German, N.Menyuk and A.Wold, J.Appl.Phys. 33 (1962) 1341.

[32] T.Shinjo and K.Kosuge, J.Phys.Soc.Japan, 21 (1966) 2622.

[33] P.H.Carr and S.Foner, J.Appl.Phys. 31 (1960) 1960.

[34] F.J.Morin, Phys.Rev. 78 (1950) 819.

[35] W.S.Carter and K.W.H.Stevens, Proc.Phys.Soc.B. 69 (1956) 1006, 76 (1960) 969.

[36] D.R.Huffmann and R.L.Wild, Phys.Rev. 148 (1966) 526.

[37] J.Chenavas, J.C.Joubert and M.Marezio, Solid State Commun. 9 (1971) 1057.

[38] D.S.McClure, "Excitons, Magnons and Phonons in Molecular Crystals", A.B.Zahlan (Ed.), Cambridge University Press, London, 1968.

[39] W.J.L.Burgers, G.Dowling, J.Sakurai and R.A.Cowley, "Neutron Inelastic Scattering", Proceedings of IAEA Symp., Copenhagen, 2 (1968) 126.

[40] J.B.Goodenough, Phys.Rev. 164 (1967) 785.

[41] H.B.Mathur, "Solid State Chemistry", C.N.R.Rao (Ed.), Marcel Dekker, New York, 1974.

[42] D.G.Wickham and W.J.Croft, J.Phys.Chem.Solids.7 (1958) 351.

[43] T.Riste and L.Tenser, J.Phys.Chem.Solids.19 (1961) 117.

[44] M.T.Evans, E.Warming and G.L.Squires, "Neutron Inelastic Scattering", Proceedings of IAEA Symp., Grenoble, 1972.

[45] W.Kudig, H.Bommel, G.Constabaris and R.H.Lindquist, Phys.Rev. 142 (1966) 327.

[46] T.J.A.Popma, C.Hass and B.Van Laar, J.Phys.Chem.Solids. 32 (1971) 581.

[47] H.F.Franzen, D.M.Strachen and R.G.Barnes, J.Solid State Chem. 7 (1973) 374.

[48] J.P.Delamaire, H.Le Brasq and F.Marion, Acad.Sci.C. 272 (1971) 2144.

[49] F.Gronvold, H.Heraldeson, B.Pedersen and T.Tufte, Rec. Chim.Min. 6 (1969) 215.

[50] C.B.Van den Berg, Ferroelectrics, 4 (1972) 117.

[51] A.B.De Vries and C.Hase, J.Phys.Chem.Solids. 34 (1973) 651.

[52] J.B.Goodenough, J.Appl.Phys. 39 (1968) 403.

[53] W.Kudig and R.S.Hargrove, Solid State Commun. 7 (1969) 223.

[54] U.Syamaprasad and C.P.G.Vallabhan, Solid State Commun. 34 (1980) 899.

[55] U.Syamaprasad and C.P.G.Vallabhan, J.Phys.C: Solid State Phys. 14 (1981) L571.

[56] U.Syamaprasad and C.P.G.Vallabhan, J.Phys.C: Solid State Phys. 14 (1981) 1865.

[57] U.Syamaprasad and C.P.G.Vallabhan, Solid State Commun. 38 (1981) 555.

[58] U.Syamaprasad and C.P.G.Vallabhan, Solid State Commun. 41 (1982) 169.

[59] U.Syamaprasad and C.P.G.Vallabhan, Phys.Lett. 89A (1982) 37.

[60] U.Syamaprasad and C.P.G.Vallabhan, Phys.Rev.B. 26 (1982) 5941.

[61] V.K.Subhadra, U.Syamaprasad and C.P.G.Vallabhan, J.Appl. Phys. 54 (1983) 2593.

[62] A.Rosencwaig, Optics Commun. 7 (1973) 305.

[63] A.Rosencwaig, Science, **181** (1973) 657.

[64] A.Rosencwaig, Phys.Today. **28** (1975) 23.

[65] A.Rosencwaig, Anal.Chem. **47A** (1975) 592.

[66] A.Rosencwaig and A.Gersho, J.Appl.Phys. **47** (1976) 64.

[67] A.Rosencwaig and S.S.Hall, Anal.Chem. **47A** (1975) 548.

[68] P.S.Bechthold, M.Campagna and T.Schober, Solid State Commun. **36** (1980) 225.

[69] R.Florian, J.Pelzl, H.Vargas and R.Wernhardt, Phys.Status Solidi.(a) **48** (1978) K35.

[70] P.Korpium, J.Baumann, E.Luscher, E.Papamokos and R.Tilgner, Phys.Status Solidi (a). **58** (1980) K13.

[71] C.Pichon, M.Leliboux, D.Fournier and A.C.Boccara, Appl. Phys.Lett. **35** (1979) 435.

[72] M.A.A.Siqueira, C.C.Ghizoni, J.I.Vargas, E.A.Menezes, H.Vargas and L.C.M.Miranda, J.Appl.Phys. **51** (1980) 1403.

[73] K.K.Kobayashi, J.Phys.Soc.Japan, **24** (1968) 497.

[74] K.H.Michel and J.Naudts, Phys.Rev.Lett. **39** (1977) 212.

[75] K.H.Michel and J.Naudts, J.Chem.Phys. **69,67** (1977) 547.

[76] B.B.Owens and G.R.Argue, Science. **157** (1967) 308.

[77] G.G. Bentle, J.Appl.Phys. 39 (1968) 4037.

[78] W.Schottky, Z.Phys.Chem.Abt. B29 (1935) 335.

[79] C.Wagner, Z.Phys.Chem.Abt. B38 (1938) 485.

[80] N.F.Mott and M.J.Littleton, Trans.Faraday Soc. 34 (1938) 485.

[81] N.F.Mott and R.W.Gurney, "Electronic Process in Ionic Crystals", 2nd ed., Oxford Press, London, 1948.

[82] A.B.Lidiard, Handbuch der Physik, Vol.20 (1957) 246.

[83] A.B.Lidiard, Phys.Rev. **94** (1954) 29.

[84] I.Boswara and A.B.Lidiard, Phil.Mag. **16** (1967) 805.

[85] R.G.Fuller, C.L.Marquardt, M.H.Reilly and J.C.Wells Jr., Phys.Rev. **176** (1968) 1036.

[86] R.G.Fuller and H.B.Rosenstock, J.Phys.Chem.Solids. **30** (1969) 2105.

[87] R.G.Fuller and M.H.Reilly, Phys.Rev.Lett. **19** (1967) 113.

[88] R.G.Fuller, Bull.Am.Phys.Soc. **15** (1970) 384.

[89] R.G.Fuller and M.H.Reilly, J.Phys.Chem.Solids. **30** (1969) 457.

[90] R.G.Fuller and F.W.Pattern, J.Phys.Chem.Solids, **30** (1970) 539.

[91] L.W.Barr and A.B.Lidiard, "Defects in Ionic Crystals, in "Physicals Chemistry An Advance Treatise", Vol.X, Academic Press, New York, 1970.

[92] D.K.Dawson and L.W.Barr, Phys.Rev.Lett. **19** (1967) 844.

[93] W.Franklin, Phys.Rev. **180** (1969) 682.

[94] G.Shennon, "Diffusion in Solids", McGraw-Hill, New York, 1963.

[95] H.R.Glyde, Rev.Mod.Phys. **39** (1954) 373.

[96] E.Pitts, Proc.Roy.Soc.A **217** (1953) 43.

[97] C.Ramasastry and Y.V.G.S.Murti, Proc.Roy.Soc. **305** (1968) 441.

[98] F.A.Kroger, J.Chem.Phys. **51** (1969) 4025.

[99] S.Chandra and J.Rolfe, Can.J.Phys. **48** (1970) 397.

[100] S.Chandra and J.Rolfe, Can.J.Phys. **48** (1970) 412.

[101] V.C.Nelson and R.J.Friauf, J.Phys.Chem.Solids. **31** (1970) 825.

[102] P.L.Read and E.Katz, Phys.Rev.Lett. 5 (1960) 466.

[103] Y.V.G.S.Murti and P.S.Prasad, Proc.Nuclear Physics and Solid State Physics Symposium (India), **17C** (1974) 67.

[104] T.M.Herrington and L.A.K.Stavely, J.Phys.Chem.Solids. 25 (1964) 921.

[105] D.Mapother, H.N.Crooks and R.J.Maurer, J.Chem.Phys. 18 (1950) 1231.

[106] D.Patterson, J.A.Morrison and G.S.Rose, Phil.Mag. 1 (1956) 393.

[107] G.Arai and J.G.Mullen, Phys.Rev. 143 (1966) 663.

[108] A.M.Karo and J.R.Hardy, Phys.Rev.B 3 (1971) 3418.

[109] H.Rabin and C.C.Klick, Phys.Rev. 117 (1960) 1005.

[110] N.L.Peterson and S.J.Rothman, Phys.Rev. 117 (1960) 1329.

[111] C.Bucci and R.Fieschi, Phys.Rev.Lett. 12 (1964) 16.

[112] C.Bucci, R.Fieschi and G.Guidi, Phys.Rev. 148 (1966) 816.

[113] T.Takamatsu and Fukada, Polym.J. 1 (1970) 101.

[114] J.Van Turnhout, Polym.J. 2 (1971) 173.

[115] R.A.Creswell and M.M.Perlman, J.Appl.Phys. 41 (1970) 2365.

[116] T.Nedetzka, M.Reichle, A.Mayer and H.Vogel, J.Phys.Chem. 74 (1970) 2652.

[117] B.T.Kolomietz, V.M.Lyubin and V.L.Averyamov, Mat.Res. Bull. 5 (1970) 655.

[118] P.R.Moran and D.E.Fields, J.Appl.Phys. 45 (1974) 3266.

[119] V.F.Zolotaryov, D.G.Semak and D.V.Chepur, Phys.Status Solidi. 21 (1967) 437.

[120] S.W.S.Mckeever and D.M.Hughes, J.Phys.D:Applied Physics. 8 (1975) 1520.

[121] C.A.Wert and R.M.Thomson, "Physics of Solids", McGraw-Hill, New York, 1970, p.393-6.

[122] J.T.Randall and M.H.F.Wilkins, Proc.Roy.Soc.A **184** (1945) 365.

[123] G.F.J.Garlick and A.F.Gibson, Proc.Phys.Soc. **60** (1948) 574.

[124] R.Capelletti and R.Fieschi, Ionic Thermoconductivity, 'A Method for the Study of the Temperature Dependent Ionic Polarisation in Condensed Matter' in "Electrets, Charge Storage and Transport in Dielectrics", M.M.Perlman (Ed.), The Electrochemical Society, Princeton, 1973.

[125] M.Campos, G.L.Ferreira and S.Mascarenhas, J.Electrochem. Soc. **115** (1968) 388.

[126] J.B.Goodenough, in "Phase Transitions", H.Henisch, R.Roy, and L.E.Cross (Ed.), Pergamon Press, New York, 1973.

[127] P.A.Fleury in "Phase Transitions", H.Henisch, R.Roy and L.E.Cross (Ed.), Pergamon Press, New York, 1973.

Chapter II

EXPERIMENTAL TECHNIQUES AND METHODS OF MEASUREMENTS

Abstract

The experimental techniques employed and methods of measurements used for carrying out the research work described in this thesis have been presented. The methods used to grow single crystals, the design and fabrication of a thin film vacuum coating unit, a metallic cell for low and high temperature electrical measurements, a low temperature photoacoustic cell for phase transition studies are also described in the present chapter.

2.1 INTRODUCTION

The experimental investigations presented in this thesis have been the result of an extensive and elaborate study on certain single crystals with the use of a number of sophisticated instruments and of a few experimental systems fabricated in the laboratory. A brief description of the various experimental techniques employed as well as the description of the experimental systems fabricated have been presented below. These experimental systems fabricated include:

(1) A high vacuum thin films coating unit for depositing metallic electrodes on to crystal surfaces, for the electrical measurements.

(2) A metallic cell which can be used for temperature variation studies of electrical properties from 80K to 450K under the vacuum conditions.

(3) A photoacoustic cell for phase transition studies in the temperature range 80K to 350K.

In addition, a brief description of the experimental procedures necessary for the study of the electrical and photoacoustic properties have also been given. Any variation from the experimental procedure required in the context of specific problem has been indicated at the appropriate places.

2.2 METHODS USED FOR CRYSTAL GROWTH

Although crystal growth has been a subject of absorbing interest for very many years, much of the recent development in both the understanding and the technology has been stimulated by increasing commercial importance of the subject. The spectacular growth of solid state electronics, so critically depends on the growth and perfection of single crystals. A host of techniques have been presently employed to grow single crystals. They include growth from solution, growth from melt, growth from vapour, flux growth, epitaxial growth, and high pressure growth etc. In this thesis most of the specimens used for the electrical and photoacoustic studies were grown from solution or from melt.

2.2.1 Growth from solution

Single crystal specimens used for the electrical and photoacoustic measurements were grown from solution by slow evaporation at constant temperature. A saturated solution of the material in an appropriate solvent is used for this process. When the solution becomes super saturated the crystal will start to grow in solution. Materials which melt incongruently, decompose before melting or undergo a phase transformation between melting point and room temperature were grown using this technique. Depending on the nature of the solvent used,solution

growth technique has been classified into aqueous solution, molten salt (flux), metallic solution and hydrothermal growth. In the present studies only the aqueous solution technique has been used. For this we have used a constant temperature water bath having a stability of ±0.01°C in the temperature range 30-50°C. Fairly large single crystals of $(NH_4)_3H(SO_4)_2$, $(NH_4)_2HPO_4$, $NH_4H_2PO_4$, $(NH_4)_2Cr_2O_7$, $NaClO_3$ and $NaNO_3$ were grown using this technique.

Doped specimens were grown from solution by adding appropriate amount of dopants into the pure solution. For example, SO_4^{2-} doped specimen of diammonium hydrogen phosphate were grown from solution by adding specific amount of $(NH_4)_2SO_4$ into the solution containing the pure diammonium hydrogen phosphate material.

From the preparation of deuterated specimen, the process of repeated recrystallisation has been used. In the present investigation the deuterated specimens of triammonium hydrogen disulphate were grown from a saturated solution obtained using heavy water of isotopic purity $\geq$ 99.8%. The presence of deuterium in the specimens used for the investigation of electrical properties has been verified by taking the infrared spectrum of these samples using an IR spectrometer (IR20).

2.2.2 Growth from melt

This method is suitable for materials that do not decompose before melting. Growth from melt is by far the fastest of the growth methods, as its rate does not depend on the mass transport process. The most common melt growth methods are

1. Bridgman,
2. Czochralski, and
3. Zone melting.

Out of these methods, we have used only the Bridgman technique to grow single crystals of pure and doped $NaClO_3$ and $NaNO_3$. Bridgman technique [1] is commonly used for growing single crystals for which volume change associated with solidification is not large. In this technique, the crystal is grown through self-seeding in contrast with the Czochralski's technique [2] where an external seed of suitable orientation is used for the starting of the growth process. In a basic Bridgman arrangement, the tappered ampule is lowered through the natural temperature gradient of a single zone furnace. The lowering rate of the ampule is controlled by a reduction gear assembly which is driven by a D.C. motor. (A photograph of the Bridgman furnace and the reduction gear assembly is shown in figure 2.2a). By

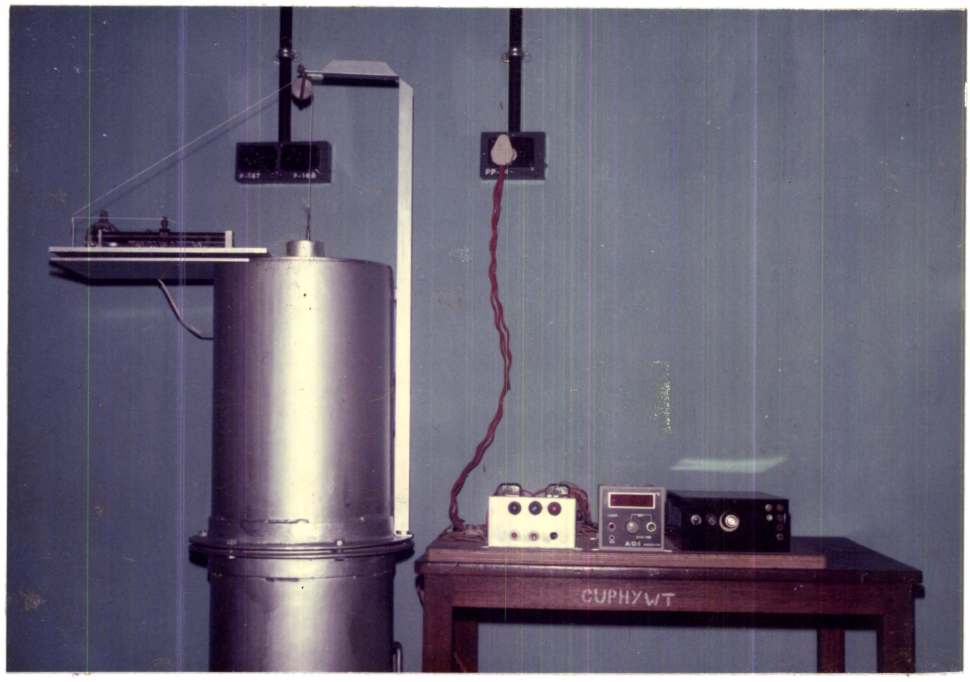

Figure 2.2a. Photograph of the Bridgman unit and the reduction gear assembly.

controlling the speed of rotation of the D.C.motor the rate of lowering can be adjusted. Using this system it is possible to get lowering rates ranging from 4 to 20 mm/h for the growth of single crystals.

2.3 PREPARATION OF SAMPLES FOR ELECTRICAL MEASUREMENTS

The starting material used for the preparation of pure single crystals were obtained after five times recrystallization of the analar grade material using triply distilled water. Large single crystals grown from solution or melt with good transparent nature were selected for the electrical and photoacoustic investigations. Samples of typical sizes 5x5x1 mm^3 were obtained by cutting slices from large single crystals and polishing with zero grade emery and ground glass. The polished faces of the specimens coated with silver conducting paint or vacuum evaporated electrodes were used for the electrical measurements. It is found that vacuum evaporated electrodes could give better electrical contacts, compared to that of silver paint. Hence, a vacuum system is designed and fabricated in the laboratory for this purpose. A brief description of this vacuum system for depositing metallic films on to crystal surfaces is presented.

2.4 VACUUM SYSTEM FOR THE DEPOSITION OF THIN FILM ELECTRODES

The metal electrodes for the electrical contact between the specimen and the electrodes were deposited by the vacuum evaporation technique. The vacuum system consists of a 4 inch oil diffusion pump (without the liquid nitrogen trap) and a baffle valve connected in series to a chrome plated circular base plate of diameter 14 inch suspended on a 1mx0.5mx1m MS frame. A 200 l/m rotatary vacuum pump was used as the backing pump. Figure 2.4a shows schematic diagram of the vacuum system for the electrode deposition. The base plate used was provided with 12 side feed-throughs for various electrical connections. A 12 inch glass bell jar placed over this base plate provided the vacuum chamber. Within this vacuum the filament holders and crystal holders, are mounted. The high current feed-throughs for the resistive heating were designed and constructed in the laboratory. Pressure down to 10^{-3} torr was measured with a pirani gauge and the pressure below this range can be monitored using a Penning gauge. A 200A step down transformer is used for the resistive heating of the vapour source for the depositing films. The various controls, and high current meters and the indicators were fitted on the front panel. A photograph of the vacuum evaporation unit fabricated for metallic coatings is shown in figure 2.4b.

2.5 METALLIC CELL FOR ELECTRICAL MEASUREMENTS

A schematic diagram of the variable temperature cell

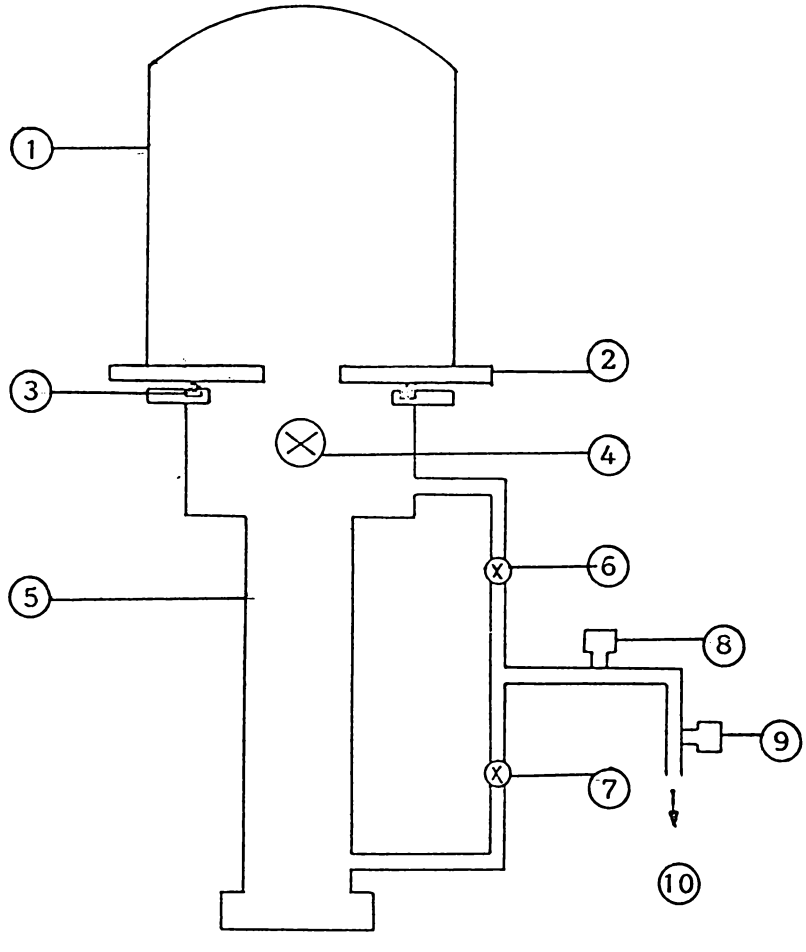

1. Glass dome
2. Base plate
3. Neoprine O-ring
4. Baffle valve
5. Diffusion pump
6. Roughing valve
7. Backing valve
8. Pirani gauge
9. Air admittance valve
10. Rotary pump

Figure 2.4a. Schematic diagram of the vacuum system for electrode deposition.

Figure 2.4a. Photograph of the thin film coating unit for electrode deposition.

used for the study of electrical properties of solids is shown in figure 2.5a. A unique feature of this design is that this cell can be used for temperature variation studies from 80K to 450K without disrupting the vacuum. Another advantage of this design is that, this cell can be used for measuring the electrical conductivity, dielectric constant, and thermally stimulated polarization and thermally stimulated depolarization measurements without affecting the vacuum conditions. Depending on the nature of information wanted and material used, different types of cell designs have been already reported in the literature [3-9]. The cell consists of an MS cylinder whose ends are permanently fixed with MS flanges. These flanges were provided with O-ring grooves for vacuum sealings. This chamber is sealed by top and bottom covers using neoprene O-rings. The top cover carries insulated leads for various measurements.Four window ports are provided to the chamber for the following uses: (1) For coupling with the rotary pump for evacuating the chamber, (2) To see whether the specimen undergo any change with temperature, (3) To perform optical excitation, for TSC studies if required, and (4) To study reflection and transmission characteristics of the specimen if necessary.

The sample holder consist of a copper cylinder one side of which is made in the form of a rectangular block as shown in figure 2.5a. The other end of the cylinder is bored to a

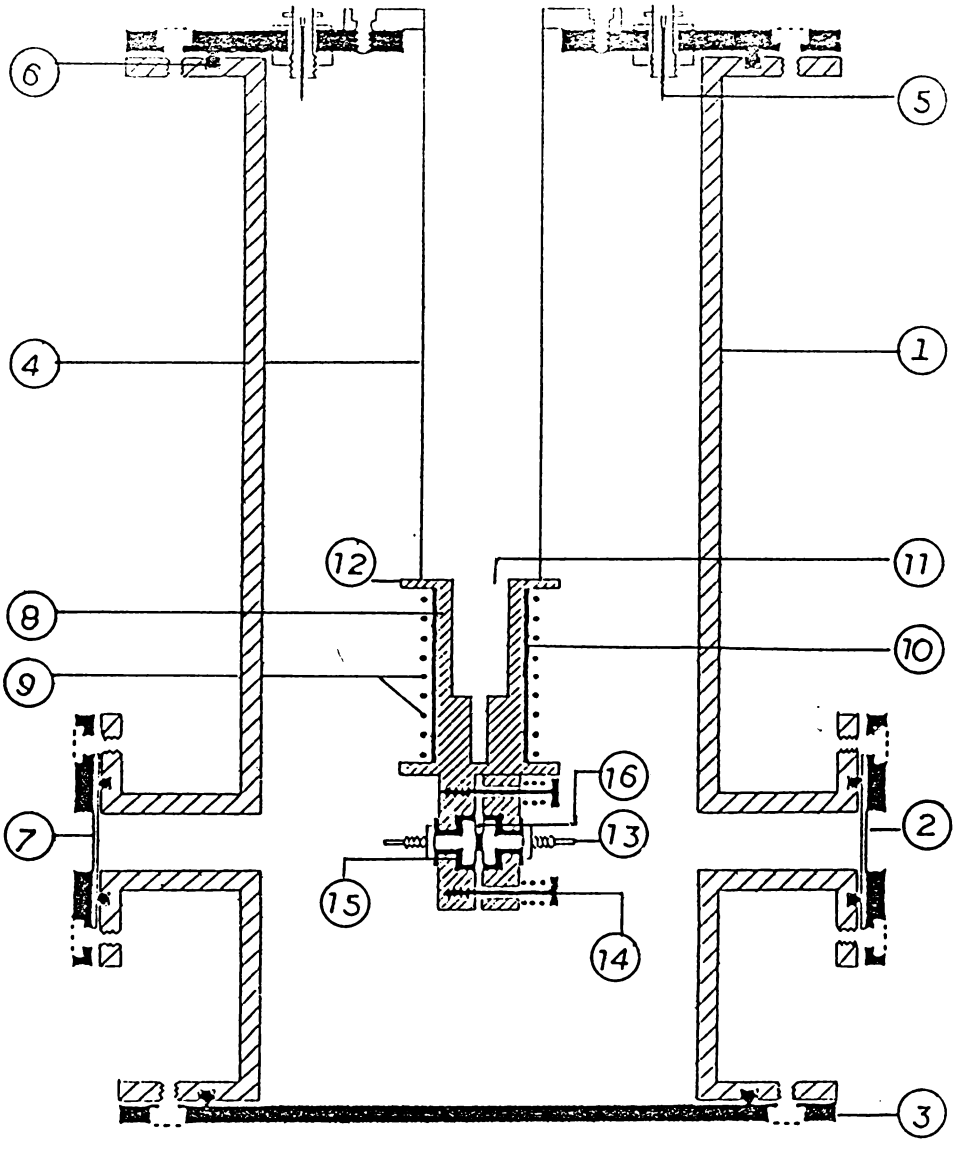

1. MS CHAMBER
2. GLASS WINDOW
3. MS FLANGE
4. SS PIPE
5. BNC
6. NEOPRINE O-RING
7. TO VACUUM PUMP
8. COPPER COLD FINGER
9. HEATER WINDINGS
10. MICA INSULATION
11. LN_2 CAVITY
12. SAMPLE HOLDER
13. COPPER ELECTRODES
14. SPRING LOADED SCREWS
15. TEFLON INSULATION
16. THERMOCOUPLE

Figure 2.5a. Schematic diagram of the temperature varying cell for the study of electrical properties.

depth such that the rectangular block is about 4 mm below the end of the bore. The outer portion of the drilled end is shaped in a suitable way to accommodate the heater windings as shown in figure 2.5a. The rectangular block is provided with teflon insulated copper electrode of certain diameter at its centre. Another movable copper block of the same dimension fixed with teflon insulated copper electrode of a smaller diameter serves the purpose of the second electrode. The second rectangular block is fixed through spring loaded screws such that the centres of the two electrodes are in a common axis. Screws are provided to the permanently fixed block to hold the thermocouples for the temperature measurements. The tip of the thermocouples are placed in thermal contact with larger electrode and they are electrically insulated using a thin mica sheet. The top end of the copper cylinder is silver brazed to a thin walled SS tube of the same diameter as that of the drilled cavity. This SS tube is permanently fixed to an MS flange forming the cold finger of the cell. This cold finger is inserted through top plate and is fixed on to this plate using O-ring and Allen screws. The length of the SS tube is adjusted such that the geometrical centre of the copper electrodes are in a line with the axis of the windows. The electrical connections for thermocouples and heater are made through teflon insulations fixed on the top plate of the chamber. Two BNC connectors are provided for electrical connections to the specimen.

The major advantages of this cell with the above design are the following:

1. The cell can be used in the temperature range 80K to 450K without disturbing the vacuum conditions.

2. The cell can be used for in situ measurements of quenched samples.

3. The cell can be used for electrical measurements at very low pressure upto 1 μ torr.

4. The liquid nitrogen consumption is found to be extremely low for a single cycle of operation.

5. The electrical properties like electrical conductivity, dielectric constant and thermally stimulated polarization and depolarization current measurements have been carried out using the same cell.

6. Major advantages of this cell design are its simplicity of construction and the favourite thermal characteristics.

2.6 METHODS OF MEASUREMENT

As mentioned in the previous chapter, a number of techniques can be employed for the study of phase transitions

in solids. Among these, the techniques employed to study the electrical properties at or near phase transition are very important in the sense that these techniques are used to characterise materials which in turn can be used for technological applications. In this context electrical properties like electrical conductivity, dielectric constant, thermally stimulated polarization and thermally stimulated depolarization currents will give extremely useful information in these materials for specific applications. A brief description of the techniques and the procedures for measuring these properties have been presented in the following discussion.

2.6.1 DC electrical conductivity

Generally in crystals containing ammonium groups, the magnitude of the conductivity is comparatively low at normal temperatures. At still lower temperatures, the magnitudes are expected to be much lower and hence low current measuring instruments have to be used for conductivity measurements. We have used electrometers (Keithley model 642 and 617) for measuring currents through the crystal. These instruments can be used for detecting currents as low as 10^{-15} A.

The dc conductivity measurements were carried out in a cell described previously. The specimen is inserted in between the spring loaded electrodes. A dc potential of the

order of 10-100V is applied across the specimen from dry batteries or from a highly stabilised power supply. (A highly stabilised dc power output ranging -100 to +100V in steps of 50 mV is available from Keithley 617 electrometer). The current through the crystal is monitored using an electrometer.By making use of the magnitude of the current, area, thickness of the specimen, and the biasing voltage, conductivity can be evaluated. A schematic diagram of the measurement of electrical conductivity is shown in figure 2.6a.

2.6.2 AC electrical conductivity

A schematic diagram of the measurement of ac electrical conductivity is shown in figure 2.6b. Alternating potential of 10-25 Vrms is applied across the specimen through a series resistance at a suitable frequency using an audio frequency oscillator and the voltage developed across the series resistance is measured using an ac microvoltmeter with a high input impedance. By knowing the magnitude of the series resistance and the voltage developed across the resistance, the current through the specimen is determined which can be used for the evaluation of ac electrical conductivity provided the area and the thickness of the specimen are known.

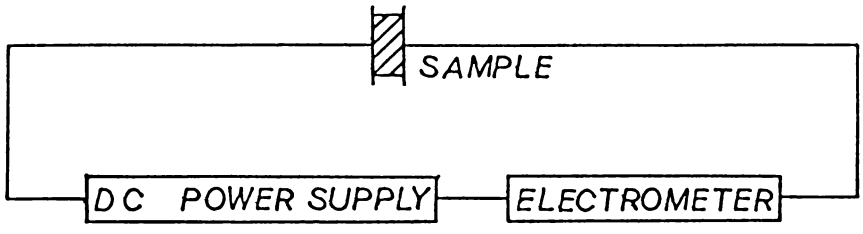

Figure 2.6a. Schematic diagram of the measurement of dc electrical conductivity.

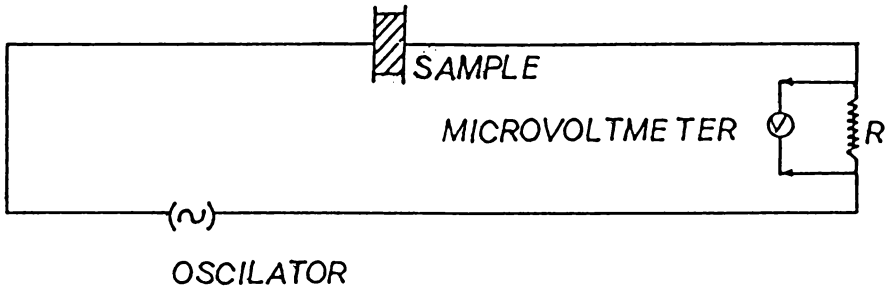

Figure 2.6b. Schematic diagram of the measurement of ac electrical conductivity.

2.6.3 Dielectric measurements

The dielectric constant of all the crystals studied here have been obtained by measuring the capacitance of a parallel plate condenser with the crystal sample as the dielectric. The main disadvantage of this technique is that it is very difficult to isolate the capacitance due to the dielectric alone from the measured capacitance as the total capacitance contains a component of lead and fringe capacitances. The conventional method generally employed to get the actual capacitance is to reset the capacitor assembly after removing the crystal to an air gap equal to the thickness of the crystal using a precision micrometer arrangement [10]. In the present investigation we have used the method suggested by Ramasastry and Syamasundara Rao [11] for accounting the effect of lead and fringe capacitances. The method relies upon measuring the total capacitance of a number of samples with varying A/d values (A being area and d, the thickness) and plotting a graph with A/d along x-axis and the measured capacitance along y-axis. A straight line will be obtained, and the intercept of this line will give the lead and fringe capacitances.

In the capacitance measurement we have used a direct reading LC meter (Vasavi Electronics VLC1) and a Digital LCR meter (Vasavi Electronics VLCR7). These instruments have the following advantages in the measurement of crystal capacitance.

1. The capacitance can be directly read from the meter without making repeated adjustments as in the case of a bridge. This enables one to take accurate readings even in the vicinity of the transition points of the crystals.

2. The conductivity of the test sample does not significantly interfere with the measurement of capacitance.

3. These instruments have maximum sensitivities of 0.05 pF for VLC1 and 0.1 pF for VLCR7 in the sensitive ranges.

The readings given by these instruments were counter-checked with a Hewlett Packard (Model 4277A) LCZ meter and it is found that they are highly reliable.

2.6.4 Thermally stimulated polarization and depolarization measurements

For the measurement of TSPC [12,13] the sample is initially cooled from room temperature (T_{RT}) to a low temperature (T_o) at which the relaxation time of I-V species is of the order of several hours and these species will be practically frozen in at random directions. Then the sample is subjected to a d.c. electric field (E_p) and with this field, the current through the specimen was monitored as a function of temperature by heating the specimen with a linear heating rate (β), and the resulting current is recorded.

On the other hand the procedure for the measurement of TSDC [13,14] consists of applying an electric field at a suitable temperature T_p for a finite time (t_p) at which the relaxation time is sufficient to polarize the I-V species at saturation. At this point, the specimen is cooled down to such a low temperature (T_o) that the relaxation time (τ) is very large. At $T = T_o$ the electric field is turned off and the short circuited current through the specimen was measured as a function of temperature by heating it at a linear heating rate (β). A schematic diagram of the comparison of TSPC and TSDC and the variation of various parameters like temperature, field and current as a function of time is shown in figure 2.6c.

A block diagram of the experimental set up used for the measurement of thermally stimulated polarization and thermally stimulated depolarization currents is shown in figure 2.6d.

The experimental set up used for the TSPC and TSDC measurements consists of a metallic cell (described previously) a low current measuring instrument (Keithley 642, 617), a home made temperature rate controller, a highly stabilised d.c. power supply and an X-Y recorder (Digital Electronics Series 2000). A photograph of the experimental set up used for the measurement of electrical properties has been shown in figure 2.6e.

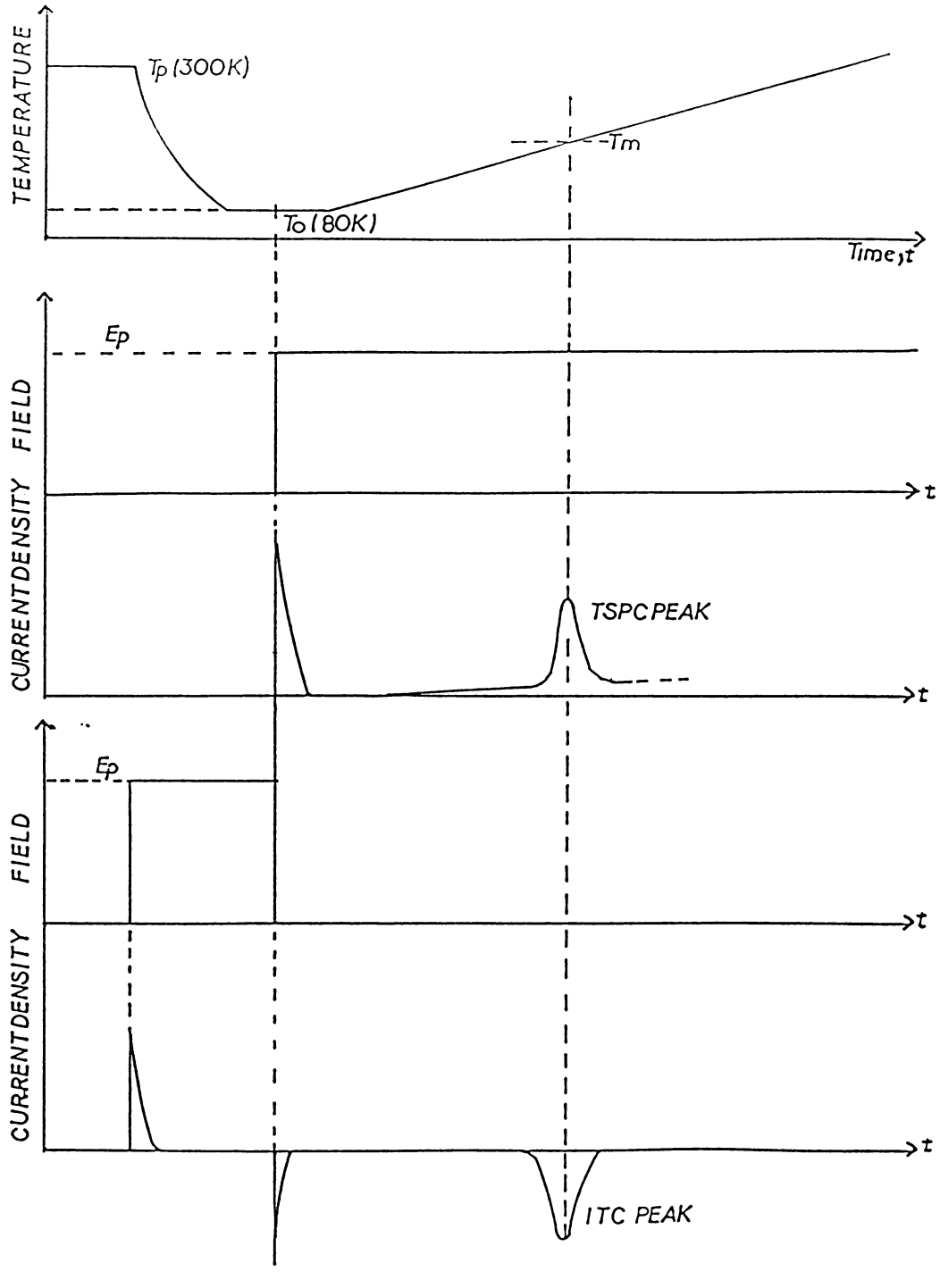

Figure 2.6c. Schematic diagram of the comparison of TSPC and TSDC measurements.

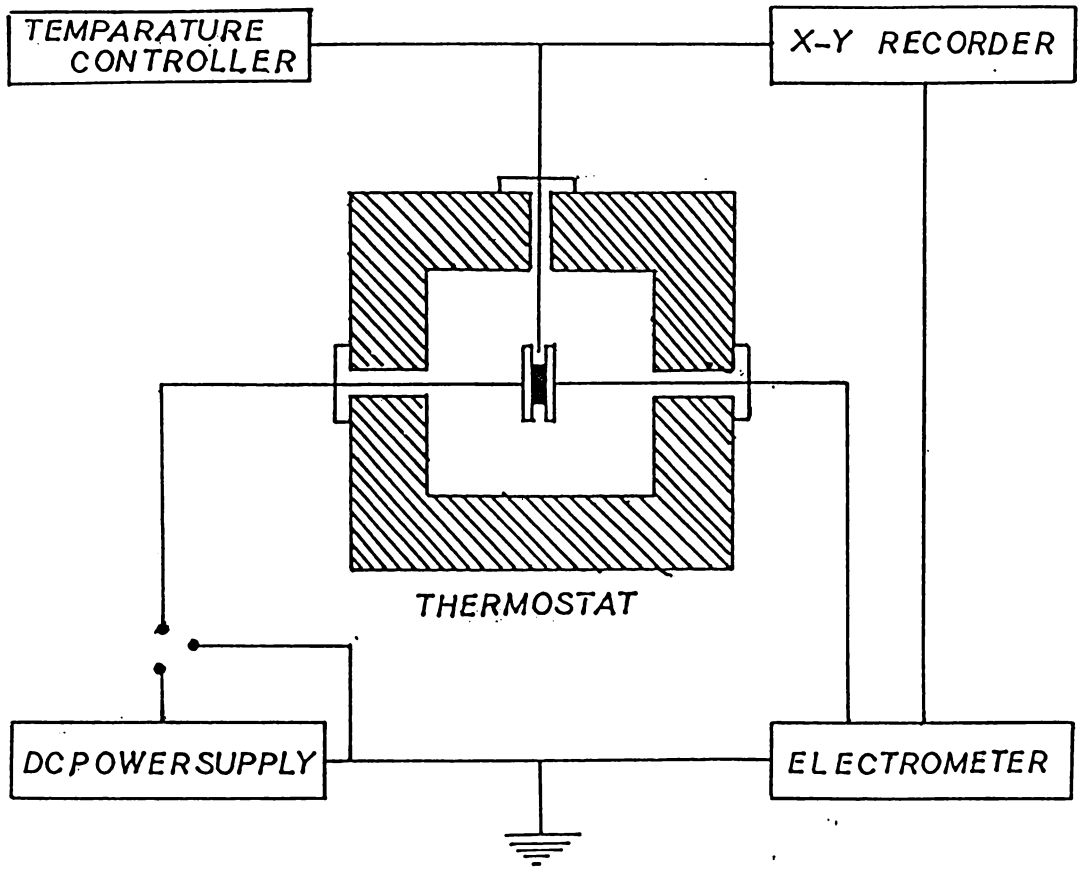

Figure 2.6d. Block diagram of the experimental set up used for the measurement of thermally stimulated polarization and depolarization currents.

2.7 Photoacoustic measurements

A block diagram of the experimental set up used for the photoacoustic studies of phase transitions in solids have been shown in figure 2.7a. The experimental set up has four parts.

1. A variable temperature photoacoustic cell with a sensitive microphone.

2. A light source.

3. A mechanical chopper for modulating the intensity of the light source.

4. A lock-in amplifier and an X-Y recorder for the detection and recording of the photoacoustic signal.

For the photoacoustic measurements, light from a 2 mW He-Ne laser (Spectra Physics) is focused on an electro-mechanical chopper (HMS light beam chopper model 230) and is then to a specially designed variable temperature photoacoustic cell (A detailed description of the cell will be given in Chapter VII) provided with a microphone (Knowles Model BT 1753). The chopped laser light falls on the specimen kept inside the cell. Then the amplitude and phase of the photoacoustic signal from the specimen are detected using a lock-in amplifier (EG & G

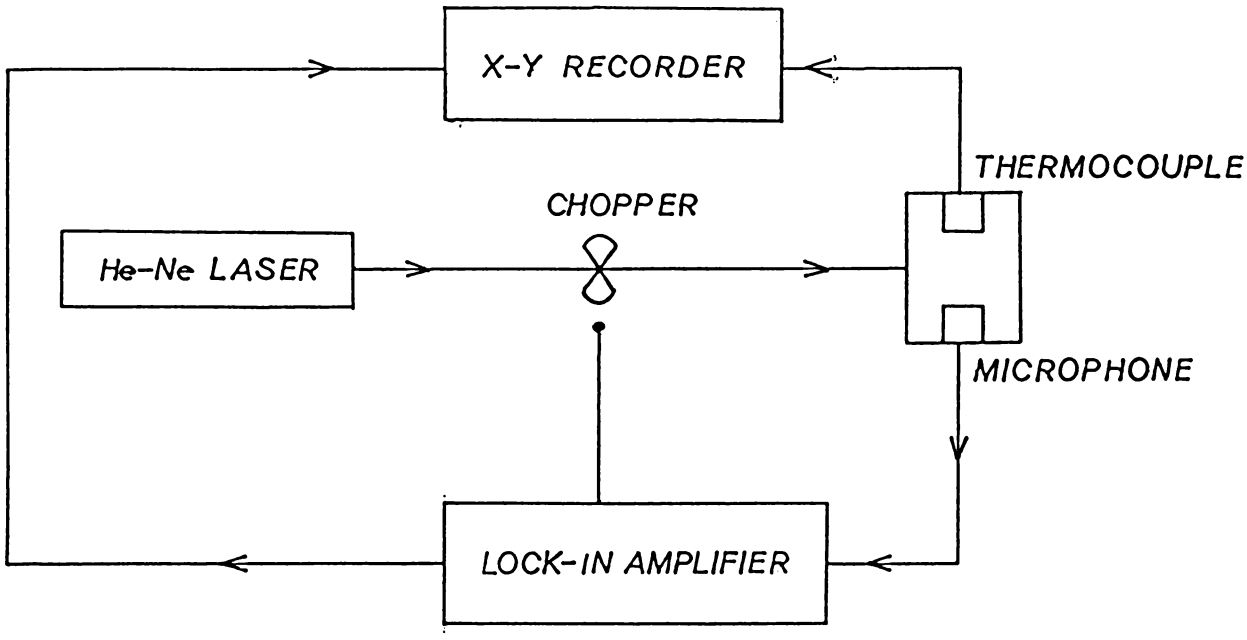

Figure 2.7a. Block diagram of the experimental set up used for the photoacoustic studies of phase transition.

PAR model 5204) and recorded (only amplitude) in an X-Y plotter. A photograph of the experimental set up is shown in figure 2.7b.

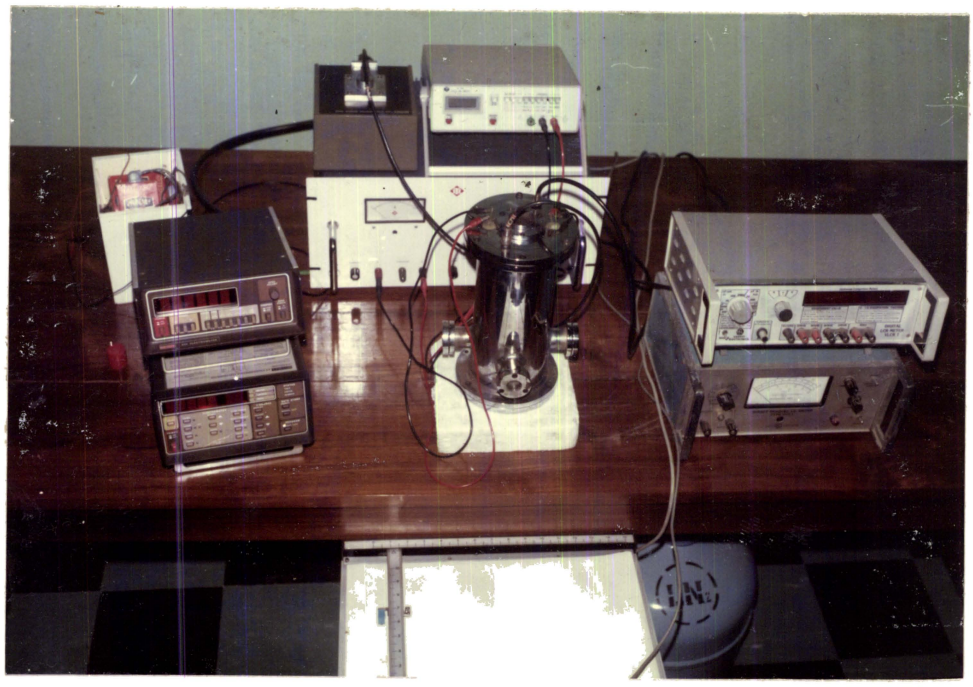

Figure 2.6e. Photograph of the experimental set up used for the measurement of electrical properties.

Figure 2.7b. Photograph of the experimental set up used for the photoacoustic study of phase transition.

2.8 REFERENCES

[1] R.A.Laudis, The Growth of Single Crystals, Prentice Hall Inc., Englewood Cliffs, New Jersey, 1970.

[2] J.Czochralski, Z.Phys.Chem. 92 (1971) 219.

[3] R.D.Gretz, Rev.Sci.Instrum. 38 (1967) 112.

[4] F.E.Card and J.J.Galen, Rev.Sci.Instrum. 32 (1961) 858.

[5] V.Kopane and V.E.Shubin, Instrum.Exp.Tech. 19 (1976) 1228.

[6] R.K.Chaudhary and L.Kishore, Cryogenics. 17 (1977) 419.

[7] H.Abachi, J.Molenat and P.Malbrunot, J.Phys.E:Sci.Instrum. 12 (1979) 706.

[8] H.Gobrecht and D.Hoffmann, J.Phys.Chem.Solids 27 (1966) 509.

[9] E.B.Podgovsak and P.R.Moran, Phys.Rev.B. 8 (1973) 3405.

[10] Annual Book of ASTM Standards 1975, Part No.40, Designation D 150-749 (Philadelphia, Pa-Am.Soc. for Testing Materials).

[11] C.Ramasastry and Y.Syamasundara Rao, J.Phys.E:Sci.Instrum. 12 (1979) 1023.

[12] S.W.S.Mckeever and D.M.Hughes, J.Phys.D:Applied Physics 8 (1975) 1520.

[13] G.Pfister and A.Abkowitz, J.Appl.Phys. **45** (1974) 1001.

[14] C.Bucci and R.Fieschi, Phys.Rev.Lett. **12** (1964) 16.

[15] C.Bucci, R.Fieschi and G.Guidi, Phys.Rev. **148** (1966) 816.

Chapter III

DC ELECTRICAL CONDUCTIVITY, DIELECTRIC CONSTANT AND PHASE TRANSITIONS IN PURE AND DEUTERATED $(NH_4)_3H(SO_4)_2$

Abstract

The results of dc electrical conductivity and dielectric constant measurements carried out in pure and deuterated single crystal specimens of triammonium hydrogen disulphate in the temperature range 30 to 180°C are presented in this chapter. The log σ vs $10^3/T$ plot shows Λ -shaped conductivity anomaly for pure sample at 140 and at 145.5°C for deuterated specimens. The dielectric constant data shows anomalous variations at 140 and 145°C respectively for pure and deuterated specimens. The mechanism of phase transition and of electrical conduction process in the two phases of this crystal are discussed in detail.

3.1 INTRODUCTION

At room temperature triammonium hydrogen disulphate (TAHDS) possesses monoclinic structure belonging to space group A2/a with 4 molecules per unit cell having dimensions $a = 10.153$ Å; $b = 5.854$ Å; $c = 15.140$ Å; and $\beta = 101.76°$ [1,2]. It has been reported that this material undergoes as many as five phase transitions accompanied with small dielectric anomalies at temperatures 140, -8, -132, -140 and -210°C [3,4]. The phases above liquid nitrogen temperature are found to be non-ferroelectric while that occurring below -210°C is a ferroelectric one [3]. Earlier, the detailed dielectric and differential thermal analysis of this material have been performed by Gesi [2] who observed three phase transitions at -8, -132 and -140°C respectively. He also noticed that the dielectric constant of TAHDS along the c^*-axis (i.e., perpendicular to the c-axis) shows breaks at -8 and -132°C while it shows a discontinuous change accompanied by a thermal hysteresis at 140°C. In addition to the above phase transitions this material also shows a broad peak for dielectric constant around -28°C [2]. Later, Gesi [5,6] found that this broad peak becomes more prominent, and this splits into two peaks as the pressure is increased beyond 4.9 bars. This pressure induced ferroelectric phase is considered to be the 6^{th} phase of TAHDS. The recently reported dc electrical conductivity measurements in pure and doped TAHDS single crystals along c^*-axis under vacuum conditions

(10^{-3} Torr) showed a conductivity anomaly at -26°C indicating the occurrence of a phase transition at this temperature. Osaka et al.[7] investigated the dielectric properties of deuterated samples of TAHDS, viz., $(ND_4)_3D(SO_4)_2$ at 1 atmospheric pressure in the temperature range between -170°C and 25°C and found that this material has two ferroelectric phases above liquid nitrogen temperature and shows a dielectric behaviour similar to that observed for normal TAHDS crystal under high pressure. This indicates a large isotopic effect on the ferroelectric activity of this remarkable crystal. However, further clarification of this effect of deuteration has been done by the same authors by investigating the dielectric properties of the deuterated analogue as a function of deuterium concentration [8], and it is concluded that the isotope effect on ferroelectric activity is very large and to some extent it is similar to the hydrostatic pressure effect on the ferroelectric property observed in the undeuterated crystal. It is found indirectly from the phase diagram of this system that, the normal crystal i.e., $(NH_4)_3H(SO_4)_2$ itself undergoes a ferroelectric phase transition at -210°C. In addition to the above mentioned investigations there exists DTA and coulometric studies [10] as well as infrared and Raman [11] and EPR studies [12] in this material. Eventhough Osaka et al. studied in detail the isotopic effect and dielectric properties as a function of temperature from liquid nitrogen to room temperature, no attempt has hitherto been made to study

the electrical properties particularly dielectric measurements of pure and deuterated TAHDS above room temperature. The present chapter describes the results obtained from dc electrical conductivity and dielectric constant measurements carried out in single crystals of pure and deuterated specimens of triammonium hydrogen disulphate in the temperature range from 30 to 180°C.

3.2 EXPERIMENTAL DETAILS

Single crystals of triammonium hydrogen disulphate were grown by slow evaporation of an aqueous solution containing 40 wt % $(NH_4)_2SO_4$ and 24 wt % H_2SO_4 at 30°C. The as grown crystals were of pseudohexagonal plates with predominant (001) faces. The specimens used for the measurement of dc electrical conductivity and dielectric constant were cut from large single crystals obtained after five recrystallisations using triply distilled water. Deuterated triammonium hydrogen disulphate (DTAHDS) specimens were prepared by repeated recrystallisation of TAHDS using heavy water of isotopic purity 99.8%. The concentration of deuterium in the deuterated specimens were verified by taking infrared spectrum of the samples after successive recrystallisations. It was observed that concentration of deuterium increases with recrystallisation process from heavy water solution and after five recrystallisations about 92% deuteration was acquired. Samples of typical sizes 5x5x1 mm^3 with their broad faces perpendicular to the (001) direction

coated with silver paint were used for the conductivity and dielectric constant measurements. The conductivity measurements were carried out by applying a steady voltage of 10-20V across the specimen and the resulting current was measured using electrometer (Keithley, model 617). Details of the sample holder, the chamber used for the temperature variation studies, the measurement of temperature etc. have been already described in chapter II. The dielectric measurements were carried out using direct reading LC meter, which has a resolution of 0.01 pf in the required ranges. The effect of lead and fringe capacitances were eliminated from the measurements using standard method [13]. To avoid surface conduction effects, the samples were annealed at 100°C for 3 hours in vacuum (10^{-3} Torr) before each measurement and all the measurements were carried out under the same vacuum conditions.

3.3 EXPERIMENTAL RESULTS

3.3.1 dc electrical conductivity

The temperature dependence of the dc electrical conductivity of single crystals of pure triammonium hydrogen disulphate is shown in figure 3.3a. Curves A and B in figure 3.3a show the variation of log σ with reciprocal of temperature for pure TAHDS single crystal along c^*-axis in the heating and cooling runs respectively. In both the heating and cooling runs TAHDS show two straight line regions characteristic of ionic crystals [14] with a well defined $\wedge$-shaped conductivity anomaly at 140°C and this evidently corresponds to a distinct

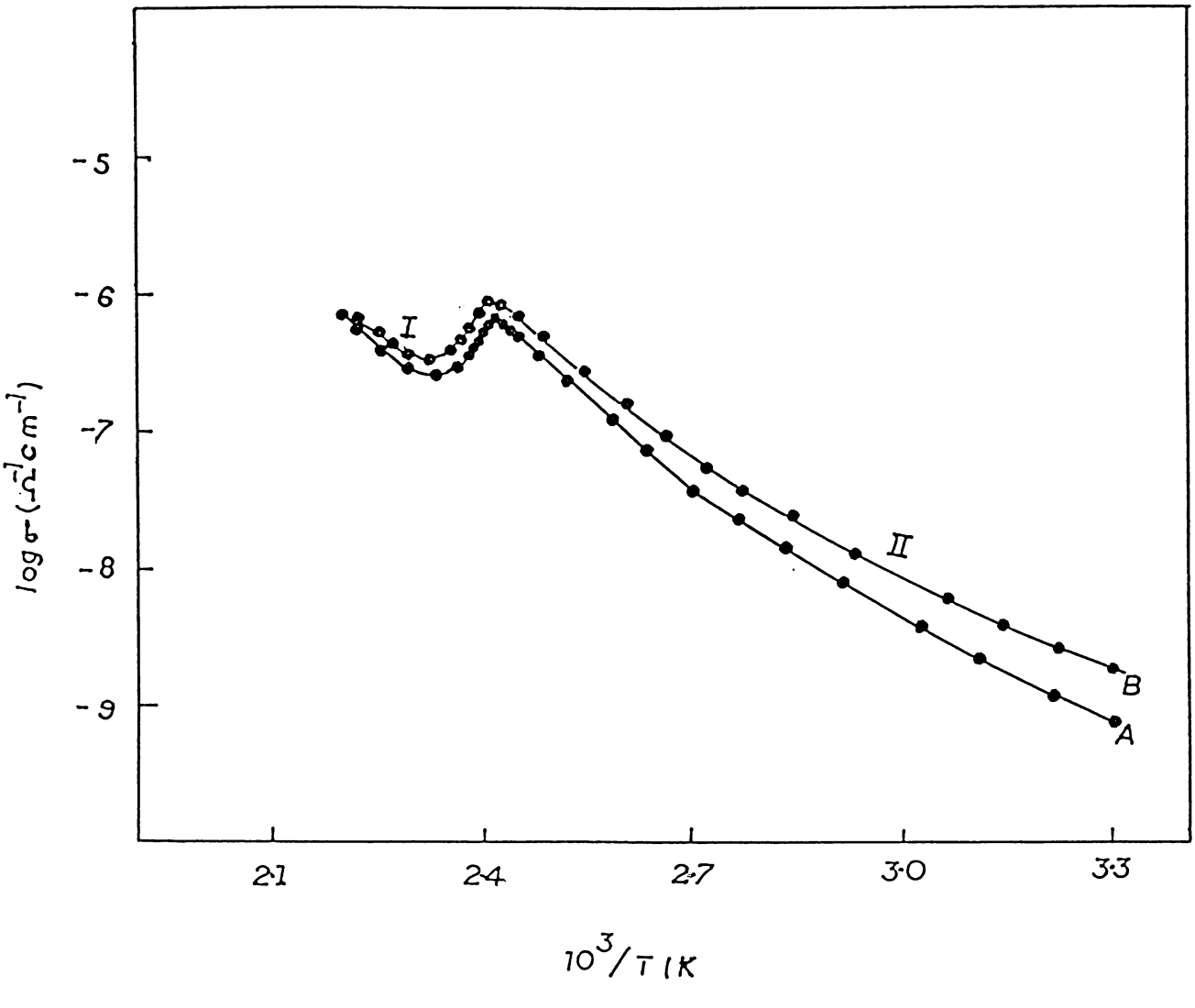

Figure 3.3a. Temperature dependence of dc electrical conductivity measurements of pure TAHDS single crystals (A) heating, (B) cooling.

phase transition occurring in this material. The corresponding two phases above and below the transition point can be denoted as I and II in the decreasing order of temperature. The transition at 140°C is found to be accompanied by a small thermal hysteresis of 2°C during heating and cooling cycles. The log σ vs $10^3/T$ plot for deuterated triammonium hydrogen disulphate (figure 3.3b) shows two distinct straight line regions but with Λ -shaped anomaly occurring at 145.5°C. Curves denoted by A and B in figure 3.3b show the variation of conductivity with temperature in the heating and cooling cycles respectively. Figure 3.3c shows the log σ vs $10^3/T$ plot for pure and deuterated triammonium hydrogen disulphate in the heating run. Clearly, the electrical conductivity in the deuterated specimen is lower by about one order of magnitude compared to that in pure TAHDS. The straight line regions for the pure and deuterated specimens can be represented by the following equations:

$$\sigma_I \text{ TAHDS} = 9.97\times10^8 \exp\left(\frac{-16442}{T}\right) \text{ohm}^{-1}\text{cm}^{-1} \qquad (3.1)$$

$$\sigma_{II} \text{ TAHDS} = 1.07\times10^2 \exp(-8101/T) \quad ,, \qquad (3.2)$$

$$\sigma_I \text{ DTAHDS} = 7.3\times10^9 \exp(-17507/T) \quad ,, \qquad (3.3)$$

$$\sigma_{II} \text{ DTAHDS} = 2.06\times10^2 \exp(-9043/T) \quad ,, \qquad (3.4)$$

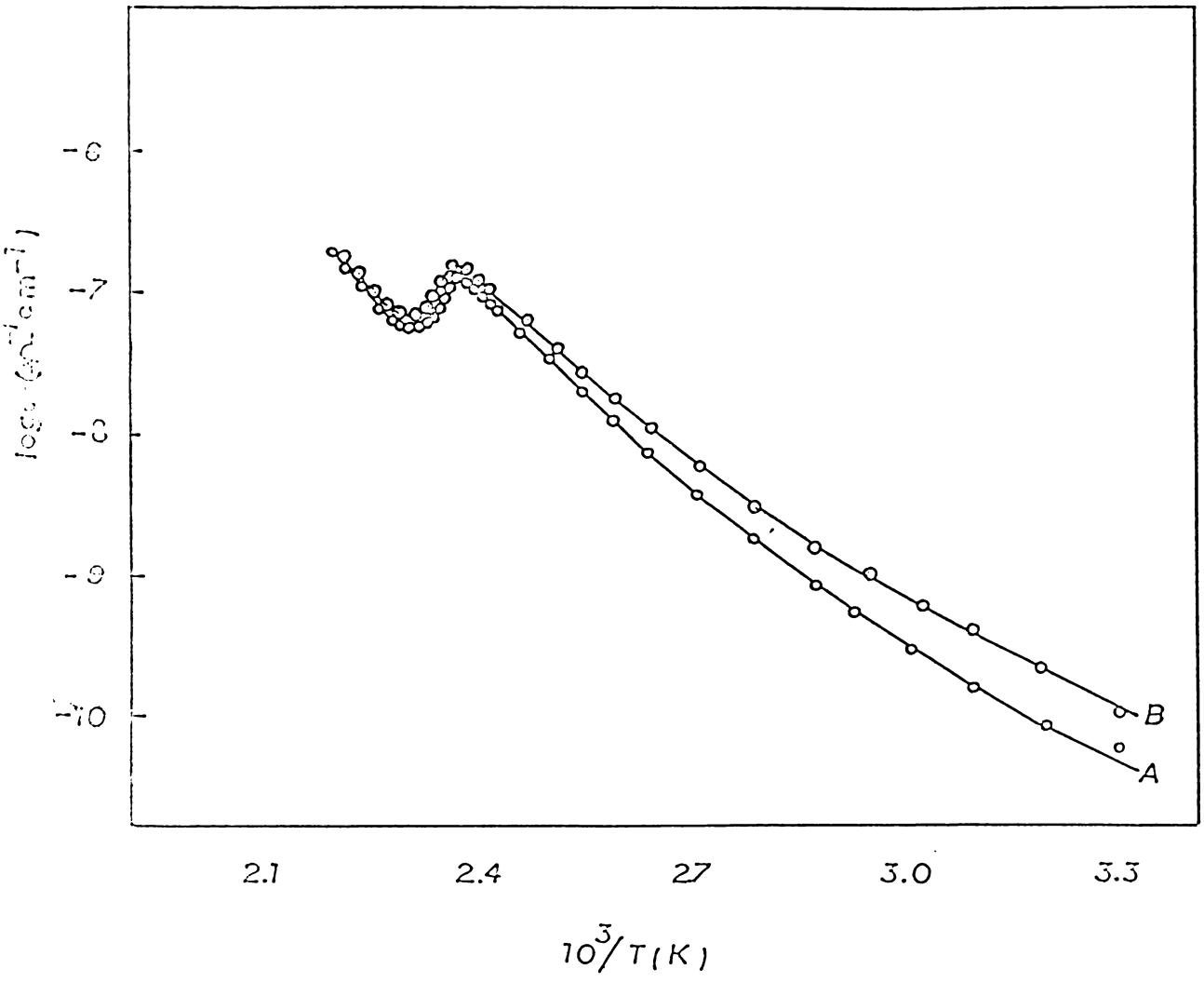

Figure 3.3b. Temperature dependence of dc electrical conductivity measure-meants of deuterated TAHDS single crystal. (A) heating, (B) cooling.

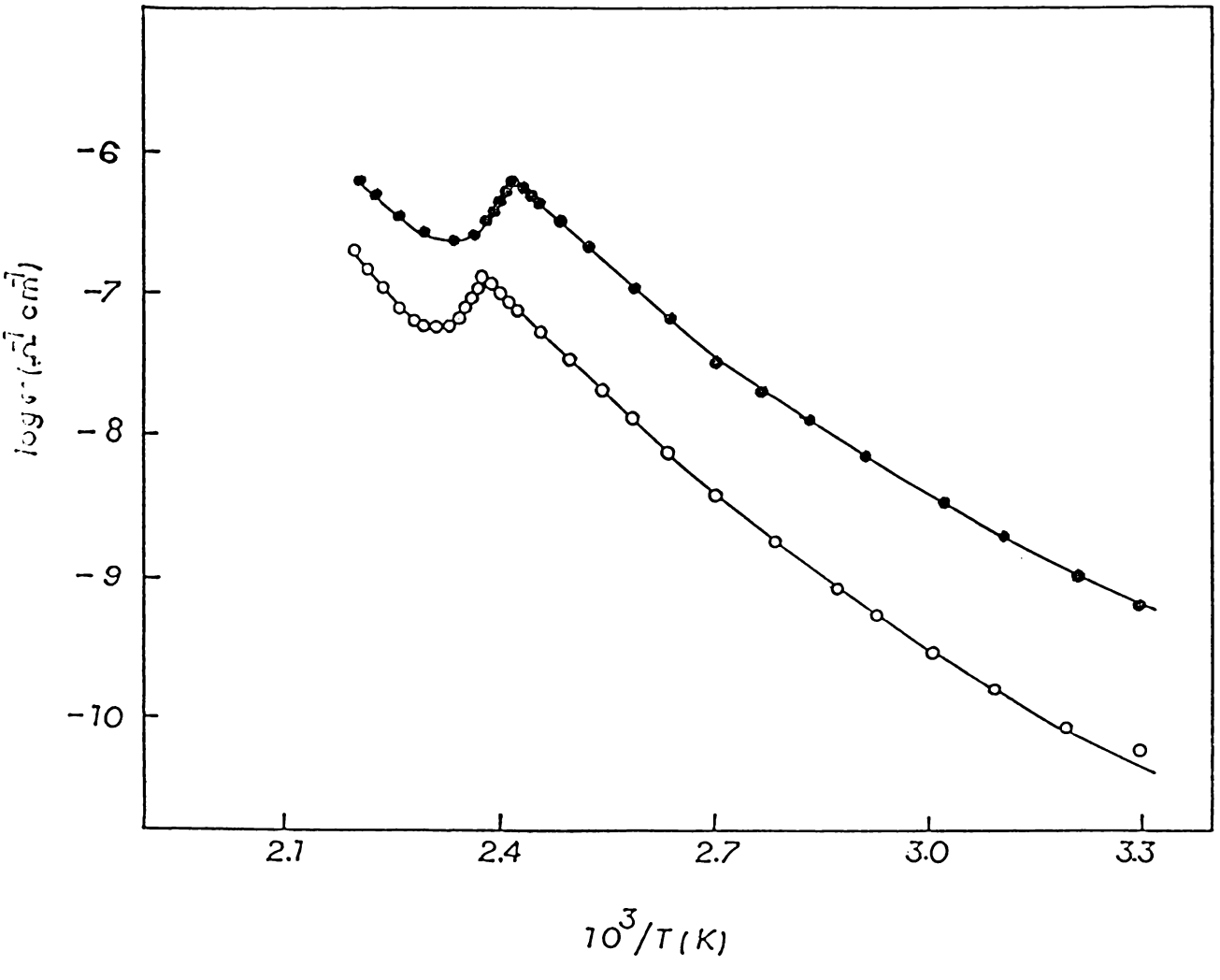

Figure 3.3c. log σ vs $10^3/T$ plot for pure and deuterated TAHDS crystals.

These equations yield activation energy values of 1.43 and 0.71 eV for TAHDS and 1.51 and 0.78 eV for DTAHDS respectively.

3.3.2 Dielectric measurements

The variation of dielectric constant ε_c as a function of temperature for pure and deuterated triammonium hydrogen disulphate measured at a frequency of 1 kHz is shown in figure 3.3d. Conductivity changes have not been found to interfere with dielectric measurements in any way at higher temperatures in this specimen. It is observed that as the temperature increases, the dielectric constant of TAHDS rises sharply at 140°C to a value of 1295 from its room temperature value of 22 and levels off beyond this temperature. On the cooling cycle the above change reverses with a thermal hysteresis of 8.5°C. In the case of deuterated TAHDS, the dielectric constant starts increasing abruptly at 145°C to a maximum value of 790 from its room temperature value of 25. The thermal hysteresis observed in this case is found to be 6°C.

3.4 DISCUSSION

Recent investigations carried out in a number of ammonium containing crystals viz., $(NH_4)_2SO_4$, $LiNH_4SO_4$, $NH_4H_2PO_4$ [15-19] show that electrical conductivity and dielectric constant measurements are very sensitive methods

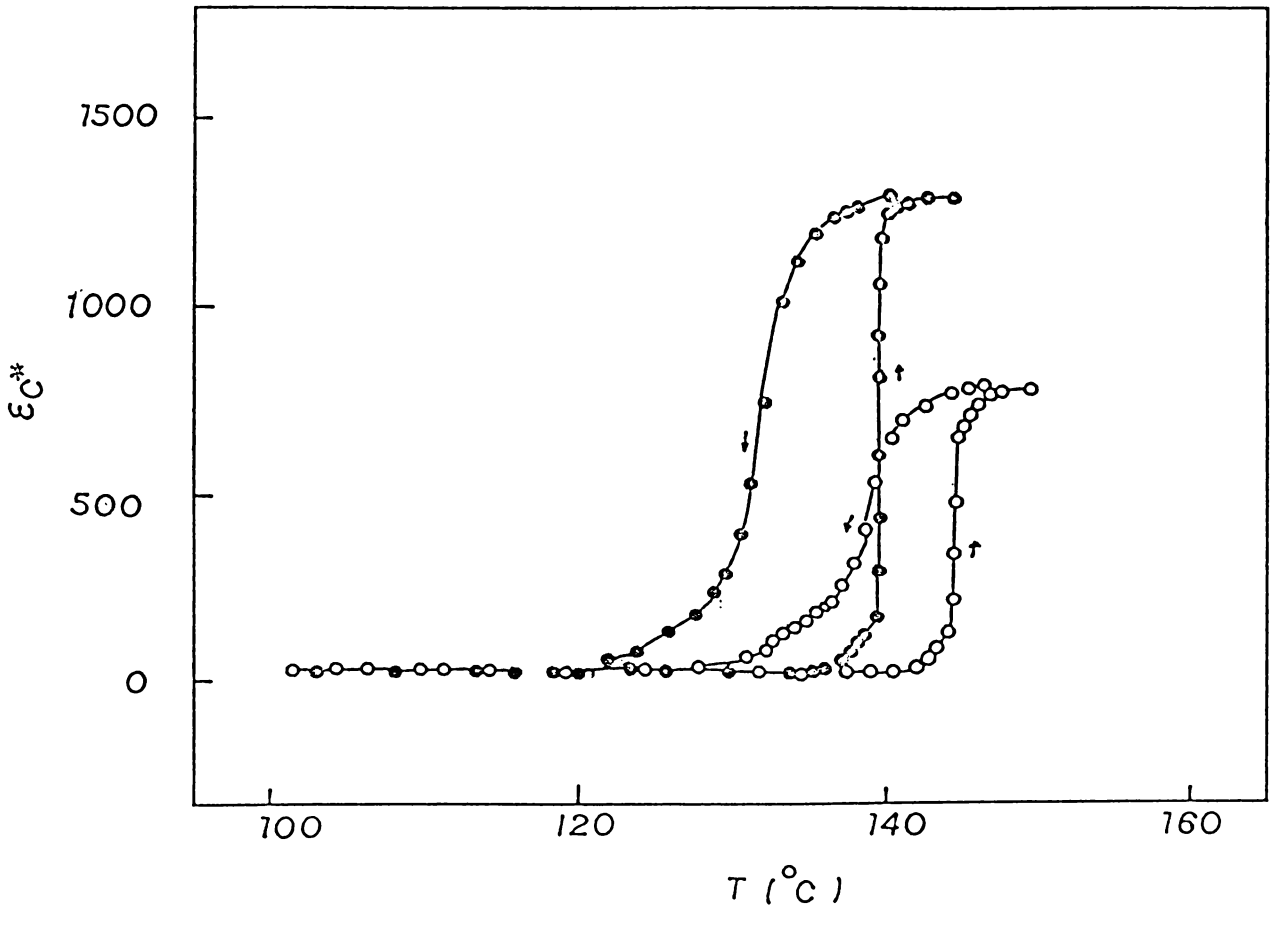

Figure 3.3d. Variation of dielectric constant ε_c^* as a function of temperature for pure and deuterated TAHDS.

for the detection of phase transitions in ferroelectrics containing NH_4^+ groups. In these materials the conductivity and dielectric constant have been found to show abrupt and anomalous variations with temperature at the transition points. Here the anomalous variations observed in pure and deuterated triammonium hydrogen disulphate from the two independent measurements of electrical conductivity and dielectric constant conclusively show that the pure material undergoes a phase transition at 140°C while the deuterated analogue has its transition temperature shifted to 145.5°C. Further, the thermal hysteresis observed in the dielectric and conductivity measurements of both pure and deuterated TAHDS confirm that this transition is a first order one as revealed by the earlier DTA results [10]. There exists complete agreement between the results obtained from conductivity and dielectric constant measurements in DTAHDS as far as the transition temperatures are concerned. The upward shift of the transition temperature by 5.5°C from conductivity measurements (5°C in the case of dielectric measurements) evidently shows the role played by the NH_4^+ groups in the mechanism of phase transition which may become fully disordered orientationally above the transition point.

In order to explain the electrical conduction mechanisms in the pure and deuterated TAHDS it is necessary to consider the electrical conduction mechanism generally operating

in NH_4^+ containing crystals. A number of mechanisms were suggested by various authors for the electrical conduction process in ionic crystals containing ammonium groups [14,17-23]. Usually in ionic crystals containing ammonium groups, the possible types of point defects are normal ionic and electronic defects and protonic defects. Of these electronic defects, electrons and holes are very small in number and hence, the contribution to the conductivity by these electronic defects can be neglected. Due to the finite sizes of NH_4^+ and HSO_4^- ions in TAHDS, the contribution to the electrical conduction process by these ions and their vacancies can also be neglected. The protonic defects associated with this material are of two category: the hydrogen ions and their vacancies belonging to NH_4^+ group and those associated with the HSO_4 group. The O-H bond is fairly strong and hence the H^+ in the HSO_4 group is not easily detachable. Thus the concentration of the former type of protonic defects is large compared to the latter and hence, it is concluded that the mechanism of electrical conduction in TAHDS single crystal is the migration of protons in the interstitial position from the NH_4 groups. The lower value of conductivity for the deuterated specimen in the whole temperature range is a direct evidence to show that the mechanism of electrical conductivity in this material is dominated by protonic conduction. In the present experiments,

the decrease in the value of conductivity obtained in the deuterated specimens is obviously due to the smaller mobility of the heavier deuterium ions compared with H^+ ions.

These experimental observations are completely in agreement with the earlier coulometric experiments suggesting that this material is a protonic conductor [10]. The activation energy values obtained from the straight line regions are in very good agreement with the values reported in other similar crystals exhibiting protonic conduction [17,19,23].

The activation energies in the case of DTAHDS is slightly higher than that obtained for the pure material. This observation is of some significance in that slight changes in the potential well might be occurring in the case of deuterated material. The vibrational amplitudes of the hydrogen atom in these substances are fairly large and hence, some anharmonic effects are likely to be observed in such materials. Since, the mass of deuterium is double that of hydrogen a substantial reduction in mean square amplitudes of vibration of these bonds must be taking place when hydrogen is substituted by deuterium. As a result, the average values of internuclear distances for the N-H and O-H bonds are likely to be slightly smaller compared with those in the case of TAHDS. Such changes in average bond lengths can cause changes in

the parameters of the potential wells to a smaller extent. The changes in the values of activation energies observed can thus be considered as a reflection of the slight rearrangements of the potential barriers encountered by the carriers due to the deuteration process.

The large dielectric constant obtained beyond the high temperature phase transition point sheds some light on the mechanism involved in this structural change. It is known that the HSO_4 group becomes partly free to reorient thus contributing significantly to the orientational part of the polarisability. The difference between the values of ε_c^* in the two cases can thus be attributed to the slight reduction on deuteration in the length of the hydrogen bonds and of N-H and O-H bond lengths as a result of the large anharmonic effects associated with the vibrations of these bonds [25].

3.5 CONCLUSIONS

1. Both dc electrical conductivity and dielectric constant measurements carried out in single crystals of pure triammonium hydrogen disulphate along the c^* axis show a Λ-shaped anomaly at 140°C, which corresponds to a phase transition occurring in this crystal at this temperature.

2. In the deuterated specimen the transition temperature is found to be raised by 5.5°C in the conductivity measurements and 5°C in the case of dielectric measurements.

3. The transition at 140°C is accompanied by a thermal hysteresis of 2°C in the conductivity and 8.5°C in the case of dielectric measurements during heating and cooling cycles whereas the transition observed in deuterated specimen shows a thermal hysteresis of 1°C and 6°C respectively in conductivity and dielectric measurements.

4. Except in the vicinity of the transition points the log σ_c^* vs $10^3/T$ plots show distinct straight line regions characteristic of ionic crystals.

5. The variation of conductivity with temperature both for pure and deuterated specimens in different phases are given by equations (3.1) to (3.4) yielding conduction activation energies 1.43 and 0.71 eV for pure TAHDS and 1.51 and 0.78 eV for DTAHDS.

6. The lower value of conductivity exhibited by deuterated specimens clearly shows that the mechanism of electrical conduction is dominated by protons.

7. The significant difference in the absolute magnitude of dielectric constant in pure and deuterated TAHDS is attributed to the slight reduction in lengths of the N-H and O-H bonds associated with the NH_4 and HSO_4 groups in the TAHDS as a result of deuteration.

3.6 REFERENCES

[1] B.Gossner, Z.Krist. 38 (1904) 110.

[2] S.Suzuki and Y.Makita,Acta.Crystallogr. B34 (1978) 732.

[3] K.Gesi, Phys.Status Solidi(a) 33 (1976) 479.

[4] K.Gesi, Jpn.J.Appl.Phys. 19 (1980) 1051.

[5] K.Gesi, J.Phys.Soc.Japan. 41 (1976) 1437.

[6] K.Gesi, J.Phys.Soc.Japan. 43 (1977) 1914.

[7] U.Syamaprasad and C.P.G.Vallabhan, J.Phys.C:Solid State Phys. 14 (1981) L571.

[8] T.Osaka, Y.Makita and K.Gesi, J.Phys.Soc.Japan. 43 (1977) 933.

[9] T.Osaka, Y.Makita and K.Gesi, J.Phys.Soc.Japan. 49 (1980) 593.

[10] A.Devender Reddy, S.G.Sathyanarayana and G.Sivaramasastry, Solid State Commun. 43 (1982) 937.

[11] .Kamoun, A.Lautie, F.Romain, A.Daoud and A.Novak, Dynamics of molecular crystals, Proceedings of the 41st International Meeting of Societe Francaise de Chimie, Divsonde Chimie Physique Grenoble, France 30 June-4 July 1986 (Amsterdam, Netherlands, Elsevier 1987) p.201-6.

[12] J.Minge and Waplak, Phys.Status Solidi(b). 123 (1984) 27.

[13] C.Ramasastry and Y.Syamasundara Rao, J.Phys.E:Sci.Instrum. 12 (1979) 1023.

[14] A.B.Lidiard, Handbuch der Physik. 20 (1957) 246.

[15] U.Syamaprasad and C.P.G.Vallabhan, Solid State Commun. 34 (1980) 899.

[16] U.Syamaprasad and C.P.G.Vallabhan, Nat.Acad.Sci.Lett. (India). 3 (1980) 364.

[17] U.Syamaprasad and C.P.G.Vallabhan, Nuclear Physics and Solid State Physics Symposium, IIT, New Delhi, Paper No. SLA 10 (1980).

[18] U.Syamaprasad and C.P.G.Vallabhan, Solid State Commun. 38 (1981) 555.

[19] V.K.Subhadra, U.Syamaprasad and C.P.G.Vallabhan, J.Appl. Phys. 54 (1983) 2593.

[20] T.M.Herrington and L.A.K.Stavely, J.Phys.Chem.Solids. 25 (1964) 921.

[21] F.A.Kroger, J.Chem.Phys. 51 (1969) 4025.

[22] Y.V.G.S.Murti and C.S.N.Murthy, J.Physique. 69 (1973) 337.

[23] Y.V.G.S.Murti and P.S.Prasad, Physica A.77 (1974) 543.

[24] Y.V.G.S.Murti and P.S.Prasad, Physica B.79 (1975) 243.

[25] R.Navil Kumar and C.P.G.Vallabhan, Phys.Status Solidi(a). (Communicated).

Chapter IV

DC/AC ELECTRICAL CONDUCTIVITY, DIELECTRIC CONSTANT AND PHASE TRANSITIONS IN $(NH_4)_2HPO_4$

Abstract

dc and ac electrical conductivity measurements carried out in single crystals of diammonium hydrogen phosphate along the c-axis show anomalous variations at 174, 246 and 416K. Low frequency dielectric constant also exhibits peaks exactly at these temperatures with a thermal hysteresis of 13°C for the peak at 416K. These specific features in electrical properties are entirely in agreement with earlier NMR second moment data and can be identified with three distinct phase transitions occurring in the crystal. The electrical conductivity values have been found to increase linearly with impurity concentration in specimens doped with specific amount of SO_4^{2-} ions. The mechanisms of phase transition and of electrical conduction process in the material are discussed in detail.

4.1 INTRODUCTION

A number of crystalline ammonium compounds undergo characteristic phase transitions resulting in drastic changes in a variety of physical properties as their temperature is changed. These physical properties have been extensively studied by various techniques like NMR, EPR, IR and Raman, Cold neutron scattering, Differential thermal analysis, Differential scanning calorimetry, Ultrasonic and X-ray diffraction. Measurement of electrical properties of such materials can also yield valuable information in relation to such phase transitions.

Diammonium hydrogen phosphate, $(NH_4)_2HPO_4$, (DAHP) is a very interesting crystal, belonging to the above category of materials. The previous investigations on this material include X-ray studies [1-4], Differential thermal analysis [5], NMR second moment calculations [6] and spin lattice relaxation time measurements [7]. The first attempt was due to Sherwin [5], who is reported to have used the DTA data in polycrystalline samples to show that this substance undergoes a crystalline transition near 418K. This transition temperature was found to be slightly influenced by the presence of water vapour and by repeated cycling through the transition, while it is little affected by the rate of heating and cooling. Later Coates and Smith [3] using X-ray powder diffraction technique determined the

high temperature structure as orthorhombic. They have also shown that the high temperature phase has 8 molecules per unit cell with 23% increase in density with respect to the low temperature phase. Watton et al. [6] using NMR proton second moment and spin lattice relaxation time measurements made with a coherent pulse spectrometer in powdered samples in the temperature range 77K to 430K suggested that the relatively high activation energies associated with the different motions of non-equivalent NH_4^+ ion groups can be attributed to hydrogen bonding between NH_4^+ groups and the surrounding nearest neighbouring oxygen atoms and that the unrealistically short interproton distance of 1.47Å as determined by X-ray diffraction may be due to the angular oscillations of the NH_4^+ groups. They also predicted that there is a possibility of the occurrence of a structural phase transition between 295 and 170K. Since, the results obtained at 215K are in agreement with the structure at room temperature, this temperature range could be limited to the region between 295 and 215K. All these previous investigations were restricted to polycrystalline or powdered samples. No attempt has so far been made to study any of the electrical properties of DAHP. In this chapter a detailed investigation of this aspect is carried out on single crystals of pure and SO_4^{2-} DAHP. We have also confirmed and accurately fixed the transition point of the previously indicated high temperature phase

transition using dc and ac electrical conductivity as well as dielectric constant data. These measurements have been extended to low temperatures to see whether this substance exhibits any phase transitions between 80K to 300K and consequently some quite interesting new results have been obtained in this region.

4.2 EXPERIMENTAL DETAILS

Single crystals of DAHP were grown by slow evaporation from an aqueous solution containing the compound (E Merck India). The material was further purified by repeated recrystallisation using triply distilled water. SO_4^{2-} doped samples were prepared by adding specific amount of $(NH_4)_2SO_4$ (between 0.02 to 0.1 mole %) into the solution. Samples of typical size 5x5x2 mm^3 were cut from large single crystals and the broad faces of the specimens coated with quick drying silver conducting paint. Details of the cryostat, sample holder and temperature measurement have been described in chapter II. For dc electrical conductivity measurements, a potential difference of 10-100V from dry batteries was applied across, the specimen kept under vacuum (10^{-3} Torr) conditions, and the resulting current was measured using Keithley model 642 electrometer. For ac conductivity measurements an LF oscillator of low output impedance was used to provide a sinusoidal voltage 10-25Vrms at 90 Hz across

the sample. An ac microvoltmeter of high input impedance along with an appropriate standard resistance was used for the current measurements. The dielectric measurements were carried out using a direct reading capacitance meter (Vasavi Electronics India, Model VLC1) and the lead and fringe capacitances were eliminated using the method of Ramasastry and Syamasundara Rao.

4.3 EXPERIMENTAL RESULTS

4.3.1 DC electrical conductivity measurements of pure and SO_4^{2-} doped diammonium hydrogen phosphate

The results of the dc electrical conductivity measurements carried out in pure and SO_4^{2-} doped single crystals of diammonium hydrogen phosphate in the temperature range from 80K to 423K are shown in figure 4.3a. The results were found to be very well reproducible for different samples. The $\log \sigma$ vs $10^3/T$ plot for pure and doped DAHP show prominent conductivity anomalies with distinct $\wedge$ -shaped peaks, one at 246K and the other at 416K. Another anomalous variation of much smaller magnitude occurs at 174K. The peak at 246K is an abrupt one and a very large variation in conductivity is observed on the low temperature side of this peak. It is found that the conductivity rise in this region covers about four orders of magnitude. On the other hand, the high

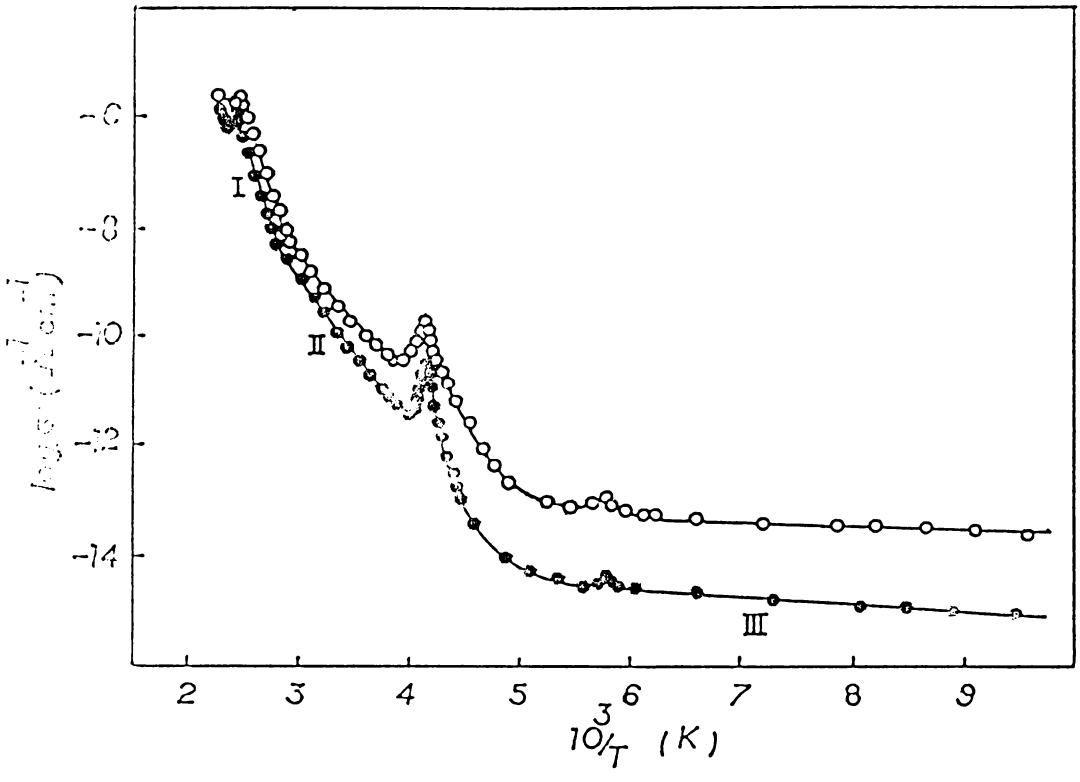

Figure 4.3a dc conductivity plots for DAHP along c-axis.

(i) pure DAHP.

(ii) SO_4^{2-} doped (0.1 mole %) DAHP.

temperature conductivity anomaly observed at 416K is confined to less than one order of magnitude. Below 416K the conductivity plots have three straight line regions designated by I, II and III (boundaries of the regions are specified elsewhere in the text) which are characteristic of ionic crystals. It is also found that in pure and doped DAHP crystals in dry nitrogen atmosphere, the magnitude of the conductivity in the respective samples are the same as those obtained under vacuum conditions.

In the low temperature range the conductivity for SO_4^{2-} doped specimens is found to be greater than that for undoped specimens. However, the temperature at which the anomalies occur are found to remain unshifted in the doped samples for the concentrations used here (0.02 to 0.1 mole %). In the high temperature regions the conductivity plots for both pure and doped samples merge together which indicates that the same mechanisms are operative in both materials.

A plot of σ vs SO_4^{2-} concentrations for the doped samples at 303K is shown in figure 4.3b. This gives a straight line, from which the mobility 'μ' of the defects created by the addition of SO_4^{2-} ions can be calculated using the equation $\frac{d\sigma}{dn} = e\mu$ where 'n' is the concentration of SO_4^{2-} defects yielding a value of $\mu = 1.27 \times 10^{-12} cm^2 V^{-1} sec^{-1}$.

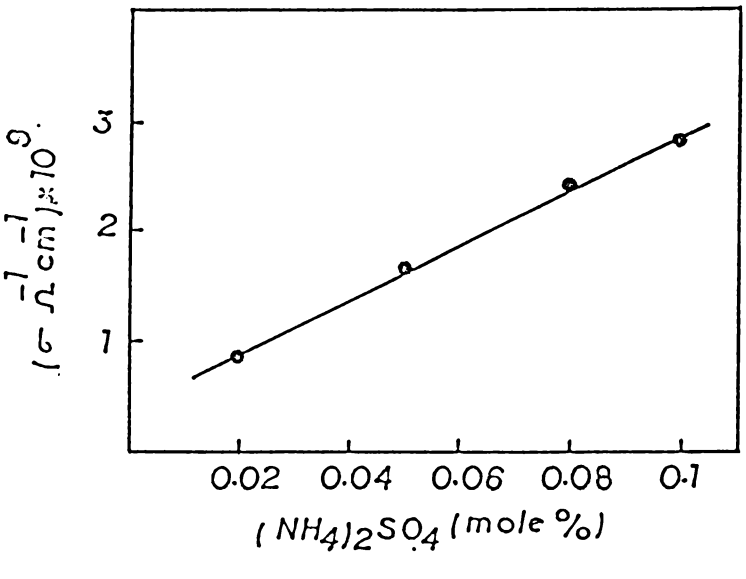

Figure 4.3b. dc conductivity vs concentration of SO_4^{2-} (in mole %) for DAHP.

Activation energy values calculated using the straight line regions of the conductivity plots are 1.48, 0.49 and 0.01 eV respectively for the regions I, II and III. These are quite close to the corresponding values (1.47, 0.46 and 0.01 eV) obtained for the SO_4^{2-} doped DAHP.

4.3.2 DC electrical conductivity measurements of pure and SO_4^{2-} doped diammonium hydrogen phosphate

The results of ac electrical conductivity measurements in pure and SO_4^{2-} doped specimens of DAHP are shown in figure 4.3c. It can be seen that the log σ vs $10^3/T$ plot shows three distinct variations at temperatures 174, 246 and 416K respectively in both pure and doped samples of DAHP. Here, the magnitude of the ac conductivity is far higher than the magnitude of the dc conductivity in both pure and doped samples. In this case also no appreciable change in conductivity results was observed, when the experiments were performed in the dry nitrogen atmosphere.

4.3.3 Dielectric measurements of pure diammonium hydrogen phosphate

The results of dielectric measurements carried out in DAHP single crystals at 1 KHz in the temperature range 80K to 303K are shown in figure 4.3d. While ε_c vs T curve

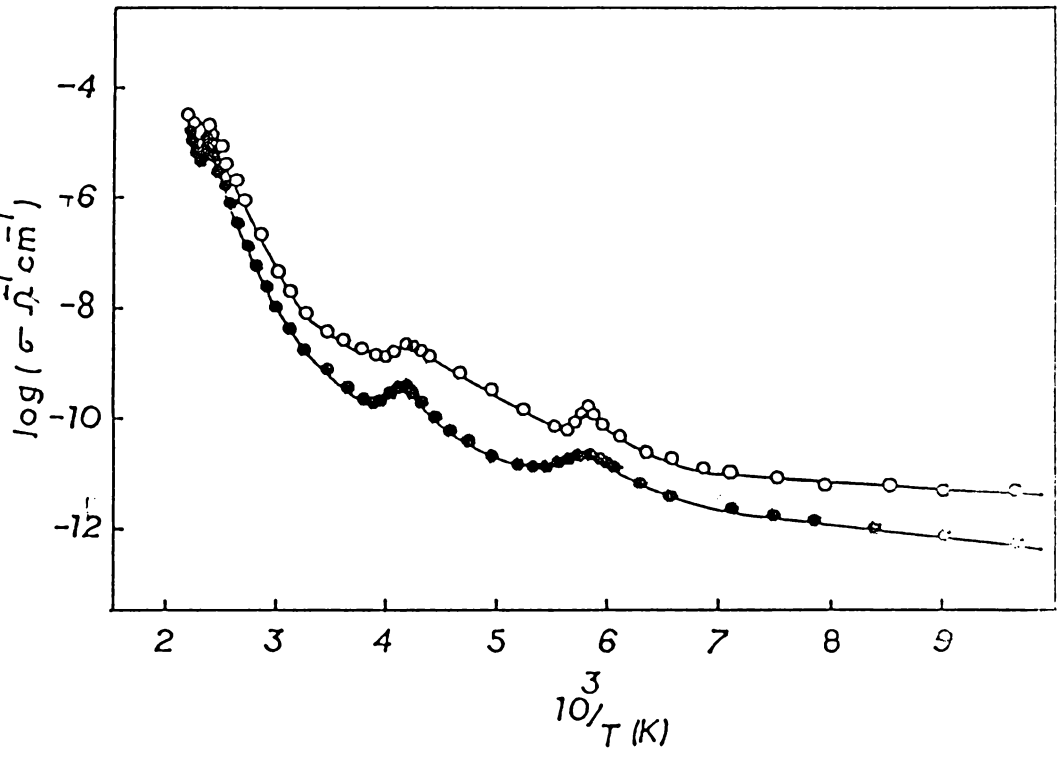

Figure 4.3c. ac electrical conductivity plots for DAHP along c-axis.

(i) —●—●—● pure DAHP

(ii) —○—○—○— SO_4^{2-} doped (0.1 mole %) DAHP.

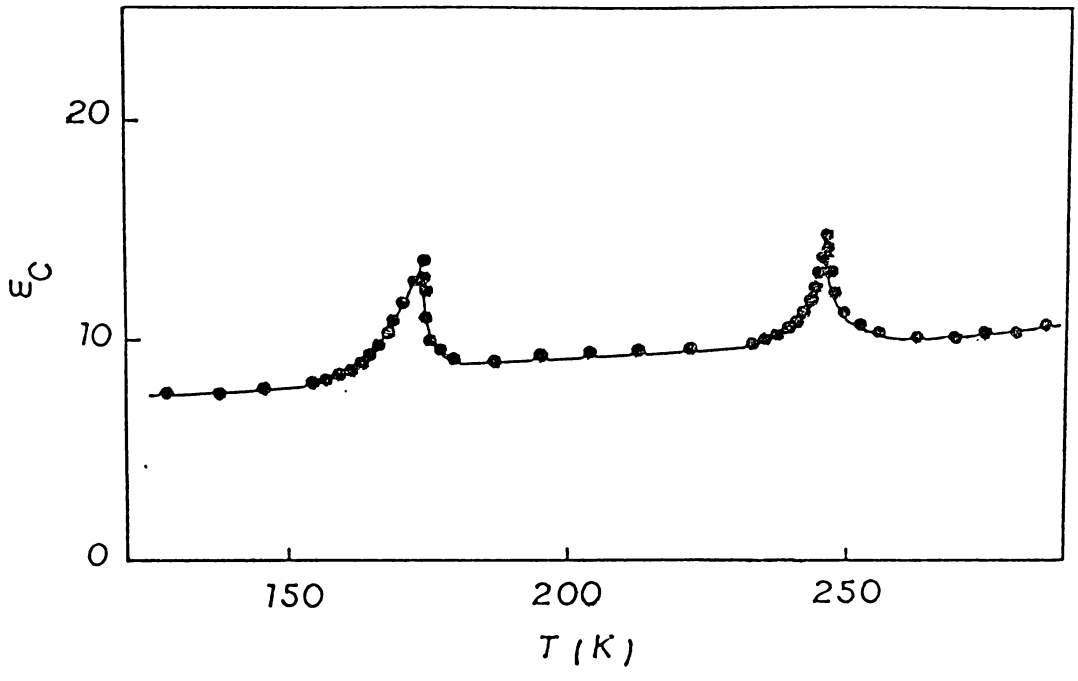

Figure 4.3d. ε_c vs. T plot for DAHP in the low temperature region.

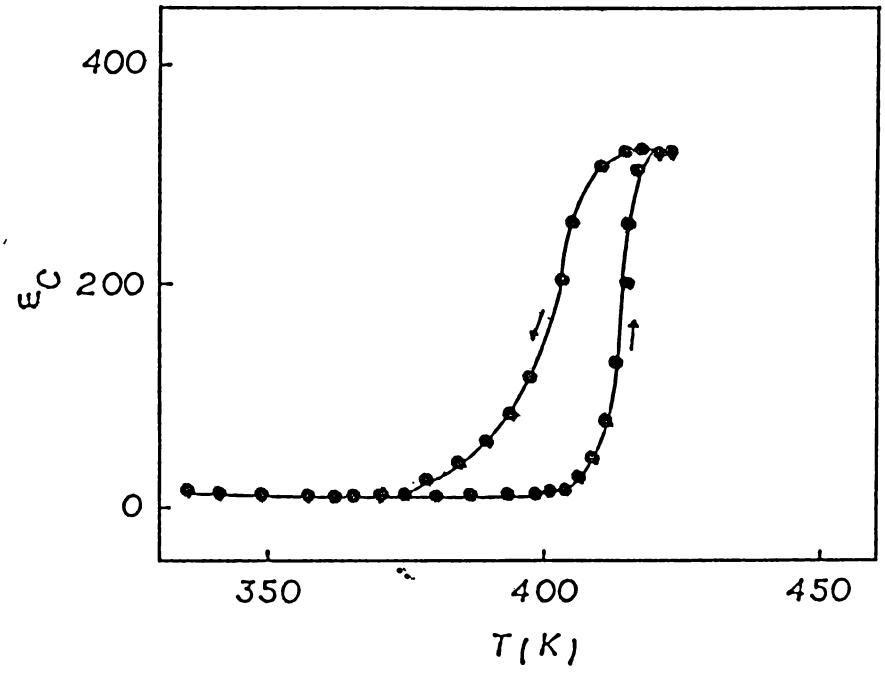

Figure 4.3e. ε_c vs T plot for DAHP in the high temperature region.

for the high temperature region (303 to 423K) is shown in figure 4.3e. The ε_c vs T plot gives abrupt variations exactly at the same temperatures where the conductivity anomalies occur viz., 174, 246 and 416K. The dielectric constant increases gradually and reaches a maximum of 13.6 at 174K and decreases thereafter as the temperature increases and again attains another maximum (14.5) giving a second peak at 246K. On further increase in temperature ε_c remains constant at the value of 10.6 upto 375K. As the temperature rises further, the dielectric constant changes abruptly from its steady value of 10.6 to 320 at 416K and then levels off beyond this temperature. On the cooling cycle the above change reverses with a thermal hysteresis of about 13°C. However, below room temperature no thermal hysteresis has been observed at 246K or 174K. For the doping concentrations employed here (0.02 to 0.1 mole %) the dielectric constant values observed for SO_4^{2-} doped samples are found to be virtually same as those obtained for pure DAHP and hence it is not shown in the figure.

4.4 DISCUSSION

Previous studies made on a series of ammonium containing crystals like $(NH_4)_2SO_4$ [8-10], $LiNH_4SO_4$ [11-14],

NH_4Cl [15], $(NH_4)_3H(SO_4)_2$ [15-17], $(NH_4)H_2PO_4$ [18] have unmistakably shown that anomalous variations in conductivity and dielectric constants of the type observed here are almost always associated with structural, orientational, or order disorder transitions occurring in these crystals at specific temperatures. In the results obtained here, there exists complete agreement between ac/dc electrical conductivity measurements and the dielectric constant data as far as the anomalous variations in these quantities are concerned. It is to be noted that proton second moment data [6] as a function of temperature also show clear variations near 246K and 174K whereas the relaxation time in the laboratory frame T_1 in $(NH_4)_2HPO_4$ clearly indicates a dip in the vicinity of 416K [6]. Thus experimental results obtained for single crystal samples of DAHP from the above independent measurements conclusively show that this substance undergoes three phase transitions at temperatures 416K, 246K and 174K respectively. The origin and mechanisms of these transitions can be understood by a detailed consideration of the structure of this compound.

At room temperature diammonium hydrogen phosphate forms colourless monocrystals with space group $p2_1/C$ having cell constants a = 11.043Å, b = 6.700Å, c = 8.043 Å, β = 113.42°

and Z = 4 [1,2] and is isomorphous to $(NH_4)_2HAsO_4$ [18]. It was suggested that the structure of DAHP consists of PO_4 and NH_4 tetrahedra connected by O-H....O and N-H....O bonds (as shown in figure 4.4a) which form infinite zig-zag chains parallel to the c-axis as shown in figure 4.4 b. In fact the structure of $(NH_4)_2HPO_4$ is determined to a large extent by these hydrogen bonds and their peculiarities. The length of these hydrogen bonds however, are not identical (H...O distances in N-H....O are 1.87, 2.07, 1.96 and 1.930Å for the first NH_4 group). The NH_4 tetrahedra in this material is slightly distorted even at room temperature as indicated by X-ray data [4]. The N-H-N angles deviate from normal tetrahedral values and they range from 105 to 115° at room temperature. It is likely that the extent of distortion of NH_4 tetrahedra is much larger at lower temperatures, where the lattice is found to be more rigid and all the hydrogen bonds are intact as suggested by the NMR investigation [6]. It is to be expected that this hydrogen bonding would become sufficiently weak at high temperatures to allow reorientations of the NH_4 group. Since the strength of these bonds are all different as indicated by their bond lengths a variety of reorientations can take place at different temperatures.

On increasing the temperature from 77K reorientations of NH_4 tetrahedra about two fold (C_2) and three fold

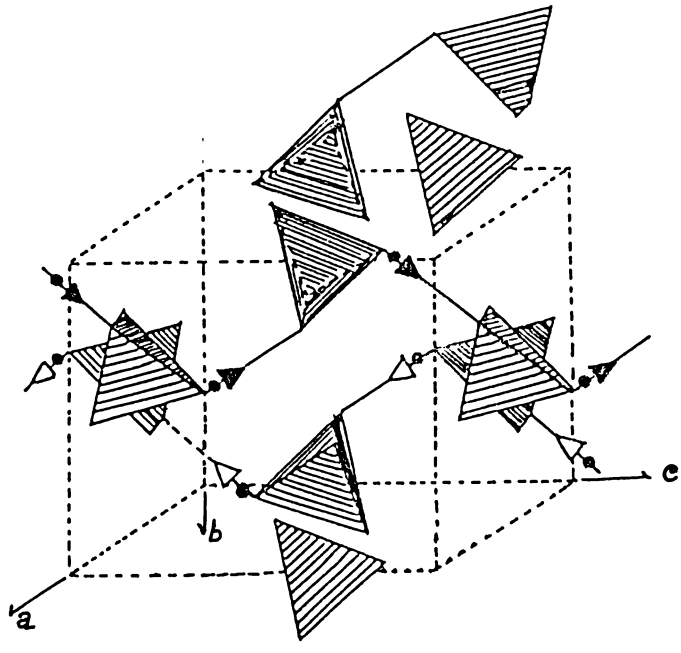

Figure 4.4a. The NH_4 and PO_4 tetrahedra connected by O-H.....O and N-H.....O bonds in diammonium hydrogen phosphate.

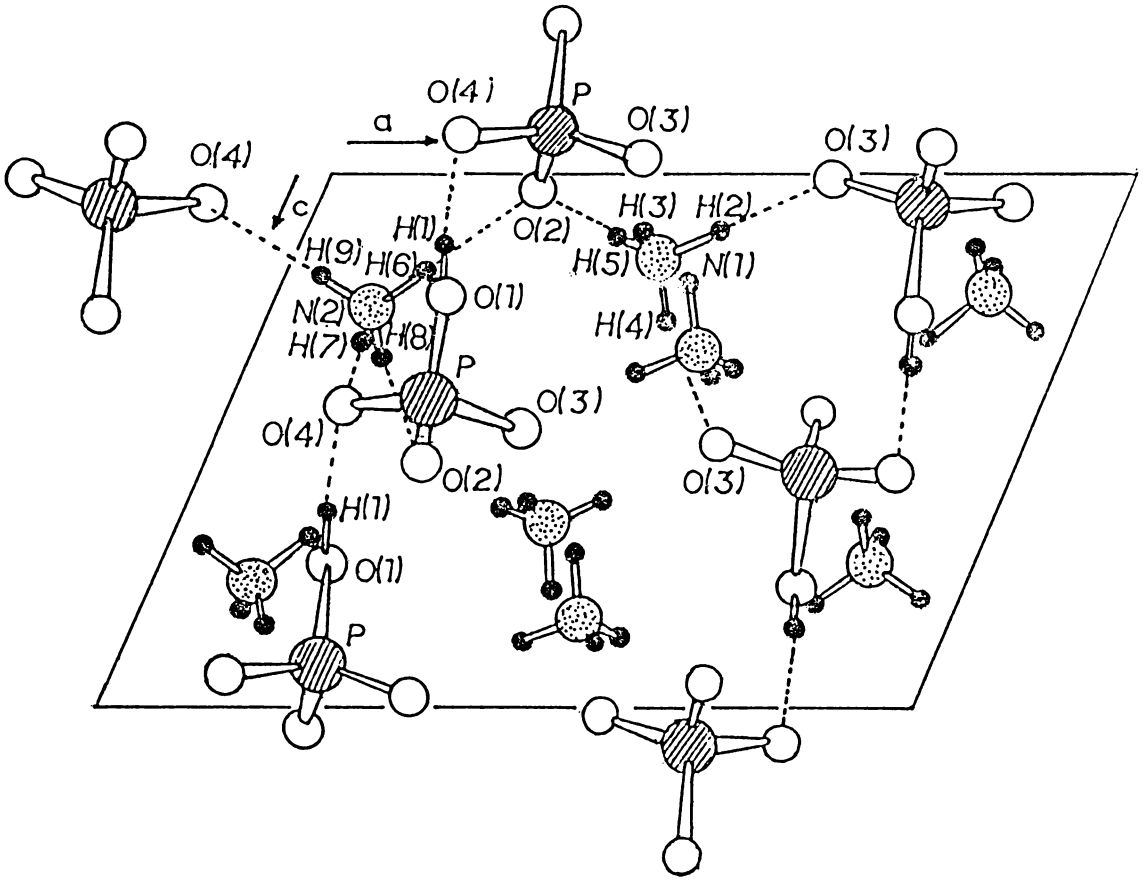

Figure 4.4b. Structure of diammonium hydrogen phosphate viewed along b-axis.

(C_3) as well as simultaneous reorientations about two independent two fold ($2C_2$) axes can take place depending on the magnitudes of the reorientational activation energies required for these changes. A satisfactory explanation for the observed experimental results from ac/dc conductivity and dielectric constant data can be obtained if we assume that the reorientation of NH_4^+ ions about the two fold axis is the cause for the transition at 174K, since it requires a comparatively lower activation energy for this type of rearrangement. The transitions observed at 246K can then be attributed to the reorientation about the three fold or simultaneous reorientation about two C_2 axes of the NH_4 tetrahedra in the crystal lattice. Thus one may conclude that NH_4^+ ions in this material undergoes sudden reorientations of different kinds at two different temperatures viz., 174K and 246K leading to the occurrence of two separate well defined transitions at low temperatures.

As the temperature of the specimen increases above room temperature the hydrogen bonds become progressively weaker and at 416K one may conclude that the hydrogen bonds associated with the ammonium tetrahedra are completely broken and the NH_4^+ ions which are assumed to be in a state of torsional oscillation now change over to a state of free rotation.

The onset of such free rotation can cause a significant change in the electrical conductivity as well as the dielectric constant at this temperature. Similar effects have been found to occur in a number of ammonium salts like $(NH_4)_2SO_4$, $NH_4H_2PO_4$ and $LiNH_4SO_4$. The present observations are in complete agreement with the earlier DTA measurements [5,6] except for a slight change in temperature from 418K to 416K. X-ray measurements [3] which also support our experimental data show that this substance undergoes a change of structure from monoclinic to orthorhombic with unit cell parameters a = 10.78, b = 14.46, c = 9.06Å at higher temperatures. Further, the variation of dielectric constant with temperature gives a clear thermal hysteresis of 13°C showing that this transition at 416K is a first order one.

To facilitate an understanding of conduction mechanism in pure and doped specimens of DAHP, a brief discussion of the peculiar features of PO_4 group in ammonium containing phosphates is required. The phosphate lattice is almost similar to that of ammonium dihydrogen phosphate, $NH_4H_2PO_4$ (shown in figure 4.4c) and potassium dihydrogen phosphate, KH_2PO_4 [20,21] with a difference that instead of two hydrogen atoms associated with PO_4 tetrahedra (H_2PO_4) only one hydrogen atom is incorporated in the present structure $(HPO_4)^{2-}$ and

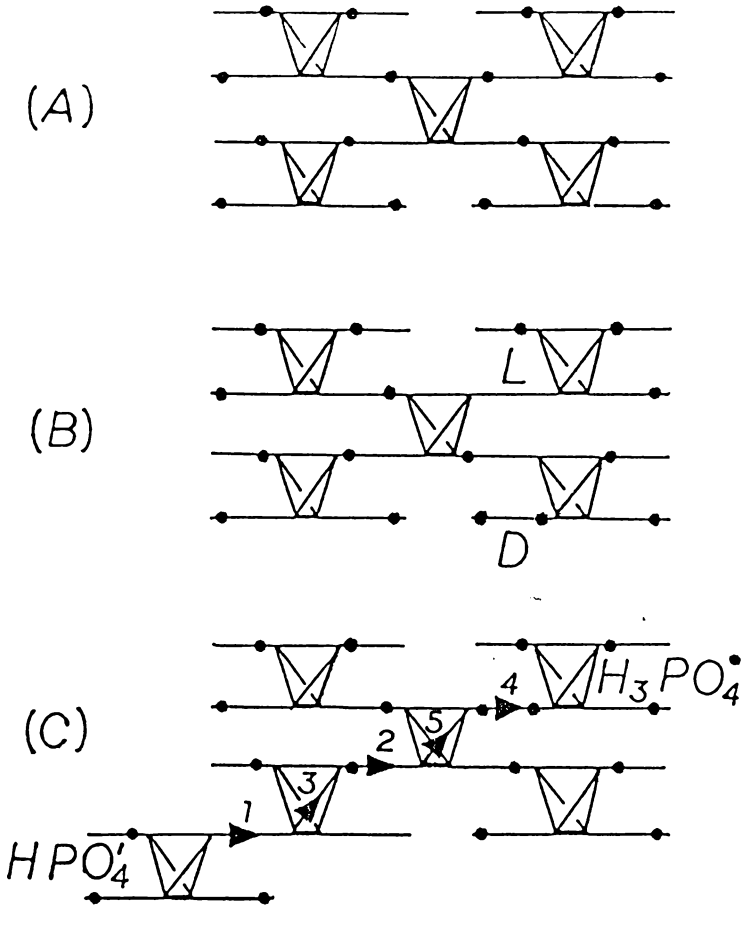

Figure 4.4c. Various types of defects observed in phosphate lattice.

(A) Ammonium dihydrogen phosphate lattice.

(B) L and D defects.

(C) Ionization defects.

as a result an open hydrogen bonded network (as shown in figure 4.4b) is formed to accommodate the cations (NH_4^+ ions) to preserve charge neutrality. Thus each hydrogen bonded network of the phosphate lattice on an average has only one position for its proton and it is located towards the end of the bond. However, configurations such as $H_2PO_4^{2-}$ or H_3PO_4 may be formed due to the transfer of a hydrogen ion from one HPO_4^{2-} group to the adjacent group or by the transfer of two hydrogen ions to an HPO_4^{2-} group. It is also possible for protons associated with the HPO_4^{2-} group to jump from one group to another along the same bond (intrabond jump) by a resonance tunnelling mechanism [22] which has been found to occur in ADP and KDP [23]. These processes are sometimes observed at fairly high temperatures resulting in the formation of such defects called ionisation defects.

Naturally it is possible for protons to jump from one bond to another bond on the same phosphate group (interbond jump) and as a result it leaves a hydrogen bond without a proton (this is known as the L-defect) as shown in figure 4.4c, or produces a bond with an H^+ in each of its proton positions. Such doubly occupied proton position is known as a D-defect [22,23]. Thus protons can migrate through the hydrogen bonded network by a series of interbond and intrabond jumps. Hence, electrical conduction in these

class of compounds can be attributed to the combined effect of individual motions of ionization defects and of L or D defects.

In addition to the above mentioned defects there exists what is known as protonic defects associated with the ammonium group which are also known as A-defects. It has been suggested that proton vacancies are generated in the NH_4 lattice by the incipient decomposition associated with the formation of NH_3 and H_3PO_4. This is mainly due to the breaking of the ammonium hydrogen bonds and the transfer of the proton directly to the neighbouring phosphate ion where it is held by electrostatic attraction [23]. This process occurs only at a much higher temperature.

Consideration of those phenomena occurring in the crystal can provide a satisfactory explanation of the electrical conduction which essentially is a defect controlled process. In the intrinsic region below the high temperature phase transition point (region 1, from T = 416K to 355K) the electrical conduction is mainly due to the generation of thermal defects as well as ionization defects. In this temperature range the transfer of protons from HPO_4^{2-} group occurs giving rise to PO_4^{3-} group. The equillibrium condition can be expressed as

$$HPO_4^{2-} \rightleftharpoons H^+ + PO_4^{3-}$$

This is in accordance with the prediction of Khan et al. [4] where it is suggested that oxygen atom O(I) in figure 4.4b associated with the HPO_4^{2-} acting as a donor in the only O-H....O bond in the structure is saturated and is not well qualified to act as an acceptor of a hydrogen bond. Thus it is quite likely that the conduction in this region is essentially due to the migration of these protons from the phosphate groups. The activation energy value of 1.48 eV obtained for pure DAHP (1.47 eV for SO_4^{2-} doped DAHP) in this temperature region is in very good agreement with those reported in the literature for similar crystals in which the mechanism of electrical conductivity is dominated by protonic conduction [15,16,18,24].

The region from T = 355K to T = 246K can be designated as region II. This is a region where impurity controlled conduction dominates over other conductivity mechanisms. This becomes clear from the effect of doping the crystal with SO_4^{2-} ions. The SO_4^{2-} ions in the lattice replace the PO_4^{3-} ions and a proton hole (L-defect) is created for charge compensation. Here, a corresponding increase in conductivity is expected. Indeed, as seen in figure 4.3b a linear increase in conductivity with SO_4^{2-} ions occurs as a result of generation of L-defects in the materials. The activation

energy of 0.46 eV for L defect mobility is in very good agreement with that observed in ADP and KDP (0.46 eV and 0.52 eV) crystals. Again the magnitude of mobility of these L defects generated by the doping of SO_4^{2-} in DAHP compares well with the values reported by several authors in other hydrogen containing phosphates [22,24,25]. In the temperature below 246K (region III, T = 174K to T = 100K) the small value of conductivity and activation energy observed could be due to the precipitation of the existing defects generated by the impurities or due to the freezing-in of defects generated by the impurity ions leading to a corresponding decrease in the number of mobile carriers.

The ac conductivity measured at 90 Hz is higher than the dc conductivity by more than one order of magnitude in the whole temperature range. The higher value is expected in this case because of the additional contribution of the polarisation component of the current. As a result the sharp change from intrinsic to extrinsic region is smeared out and the conductivity plots show much smoother variations with respect to temperature. At still lower frequencies, the conductivity plots do exhibit the distinct regions I, II and III as obtained in the case of dc measurements.

4.5 CONCLUSIONS

The electrical measurements carried out in single crystals of pure and SO_4^{2-} doped diammonium hydrogen phosphate lead to the following conclusions.

1. dc and ac electrical conductivity and dielectric constant measurements in single crystals of $(NH_4)_2HPO_4$ show anomalous variations at 174, 246 and 416K corresponding to three distinct phase transitions occurring in this crystal.

2. The experimental observations are found to be in good agreement with the earlier DTA and NMR second moment calculations.

3. The phase transition observed at 416K can be identified with the structural change indicated by X-ray measurements and it is of first order.

4. The transitions at 246 and 174K are attributed to the different reorientations of NH_4^+ groups in DAHP.

5. The activation energy and mobility for carriers in this material show that protonic conduction is the dominant mechanism responsible for the electrical conductivity of this material.

4.6 REFERENCES

[1] J.P.Smith, J.R.Lehr and W.E.Brown, Acta.Cryst. **10** (1957) 50.

[2] J.P.Smith, J.R.Lehr and W.E.Brown, Acta.Cryst. **10** (1957) 709.

[3] R.V.Coates and P.S.Smith, Acta.Cryst. 23 (1967) 504.

[4] A.A.Khan, M.E.Straumanis and W.J.James, Acta.Cryst. B28 (1972) 2065.

[5] K.A.Sherwin, J.Sci.Instrum. **41** (1964) 7.

[6] A.Watton, E.C.Reynhardt, H.C.Sandhu and H.E.Petch, J.Chem. Phys. 67 (1977) 887.

[7] F.Koksal, Z.Naturforsh. 36A (1981) 203.

[8] U.Syamaprasad and C.P.G.Vallabhan, J.Phys.C:Solid State Phys. 14 (1981) L865.

[9] U.Syamaprasad and C.P.G.Vallabhan, Solid State Commun. 38 (1981) 555.

[10] U.Syamaprasad and C.P.G.Vallabhan, Solid State Commun. 41 (1982) 169.

[11] U.Syamaprasad and C.P.G.Vallabhan, Solid State Commun. 34 (1980) 899.

[12] U.Syamaprasad and C.P.G.Vallabhan, Nat.Acad.Sci.Lettters (India). 3C (1980) 364.

[13] U.Syamaprasad and C.P.G.Vallabhan, Phys.Lett. 89A (1982) 37.

[14] U.Syamaprasad and C.P.G.Vallabhan, Phys.Rev.B 26 (1982) 5941.

[15] Y.V.G.S.Murti and P.S.Prasad, Physica. 79B (1975) 243.

[16] U.Syamaprasad and C.P.G.Vallabhan, J.Phys.C: Solid State Physics. 14 (1981) L571.

[17] A.Devendar Reddy, S.G.Sathyanarayana and Sivarama Sastry, Solid State Commun. 43 (1982) 937.

[18] V.K.Subhadra, U.Syamaprasad and C.P.G.Vallabhan, J.Appl. Phys. 54 (1983) 2593.

[19] A.A.Khan, M.E.Straumanis and W.J.James, Acta.Cryst.B26 (1970) 1889.

[20] L.Tenzer, B.C.Frazer and R.Pepinsky, Acta.Crtyst.B26 (1958) 505.

[21] F.Jona and G.Shirane, Ferroelectric crystals (Pergamon, Oxford, London, 1962), p.88.

[22] E.J.Murphy, J.Appl.Phys. 35 (1964) 2609.

[23] L.B.Harris and G.J.Vella, J.Chem.Phys. 58 (1973) 4550.

[24] M.O'Keefe and C.T.Perrino, J.Phys.Chem.Solids 28 (1967) 211.

[25] C.T.Perrino and P.Wentrcek, J.Solid State Chem. **10** (1974) 36.

Chapter V

THERMAL DEPOLARISATION STUDIES OF PURE AND DOPED DIAMMONIUM HYDROGEN PHOSPHATE

Abstract

The results of thermal depolarisation current (TDC) measurements carried out in pure and doped diammonium hydrogen phosphate in the temperature range 80K to 423K are presented in this chapter. The depolarisation current spectrum shows three distinct peaks in the pure diammonium hydrogen phosphate and four peaks in the SO_4^{2-} doped diammonium hydrogen phosphate crystals. Detailed investigations of TDC carried out in these materials as a function of impurity concentration, poling field, poling temperature and heating rate reveal the origin and nature of each of these peaks. The observed experimental results are in very good agreement with those obtained from earlier conductivity and dielectric constant measurements. The DSC measurements of this material also support the conclusions drawn from the TDC studies.

5.1 INTRODUCTION

Many ammonium compounds exhibit characteristic transitions and these affect a variety of physical properties as their temperature or pressure is changed. Among these materials crystals containing NH_4 and PO_4 groups have been of great interest in recent years in view of their dielectric, ferroelectric and thermal properties. The hydrogen bonds of O-H....O and N-H....O type in these crystals play an important role in determining some of their physical properties. Diammonium hydrogen phosphate (DAHP) is an interesting crystal belonging to this class of materials. Though a fairly good number of investigations are already reported in DAHP [1-7] no attempt has so far been made in studying the detailed electrical properties of these materials except for some very recent conductivity and dielectric measurements [8]. In the present chapter a detailed investigation carried out in single crystals of pure and SO_4^{2-} doped diammonium hydrogen phosphate using thermal depolarisation current technique is depicted. We report here the observation of three distinct peaks in the thermal depolarisation current spectrum of pure DAHP and four peaks in the SO_4^{2-} doped specimens of diammonium hydrogen phosphate within the temperature range studied here. Detailed analysis of these peaks is made by studying their characteristics as a function of poling field, poling temperature, impurity concentration and heating rate.

The study of thermal depolarisation current measurements originally proposed by Bucci et al. [9,10] has evoked considerable interest in recent years in view of the information one can draw about various phenomena such as relaxation, solubility and precipitation process of impurity vacancy (I-V) complexes, phase transitions and space charge effects associated with ions, electrons and holes in ionic and ceramic materials as well as in polymeric solids. The method in its essence consists of four distinct steps.

(i) The polarisation of the sample by the application of an electric field at a temperature for which the relaxation time associated with the I-V dipole complexes is short compared to the time scale of the experiment.

(ii) Cooling the specimen rapidly to a very low temperature with the field intact at which the relaxation time is very large.

(iii) Then the sample is heated in a linear fashion at a constant rate with the field removed.

(iv) Recording the discharge current as a function of temperature.

From the nature of the discharge current as a function of temperature and from the position of the discharge current peak,

the activation energy and the reciprocal frequency factor can be obtained by using the first order reorientation kinetic equation [10].

5.2 EXPERIMENTAL DETAILS

The method of preparation of single crystals of DAHP is already given in chapter IV. The single crystals used in the present investigation were obtained after three recrystallisations using triply distilled water. Sulphate doped specimens of DAHP were grown by adding specific amount of $(NH_4)_2SO_4$ into the solution. The nominal concentration of impurities added ranges from 0.02 to 0.1 mole %. The presence of SO_4^{2-} ions in the specimens of DAHP were verified by taking the Laser Raman spectrum of the doped material. The samples used for the depolarisation measurements were prepared by cutting slices of typical sizes 5x5x1 mm^3 from large single crystals. For good electrical contact between the crystal and the electrodes, the broad faces of the specimen were coated with silver paint. The sample holder, vacuum chamber for temperature variation studies, measurement of temperature etc., have been already described in chapter II. The thermal depolarisation current measurements were carried out by polarising the specimen with a voltage of 100-600 V for a polarising time of 1-10 minutes at the polarising temperature ranging from 300 to 400K. With polarising field still on, the crystal was cooled down to a very low temperature (80K)

where the electric field was removed. The crystal was then connected to an electrometer (Keithley model,642) for the depolarisation current measurement and the discharge current along with the temperature of the specimen was recorded using an X-Y recorder by increasing the temperature of the specimen at a constant linear heating rate ranging from 0.01 to 0.1K/sec. The differential scanning calorimetric (DSC) studies were made using a Perkin Elmer Delta Series Model DSC7 instrument.

5.3 EXPERIMENTAL RESULTS

5.3.1 Pure diammonium hydrogen phosphate

The thermal depolarisation current spectrum of undoped diammonium hydrogen phosphate crystals recorded in the temperature range of 80K to 423K with a heating rate of 0.07K/sec. is shown in figure 5.3a. The spectrum obtained by polarising the specimen at 300K for 2 minutes with a poling field of 3KV/cm shows three distinct current peaks (denoted as A,B and C) of varying magnitude with their current maxima located at temperatures 174, 248 and 418K. It is to be noted that the peak B is quite sharp and narrow with a height more than twice that of the peak A. The height of the peak C is about one order of magnitude greater than that of peak A. The exact shape of the peaks A and B are separately shown in the inset of figure 5.3a.

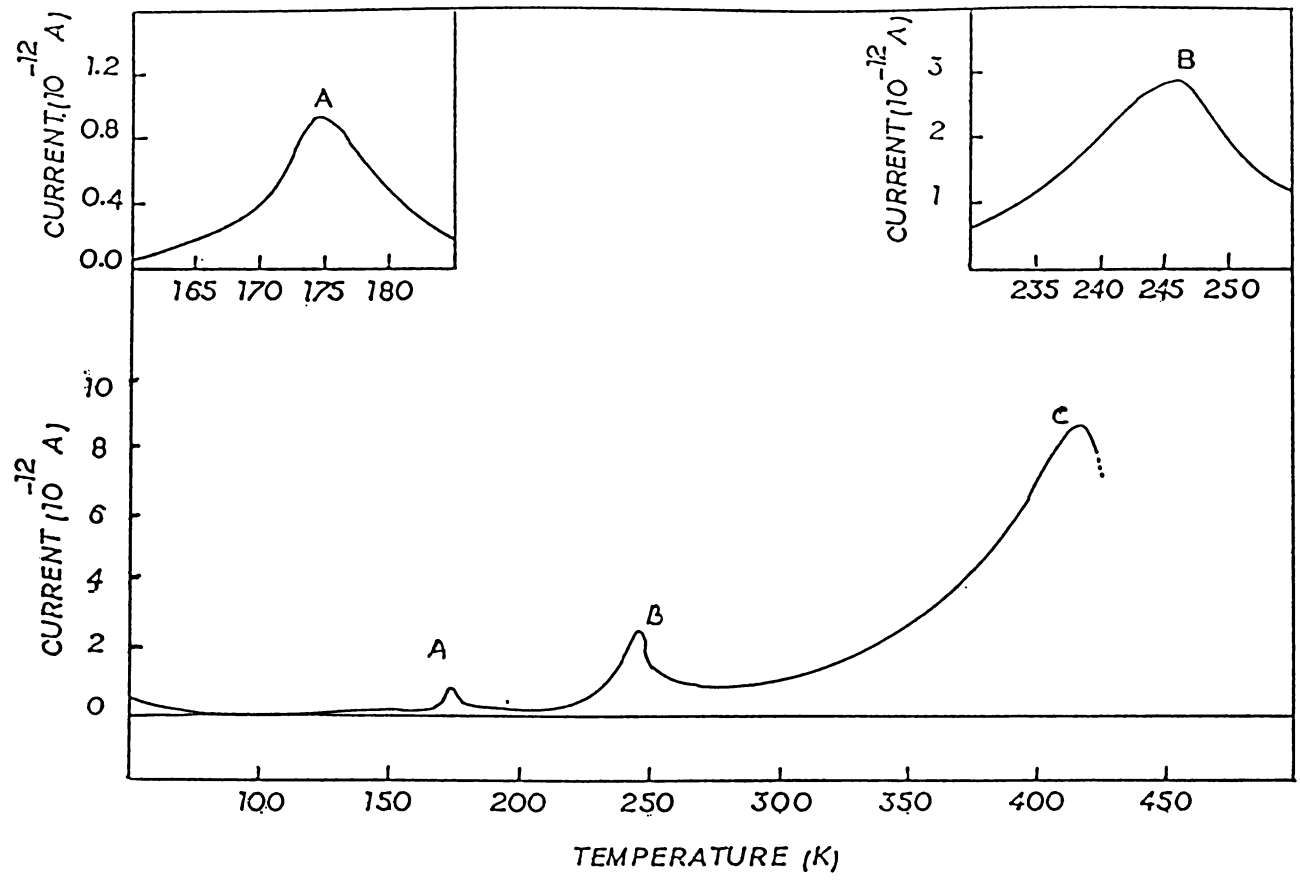

Figure 5.3a. Thermal depolarization current spectrum of pure diammonium hydrogen phosphate crystal. Inset show the details of the current peaks A and B.

5.3.2 SO_4^{2-} doped diammonium hydrogen phosphate

The depolarisation current spectra obtained for SO_4^{2-} doped (0.1 mole %) specimens of DAHP by polarising it at 300K with a field of 3 KV/cm (for 2 minutes) with a heating rate of 0.07K/sec. is shown in figure 5.3b. In addition to the three current peaks (denoted as A,B and C) observed in undoped DAHP specimens an additional current peak (denoted as D) is also observed in this material at 296K. This current peak is a broader one with a height which is three times larger than that of A in the undoped diammonium hydrogen phosphate. The height of the peaks are found to be slightly enhanced in the SO_4^{2-} doped specimens compared with the corresponding peaks in the undoped materials under the same conditions. However, the temperatures corresponding to the current maxima for the peaks A,B and C in the case of SO_4^{2-} doped specimens are found to be approximately the same as those in the case of pure DAHP when lower levels of doping concentrations are used, whereas these are slightly affected at higher doping levels.

5.3.3 Effect of poling field on the TDC spectra of pure and doped DAHP

The effect of poling field (1-6 KV/cm) on the variation of the height of the peaks A, B and C is shown in figure 5.3c. The plots show no appreciable change either in shape or in the magnitude of any of these peaks. However, on increasing the

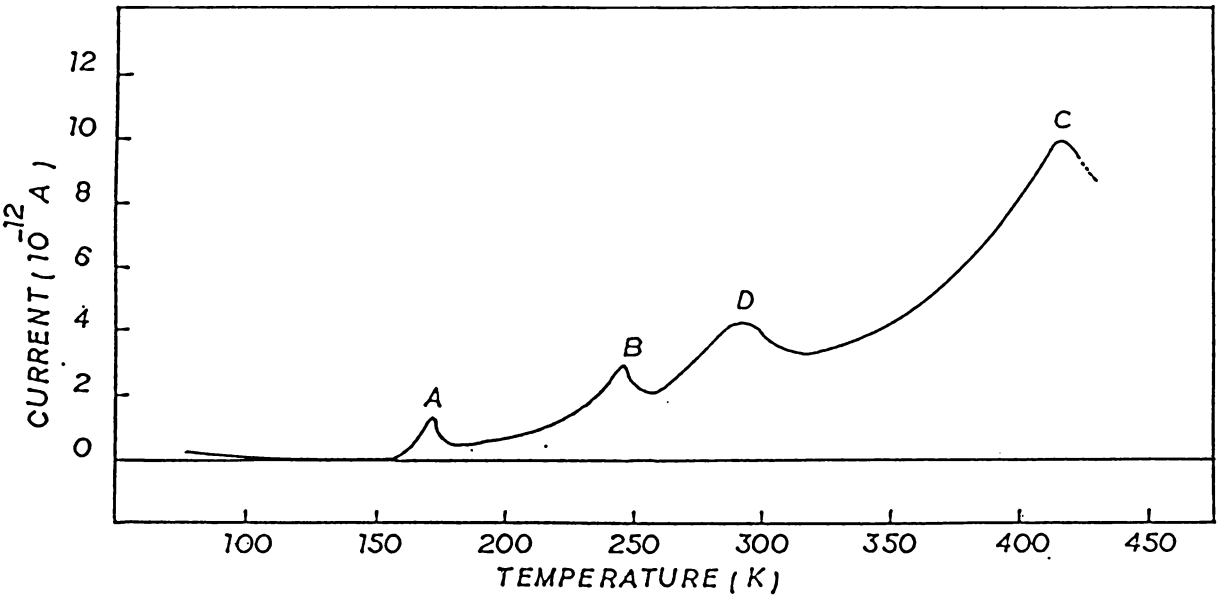

Figure 5.3b. Thermal depolarization current spectrum obtained for SO_4^{2-} doped (0.1 mole %) diammonium hydrogen phosphate crystal.

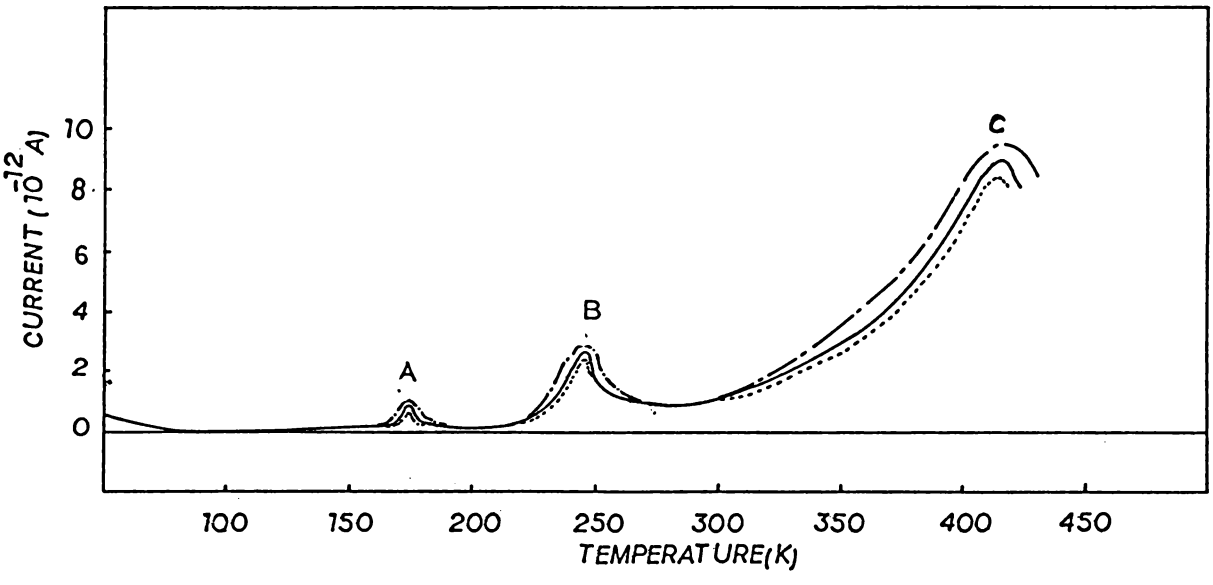

Figure 5.3c. Effect of poling field on the variation of the height of the current peaks A,B and C.

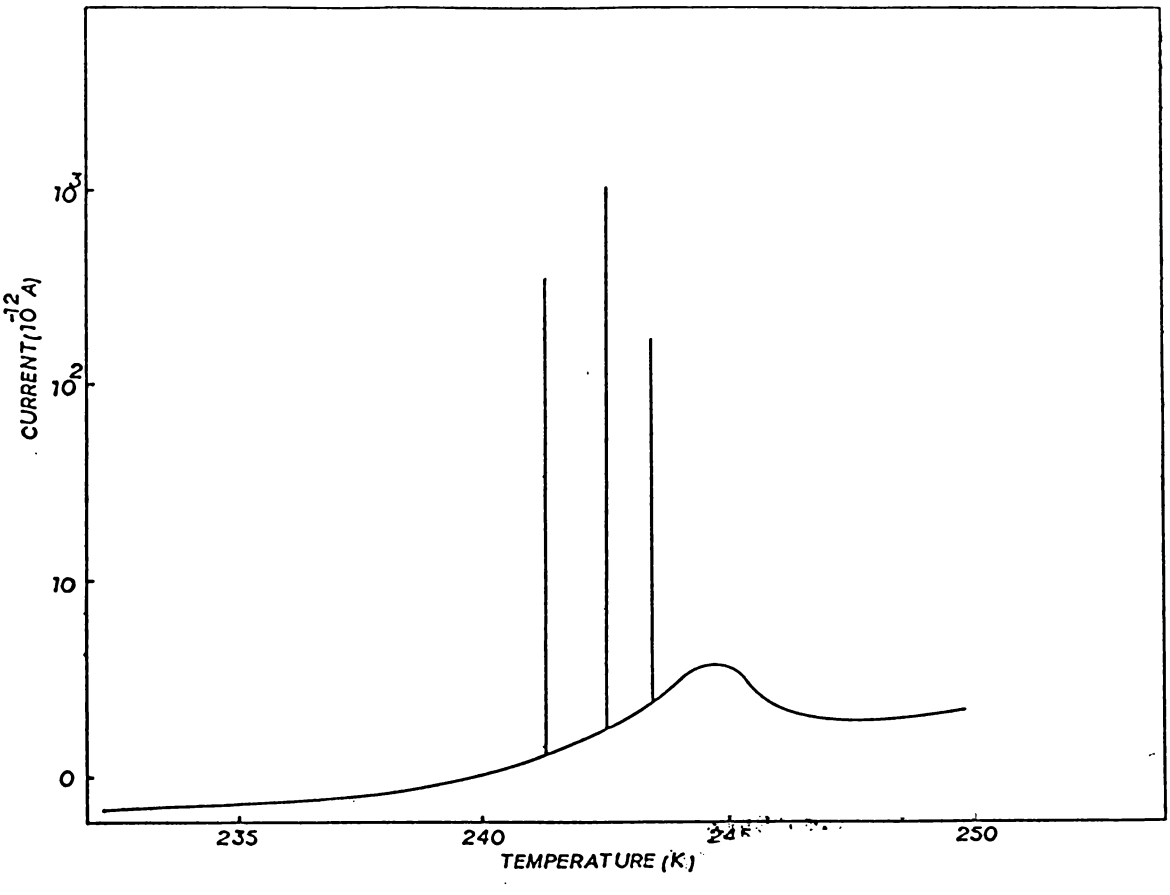

Figure 5.3d. Current spikes observed in the first heating cycle of the ITC measurement in DAHP crystal. Poling field 6.5 KV/cm.

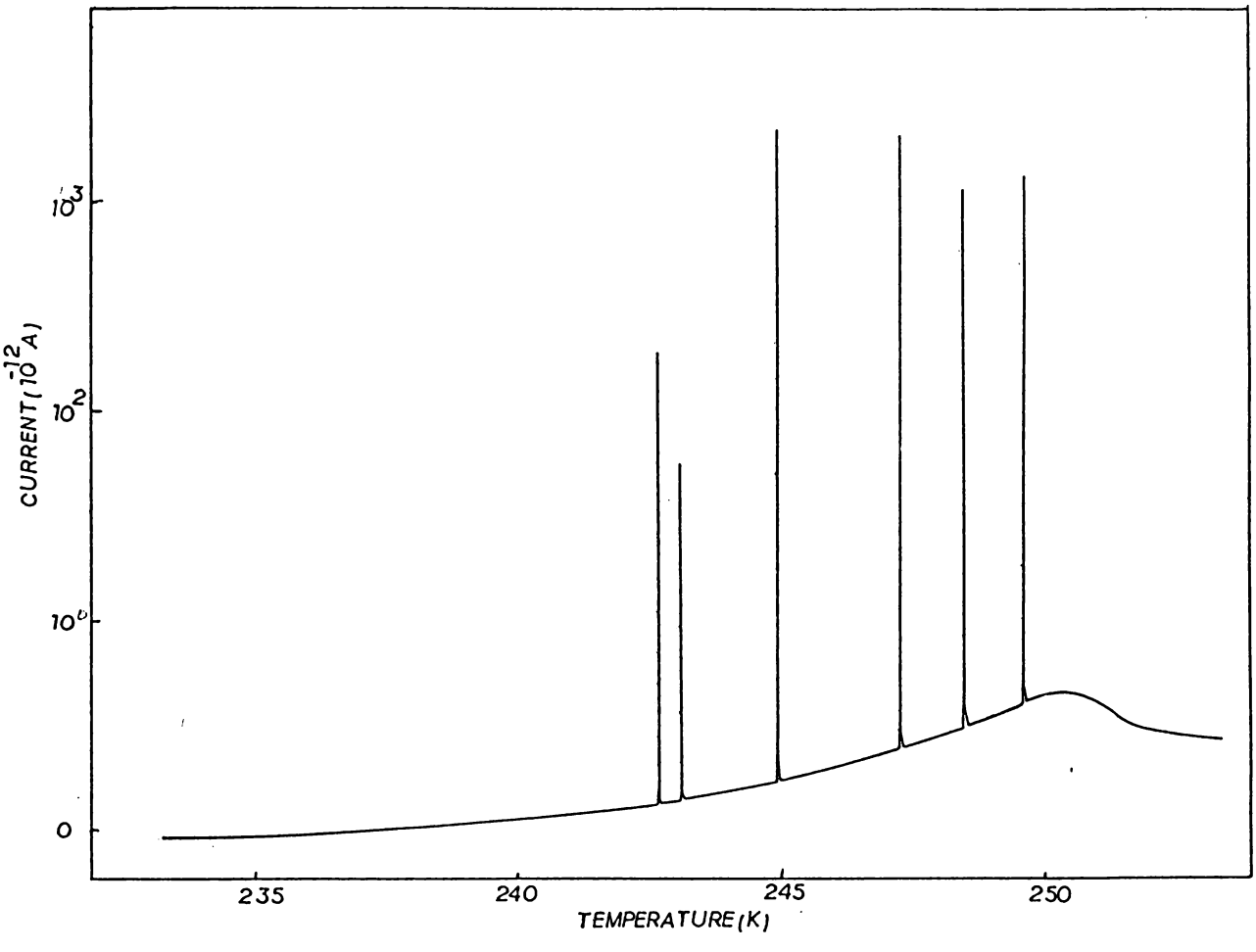

Figure 5.3e. Current spikes observed in the second heating cycle of ITC measurement in pure DAHP crystal. Poling field 6.5 KV/cm.

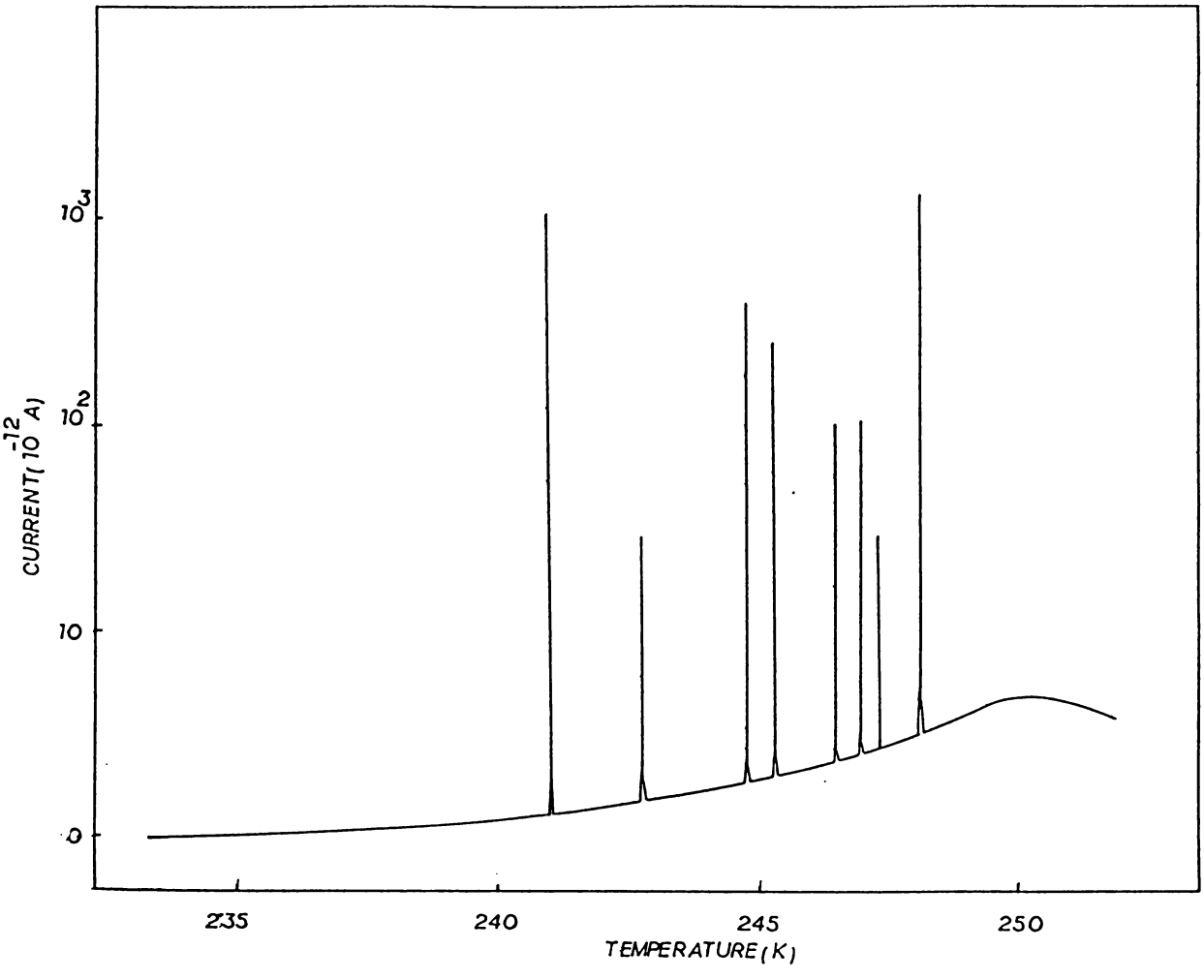

Figure 5.3f. Current spikes observed in the third heating cycle of ITC measurement in pure DAHP crystal. Poling field 6.5 KV/cm.

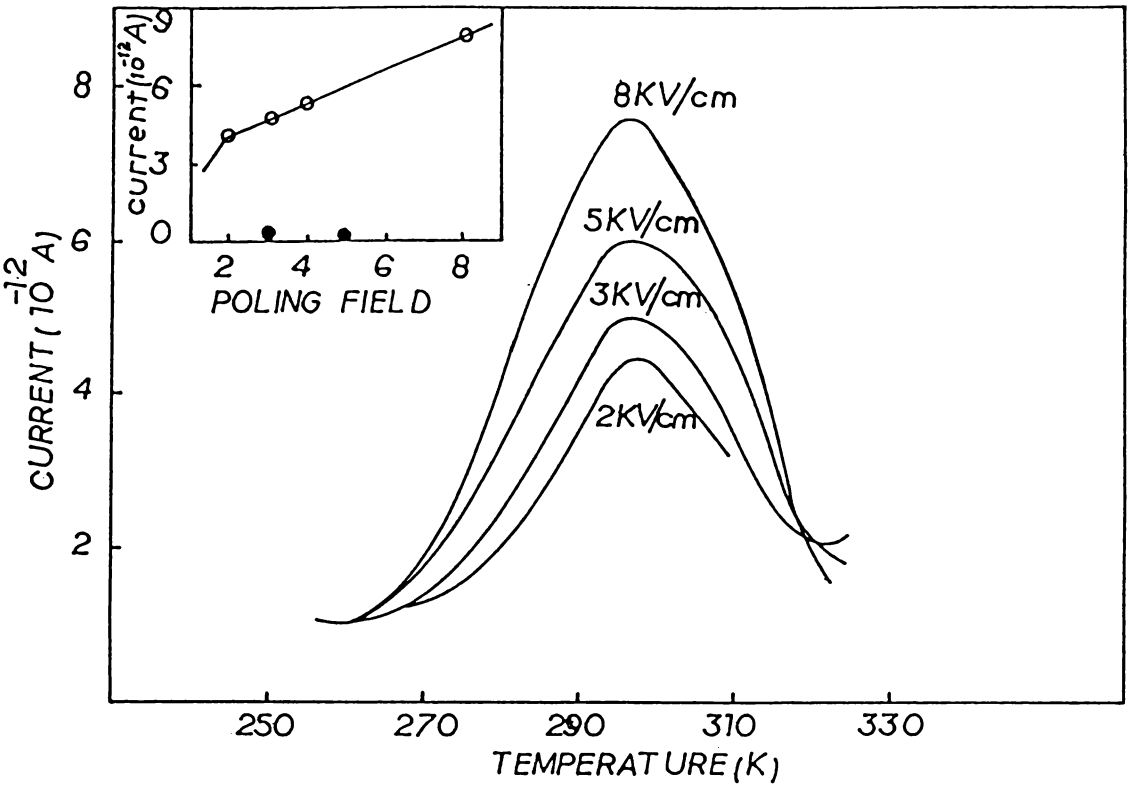

Figure 5.3g. Effect of poling field on the variation of the current peak D. The inset shows the linear variation of the height of the current peak D.

poling field above 6 KV/cm, just before the second peak, a number of current spikes have been observed. The heights of these current spikes varies upto three orders of magnitude as shown in figure 5.3d. It is to be noted that the number of these spikes is not constant for each repetition of the depolarisation current measurement. Figures 5.3e and 5.3f show the nature of variation of these anomalous current spikes observed in the second and third consecutive repetition of the depolarisation measurement. Inspite of the occurrence of these fluctuations at higher poling fields it is possible to recover the clear and transparent crystal without damage even after heating it upto 423K. Figure 5.3g illustrates the effect of poling field on the magnitude of the current peak D and the inset shows the linear variation of the current maximum with the applied field. It is found that the variation of poling field has no effect on the height or shape of the TDC peaks A,B and C in the SO_4^{2-} doped DAHP and hence they have not been shown in this figure.

5.3.4 Effect of poling temperature

Figure 5.3h which shows the effect of poling temperature on the height of the peak D in the 0.1 mole % SO_4^{2-} doped specimens of DAHP obtained by polarising it with a field of 3KV/cm for 2 minutes, indicates that the height of the peak decreases with the increase of poling temperature. However, the intensity and shape of the peaks A,B and C in both pure and doped DAHP specimens are found to be unaffected by this treatment.

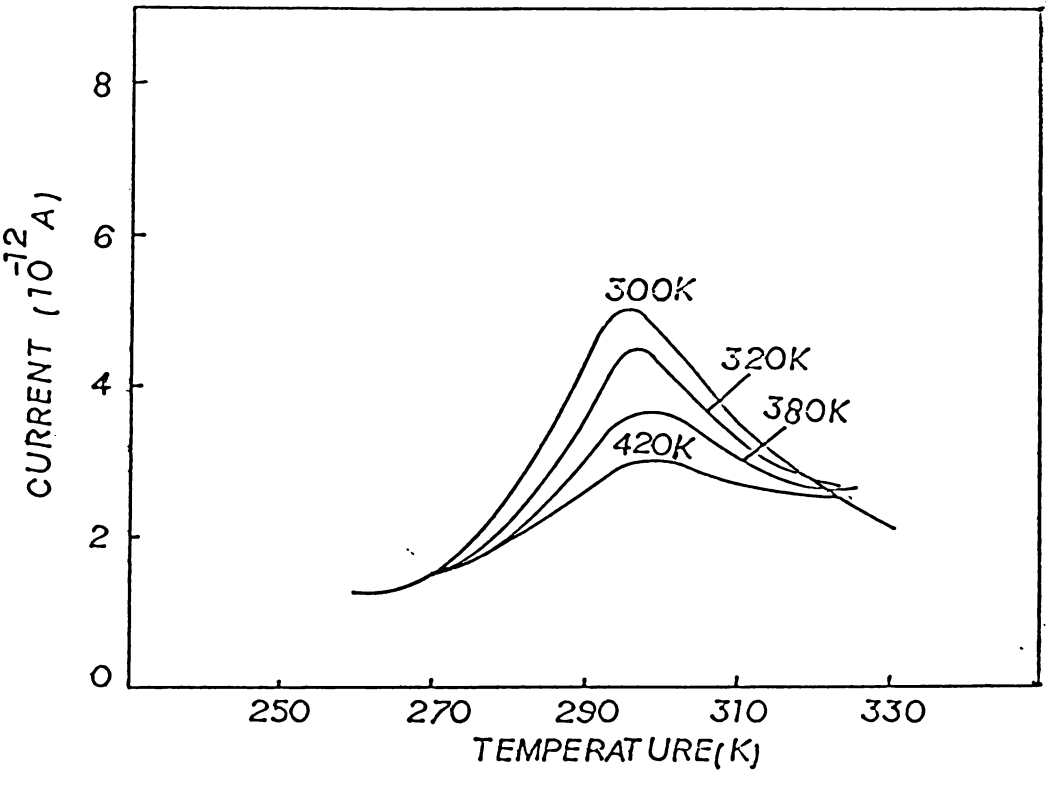

Figure 5.3h. Effect of poling temperature on the variation of the current peak D.

5.3.5 Effect of impurity concentration

The nature of variation of the current peak D as a function of temperature for various amount of SO_4^{2-} (ranging from 0.02 to 0.1 mole %) doped DAHP crystals poled at 300K for 2 minutes with a field of 3 KV/cm is shown in figure 5.3i. It is to be noted that the height and shape of the peak D varies in proportion to the concentration of SO_4^{2-} ions added in the pure material. Figure 5.3j shows the effect of SO_4^{2-} concentration on the magnitude of the current maxima for the peak D. It shows a linear variation implying that the impurity ions are responsible for this change. The current peak D isolated from the main TDC spectrum obtained for SO_4^{2-} (0.1 mole %) doped DAHP crystal using thermal peak cleaning technique [10] is shown in figure 5.3k. The log I vs T^{-1} plot obtained for this isolated peak given in figure 5.3l, yields an activation energy value of 0.53 eV and a pre-exponential factor of 4.4×10^{-12} sec.

5.3.6 The effect of heating rate

The effect of heating rate on the nature of variation of the TDC peaks both in pure and doped DAHP crystals obtained by polarising it with a field of 3 KV/cm for 2 minutes at 300K is such that the temperature corresponding to the current maxima depends slightly on the rate of heating whereas the areas delineated by all the peaks A,B and C are found to be

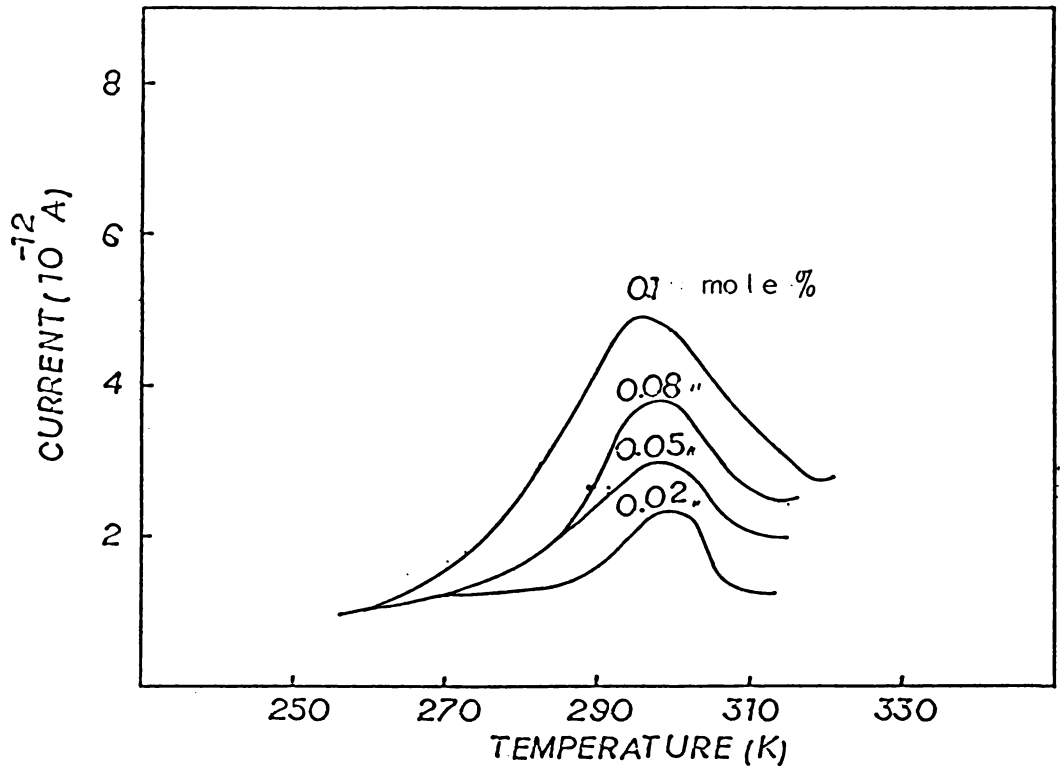

Figure 5.3i. Effect of SO_4^{2-} concentration on the variation of the current peak D.

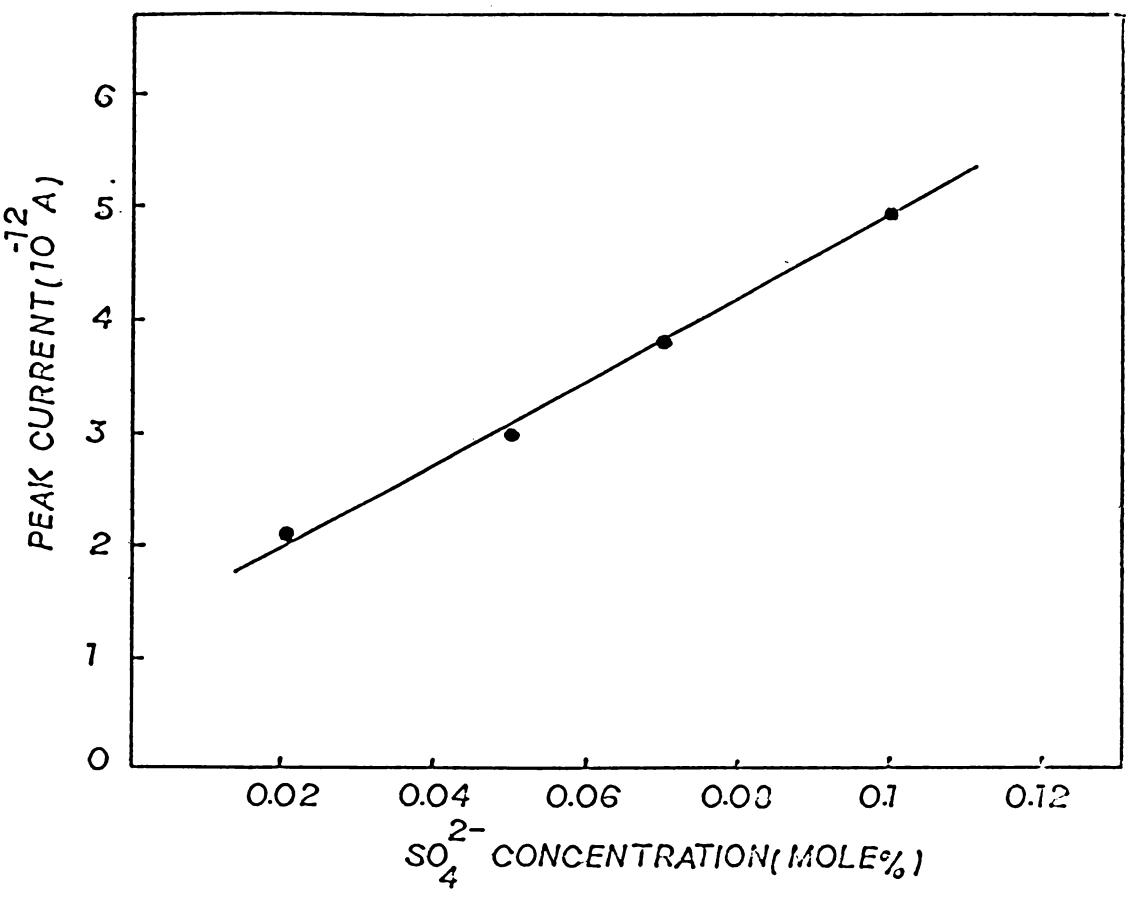

Figure 5.3j. Effect of SO_4^{2-} concentration on the peak height of the current peak D.

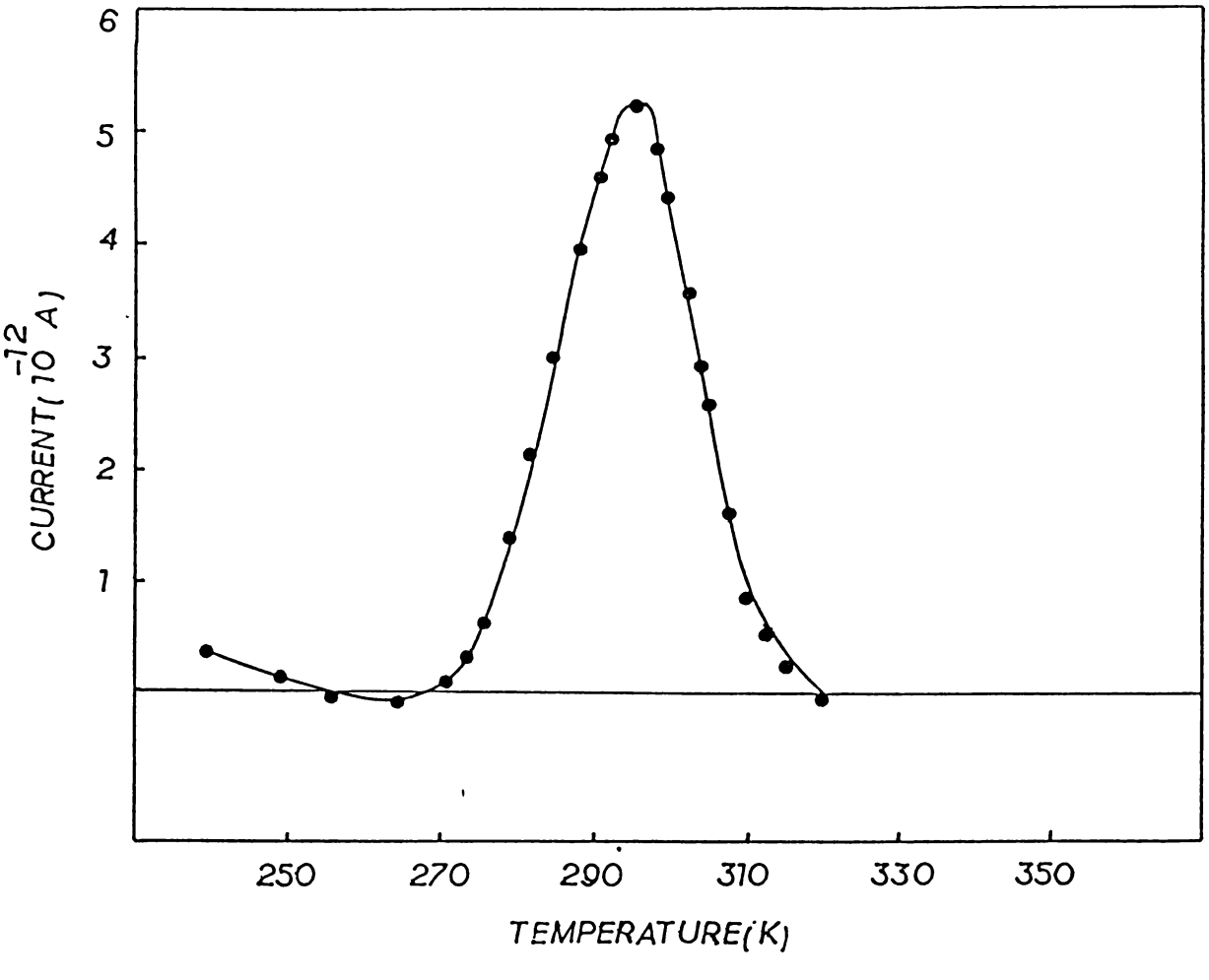

Figure 5.3k. ITC peak of SO_4^{2-} doped DAHP crystal using thermal peak cleaning technique.

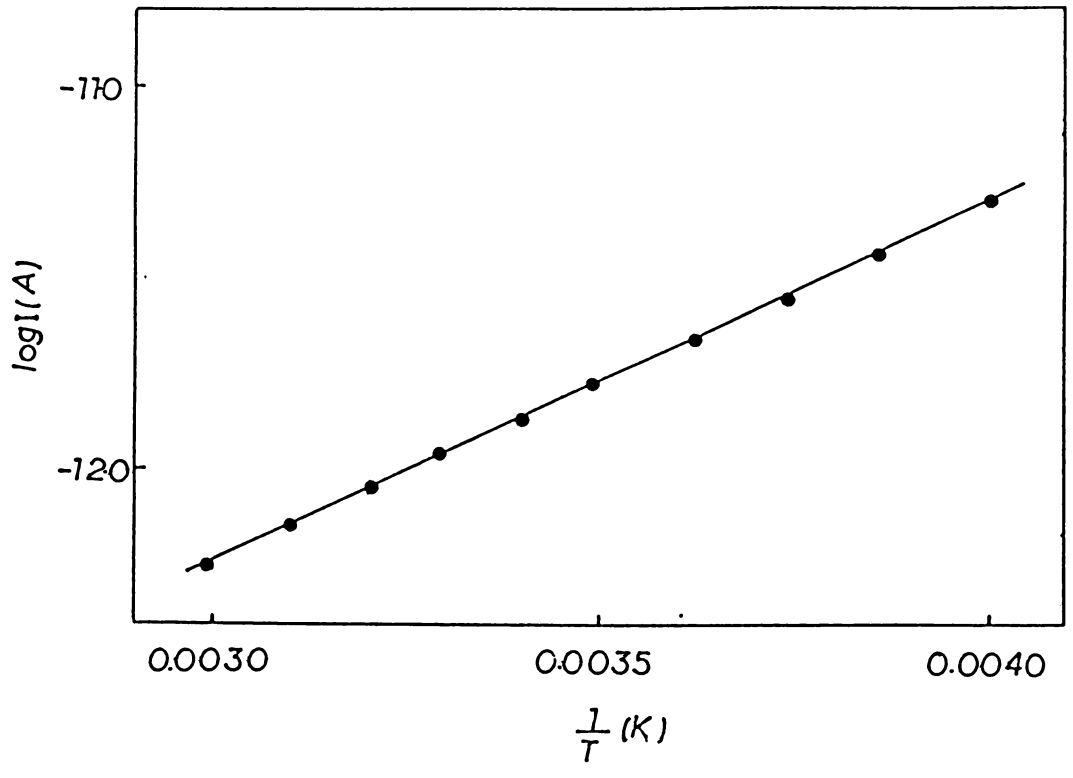

Figure 5.31. Log I vs 1/T plot for an isolated ITC peak of doped DAHP crystal.

unaffected by the change in heating rate. It is also observed that for higher heating rates the height of all the current peaks show a slight increment.

5.3.7 Results obtained from DSC studies

Figure 5.3m shows the DSC spectrum recorded for DAHP in the temperature range 100K to 300K with a heating rate of 20°C/m in the heating cycle. The spectrum obtained shows two distinct variations in the heat flow indicative of the occurrence of two phase transitions.

5.4 DISCUSSION

The conductivity, dielectric and NMR studies made earlier in ammonium containing ionic crystals like NH_4Cl [11, 12], $(NH_4)_2SO_4$ [13-16], $LiNH_4SO_4$ [17,19], $(NH_4)_3H(SO_4)_2$ [20-22], $(NH_3)_2HPO_4$ [8], $(NH_4)H_2PO_4$ [23-25] reveal that at elevated temperatures the reorientation or free rotation of the ammonium groups in these crystals can lead to phase transitions and such motional effects of ammonium group generate a large number of protonic effects which contribute significantly to the conduction process. As already mentioned in chapter IV pure diammonium hydrogen phosphate (DAHP) undergoes three well defined transitions at temperatures 174, 246 and 416K and that the origin of these transitions has been discussed in detail. Therefore the field independent depolarisation current

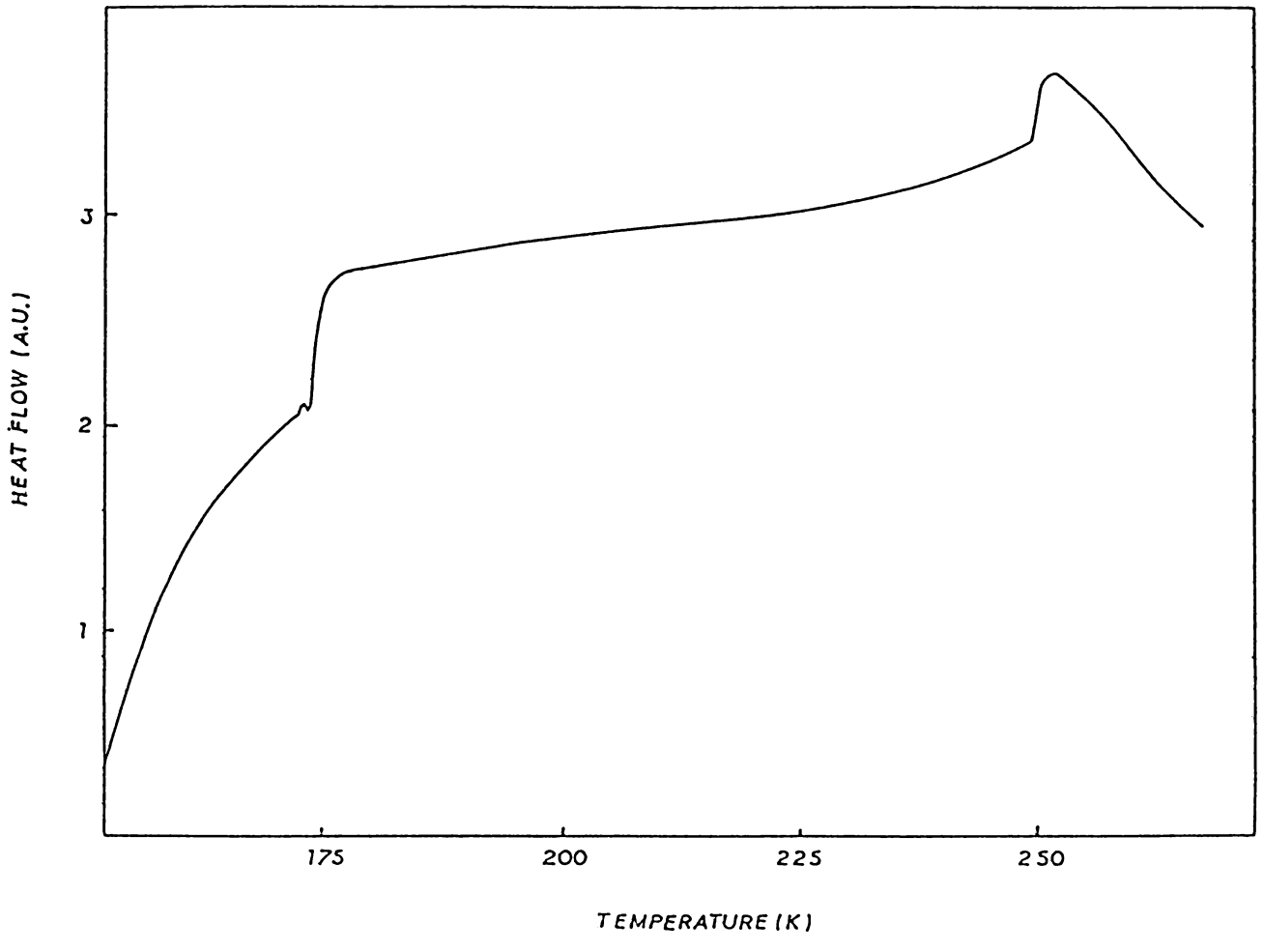

Figure 5.3m. DSC spectrum of DAHP material obtained with a heating rate of $10^{o}C$/min.

peaks observed in diammonium hydrogen phosphate at temperatures 174, 248 and 418K can be assigned directly as due to the occurrence of three distinct phase transitions in this material, at the above temperatures. Similar TDC peaks have been found to appear at transition points in many materials. These results obtained are further verified by taking the DSC spectrum of this material. The slight difference in transition temperatures observed on both in TDC and DSC measurements compared with that observed in electrical conductivity and dielectric constant measurements can only be due to the higher heating rate employed in the former cases. The three current peaks A,B and C occurring in the pure material also appear virtually unchanged in the SO_4^{2-} doped DAHP material. The fact that, the three peaks, A,B and C in SO_4^{2-} doped DAHP material suggests that the defect structure created by the addition of SO_4^{2-} ions has no role in determining the characteristics of this three peaks, and therefore A,B and C peaks should be attributed as innate property of the original material.

The occurrence of additional peak D in the case of SO_4^{2-} doped DAHP specimen clearly shows that this peak arises due to the substitution of the impurity ion in the host lattices. As already indicated in chapter IV, the $(NH_4)_2HPO_4$ consists of NH_4 and PO_4 tetrahedra held together by N-H....O and O-H....O bonds. When the host PO_4^{3-} ion is substituted by an aliovalent impurity ion like SO_4^{2-} the charge compensation

is usually achieved by the creation of proton vacancies as generally observed in KDP and ADP type crystals [26,27]. This is true in the present case also as revealed from the conductivity studies. If the charge compensating species is in the local environment of the impurity ion then a dipolar complex is formed which may reorient by a thermally activated jump of one of the constituents of the complex. Thus the detection of dipoles with relaxation parameters of the appropriate magnitude would support a predominant vacancy transport mechanism. If the charge transport in the crystal proceeds via cation or anion vacancies, then such dipoles formed by the association of these vacancies with divalent impurity ions should be detected by the TDC technique. Again the frequency associated with the relaxation of these dipoles is expected to be of the order of lattice vibration frequency (10^{12} to 10^{14} sec^{-1}) [28]. Thus the detection of dipoles with relaxation parameters of appropriate magnitude would support a vacancy charge transport mechanism in the material. In the present case substitution of bivalent anions i.e., SO_4^{2-} ions for PO_4^{3-} would require a cation vacancy for maintaining the charge neutrality of the crystal, thus giving rise to charge compensating vacancy dipoles. These dipoles alter their orientation when the associated defect jumps from one lattice site to another around the impurity ion. Consequently, the pre-exponential factor of the relaxation time of the dipoles is expected to be of the order of inverse of lattice vibrational frequency.

Considering these facts, it is clear that the peak occurring at 296K with an activation energy of 0.53 eV and pre-exponential factor 4.4×10^{-12} sec is due to the anion impurity cation vacancy (i.e., L defects) dipole complexes. Since, the mechanisms for conductivity and thermal depolarisation involve identical proton vacancy jumps, one can correlate the conductivity and the thermal depolarisation results. As noted in chapter IV the electrical conductivity of SO_4^{2-} doped DAHP crystal gives activation energy of 0.46 eV which is found to be fairly in good agreement with 0.53 eV obtained from TDC measurements. The conductivity in these crystals have been found to be due to the migration of proton vacancies, i.e., L defects. Based on the arguments given above, one may conclude that the impurity - proton vacancy dipoles are responsible for the observed, thermal depolarisation current peak at 296K.

The TDC studies extended in SO_4^{2-} doped specimens of DAHP as a function of poling field and SO_4^{2-} concentration strongly support the above conclusion that the origin of the peak observed at 296K is due to the formation of I-V complex by the substitution of SO_4^{2-} in the PO_4 lattice. The effect of poling temperature on the peak height of TDC peak observed at 296K suggests that the dissociation of these I-V complexes results at higher poling temperatures causing corresponding decrease in the number of I-V dipoles and hence a reduction in the TDC peak D.

5.5 CONCLUSIONS

The thermal depolarisation current measurements carried out in pure and SO_4^{2-} doped single crystals in the temperature range 90K to 423K as a function of poling field, poling temperature, impurity concentrations and heating rate, lead to the following conclusions.

1. The thermal depolarisation current spectrum obtained for pure DAHP gives three distinct peaks (denoted as A,B and C) whereas in SO_4^{2-} doped DAHP an additional peak (denoted as D) is also observed.

2. Peaks A and B in both pure and doped DAHP can be assigned as due to the reorientation of the NH_4 tetrahedra and the peak C as due to the structural change taking place in this material.

3. The nature of variation of the peaks A,B and C as a function of poling field, poling temperature and SO_4^{2-} concentration does not show characteristics of TDC peaks whereas D exhibits the typical characteristics of a TDC peak.

4. The additional peak observed in SO_4^{2-} doped DAHP crystal at 296K can be assigned unambiguously to the reorientation of the I-V complexes.

5. Log I vs T^{-1} plot yield an activation energy of 0.53 eV and a pre-exponential factor of 4.4×10^{-12} sec. The activation energy value compares well with that obtained from dc conductivity measurements.

6. The peak D observed in the TDC spectrum of SO_4^{2-} doped specimen arises due to the formation of impurity ion-cation vacancy dipole by the substitution of SO_4^{2-} ions in the $(NH_4)_2HPO_4$.

5.6 REFERENCES

[1] J.P.Smith, J.R. Lehr and W.E.Brown, Acta.Cryst. 10 (1953) 50.

[2] J.P.Smith, J.R.Lehr and W.E.Brown, Acta.Cryst. 10 (1957) 709.

[3] K.A.Sherwin, J.Sci.Instrum. 41 (1964) 7.

[4] R.V.Coates and P.S.Smith, Acta.Cryst. 23 (1967) 504.

[5] A.A.Khan, J.P.Roux and W.J.James, Acta.Cryst. B28 (1972) 2065.

[6] A.Watton, E.C.Reynhardt, H.S.Sandhu and H.E.Petch, J.Chem. Phys. 67 (1977) 887.

[7] F.Koksal, Z.Naturforsh 36A (1981) 203.

[8] R.Navilkumar and C.P.G.Vallabhan, J.Phys:Condensed Matter (in press).

[9] C.Bucci and R.Fieschi, Phys.Rev.Lett. 12 (1964) 16.

[10] C.Bucci, R.Fieschi and G.Guidi, Phys.Rev. 148 (1966) 816.

[11] Y.V.G.S.Murti and P.S.Prasad, Physica 79B (1975) 243.

[12] Y.V.G.S.Murti and P.S.Prasad, Proc.Nuclear Phys. and Solid State Phys.Symp. (India) 17C (1974) 67.

[13] U.Syamaprasad and C.P.G.Vallabhan, Solid State Commun. 38 (1981) 555.

[14] U.Syamaprasad and C.P.G.Vallabhan, Proc.Nuclear Phys. and Solid State Phys.Symp. (India), Paper No.SLA10 (1980).

[15] U.Syamaprasad and C.P.G.Vallabhan, Solid State Commun. 41 (1982) 169.

[16] U.Syamaprasad and C.P.G.Vallabhan, J.Phys.C: Solid State Phys. 14 (1981) 1865.

[17] U.Syamaprasad and C.P.G.Vallabhan, Solid State Commun. 34 (1980) 899.

[18] U.Syamaprasad and C.P.G.Vallabhan, Nat.Acad.Sci.Lett.(India) 3 (1980) 364.

[19] U.Syamaprasad and C.P.G.Vallabhan, Phys.Lett. 89A (1982) 37.

[20] U.Syamaprasad and C.P.G.Vallabhan, J.Phys.C:Solid State Phys. 14 (1981) L571.

[21] R.Navilkumar and C.P.G.Vallabhan (Communicated).

[22] R.Navilkumar and C.P.G.Vallabhan, Solid State Phys.Symp. Vol.28A (1985) 240.

[23] B.V.R.Chowdri and Y.Ravi Sekhar,Solid State Commun. 29 (1979) 687.

[24] B.V.R.Chowdri and Y.Ravi Sekhar, Phys.Stat.Solidi (a) 54 (1979) 413.

[25] V.K.Subhadra, U.Syamaprasad and C.P.G.Vallabhan, J.Appl.Phys. 54 (1983) 2593.

[26] M.O'Keefe and C.T.Perrino, J.Phys.Chem.Solids 28 (1967) 211.

[27] C.T.Perrino and P.Wentrcek, J.Solid State Chem. 10 (1974) 36.

[28] F.Jona and G.Shirane, Ferroelectric Crystals, Macmillian, New York (1962).

Chapter VI

DC AND AC ELECTRICAL CONDUCTIVITY, DIELECTRIC CONSTANT, IONIC THERMOCURRENT AND PHASE TRANSITIONS IN PURE AND DOPED $(NH_4)_2Cr_2O_7$ CRYSTALS

Abstract

Ammonium dichromate (AD) crystal has been investigated by dc and ac electrical conductivity, dielectric constant and ionic thermocurrent measurements. These measurements carried out along c-axis in the temperature range 80K to 435K show three distinct anomalous reversible changes at temperatures 128, 156 and 268K. Similar and supportive data were obtained with DSC measurements performed in the same temperature range. These experimental results indicate that $(NH_4)_2Cr_2O_7$ undergoes three phase transitions below room temperature. The mechanism of phase transition and of electrical conduction process in this material have been discussed and the activation parameters are evaluated.

6.1 INTRODUCTION

Ammonium containing crystals have been studied extensively using nuclear magnetic resonance. The proton resonance line shapes and second moments of various ammonium salts [1-8] show interesting changes as a function of temperature. Some of these changes can be interpreted readily in terms of the crystal structure of the salt and of various types of molecular motion occurring in them. Some of the salts, however, have nuclear resonance spectra which are not so easily interpreted, and more experimental and theoretical work is necessary to understand them. Careful measurements of spin lattice relaxation times as a function of temperature might very well provide important and detailed information about the molecular motion in these substances.

Gutowsky, Pake and Behrson [1] have investigated the second moments of the hydrogen resonance of ammonium chloride and ammonium bromide as a function of temperature and they found that this method is very suitable for determining the N-H distances in these compounds. The hindered rotation of NH_4^+ in ammonium compounds has been well investigated by the measurement of proton spin lattice relaxation time T_1 in the laboratory frame and $T_{1\rho}$ in the rotating frame. However, because of the poor natural abundance of ^{17}O

(0.037%), it is very difficult to study the motion of oxygens by NMR. Shimomura et al. [6] reported that the temperature dependence of the dipolar relaxation time T_{1D} goes through minimum values in NH_4ClO_4, $(NH_4)_2S_2O_8$ and $(NH_4)_2Ce(NO_3)_6$. They have proposed a spin-rotational model to explain these $(T_{1D})_{min}$, in which it is considered that the rotation of NH_4^+ is triggered by the reorientation of the anions.

The reorientational motion of ammonium ions in $(NH_4)_2Cr_2O_7$ was thoroughly studied by Richards and Schaefer [9] using proton magnetic resonance. They have suggested a low barrier for the reorientational motion for the NH_4 ions. The neutron scattering cross section values [10,11] showed a much greater freedom of rotation and weaker hydrogen bonding for ammonium ions in this compound than in $(NH_4)_2Cr O_4$. Vibrational spectra of $(NH_4)_2Cr_2O_7$ have been reported at room temperature by various investigators [12-15] and the temperature dependence of the infrared studies by Schutte and Heyns [16]. The first attempt to study the phase transitions in $(NH_4)_2Cr_2O_7$ was carried out by Jaffray [17] using differential thermal analysis and specific heat measurements. These measurements show that this material undergoes anomalous changes which may correspond to phase transitions at temperatures 128, 155 and 268K.

The temperature dependence of the relaxation time in the laboratory frame T_1, and in the rotatory frame $T_{1\rho}$ in pure and deuterated $(NH_4)_2Cr_2O_7$ (the concentration of deutrons is about 75%) have been reported by Morimoto [18]. The values of relaxation time in the laboratory frame for deuterated $(NH_4)_2Cr_2O_7$ are about three times larger than those in pure $(NH_4)_2Cr_2O_7$ below 143K suggesting that the inter molecular dipolar interaction of protons among NHD_3^+ in deuterated $(NH_4)_2Cr_2O_7$ is responsible for this change. On the other hand the temperature dependence of $T_{1\rho}$ in deuterated $(NH_4)_2Cr_2O_7$ shows minimum values between 313K and 299K. The minimum values of $T_{1\rho}$ observed in ammonium perchlorate and in ammonium dichromate by the same author [18] are about 10^5 times larger than the theoretical predictions, suggesting that the origin of the $(T_{1\rho})_{min}$ can be understood as the effect of dipolar interaction between protons (^1H) of ammonium ions and ^{17}O of the anions. Further, the large anions will re-orientate about the symmetrical axes and then modulate the dipolar interaction between ^1H and ^{17}O causing the corresponding decrease in the values of $T_{1\rho}$. Eventhough Morimoto [18] studied the spin lattice relaxation times in pure and deuterated $(NH_4)_2Cr_2O_7$ in the temperature range 80K to 400K, no anomalous change has been observed in T_1 as well as in $T_{1\rho}$ values of these species at the

transition points reported earlier from specific heat and differential thermal analysis investigations. Moreover, no attempt has hitherto been done to investigate the electrical properties of this material as a function of temperature.

In the present chapter a detailed investigation carried out in single crystals of pure and SO_4^{2-} doped $(NH_4)_2Cr_2O_7$ along c-axis in the temperature range 80K to 435K using dc and ac electrical conductivity, dielectric constant, ionic thermocurrent and differential scanning calorimetric studies is presented.

6.2 EXPERIMENTAL DETAILS

The method suggested by Kozlova et al. [19] to grow single crystals of $(NH_4)_2Cr_2O_7$ from solution by lowering the temperature of the aqueous solution near 24° from 53°C could not produce good transparent single crystals of suitable dimensions for the electrical measurements. We have used the method of slow evaporation to grow single crystals of this materials. The starting material after three times recrystallization using triply distilled water is used for the growth process. The saturated solution of the recrystallized material is kept in a constant

temperature water bath at 36°C. After three to four weeks large transparent single crystals of $(NH_4)_2Cr_2O_7$ will be obtained. SO_4^{2-} doped single crystals of $(NH_4)_2Cr_2O_7$ were prepared by adding appropriate amounts of $(NH_4)_2SO_4$ into the solution containing the pure material. The specimen used for the electrical measurements were prepared by cutting slices from large single crystals with typical dimensions 5x5x1 mm^3 and by polishing it with zero grade emery and ground glass. Electrical contacts were made using aluminium electrodes evaporated on to the broad faces of the specimen parallel to (001) faces of the specimen. The electrical measurements were carried out in the cell with the normal procedures described in chapter II. The DSC studies were made in a Perkin Elmer Delta Series DSC7 calorimeter with a heating rate of 10°C/m in the temperature range 100K to 300K.

6.3 EXPERIMENTAL RESULTS

6.3.1 DC electrical conductivity measurements of pure and doped $(NH_4)_2Cr_2O_7$

The dc electrical conductivity measurements carried out in single crystals of pure and doped specimens of $(NH_4)_2Cr_2O_7$ along c-axis in the temperature range 80K to 435K are shown in figure 6.3a. The results obtained were found to be very well reproducible for different samples

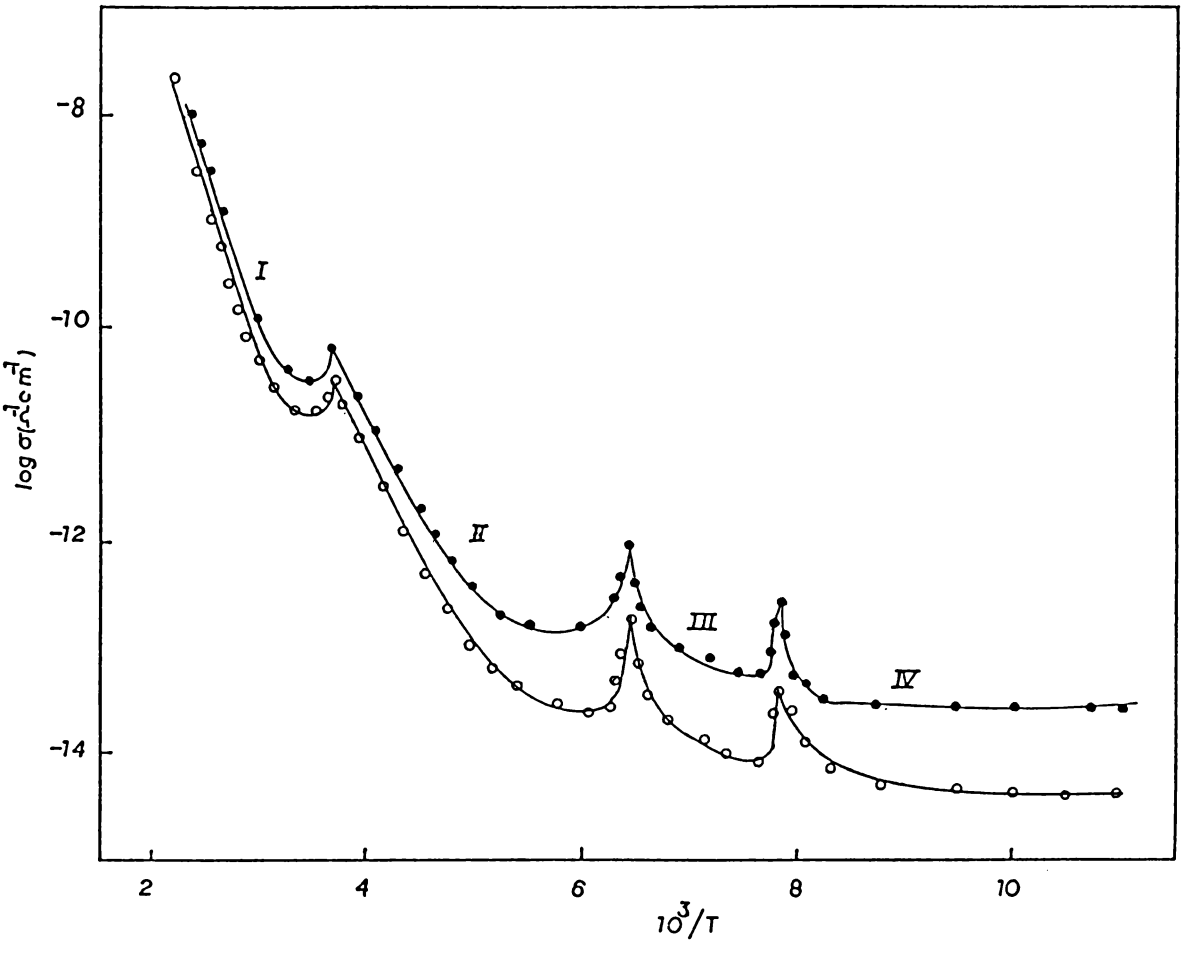

Figure 6.3a. Log σ vs $10^3/T$ plot for ammonium dichromate crystals. (1)—●—●— pure, (2) —O—O—O— SO_4^{2-} doped.

as well as for different heating and cooling cycles. The $\log\sigma$ vs $10^3/T$ plot obtained for pure and doped specimens of ammonium dichromate shows three distinct Λ-shaped peaks at temperatures 128, 156 and 269K respectively. These anomalous changes in the conductivity plot divides the entire temperature range into four distinct straight line regions (Let us denote these regions as I, II, III and IV in the decreasing order of temperature). The transitions observed in pure $(NH_4)_2Cr_2O_7$ at 128 and 156K are quite abrupt and there is an enormous increase in conductivity observed at these points. Here the magnitude of the conductivity rises to more than one order, while the peak observed at 269K is less sharp and the increase in conductivity is about one order of magnitude. It is observed that for slower rate of variation of temperature the peaks are found to be sharper. No measurable thermal hysteresis has been observed in the transition regions. The activation energy values obtained from the straight line regions are 0.72, 0.34 and 0.08 eV respectively, for phases I, II and III in pure $(NH_4)_2Cr_2O_7$ (Since the IV phase does not yield measurable slope, no activation energy calculation has been done).

In the higher temperature region the conductivity plots for both pure and SO_4^{2-} doped specimens merge

together which indicates that the same electrical conduction process are operative in both these materials. However, in the lower temperature region the conductivity of SO_4 doped specimens is approximately one order of magnitude less compared to that in pure $(NH_4)_2Cr_2O_7$. No shift in the transition temperatures were observed in doped specimens in the range of doping concentrations used here. The activation energy values obtained in the case of SO_4^{2-} doped specimens of $(NH_4)_2Cr_2O_7$ are 0.73, 0.37 and 0.085 eV respectively for first three phases.

6.3.2 AC electrical conductivity measurements in pure and doped $(NH_4)_2Cr_2O_7$

The ac electrical conductivity measurements carried out in pure and SO_4^{2-} doped specimens of $(NH_4)_2Cr_2O_7$ at 90 Hz in the temperature range 80K to 435K is shown in figure 6.3b. The $\log\sigma$ vs $10^3/T$ plot shows three distinct variations at temperatures 128, 156 and 269K respectively in both pure and doped $(NH_4)_2Cr_2O_7$ crystals. The magnitude of conductivity in the SO_4^{2-} doped specimens is found to be less compared to that in pure material. However, the magnitude of ac conductivity is about one order of magnitude higher than that of the corresponding dc conductivity value in the whole temperature range studied here.

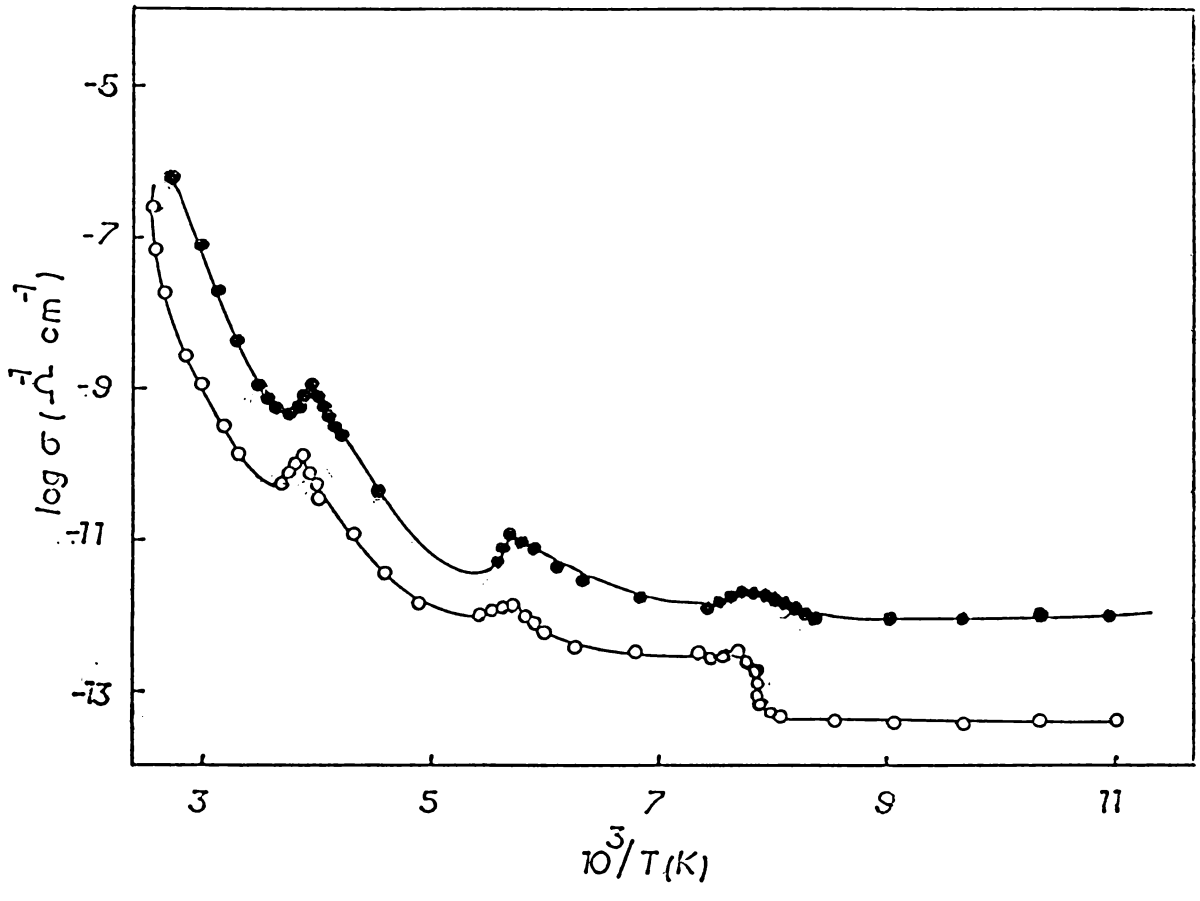

Figure 6.3b. Log σ vs $10^3/T$ plot for pure (—●—●—) and SO_4^{2-} doped (—o—o—o—) specimen from ac conductivity measurements.

6.3.3 Dielectric measurements

The dielectric constant measurements carried out in single crystals of pure ammonium dichromate along c-axis at 1 kHz in the temperature range 80K to 300K is shown in figure 6.3c. The plot gives anomalous variations exactly at the same temperatures where the dc and ac conductivity anomalies occur viz., 128, 156 and 269K. The dielectric constant increases gradually from 5.2 at 80K and reaches a maximum value of 10.1 at 128K and decrease thereafter as the temperature increases and attains another maximum of 16.25 at 156K. As the temperature increases the dielectric constant decreases and remains constant at 6.2 upto 200K and then slowly increases and attains a third maximum (12.8) forming a $\wedge$-shaped dielectric anomaly at 269K. On further increase in temperature the dielectric constant slowly increases and attains a value about 12.5 at room temperature. On the cooling cycle no appreciable deviation was observed in dielectric values from that obtained in the heating runs and hence it is not shown in figure 6.3c. Also, the dielectric constant values obtained for 0.1 mole % SO_4^{2-} doped specimens of $(NH_4)_2Cr_2O_7$ do not deviate much from the values obtained for pure $(NH_4)_2Cr_2O_7$ and hence they are not in the figure 6.3c.

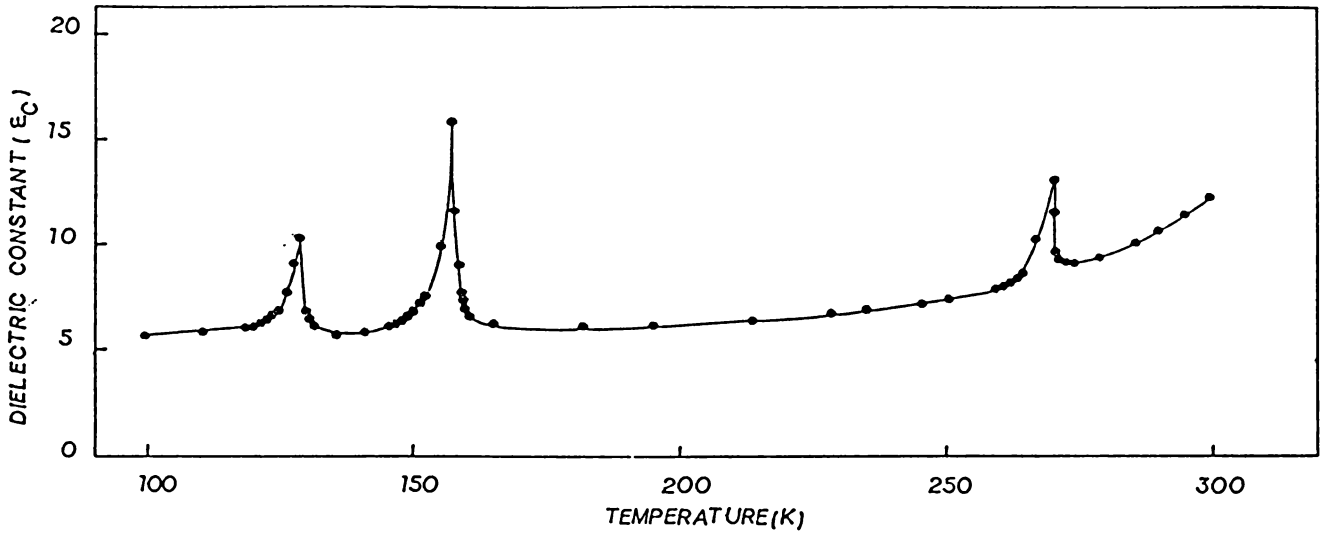

Figure 6.3c. ε_c vs T plot for pure ammonium dichromate crystal.

6.3.4 Ionic thermocurrent measurements

The ionic thermocurrent measurements carried out in single crystals of pure $(NH_4)_2Cr_2O_7$ by polarising the specimens at 300K with a field of 3 KV/cm for 5 minutes are shown in figure 6.3d. The ITC spectrum obtained with a heating rate of 0.07 K/sec shows three distinct current peaks at temperatures 130, 159.5 and 271K. Let these peaks be denoted as A, B and C in the increasing order of temperature. The height of the peak B is twice that of A while peak C is approximately the same magnitude as that of peak A. The peaks A and B are quite sharp whereas the peak C is fairly broad. The height of the current peak is found to be slightly increased with increase in the poling field. However no change in magnitude has been observed for these peaks with the change in poling temperature and poling time.

6.3.5 Differential scanning calorimetric studies

Figure 6.3e shows the DSC spectrum recorded for pure $(NH_4)_2Cr_2O_7$ in the temperature range 100K to 300K with a heating rate of 10°C/m. The spectrum obtained shows three distinct variations in the heat flow at temperatures close to the point where earlier electrical and dielectric anomalies were observed.

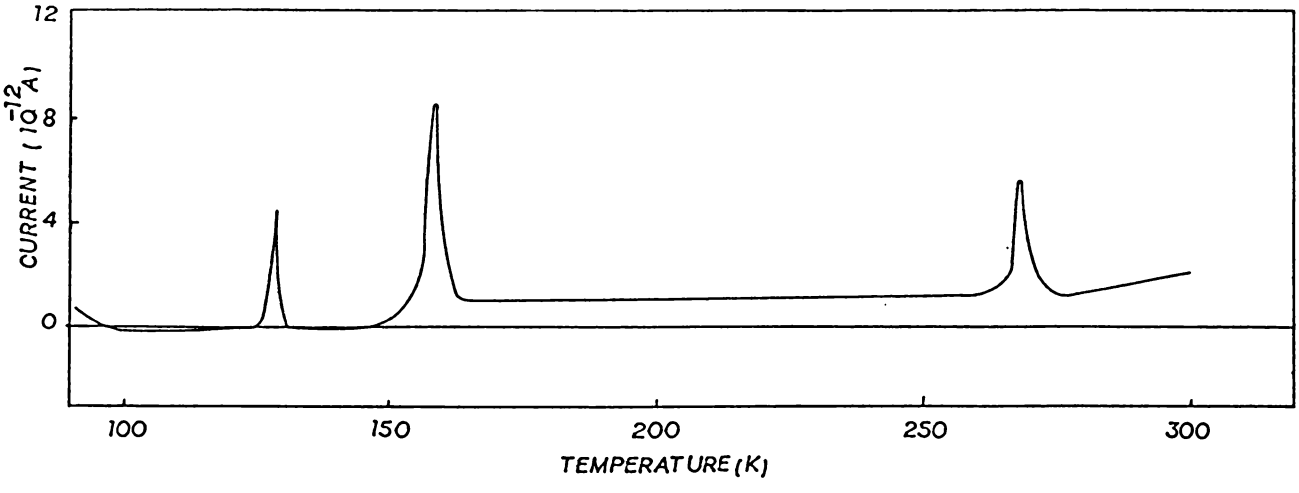

Figure 6.3d. Ionic thermocurrent spectrum obtained for pure ammonium dichromate crystal.

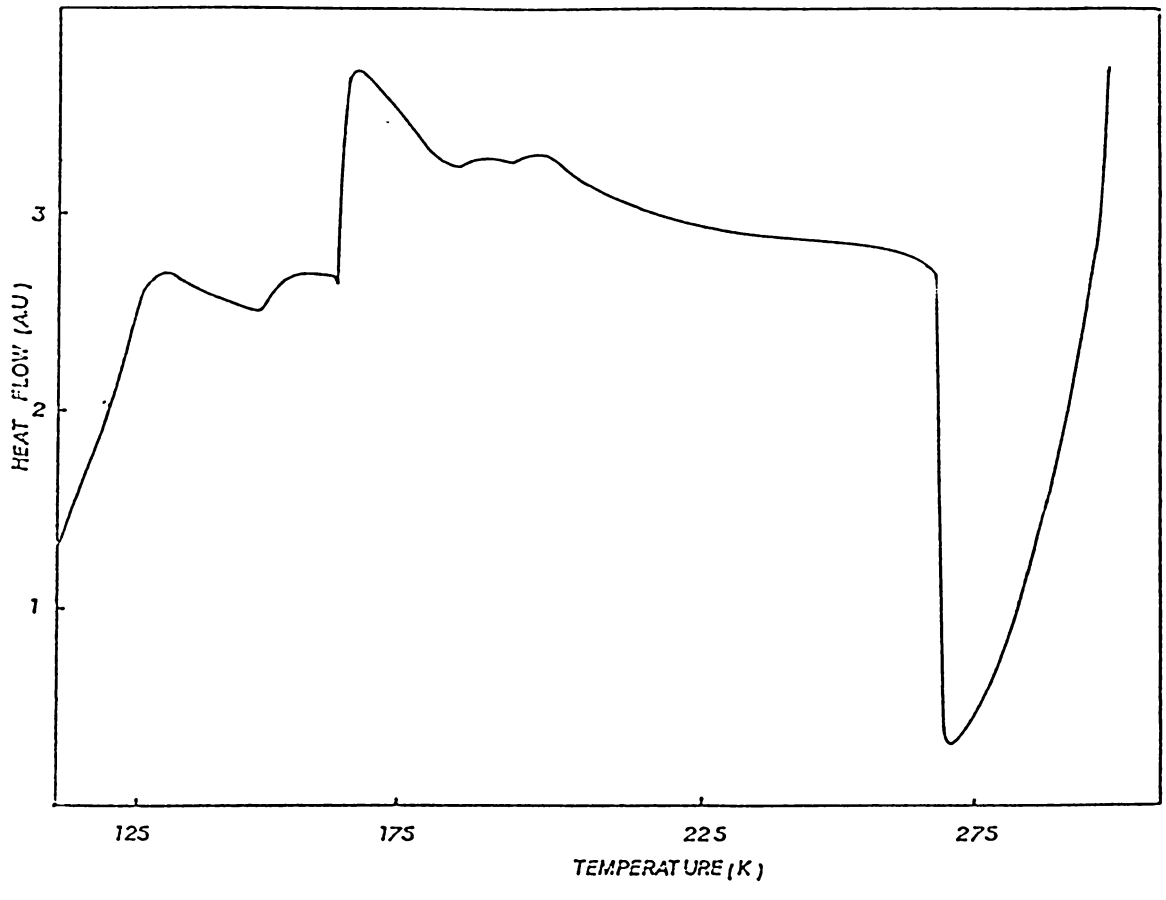

Figure 6.3e. DSC spectrum of ammonium dichromate material.

6.4 DISCUSSION

The results obtained for pure and doped $(NH_4)_2Cr_2O_7$ from various experimental techniques employed, it is clear that this material undergoes three anomalous variations at temperatures 128, 156 and 269K. Also there exists complete agreement between the dc and ac conductivity measurements and dielectric measurements as far as the temperature corresponding to the anomalous variations are concerned. The shift in the temperatures in ITC and DSC measurements is probably due to the higher heating rates employed in these measurements. Though the experimental results obtained for $(NH_4)_2Cr_2O_7$ from the present investigations are in complete agreement with results reported by Jaffray [17] from DTA and specific heat measurements and Schuttle and Heyns from infrared studies [16], no correlation has been observed from the results of NMR spin lattice relaxation time measurements [18]. Again, these earlier results could not explain the origin of the observed anomalous variations in these materials occurring at different temperatures. The transitions observed at the lower temperatures can in fact, be explained by considering the nature of hydrogen bonding in this material.

The structure of $(NH_4)_2Cr_2O_7$ is monoclinic with space group C_{2h}^3 or C_{2h}^6 according to Gossner and Mussgnug [20]. The determination of the unit cell parameters from

powder photographs (Cr-K radiation, λ_a = 2.2909 Å) gives the following cell dimensions agreeing well with Gossner's and Mussgnug's values: a = 13.26 Å, b = 7.54 Å, c = 7.74 Å and β = 93.2° with four formula units in the unit cell. The crystal structure of $(NH_4)_2Cr_2O_7$ is shown in figure 6.4a. The chromium atoms are surrounded by four oxygen atoms, situated at the corners of a distorted tetrahedron. The Cr_2O_7 group is formed by the sharing of one corner oxygen atom by the two distorted tetrahedra. The Cr-O_4-Cr angle is 115° and the Cr-Cr distance in the bridge is 3.2 Å. The Cr-Cr distances between different Cr_2O_7 groups are much longer being 4.8 Å. The stable arrangement of the $Cr_2O_7^{2-}$ group, consists of two Cr atoms and the shared oxygen atoms. The strong distortion of the dichromate group in the material is considered as due to the formation of strong N-H-O bonds but the accuracy of the NH_4-O (or rather N-O) distances is so low that it is not possible to decide whether this explanation is likely to be true or not. It is highly probable that the NH_4 tetrahedra in $(NH_4)_2Cr_2O_7$ also are highly distorted to give distinct orientations at lower temperatures where the lattice is found to be more rigid as in the case of $(NH_4)_2SO_4$ [21] and $(NH_4)_2HPO_4$ [22].

As observed in the infrared studies, the spectra obtained below 268K phase transition point differs very little

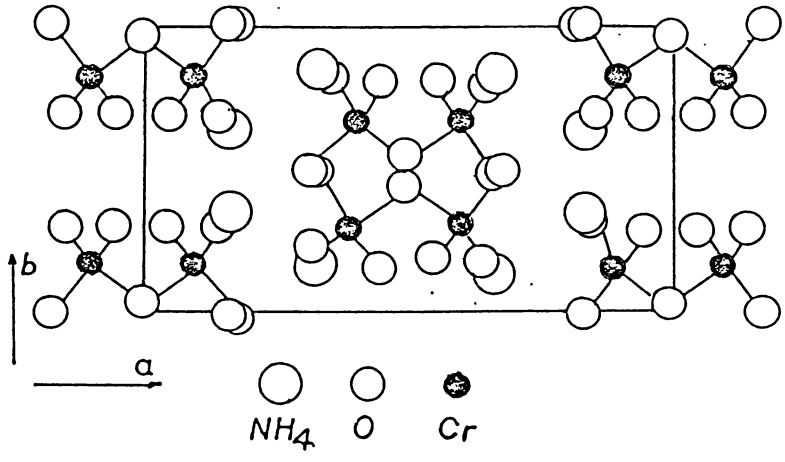

Figure 6.4a. The crystal structure of ammonium dichromate viewed along c-axis.

from that obtained at room temperature. When temperature is varied, a very broad band develops gradually in the region 1750 cm^{-1} and 1600 cm^{-1} and it splits into two weak broad bands at 1720 cm^{-1} and 1650 cm^{-1} below this transition point. It is also observed that the ν_4 band of the NH_4 ion also becomes more assymetric on the high frequency side as the temperature decreases below 268K. On further decrease in temperature below 155K just below the second phase transition a definite shoulder appears in the infrared spectrum at 1430 cm^{-1} (ν_{4a}) and a change in intensities of the $Cr_2O_7^{2-}$ bands is observed. As the temperature decreases below the phase transition point at 128K, the 875 cm^{-1} band of the Cr_2O_7 ions is split into two components at 868 cm^{-1} and 878 cm^{-1} and abrupt changes occur in the intensities of some of the $Cr_2O_7^{2-}$ absorptions. From these experimental results it is concluded that NH_4^+ begins to execute free rotations (as observed in NH_4I [23]) at and above 128K. At lower temperatures because of the hindrance to the rotational motion and change in the torsional mode different variety of orientations are taking place. The distorted NH_4 ions are expected to possess a significant electric dipolemoment. The high value of dielectric constant observed at temperatures 128, 156 and 269K can be attributed to the dipolar contribution to dielectric constant of $(NH_4)_2Cr_2O_7$ as a result of motional effect of NH_4^+ ions. This is in accordance with the results of NMR investigations. Similar effects

have been found to occur in ammonium sulphate [24], diammonium hydrogen phosphate [22] and in ammonium dihydrogen phosphate [25]. A detailed study of NMR measurements and low temperature structural studies preferably with neutron diffraction will be required to get a better understanding of the nature of reorientation of the various ion groups in this material.

As already discussed in chapter III the mechanism of electrical conduction in the material can also be explained by considering the nature of defect phenomena generally observed in crystals containing ammonium groups. In crystals containing ammonium groups, the types of defects usually observed are normal ionic, electronic and protonic defects. The contribution to the electrical conductivity by the NH_4^+ and $Cr_2O_7^{2-}$ group and their vacancies can be neglected in considerations based on their sizes.

From the experimental results obtained for pure and doped material, it has been suggested that the conduction mechanism in the region is predominantly due to the cation vacancies created by thermal generation of the detached ammonium groups in this material or due to the generation of protonic defects. The activation energy values obtained in the phase I, for pure and doped material clearly show that

electrical conduction mechanisms are responsible in this region for both kind of crystals.

The lower value of conductivity observed in the case of SO_4^{2-} doped specimens of $(NH_4)_2Cr_2O_7$ can be explained by considering the nature and role of SO_4^{2-} ions in the $(NH_4)_2Cr_2O_7$ lattice. When a divalent anionic impurity is substituted in an ionic crystal like $(NH_4)_2Cr_2O_7$, the charge compensation is generally accomplished by the creation of anionic vacancies in the host lattice. Since in the $(NH_4)_2Cr_2O_7$ lattice, the size of the anions are fairly large compared with that of the impurity ions, the probability of the migration of interstitials as well as vacancies is less likely. Therefore, the SO_4^{2-} ions form complexes with only the mobile ions viz., hydrogen associated with the NH_4^+ groups in $(NH_4)_2Cr_2O_7$. Complexes thus formed are predominantly HSO_4^- ions which have lesser mobility. Thus it is clear that the reduction in the magnitude of conductivity at lower phases can be due to the formation of these complexes provided the dominant mechanism of electrical conduction is by migration of interstitial hydrogen ions. The experimental results reveal that the above mechanism is operative in phases II and III causing a significant reduction in the magnitude of conductivity compared to that in pure $(NH_4)_2Cr_2O_7$. At fairly high temperatures probably the dissociation of these complexes can also affect

the electrical conduction process in this material and in this region one can hence expect a higher value for σ.

As already indicated $(NH_4)_2Cr_2O_7$ undergoes phase transitions at different temperatures due to free rotation and hindered rotations of the NH_4 ions. This gives rise to free charge carriers, causing a corresponding peaks in the ITC spectrum. Thus the observed peaks in the ITC spectrum attributed to the space-charge formation at the phase transition points. As these peaks are rather sharp they are not likely to be due to reorientation of any I-V dipoles. This result is a further confirmation that ITC measurement is a sensitive technique for the detection of a phase transition in solid.

6.5 CONCLUSIONS

The dc and ac conductivity, dielectric constant ionic thermocurrent and DSC studies carried out in single crystals of pure and doped $(NH_4)_2Cr_2O_7$ along c-axis in the temperature range 80K to 435K give the following conclusions.

1. The dc and ac electrical conductivity and dielectric constant measurement show anomalous variations at temperatures 128, 156 and 269K corresponding to three phase transitions.

A small shift in transition temperatures were observed in the ionic thermocurrent and DSC studies.

2. The shift in the transition temperatures observed in ITC and DSC studies could be due to the higher heating rates employed in these techniques.

3. The transition observed in this material at different temperatures could be due to free rotation, reorientation and hindered internal rotation of the NH_4 groups in these materials.

4. The activation energy values obtained in phase I in both pure and doped $(NH_4)_2Cr_2O_7$ indicate that the electrical conduction mechanism in this region is predominantly due to protons.

5. The higher magnitude of conductivity observed in ac measurements compared to that in dc measurements is probably due to the additional component of polarization current in the ac measurements.

6. The activation energy values obtained from the straight line regions of the phases I, II and III are 0.72, 0.34 and 0.08 and 0.73, 0.37 and 0.08 respectively for pure and doped $(NH_4)_2Cr_2O_7$.

6.6 REFERENCES

[1] H.S.Gutowsty, G.E.Pake and R.Behrson, J.Chem.Phys. 22 (1954) 643.

[2] W.Guttler and J.V.von Schutz, Chem.Phys.Wett, 20 (1973) 133.

[3] J.E.Tuohi, E.E.Ylinen and M.Punkkinen, Phys.Ser. 13 (1976) 253.

[4] R.L.Armstrong, J.A.J.Lourens and K.R.Jaffrey, J.Mag.Res. 23 (1976) 115.

[5] I.Svare, J.Phys.C:Solid State Phys. 10 (1977) 4137.

[6] K.Shimomura, Y.Yoshida, A.Sanjoh and H.Negita, Phys.Lett. 81A (1981) 189.

[7] R.E.Code, J.Higinbothan and A.R.Sharp, Can.J.Phys. 54 (1976) 239.

[8] A.Watton, E.C.Reynhardt and H.E.Petch, J.Chem.Phys. 65 (1976) 4370.

[9] R.E.Richards and T.Schaefer, Trans.Faraday Soc. 57 (1961) 210.

[10] J.J.Rush, T.I.Taylor and W.W.Havens Jr., J.Chem.Phys. 35 (1961) 2265.

[11] J.J.Rush, T.I.Taylor and W.W.Havens.Jr., J.Chem.Phys. 37 (1962) 234.

[12] F.A.Miller and C.H.Wilkins, Anal.Chem. 24 (1952) 1253.

[13] F.A.Miller, G.L.Carlson, F.F.Bentlay and W.H.Jones, Spectrochim. Acta. 16 (1960) 135.

[14] H.Stammreich, D.Bassi, O.Sala and H.Siebert, Spectrochim. Acta. 13 (1958) 192.

[15] J.A.Campbell, Spectrochim.Acta. 21 (1965) 1333.

[16] C.J.H.Schutte and A.M.Heyns, Chem.Phys.Lett. 1 (1967) 487.

[17] J.Jaffray, Compt.Rend. 241 (1955) 1114.

[18] K.Morimoto, Solid State Commun. 49 (1984) 1169.

[19] O.G.Kozlova, Yu.A.Kharitonov and Academician N.V.Belov, Sov.Phys.Dokl. 24(7) (1979) 509.

[20] B.Gossner and F.Mussgnug, Z.Krist. 72 (1930) 476.

[21] U.Syamaprasad and C.P.G.Vallabhan, Solid State Commun. 38 (1981) 555.

[22] R.Navil Kumar and C.P.G.Vallabhan, J.Phys:Condensed Matter (in press).

[23] W.Vedder, "The Infrared Absorption Spectrum of the Ammonium Ion in Lattices of NaCl Type", Thesis, University of Amsterdam, 1958.

[24] U.Syamaprasad and C.P.G.Vallabhan, J.Phys.C:Solid State Physics, **14** (1981) L865.

[25] V.K.Subhadra, U.Syamaprasad and C.P.G.Vallabhan, J.Appl. Phys. **54** (1983) 2593.

Chapter VII

PHOTOACOUSTIC STUDIES ON PHASE TRANSITIONS IN $(NH_4)_2\ Cr_2O_7$ AND $NH_4H_2PO_4$

Abstract

The design and fabrication of a resonant photoacoustic cell for the amplitude and phase measurements of photoacoustic signal over a wide temperature range is described. With this set up the sample can be cooled down to 80K without affecting the microphone performance. The cell calibration procedures have been evolved and the performance of the cell has been evaluated. The feasibility and sensitivity of this photoacoustic system for the in situ studies of phase transitions in solids have been demonstrated by carrying out PA investigations in $(NH_4)_2Cr_2O_7$ and in $NH_4H_2PO_4$ as a function of temperature.

7.1 INTRODUCTION

The photoacoustic or optoacoustic effect was discovered by Alexander Graham Bell in 1890 [1-3]. He found that a periodically interrupted light beam impinging on a solid generates a sound wave in the gas above the solid. This generated a flurry of activity for a year or so which included work by Tyndall [4,5], Rontgen [6] and Lord Rayleigh [7]. The field was dormant until 1938 when Veingerov [8] in Russia made a spectrophone for the study of gases. This work was generally ignored until after world war II, when some sporadic gas studies were made. With the technical developments of sensitive electret condenser microphones, intense laser light sources, and commercial lock-in amplifiers, it became possible to build viable PA spectrometers. Kreuzer [9,10] used photoacoustic methods to detect trace pollutants in gases. Harshbarger and Robin [11] review much of the gas phase work. In recent times Rosencwaig [12,13] was the first to apply photoacoustic spectroscopy (PAS) to solids. A number of review articles has covered subsequent work [14-18] in this area.

Several theoretical models have been developed to explain the photoacoustic signal observed from solids. The first was by Parker [19] which was later given further refinements [20]. Next Rosencwaig and Gersho [21] presented the

most widely used theory which assumes that the PA signal is generated solely by periodic heat flow from the sample to the gas. Bennett and Forman [22] gave a theory for nearly transparent sample based on linearised hydrodynamic equations which included both acoustic and thermal diffusion terms. Bennett claims that the acoustic term is dominant in the intermediate frequency range which is the one currently encountered experimentally. McDonald and Wetsel [23] have extended the Rosencwaig-Gersho theory to include mechanical vibration of the sample. This is particularly important for liquid samples. They present three versions of the theory. The complete coupled equations for acoustic wave motion and thermal diffusion are presented and solved numerically. Since each is based on somewhat different assumptions and conditions the philosophy of this work has been to insert relevant parameters into computer programs which calculate the photoacoustic (PA) signal based on each theory and compare the results with experiment. These computer programs calculate the theoretical PA signal amplitude and phase with respect to the lock-in amplifier reference signal as a function of chopping frequency.

Since the generation and propagation of thermal wave in a sample depend critically on the thermoelastic

and other physical properties, a detailed analysis of the amplitude and phase of the PA signal enables one the determination of properties like thermal diffusivity, specific heat, thermal conductivity and phase transitions. This ensures the possibility to carry out non-destructive testing of samples which possess defects. Since the PA signal is determined by the characteristics of thermal propagation within the sample, it is possible to evaluate the thermal properties of a sample with great accuracy [24,25]. Also, the study of thermal wave propagation through the various layers of the sample provides the values of thermal properties of the sample in a non-destructive fashion. Using PA technique, thermal diffusivities of glass, metals and various polymer samples have been determined precisely and such measurements provide the absolute values of thermal diffusivity of samples as a function of temperature. Since, the thermal parameters of a material generally vary when the material undergoes phase transition, monitoring the PA signal as a function of temperature should provide information on the occurrence and characteristics of phase transitions. This method has been recently revived as a very useful technique for the spectroscopic investigation of samples where conventional optical absorption and reflection spectroscopy cannot be used. The first attempt to

study phase transition employing the PA effect was by Florian et al. [26] who studied first order phase transitions. Although there have been a number of papers [27-30] on this topic, a quantitative evaluation in terms of the predictions of the Rosencwaig-Gersho theory has been attempted only in certain specific cases.

In the present chapter, a detailed description of a resonant photoacoustic cell designed and fabricated for the temperature varying studies and phase transitions in solids have been presented. We also describe the complete characterisation of the cell by using a thin layer of carbon black which has well known thermal properties. By exploring the dependence of photoacoustic signal on the thermal properties of the sample, we demonstrate experimentally the usefulness of the photoacoustic effect for investigating phase transitions in solids. Specific studies have been made in the case of $(NH_4)_2Cr_2O_7$ and $NH_4H_2PO_4$ single crystals.

7.2 EXPERIMENTAL DETAILS

7.2.1 Photoacoustic cell for phase transition studies

The two type of cell designs has principally been used in photoacoustic spectroscopy. They are (1) Resonant cell, and (2) Non-resonant cell.

In the present photoacoustic system which is a Helmholtz resonant cell [31], the microphone is separated from the sample chamber by a long narrow tube. Such a cell shows acoustic resonances at frequencies which are well within the frequency range used in photoacoustic experiments. This type of PA cells are very convenient for use in temperature varying studies. On the other hand, in the non-resonant photoacoustic cell the microphone is located in close proximity of the sample [31]. To reduce the spurious signals it is protected from direct illumination. Non-resonant cells are operated at frequencies much below that of the cell cavity. The frequency response of these cells most closely follows the predictions of the Rosencwaig-Gersho theoretical model [21].

The resonant photoacoustic cell described here has been constructed with a view to get high sensitivity and to expand the operating ranges for temperature and frequency specifically for the study of phase transition in solids.

A schematic diagram of the low temperature photoacoustic cell is shown in figure 7.2a. The whole PA cell is kept within a main chamber. This main chamber enclosing the photoacoustic cell has the same form as that of the

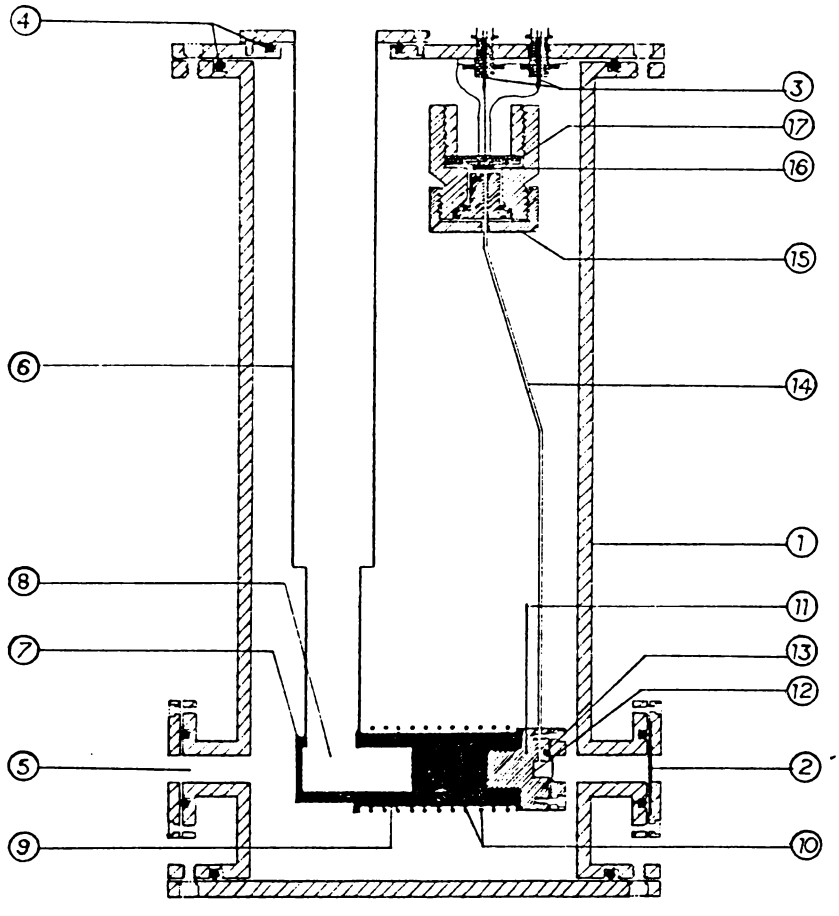

1. MS OUTER CHAMBER
2. GLASS WINDOW
3. BNC
4. NEOPRINE O-RINGS
5. TO VACUUM PUMP
6. SS TUBE
7. COPPER BLOCK
8. LN_2 CAVITY
9. MICA INSULATION
10. HEATER WINDINGS
11. SS PA CELL
12. SAMPLE CHAMBER
13. INDIUM O-RINGS
14. SS PIPE
15. MICROPHONE ASSEMBLY
16. MICROPHONE
17. EBONITE MICROPHONE HOLDER

Figure 7.2a. Schematic diagram of low temperature photoacoustic cell.

chamber used for the study of electrical properties as discussed in chapter II. This chamber is sealed by two MS flanges fixed at the top and bottom by using neoprene O-rings. Four window ports are provided to the main chamber for the following uses.

1. For connecting rotary pump for evacuating the chamber to minimise the background noise level and to avoid the condensation of moisture on the window adjacent to the sample.

2. To let in the light beams for the optical excitation of the sample for the photoacoustic measurements.

3. To observe whether the sample is undergoing any physical changes (such as cracking) with the temperature.

The samsple is kept in a cylindrical cavity of inner diameter 7 mm and depth 7 mm and made out of copper which is chrome plated. This cavity is sealed onto the cell body with a copper flange using indium O-ring. The copper flange is provided with a highly polished circular glass plate which is fixed on to it using Araldite. The sample is maintained in the cavity by inserting a concentric

SS hollow cylinder with a transverse opening which is directed towards the microphone chamber. The rear side of the sample cavity is threaded and it is screwed to a cold finger provided with heater windings (60W) used for heating the sample. The cold finger is permanently joined to an SS tube through an L-joint such that the sample cavity is pointed towards one of the window ports. The length of the SS tube is adjusted such that the centre of the sample cavity is on the axis of the window ports. The top end of the SS tube is permanently fixed to an MS flange which is vacuum sealed to the top flange of the main chamber using neoprene O-ring and allen screws. The temperature of the sample is monitored by inserting a chromel alumel thermocouple on the rear side of the sample cavity by drilling 1 mm bore on the PA cell assembly. The tube which connects the sample chamber and the microphone chamber is made out of stainless steel and has a bore of 1 mm and a length of 19 cm. The microphone is mounted on the top of the microphone chamber and the assembly is attached to the top flange of the main chamber. The electrical connections to the heaters, thermocouples and, microphone biasing are made through teflon insulations fixed on the top of plate of the chamber. The PA signal is taken out using a BNC connector fixed on the top plate. A photograph of the PA cell thus fabricated is shown in figure 7.2b. The photoacoustic cell has the following advantages.

Figure 7.2b. Photograph of the photoacoustic cell.

1. The cell can be used for phase transition studies in the temperature range 80K to 350K.

2. Since the outer part of the PA cell assembly is evacuated the system is virtually immune to ambient noise level.

3. The liquid nitrogen consumption needed for cooling the sample to the low temperature (80K) is found to be very small for a single cycle of operation.

4. The major advantage of the PA cell is its simplicity of construction and extremely good temperature stability.

7.2.2 Calibration of the PA cell

The experimental set up used for the PA measurements is already shown in chapter II. For calibration of the cell 2 MW He-Ne laser was used as the light source. The laser beam was chopped by a mechanical chopper. An electret microphone together with a lock-in amplifier was used for the PA signal detection. The PA cell calibration was carried out with carbon black (prepared from soot) as the reference. The calibration of the PA cell has been done by measuring the photoacoustic amplitude and phase as a function of temperature or as function of chopping frequency at a constant temperature.

7.2.3 Preparation of the samples for photoacoustic investigation

The photoacoustic measurements on ammonium dichromate, were carried out with pressed powder samples obtained after three times recrystallisation whereas the measurements on ammonium dihydrogen phosphate were carried out with single crystals grown from solution . Disc shaped specimens of typical dimensions 7 mm diameter and thickness ranging from 0.1 mm to 1 mm were used for the photoacoustic measurements. A He-Ne laser (λ = 632.8 nm) of 10 mW power is used as the source of illumination.

7.3 EXPERIMENTAL RESULTS

7.3.1 Response characteristics of the cell

Figure 7.3a shows the dependence of the PA signal (both amplitude and phase) as a function of temperature, at a modulation frequency 70 Hz. It is observed that the amplitude of the PA signal increases with decrease in temperature whereas the phase increases with rise in temperature. Figure 7.3b shows the frequency response of the PA amplitudes at temperatures 100, 120, 200, 250 and 300K. The signal amplitude versus chopping frequency was measured in the frequency range 30-1000 Hz. The phase of the photoacoustic signal gets automatically adjusted to give the maximum amplitude where an autoranging lock-in amplifier

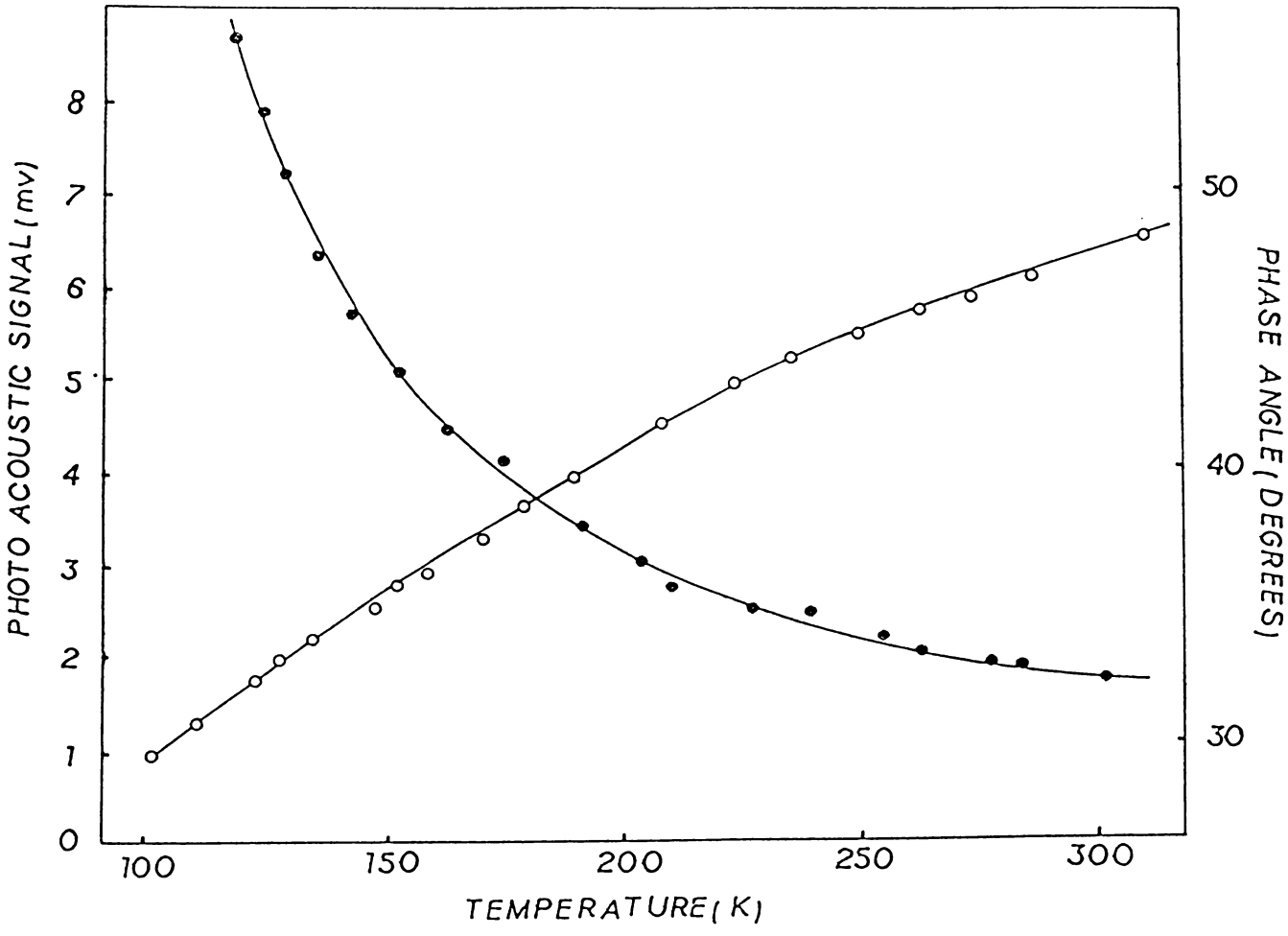

Figure 7.3a. Variation of photoacoustic signal as a function of temperature. (1) —●—●— amplitude, (2) —○—○—○— phase, f = 70 Hz.

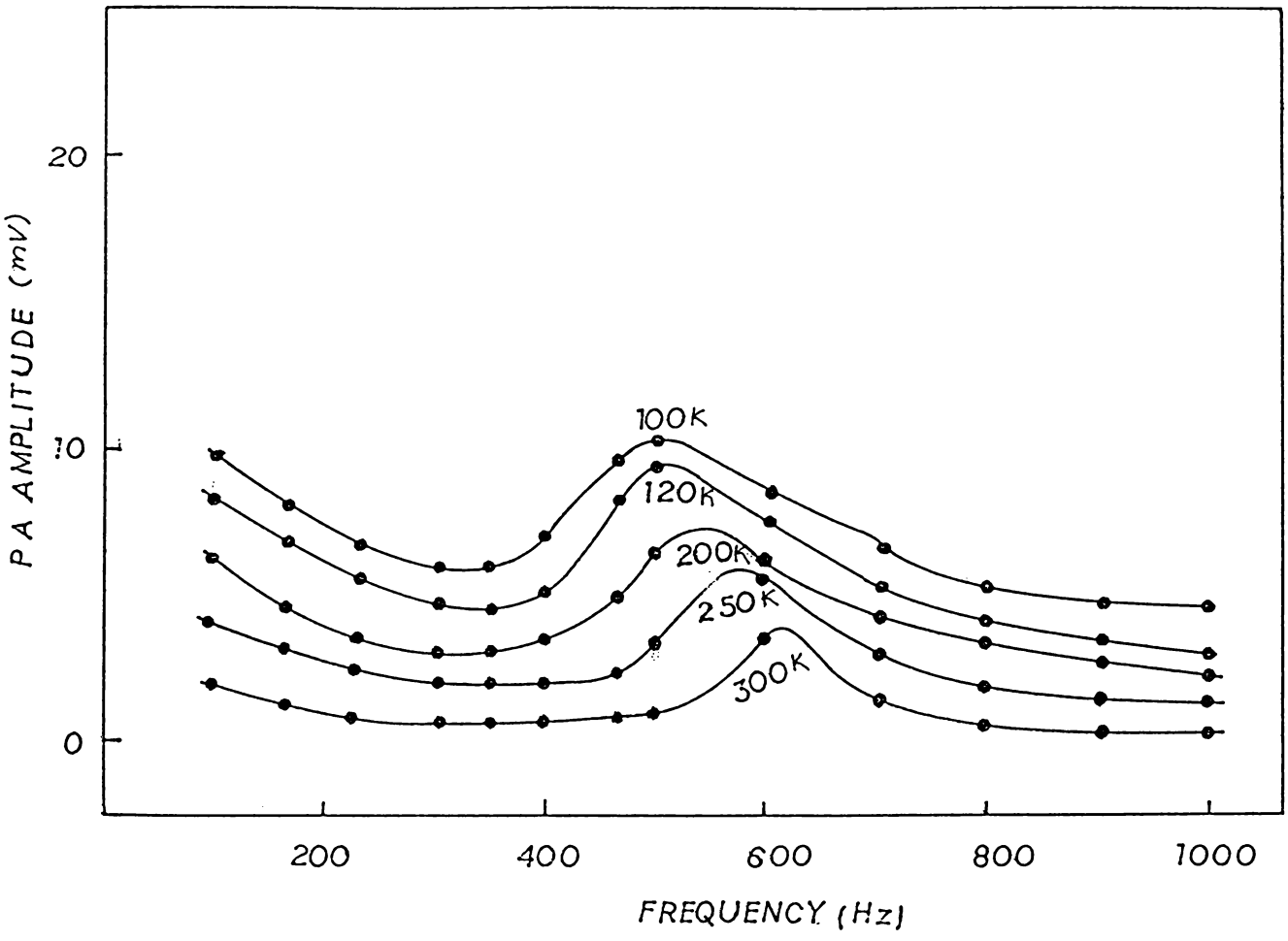

Figure 7.3b. Frequency response of photoacoustic amplitude at different temperatures.

(EG&G Model 5208) is used. It is observed that the frequency versus amplitude shows a resonant peak at 630 Hz. It is also observed that the resonant peak is shifted to the lower frequency values and a considerable enhancement of the photoacoustic signal occurs as the temperature decreases from 300K to 80K.

7.3.2 Photoacoustic measurements on $(NH_4)_2Cr_2O_7$ and $NH_4H_2PO_4$

The photoacoustic studies carried out in $(NH_4)_2Cr_2O_7$ pressed pellets in the temperature range 80K to 300K are shown in figure 7.3c. The recorded response obtained with a chopping frequency of 70 Hz (without adjusting the phase) shows three distinct anomalous variations in the photoacoustic amplitude at temperatures 128, 156 and 269K. The magnitude of the PA signal is found to be small for the variation at 268K and maximum for the variation at 156K. Figure 7.3d shows the variation of the phase angle with temperature. Here also, the photoacoustic phase shows three distinct variations around 128, 156 and 268K.

The PA measurement carried out in single crystals of $NH_4H_2PO_4$, the front surface(perpendicular to c-axis)of which was coated with carbon black,with a chopping frequency of 70 Hz

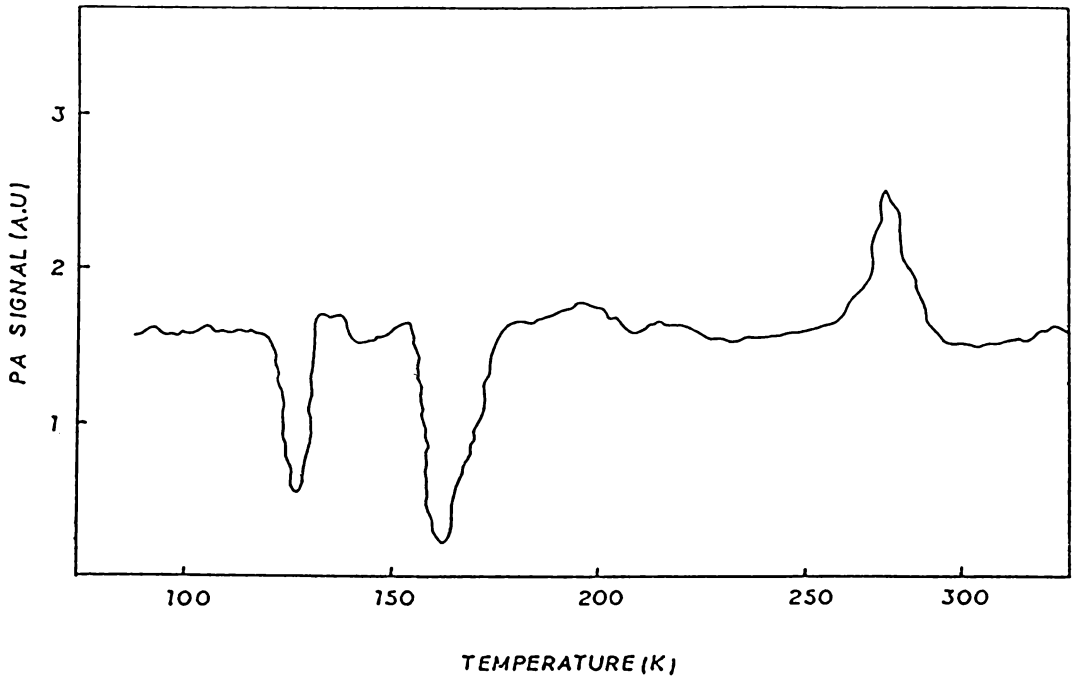

Figure 7.3c. Variation of photoacoustic signal (amplitude) as a function of temperature. f = 70 Hz.

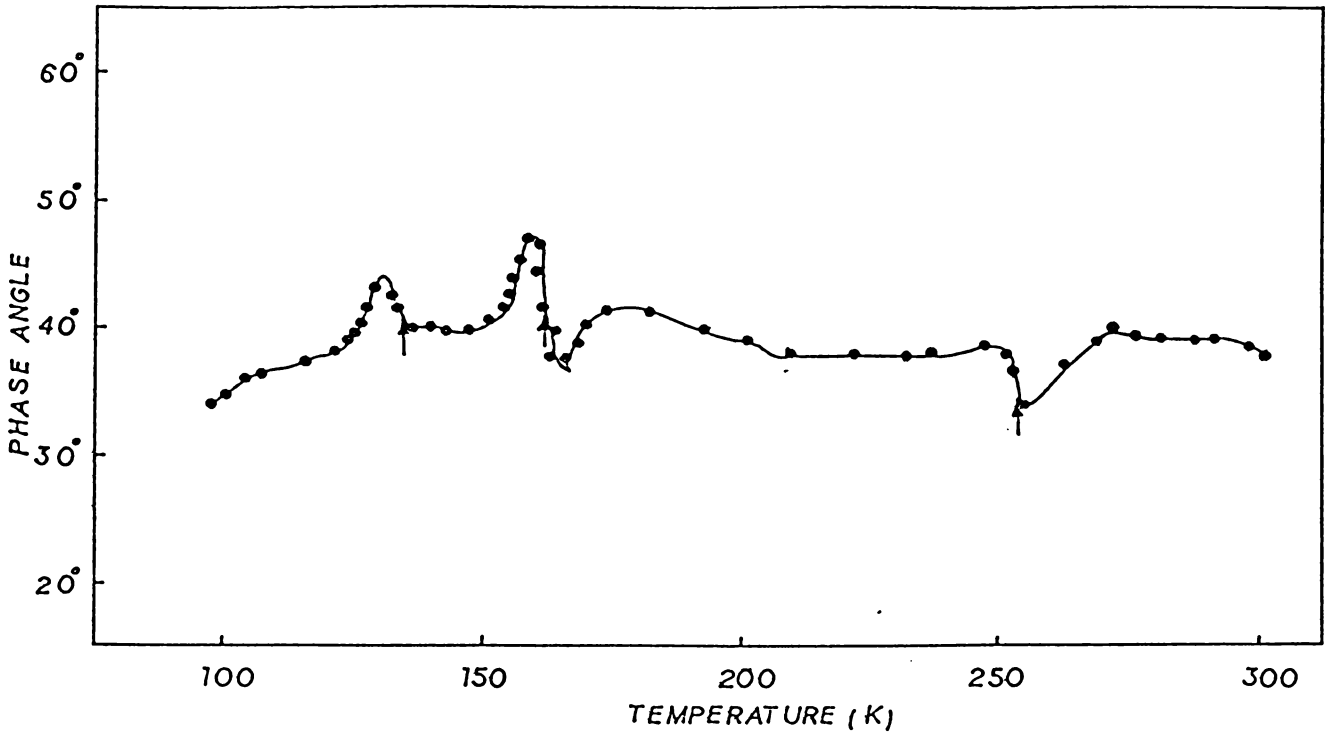

Figure 7.3d. Variation of photoacoustic phase as a function of temperature for ammonium dichromate material.

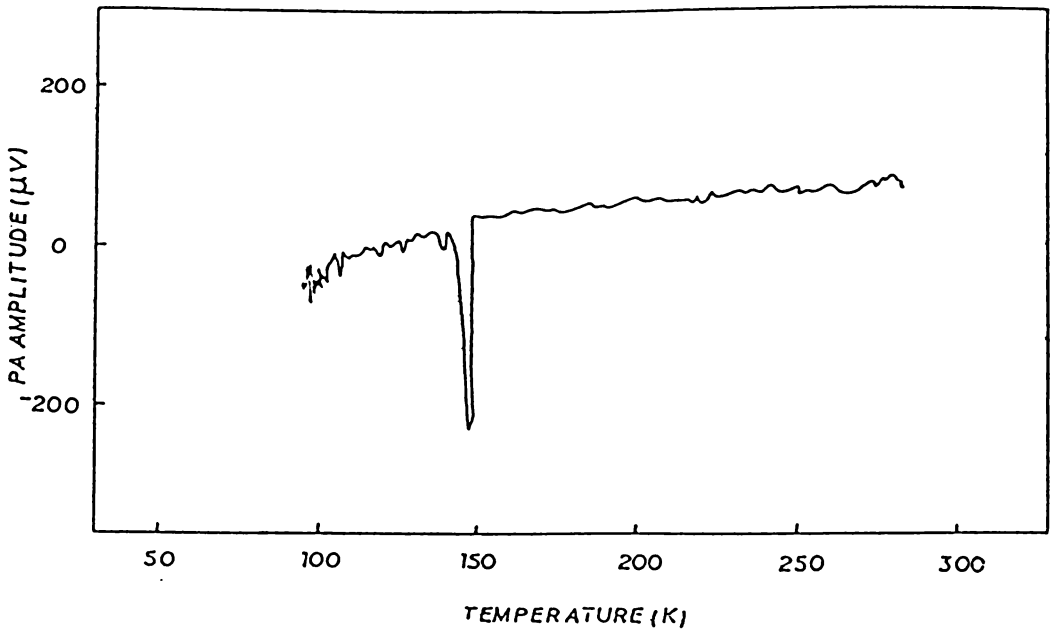

Figure 7.3e. Temperature dependence of photoacoustic signal (amplitude) of ammonium dihydrogen phosphate crystal. f = 70 Hz.

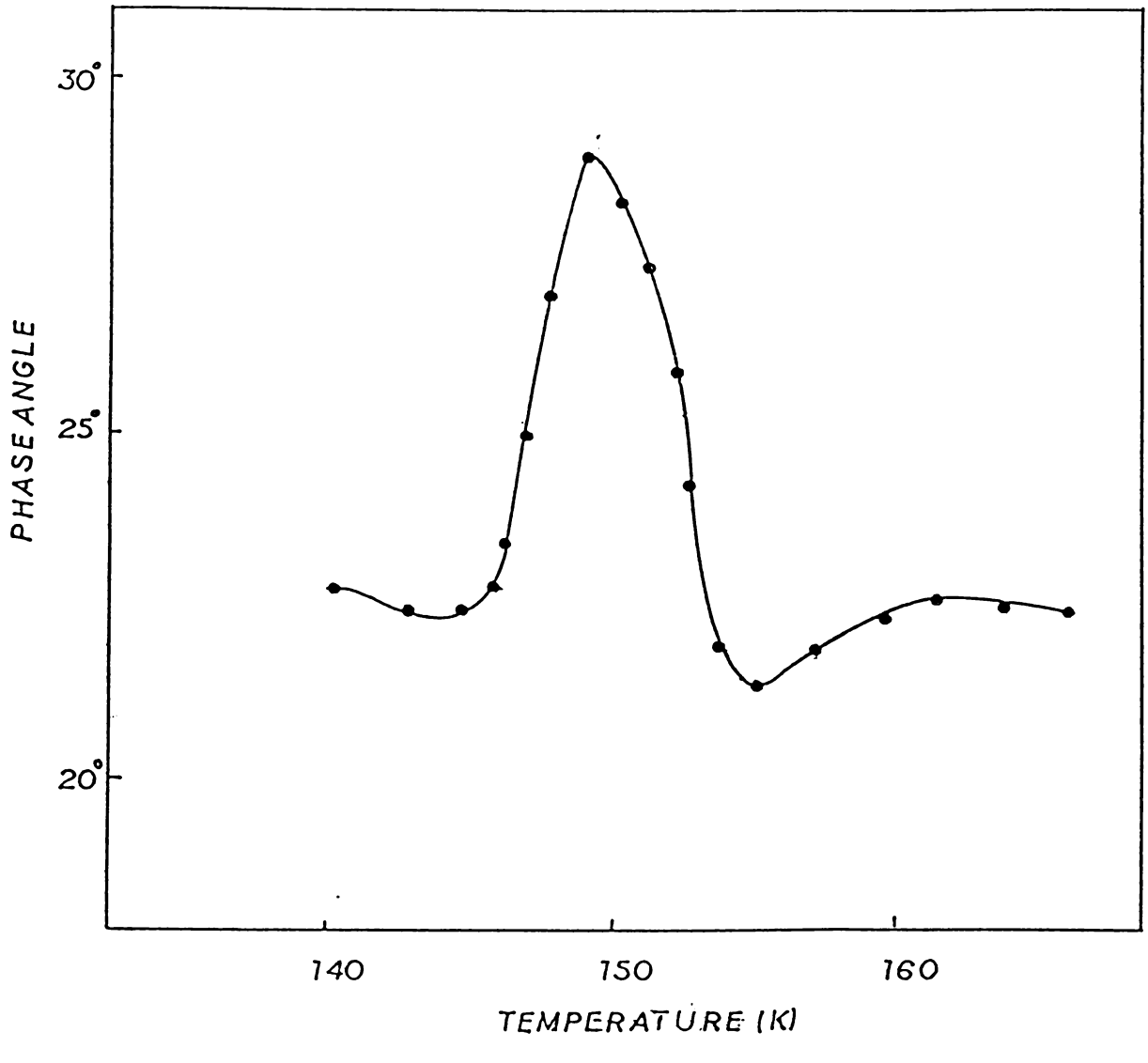

Figure 7.3f. Variation of photoacoustic signal (phase) as a function of temperature for ammonium dihydrogen phosphate crystal. f = 70 Hz.

is shown in figure 7.3e. It is observed that the photo-acoustic signal drastically changes (reduced) at 148K corresponding to a phase transition known to occur in this material. The change in absolute magnitude of the PA signal is about 235 μV from its room temperature value. The phase angle plotted against temperature for this material is shown in figure 7.3f. Here the phase angle slowly rises and reaches a maximum and then decreases as the temperature changes, forming a peak at 148K.

7.4 DISCUSSION

The resonant frequency of a resonant PA cell is given by the relation

$$f = \frac{C \cdot D}{2\sqrt{\pi}} \left[\frac{V_1 + V_2}{V_1 V_2 (L + 1.7D)} \right]^{\frac{1}{2}} \qquad (7.1)$$

Here C is the velocity of the acoustic wave at room temperature, D the diameter of the interconnecting channel, V_1 the volume of the sample cavity, V_2 the volume of the microphone cavity and L the length of the interconnection tube. By substituting the known values, the resonant frequency calculated was found to be 672 Hz. The theoretical value is in reasonably good agreements with the experimentally observed value. From equation (7.1) it is evident that

the low temperature behaviour of the cell be principally related to the decrease in the velocity of the acoustic wave upon the reduction in temperature. As a result, the resonant frequency is to be reduced as the temperature decreases from 300K to 80K. The increase of the photoacoustic amplitude with decrease in temperature can be attributed to the temperature dependent parameters of the gas in the PA cell.

Rosencwaig and Gersho [21] have shown that for an optically opaque and thermally thick sample the photoacoustic signal is independent of the optical absorption coefficient and can be written as

$$Q = \frac{A\, f(T)}{\left[C_s(T)\, K_s(T)\right]^{3/2}} \qquad (7.2)$$

where A is the conversion coefficient representing all the factors, independent of the temperature T, in the generation of the PA signal The function f(T) accounts for all the thermal properties of the cell and internal gas and Cs(T) and Ks(T) are the specific heat at constant pressure and thermal conductivity of the sample respectively. It follows from the above equation that by varying temperature, the photoacoustic signal should exhibit a sudden

change at a phase transition as the specific heat jumps at the transition temperature.

Indeed, the experimental results of the temperature dependence of the PA signal obtained for both $(NH_4)_2Cr_2O_7$ and $NH_4H_2PO_4$ samples clearly show that these materials undergo phase transitions at temperatures mentioned and the PA technique is a good method for the detection of these transitions.

As indicated in the infrared measurements [32] the transition at 269K in AD appear to be the result of the onset of free rotation of the NH_4 group. Below this temperature it is most likely that the NH_4 group may be executing hintered internal rotations. Thus between 156 and 269K one may assume that the NH_4 tetrahedra in AD is in partially disoriented form. The doubling of the ν_4 vibrational mode of NH_4 group in the infrared spectrum could be the result of crystal field splitting due to non-equivalent NH_4 group arising from different orientations. Most ammonium crystal lattices become very rigid at lower temperatures. It is very likely that this can distort the NH_4 tetrahedra or Cr_2O_7 group below 128K. Thus the last of the transitions at lower temperature could be the result of a structural change taking place in the crystal

at this temperature. X-ray or neutron diffraction analysis could throw more light on the structure of the crystal below this transition. The present results offers enough justification for making diffraction studies below 128K. The transitions in ADP crystals are well studied [33-36]. The present results obtained with PA technique completely confirm the earlier observations in this case.

7.5 CONCLUSIONS

The results obtained from photoacoustic measurements carried out in the temperature range 80K to 300K lead to the following conclusions.

1. A resonant photoacoustic cell has been designed and the response characteristics are evaluated.

2. Anomalous changes have been observed in PA signal at 128, 156 and 269K in $(NH_4)_2Cr_2O_7$ and at 148K in $(NH_4)H_2PO_4$ corresponding to different phase transitions occurring in these materials.

7.6 REFERENCES

[1] A.G.Bell, Am.J.Sci. 20 (1880) 305.

[2] A.G.Bell, Proc.Am.Assoc. Advancement of Science. 29 (1880) 115.

[3] A.G.Bell, Phil.Mag. 11 (1881) 510.

[4] J.Tyndall, Proc.Roy.Soc.London. 31 (1881) 307.

[5] J.Tyndall, Proc.Roy.Soc.London. 31 (1881) 478.

[6] W.C.Roentgen, Phil.Mag. 11 (1881) 308.

[7] Rayleigh, Nature 23 (1881) 274.

[8] M.L.Veingerov, Dokl.Akad.Nauk SSSR. 19 (1938) 687.

[9] L.B.Kreuzer, J.Appl.Phys. 42 (1971) 2934.

[10] L.B.Kreuzer and C.K.N.Patel, Science 173 (1971) 45.

[11] W.R.Harshbarger and M.B.Robin, Accounts of Chemical Research 6(10) (1973) 329.

[12] A.Rosencwaig, Opt.Commun. 7 (1973) 305.

[13] A.Rosencwaig, Science 181 (1973) 657.

[14] A.Rosencwaig, Phys.Today 28(9) (1975) 23.

[15] A.Rosencwaig, Anal.Chem. 47(6) (1975) 592A.

[16] A.Rosencwaig, Rev.Sci.Instrum. 48 (1977) 1133.

[17] A.A.King and G.F.Kirkbright, Laboratory Practice 25(6) (1976) 377.

[18] A.Rosencwaig, in "Advances in Electronics and Electron Physics", L.Marton (Ed.), Academic Press, New York, 1978, Vol.46, p.207.

[19] J.G.Parker, Appl.Optics. 12 (1973) 2974.

[20] L.C.Aamodt, J.C.Murphy and J.G.Parker, J.Appl.Phys. 48 (1977) 927.

[21] A.Rosencwaig and A.Gersho, J.Appl.Phys. 47 (1976) 64.

[22] H.S.Bennett and R.A.Forman, J.Appl.Phys. 48 (1977) 1432.

[23] F.A.McDonald and G.C.Wetsel,Jr., J.Appl.Phys. 49 (1978) 2313.

[24] K.O.Park, S.I.Yun and C.S.Sol, New Physics, (Korean Physical Society) 3 (1981) 183.

[25] Andre' Lacharine and Patric Poulet, Appl.Phys.Lett. 45 (1984) 953.

[26] R.Florian, J.Pelzl, M.Rosenberg, H.Vargas and R.Wernhardt, Phys.Status Solidi (a) 48 (1978) K35.

[27] C.Pichon, M.Le Libonx, D.Fournier and A.C.Boccara, Appl. Phys.Lett. 35 (1979) 435.

[28] P.Korpiun, J.Boumann, E.Lusher, B.E.Papamoko and R.Tilgner, Phys.Status Solidi (a) 58 (1980) K13.

[29] P.Korpiun and R.Tilgner, J.Appl.Phys. 51 (1980) 6115.

[30] P.S.Bechthold, M.Campagna and T.Schober, Solid State Commun. 36 (1980) 225.

[31] A.Rosencwaig, "Photoacoustic Spectroscopy of Solids", Rev.Sci.Instrum. 48 (1977) 1133.

[32] C.J.H.Schuttle and A.M.Heyns, Chem.Phys.Lett. 1 (1967) 487.

[33] R.Ueda, J.Phys.Soc.Japan, 3 (1948) 328.

[34] L.Tenzer, B.C.Frazer and R.Pepinsky, Acta.Cryst. 11 (1958) 506.

[35] C.C.Stephenson and A.C.Zettlemoyer, J.Am.Chem.Soc. 66 (1944) 1405.

[36] E.Wiener-Avnear, S.Levin and I.Pelah, J.Chem.Phys. 52 (1970) 2891.

Chapter VIII

IONIC THERMOCURRENT STUDIES IN PURE AND DOPED $NaClO_3$ CRYSTALS

Abstract

An evaluation of the ionic thermocurrent technique has been performed by monitoring the relaxation of divalent impurity-cation vacancy dipoles formed from various divalent cationic impurities incorporated into the monocrystalline sodium chlorate. The observations have been compared with the predictions based on the relaxation of a nearest neighbour impurity-vacancy dipole model. The results obtained from these measurements show that the activation energy for the reorientation of impurity-vacancy dipoles is strongly depending on the ionic radius of the dopant ion and it is found that the activation energy increases with the increase in the ionic radius. The kinetic parameters are evaluated and the results obtained are discussed in detail.

8.1 INTRODUCTION

At room temperature, $NaClO_3$ monocrystals have non-centro symmetric cubic structure of tetrahedral class given by the space group $T^4(P2_13)$ with four formula units per primitive cell [1]. The peculiar structural configuration of ClO_3 group in the $NaClO_3$ where oxygen atoms are arranged on an equilateral triangle with the chlorine atom located only a short distance (0.48Å) above the plane and centre of gravity of the oxygen atoms, markedly affect the thermal behaviour of this material [2]. There has been considerable amount of work in this material, perhaps because it grows easily from solution and shows interesting properties like optical activity and piezoelectricity. Several properties of this crystal such as thermal expansion [2] elastic constants [3,4], optical properties [5,6], vibrational spectral analysis [7,8] and microhardness [9] have been studied in great detail. The dielectric constant of this material has been measured at 1 KHz by Mason [2] in the range of temperature -100°C to 200°C. Measurement of static dielectric constant has been reported by Bechmann and Taylor [10], but the details regarding the frequency and temperature are not available. However, it is known that the presence of impurities in minute quantities or defects will show up as increase in the dielectric constant at low frequencies. This frequency dependence is due to the space charge polarisation. But at

certain higher frequency range, the dielectric constant becomes frequency independent and the effect of defects and impurities is negligible [11,12]. Ionic conductivity of single crystals of sodium chlorate as a function of temperature was reported by Ramasastry, Viswanatha Reddy and Murthy [13]. The measurements extended in the temperature range 70 to 250°C inferred that the charge transport was by the mechanism of cation vacancy migration in the low temperature (structure sensitive) region. But the defect parameters such as the jump and formation energies could not be obtained as the energy of association between the aliovalent impurities and the charge compensating defects was not known. However, their measurements on $NaClO_3$ crystals containing divalent cationic impurities show that the increase of conductivity is due to the creation of positive ion vacancies or negative ion interstitials, either of which can compensate the excess positive charge of the added divalent cationic impurity in place of sodium to satisfy the electrical neutrality condition.

Ionic thermo current (ITC) measurements have recently become accepted as an ideal technique for studying the dynamics and thermal behaviour of impurities in a crystalline lattice. In the case of substantial concentration of divalent impurity ions in normal ionic solids, like alkali halides, halates and in crystals with fluorite structure, the compensation process is accomplished by the generation of equal number of lattice

vacancies or interstitial host ions depending on the nature of the added impurity [14,15]. Due to coulombic attraction these vacancies generally take nearest neighbour or next nearest neighbour positions in the lattice with respect to the added impurity ion thereby forming impurity-vacancy (I-V) complexes. Such I-V complexes are invariably dipolar in nature and usually they oriented in random directions. However, in an external electric field a major part of these complexes will be aligned in the field direction, provided sufficient amount of thermal activation does take place. On cooling with the field, all the oriented dipoles get frozen-in and they continue to remain in the oriented condition even when the field is removed as their relaxation times are of the order of several hours. On warming the specimen at a constant heating rate, it gives rise to the characteristic ionic thermocurrent spectrum with distinct current peaks resulting from the randomisation process of I-V dipoles [16]. The mathematical expression representing the ITC peaks is given by the first order kinetic equation

$$I(T) = \frac{A P_0}{\tau_0} \exp - \left\{ \frac{E}{kT} + \frac{1}{\beta \tau_0} \int_{T_0}^{T} \exp\left(\frac{-E}{kT'}\right) dT' \right\} \qquad (8.1)$$

where A is the area of cross-section of the specimen, τ_0 is the characteristic relaxation time, β is the constant heating rate and P_0 is the maximum amount of polarisation possible

at temperature T_o given to a first approximation by Langevin's equation [17],

$$P_o = \frac{N_D \mu^2 E}{3kT} \qquad (8.2)$$

where N_D is the concentration of dipoles

E - the local electric field

μ - the dipolemoment.

A detailed study of the ionic thermocurrent spectrum yields valuable information on the relaxation process of such I-V complexes.

In the present chapter an exhaustive investigation carried out in single crystals of pure and doped $NaClO_3$ using ionic thermo current technique is presented. This presumably, is the first attempt of an ITC investigation in an alkali halate crystal. Investigations have also been extended to study the effects of dopant concentration, poling temperature, poling field and polarising time and heating rate on the ITC spectra of doped $NaClO_3$ crystals.

8.2 EXPERIMENTAL DETAILS

Single crystals of pure $NaClO_3$ can be conveniently prepared by slow evaporation of a saturated solution in

petri dishes. $NaClO_3$ doped with Ca^{2+}, Sr^{2+}, Pb^{2+} and Ba^{2+} impurities can be grown by slow evaporation of a mixture of the saturated solution of $NaClO_3$ with small quantities of corresponding halates solution in different proportions. These crystals cannot be cleaved. Fortunately they grow as rectangular parallelepipeds with sharp edges between adjacent faces mutually inclined at right angles. Specimens of typical sizes 5x5x1 mm^3 cut from large single crystals with their broad faces parallel to the $\langle 100 \rangle$ direction were used for the investigation. Electrical contacts were made using aluminium electrodes evaporated on to the broader faces of the crystal. The details of the cryostat used for the ITC measurements under vacuum conditions have been already described in Chapter II. A linear heating rate ranging from 0.01 to 0.1 K/sec have been used in the temperature range used here. The thermocurrent generated by the sample was measured using Keithley model 617 programmable electrometer and recorded along with the temperature on the X-Y recorder.

8.3 EXPERIMENTAL RESULTS

8.3.1 Effect of impurity concentration on ITC spectra

The ionic thermocurrent spectrum for pure $NaClO_3$ single crystals along (100) direction obtained by polarising the specimen with a field of 2 kV/cm at 303K for 5 minutes with a heating rate of 0.07K/sec is shown in figure 8.3a.

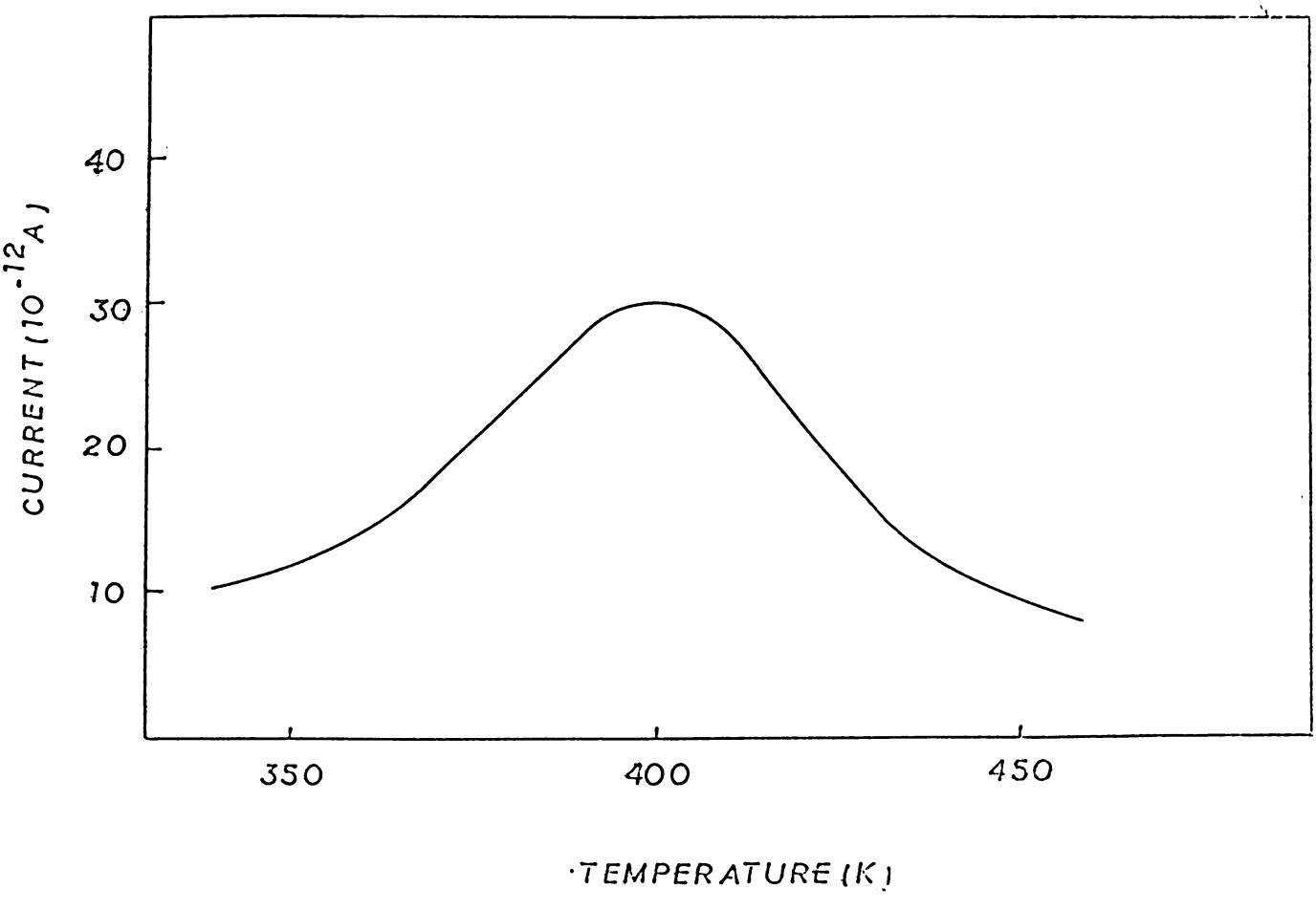

Figure 8.3a. Ionic thermocurrent spectrum of pure $NaClO_3$ crystal. Poling field 2kV/cm, poling temperature 303K, poling time 5 min. and heating rate 0.07 K/sec.

The spectrum obtained in the temperature range 80 to 450K shows a broad current peak with a maximum at 402K. It is observed that the temperature corresponding to the current maximum (T_m) is found to remain independent of the poling field and poling time, where as it is slightly affected by the change in polarising temperature. The ionic thermocurrent spectra obtained for $NaClO_3$ doped with four different divalent cationic impurities viz., Ca^{2+}, Sr^{2+}, Pb^{2+} and Ba^{2+} for three different concentrations (100, 250 and 500 ppm) at 303K for 5 minutes with a heating rate of 0.07 k/sec are shown in figures 8.3b to 8.3e. The spectra obtained for the doped $NaClO_3$ crystals shows two distinct current peaks of varying magnitude in all the four specimens. Let us denote these peaks as A and B in the increasing order of temperature. The peaks observed below room temperature i.e., peaks A, are fairly sharp in nature and the peaks observed above room temperature are much broader in all the doped specimens of $NaClO_3$. It is observed that, the temperature corresponding to the current maxima's for peaks A and B is different for different impurity doped specimens. Table 1 gives the different T_m values obtained for the two peaks A and B in each of the four different impurity doped specimens of $NaClO_3$.

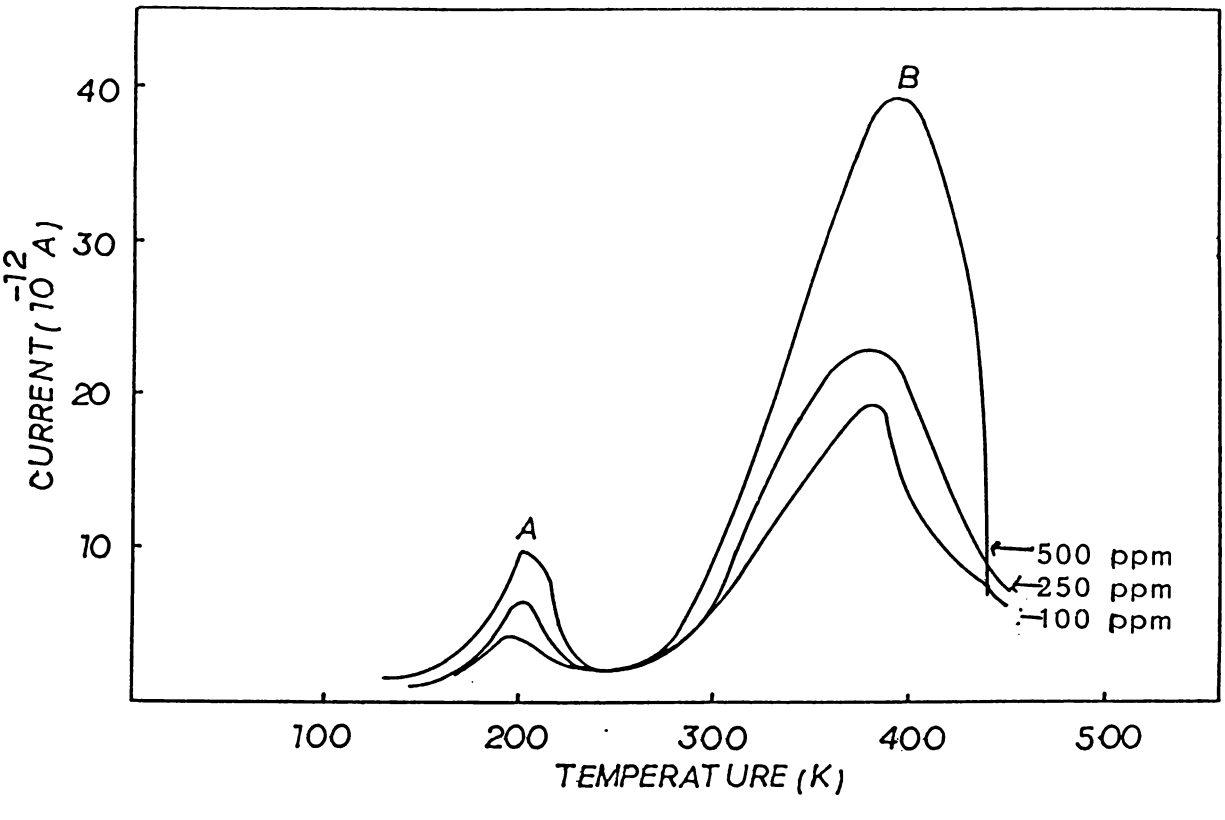

Figure 8.3b. ITC spectrum of $NaClO_3:Ca^{2+}$ crystals for three different concentrations.

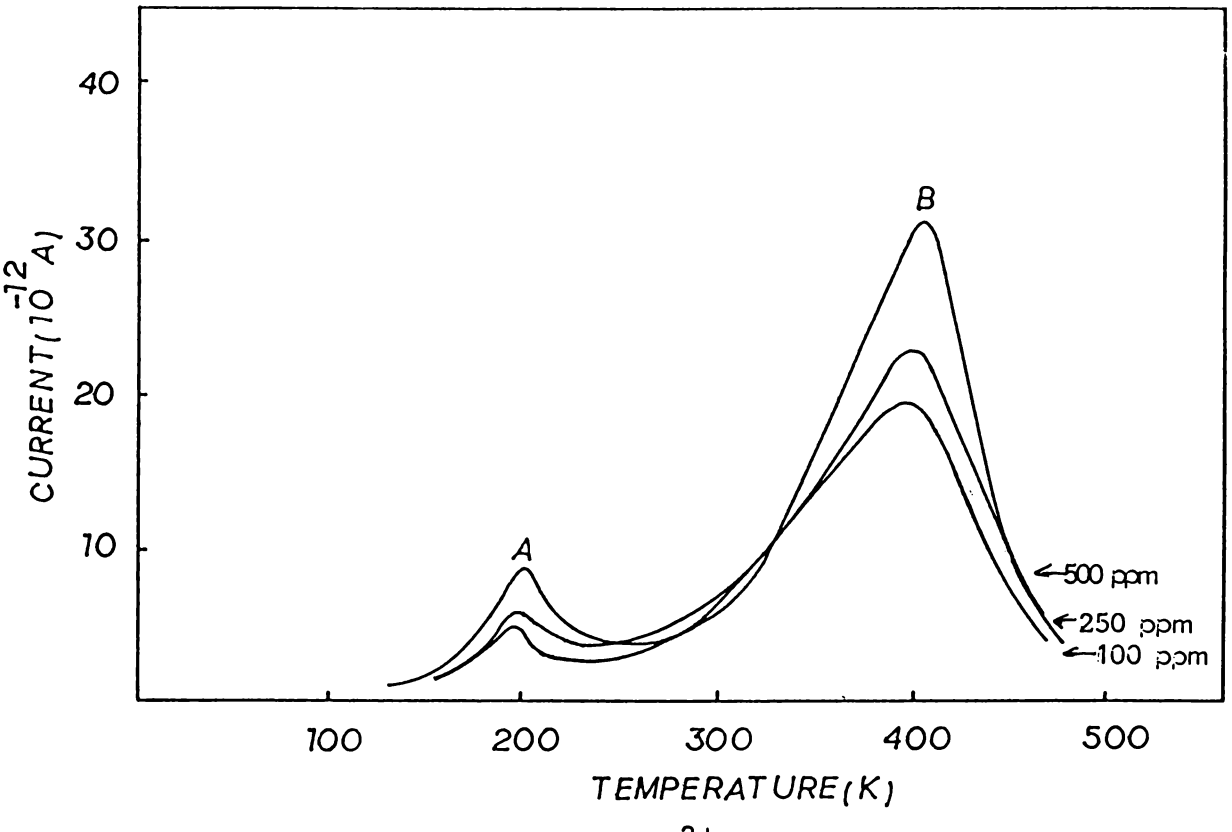

Figure 8.3c. ITC spectrum of Sr^{2+} doped $NaClO_3$ crystals for three different concentrations.

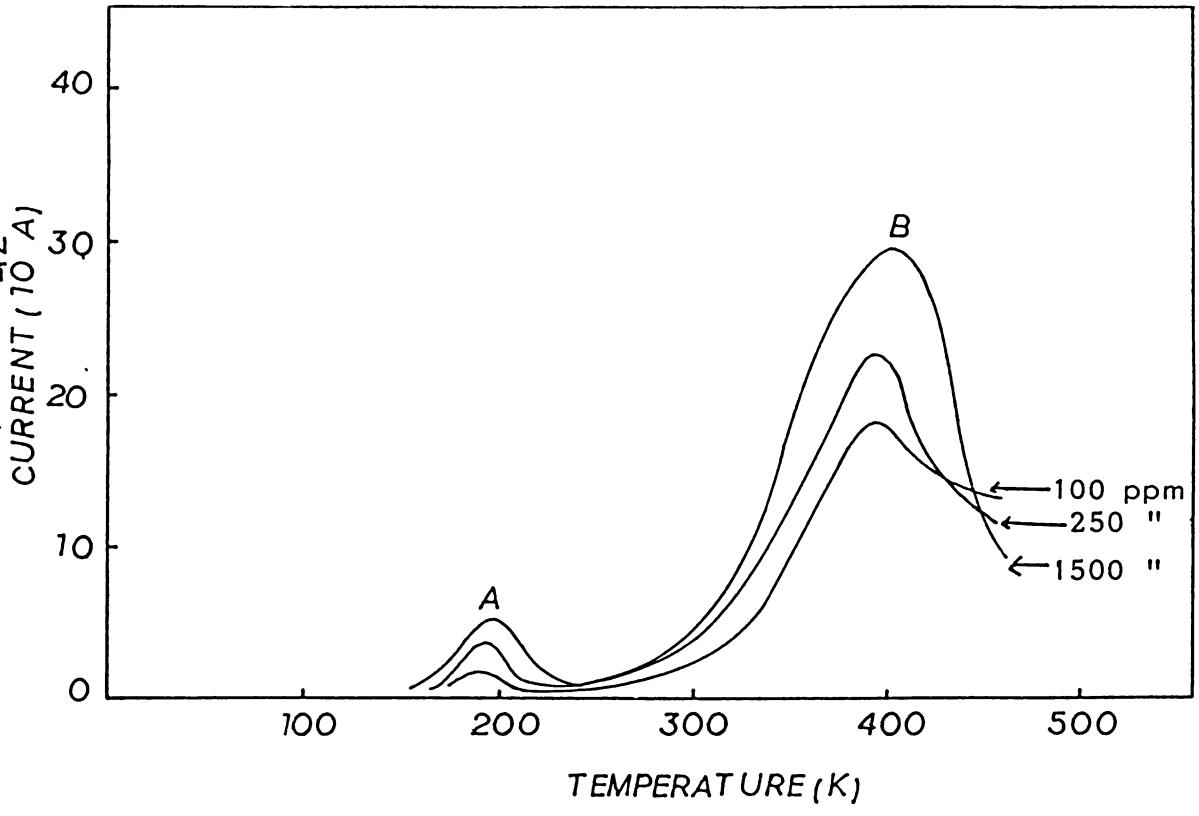

Figure 8.3d. ITC spectrum of Pb^{2+} doped $NaClO_3$ crystals for three different concentrations.

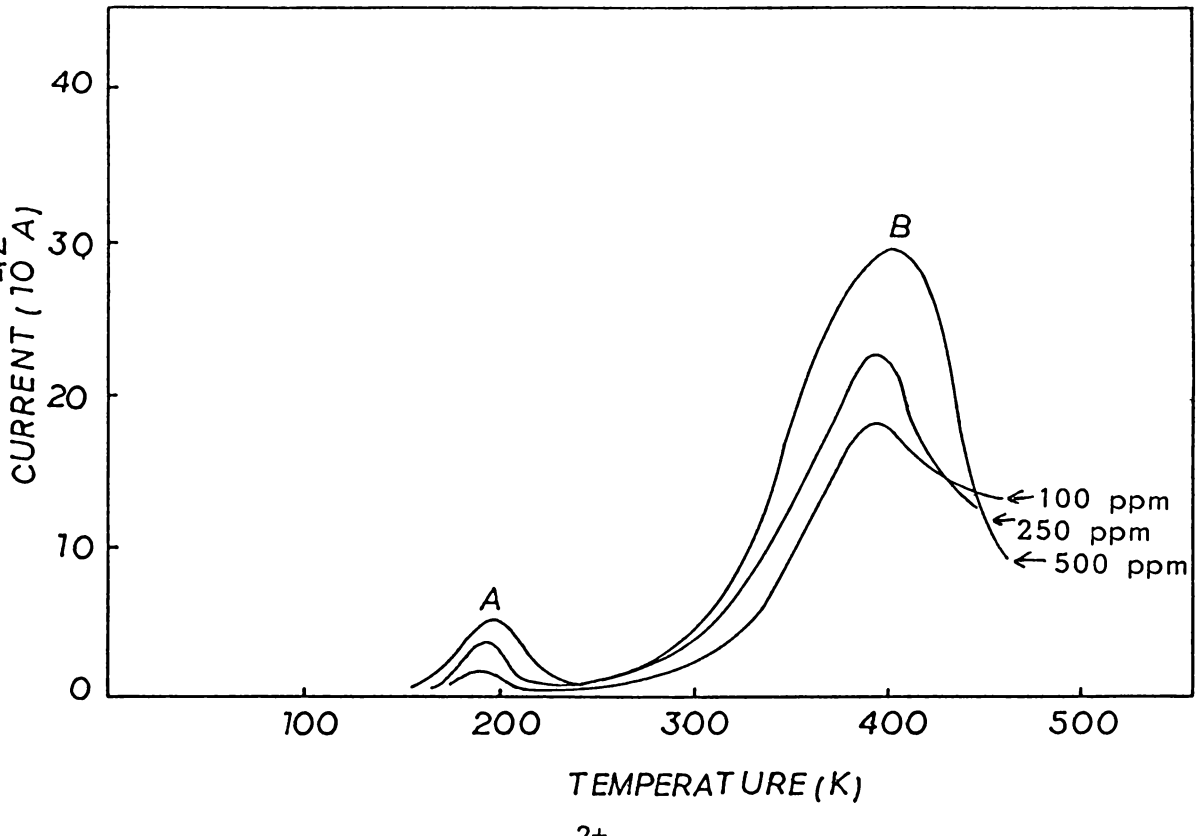

Figure 8.3e. ITC spectra of Ba^{2+} doped $NaClO_3$ crystals for three different concentrations.

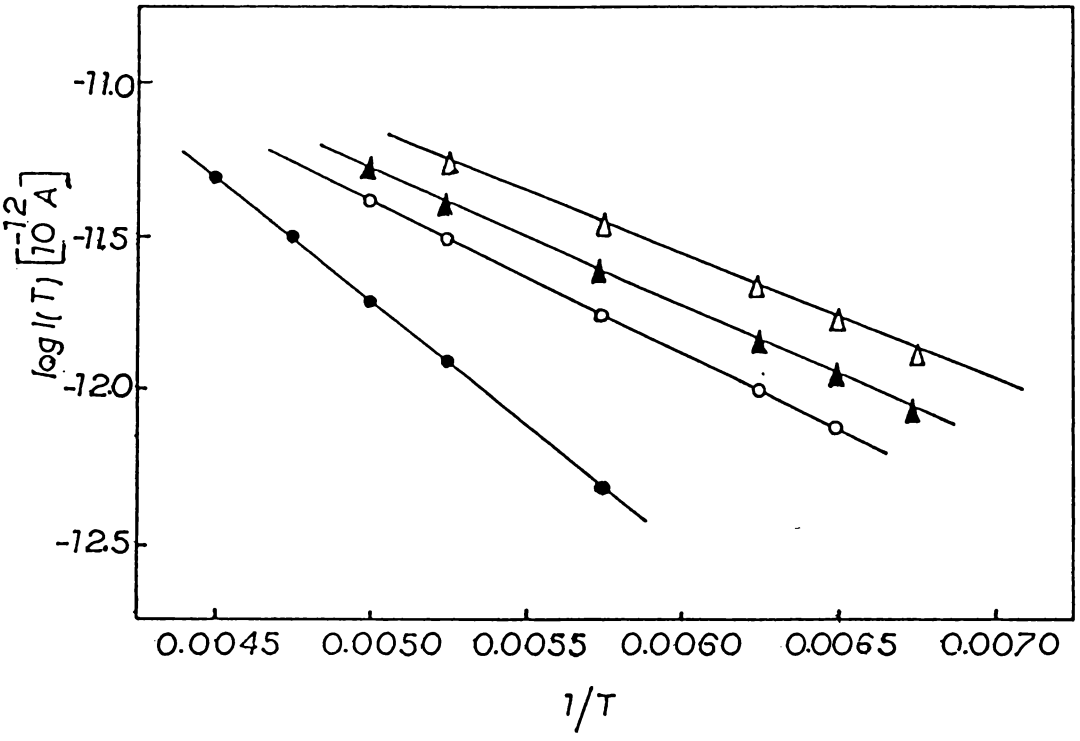

Figure 8.3f. Log I(T) vs 1/T plot for doped $NaClO_3$ crystals. (1) Ba^{2+}, (2) Pb^{2+}, (3) Sr^{2+} and (4) Ca^{2+}.

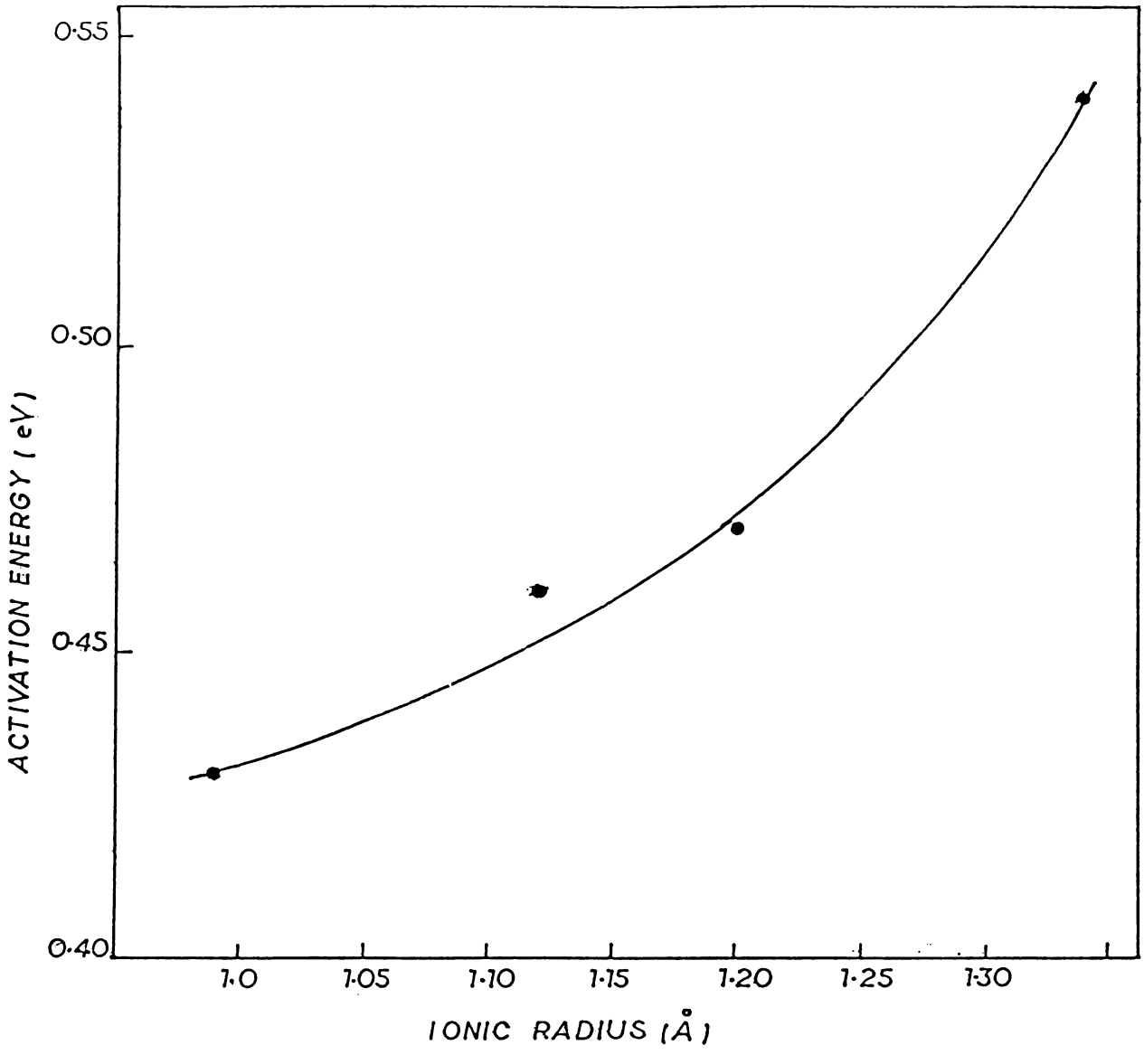

Figure 8.3g. Variation of activation energy with ionic radii for various impurities doped $NaClO_3$ crystals.

Table 1 The various T_m values obtained for peaks A and B for different impurities in $NaClO_3$ crystals

Sample	Peak A T_m (K)	Peak B T_m (K)
$NaClO_3$: Ca^{2+}	201.0	391.0
$NaClO_3$: Sr^{2+}	205.0	403.5
$NaClO_3$: Pb^{2+}	208.5	405.0
$NaClO_3$: Ba^{2+}	218.0	409.2

Table 2 Activation energies and pre-exponential factors calculated for the various impurities doped $NaClO_3$ crystals

Impurity Ion	Activation energy E (eV)	Pre-exponential factor τ_o (sec.)
Ca^{2+}	0.43	1.95×10^{-9}
Sr^{2+}	0.46	5.65×10^{-10}
Pb^{2+}	0.47	5.2×10^{-10}
Ba^{2+}	0.54	3.6×10^{-11}

The height of the peaks A and B in all the four different impurity doped $NaClO_3$ crystals is found to exhibit definite increase with impurity concentration for fixed values of poling field, poling time and polarising temperature. The plots of $\log_{10} I(T)$ vs T^{-1} for the low temperature tails of the peaks A for all the doped specimens with fixed impurity concentration (250 ppm) give four straight line regions with different slopes as shown in figure 8.3f. By making use of equation (8.1) after eliminating the integral term, the activation energy values and the pre-exponential factors obtained are shown in table 2. The variation of activation energy with ionic radii is shown in figure 8.3g. It is observed that, the activation energy increases with increase in ionic radius.

8.3.2 Effect of poling temperature

To study the effect of poling temperature on the nature of the ITC peaks, the samples were polarized at different temperatures for a poling time of 5 minutes and then quenched to liquid nitrogen temperature, which is a method similar to the usual thermal peak cleaning technique. The ITC spectra for doped (250 ppm) samples polarized at 260, 300, 370 and 430K with a poling field of 35 KV/cm are shown in figure 8.4h. It is found that the sample polarized at 260K shows a maximum height for the peaks A and minimum for peaks B in all the four

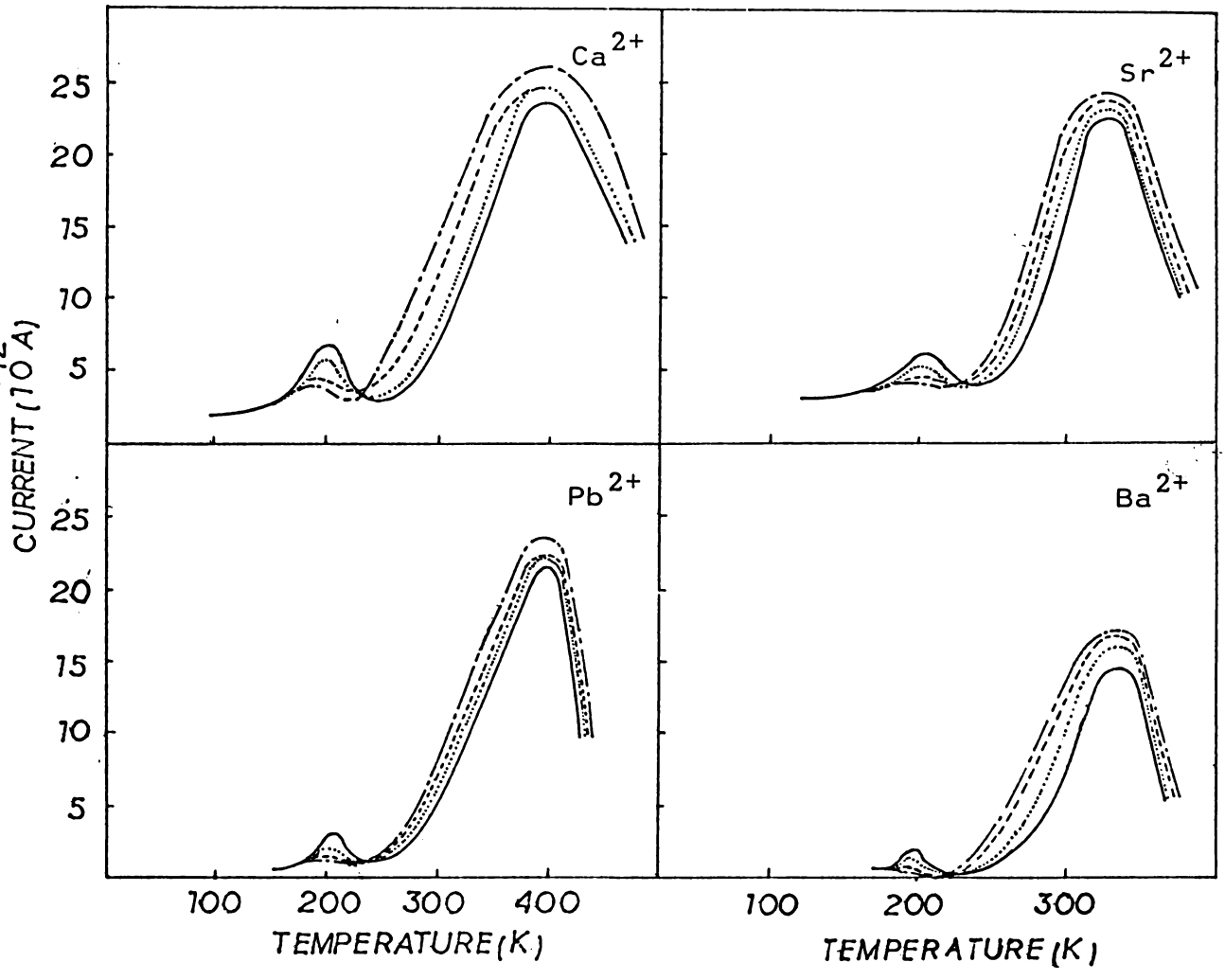

Figure 8.3h. Effect of poling temperature on the variation of the ITC spectra of doped $NaClO_3$ crystals. (1) ——— 260K, (2) ..... 300K, (3)----- 370K and (4).-.-.-. 430K.

different impurity doped specimens, whereas for higher poling temperatures, the height of the peaks B increases at the expense of the peaks A. It is also found that the temperature corresponding to the current maxima for peaks A is unshifted by this process. The temperature corresponding to the current maxima for peaks B is found to be shifted to the higher temperature in all the doped $NaClO_3$ crystals.

8.3.3 Effect of poling field

Figure 8.3i shows the variation of the height of the peaks A obtained for the four different impurities doped (250 ppm) specimens of $NaClO_3$ as a function of polarizing field. It is found that all the four specimens show a linear variation throughout the range 1-6 KV/cm and for very high field strengths (10KV/cm) they show saturation effects. Figure 8.3j shows the variation of the peak height with poling field obtained for the different impurities doped $NaClO_3$ crystals in the case of peak B. they show drastic saturation effects in the range 1-6 KV/cm. It is also found that the temperature corresponding to the current maxima for both the peaks in all the four different doped specimens of $NaClO_3$ is unaffected by this process.

8.3.4 Effect of poling time

It is well known that the ionic conductivity and the polarization are extremely sensitive to thermal treatments like annealing or quenching. The study of ITC measurements

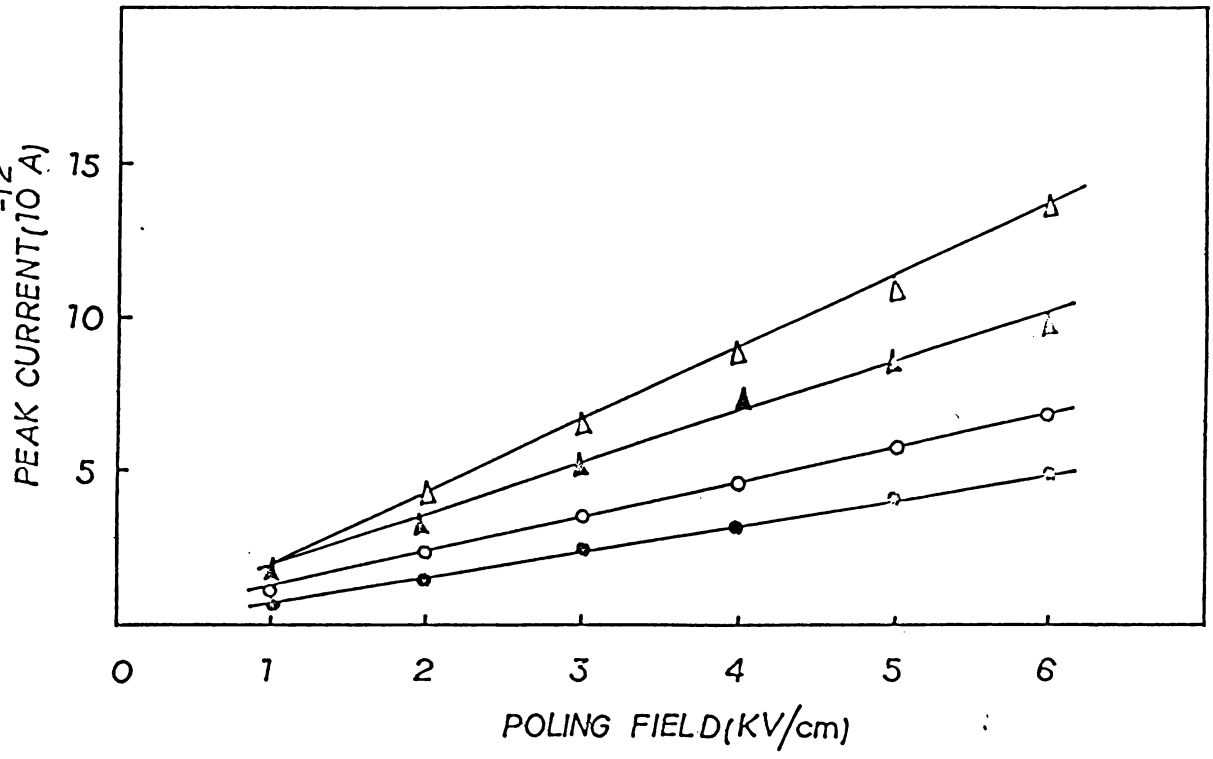

Figure 8.3i. Effect of poling field on the variation of the height of the current peaks A for different impurities doped $NaClO_3$ crystals.
(1) Ba^{2+}, (2) Pb^{2+}, (3) Sr^{2+}, and (4) Ca^{2+}.

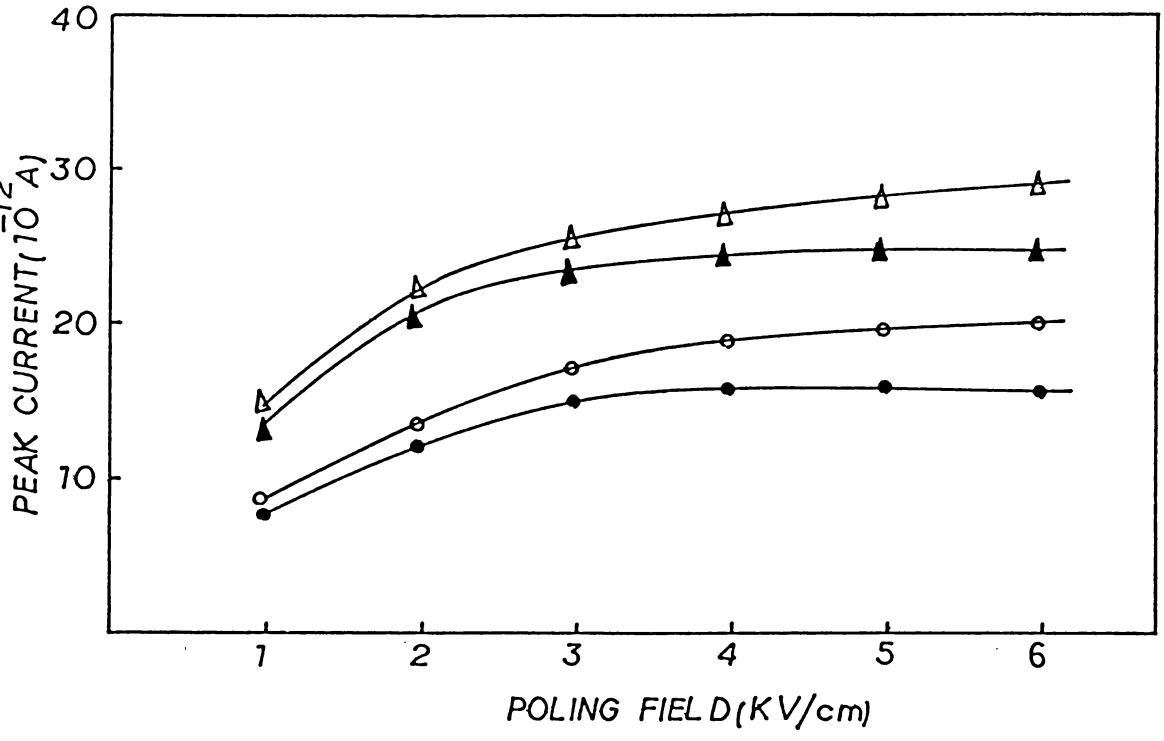

Figure 8.3j. Effect of poling field on the variation of the height of the current peaks B for different impurities doped $NaClO_3$ crystals.
(1)●—●—● Ba^{2+}, (2)○—○—○ Pb^{2+}, (3)▲—▲—▲ Sr^{2+} and (4)△—△—△ Ca^{2+}.

of samples containing a fixed amount of impurity ion by varying poling time, while keeping the polarizing field constant, can yield valuable information regarding the behaviour of the thermally generated defects on the electrical conduction process. Figure 8.3k and 8.3l show the variation of the current maxima for peaks A and B for the four different impurity doped specimens of $NaClO_3$ for a fixed poling field (3.5 KV/cm) as a function of poling time. The magnitude of the peak current increases gradually for both A and B peaks in all the doped specimens as the poling time increases from 1 to 10 minutes. This effect is found to be more pronounced at higher poling temperatures and for higher impurity concentrations.

8.3.5 Effect of heating rate

The measurement of the effect of heating rate on the height of the current peaks obtained for the doped specimens of $NaClO_3$ shows that for higher heating rates, the temperature corresponding to the current maxima shifts slightly to the higher temperature region and the magnitude of the peak current increases with the heating rate for both the two peaks. However, the total integrated charge for these peaks is found to be unaffected by the change in heating rate.

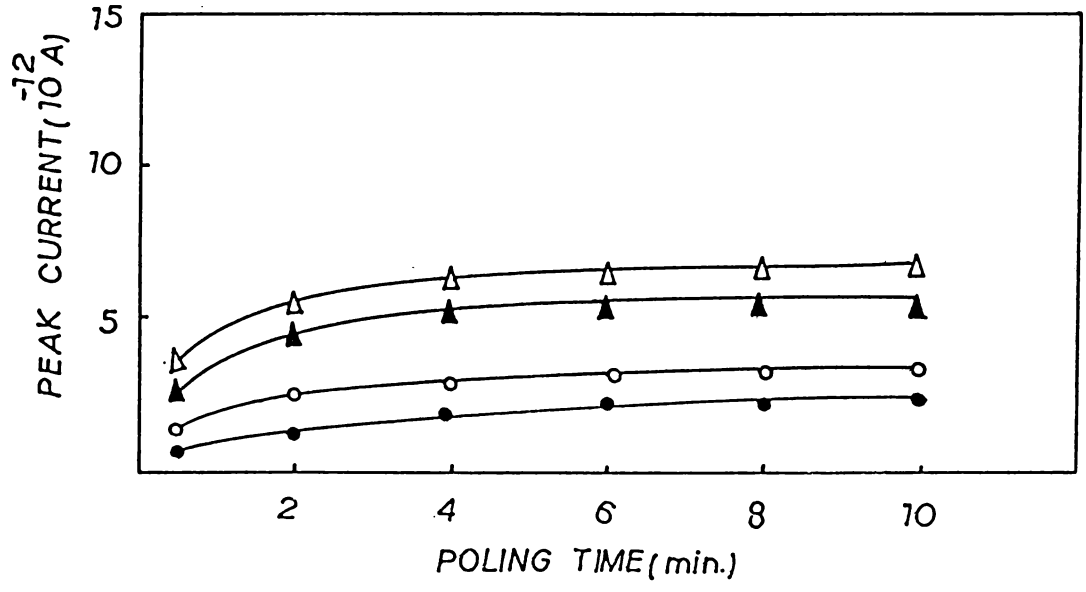

Figure 8.3k. Variation of the current maxima for peaks A in doped $NaClO_3$ crystals as as a function of poling time. (1)—●—●—●— Ba^{2+}, (2)—o—o—o— Pb^{2+}, (3)—▲—▲—▲— Sr^{2+} and (4)—△—△—△— Ca^{2+}.

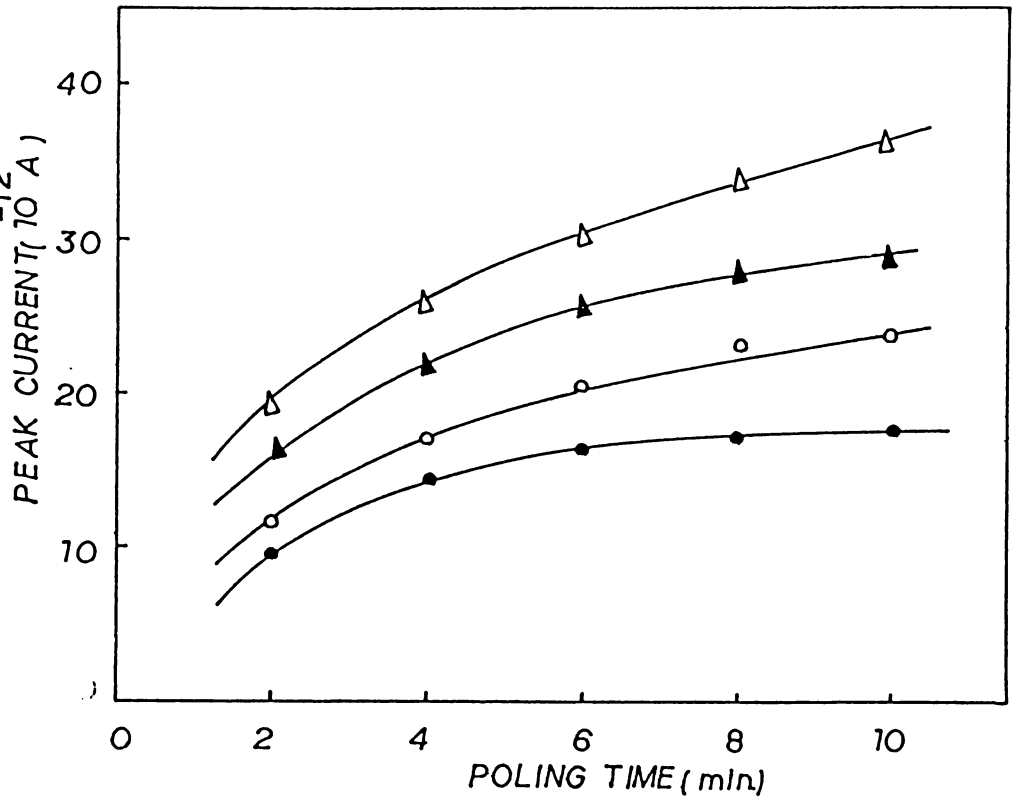

Figure 8.31. Variation of current maxima for peaks B in doped $NaClO_3$ crystals as a function of poling time. (1)-●-●-● Ba^{2+}, (2)-○-○-○ Pb^{2+}, (3)-▲-▲-▲ Sr^{2+} and (4)-△-△-△-Ca^{2+}.

8.4 DISCUSSION

It is obvious from the nature of variation of the current peak observed in pure $NaClO_3$ crystals and from its behaviour towards various experimental parameters that the high temperature current peak A, does not originate from the I-V complexes. It is presumably due to the release of ionic space charges accumulated during the polarisation process at the poling temperature due to the formation of charge carriers by the inherent impurities present in the $NaClO_3$ material. Since even the pure material contains inherent impurities of the order of 10^{-6} molar fraction these impurities play a major role in giving rise to this current peak in the ITC spectra of pure $NaClO_3$. On the other hand, the two distinct peaks occurring in the ITC spectra in the case of doped specimens have entirely different characteristics. Here the integrated charges vary in accordance with the impurity concentration. The activation energy value as well as the temperature of the current peaks depend on the type of impurity added. Hence one may attribute them directly to the presence of impurities added into the crystal.

It is well known [18-24] that by the suitable addition of divalent cationic impurities, vacancies and interstitials can be created. Therefore, it is possible to create lattice

vacancies associated with impurity ions in which they form complexes and higher agglomerates. Both free charge carriers and complexes cause ITC peak in polar crystals.

As already reported by Ramasastry et al. [13,25], when divalent cationic impurities like Ba^{2+}, Ca^{2+} are substituted in monocrystalline $NaClO_3$, the condition for electrical neutrality requires that positive ion vacancies or negative ion interstitials should be created and these could be generated in equal numbers. In view of the relatively large mass and size of the chlorate ion, they have neglected the occupation of ClO_3 group in the interstitial position. This inference is again strongly supported by the fact that ClO_3 ion has low mobility and an unfavourable shape (planar) for migration, and high electronic polarizability. Hence, they came to the conclusion that it is the movement of the sodium ions with small Goldschmidt radius (98 pm) and low electronic polarizability (0.41×10^{-24} cm^3) that should be mainly responsible for the electrical conduction process in the pure material. Thus the conduction in this substance is caused by the migration of positive ions and their vacancies under the influence of applied electric field.

The above considerations lead to the fact that the current peaks observed below room temperature in all the four

different impurity doped specimens of $NaClO_3$ are due to the reorientation of the impurity vacancy dipoles formed by the substitution of divalent cationic impurities in the $NaClO_3$ lattice. Theoretical calculations performed for a general cation Me^{2+} (Me^{2+} = Mn^{2+}, Pb^{2+}, Ca^{2+}, Ba^{2+}, Sr^{2+} ....) [18] as well as for some other well defined systems [19-21] have revealed that, the interaction energies of cation vacancies with Me^{2+} both for the nearest neighbour (nn) and next nearest neighbour (nnn) state are nearly the same. Later, this theoretical predictions were experimentally verified in NaCl and LiF by actual substitution of Mn^{2+} ion. It was also found from the above experimentation that for I-V dipoles created by Me^{2+} impurity having an ionic radius larger than that of the host lattice cation, the relaxation processes as reflected by the ITC curves are solely due to the nearest neighbour dipole interaction. For Me^{2+} impurities with smaller ionic radii a departure from the above model is observed [26]. Therefore, it is possible to extend the above model in the present case also, since, $NaClO_3$ is an ionic crystal and the dopants used in the ITC investigation have ionic radii larger than that of the Na^+ ion. Consequently, the observed low temperature peaks (A) in the doped specimens of $NaClO_3$, undoubtedly are due to the formation of I-V dipoles in the nearest neighbour positions. Again the behaviour of these peaks towards the

poling field and poling temperature is typical of an ITC peak stimulated by I-V dipole reorientation. The activation energy values calculated from ITC measurements are found to be in very good agreement with those reported from ionic conductivity measurements [13,25]. Thus it becomes evident that the same cation vacancy hopping mechanism is operative in the electrical conduction process as well as in I-V dipole relaxation.

The substitution of divalent impurity ions cause a local distortion in the host lattice, and it is to be expected that the lattice distortion will affect the relaxation behaviour of these dipoles. From the activation parameters reported in the table 2 it is possible to observe that, the value for the reorientation activation energy increases as the ionic radius of the impurity ion increases. Such variation of activation energy with impurity ions arises from the change in the Born-Mayer potentials [27-29] resulting from substitution process.

In order to find the origin of the peaks 'B' observed at higher temperatures let us consider the effect of various parameters on the ITC spectra of this material. It is clear from the peak heights obtained for doped $NaClO_3$ crystal as a function of poling temperatures that the complexes responsible for low temperature ITC peak now gradually begin to dissociate

at higher temperatures, and when one quenches the sample from higher temperature to the liquid nitrogen temperature, the carriers thus generated are immobilised, giving rise to a non-uniform space charge. Therefore the high temperature peaks (B) observed in all the doped specimens of $NaClO_3$ are due to the space charge created by the dissociation of I-V complexes in the material. The observed decrease with the poling temperature in the magnitude of the height of the lower temperature peaks (A) of all the four systems readily leads to the conclusion that, the decrease of the total integrated charge with increasing poling temperature is a consequence of the decrease due to dissociation in the effective number of complexes. The resulting space charge should then certainly show up in the peak B, the height of which should increase with poling temperature. Indeed such an effect is observed as expected and this lends conductivity to the structure proposed here for the origin and nature of the ITC peaks in pure as well as doped sodium chlorate.

8.5 CONCLUSIONS

The detailed investigations carried out in single crystals of pure and doped $NaClO_3$ using ITC technique in the temperature range 80 to 450K lead to the following conclusions:

1. The ITC spectrum obtained for pure $NaClO_3$ crystals shows only a broad peak with a maximum at 402K. The origin

of this current peak can be assigned as due to the formation of space charges by the inherent impurities present in the pure sample.

2. The ITC spectra obtained for doped $NaClO_3$ crystals show two distinct current peaks whose temperature values corresponding to the current maxima depend upon the nature and size of the divalent impurity added.

3. The origin of the low temperature peaks (A) observed in all the four different doped specimens can be assigned to the formation of impurity-vacancy dipoles in the nearest neighbour positions by the added divalent cationic impurity in the $NaClO_3$ lattice.

4. The peaks (B) observed above room temperature can be assigned as due to the non-uniform distribution of space charge formed by the dissociation of the I-V complexes.

5. Activation energy values for reorientation of I-V complexes are found to increase with the increase of the ionic radius of the impurity ion.

6. Activation energy values obtained from ITC measurements are found to be in good agreement with the values obtained

from conductivity measurements. Hence the same hopping mechanism must be active both in conduction process and in I-V dipole reorientation.

8.6 REFERENCES

[1] R.W.G.Wyckoff, Crystal Structures (2nd Edition), Vol.2, p.380-91, Interscience, New York (1971).

[2] W.P.Mason, Phys.Rev. 70 (1946) 529.

[3] V.Radha and E.S.R.Gopal, J.Ind.Inst.Sci. 50 (1968) 26.

[4] S.Bhagavantham, Proc.Ind.Acad.Sci. XLI (1955) 72.

[5] S.C.Abraham, A.M.Gloss and K.Marsau, Solid State Commun. 24 (1977) 515.

[6] S.B.S.Sastry, R.B.Tripathi and C.Ramaswamy, J.Phys.Chem. Solids 34 (1973) 473.

[7] A.D.Prasad Rao, R.S.Katiyar and S.P.S.Porto, Phys.Rev.Lett. 28 (1972) 665.

[8] A.D.Andrea, B.Fornari, G.Mattel, M.Pagannone and M.Scrocco, Phys.Status Solidi (b) 53 (1972) 577.

[9] P.Dawson, Phys.Status Solidi (b) 50 (1972) 571.

[10] R.Bechmann and R.Taylor, Selected Engineering Reports, Post Office Research Station (London), 1957.

[11] K.V.Rao and A.Smakula, J.Appl.Phys. 37 (1966) 319.

[12] Y.R.Reddy and L.Sirdeshmukh, Solid State Commun. 51 (1984) 407.

[13] C.Ramasastry, K.Viswanatha Reddy and V.S.Murthy, Proc.R.Soc. Lond. A. 325 (1971) 347.

[14] A.B.Lidiard, in Handbuch der Physik edited by S.Flugg (Springer-Verlag, Berlin, 1957), Vol.XX, p.246.

[15] A.B.Lidiard, in Crystals with the Fluorite Structure, ed. W.Hayes (Oxford U.P., London, 1974), Ch.3.

[16] C.Bucci, R.Fieschi and G.Guidi, Phys.Rev. 148 (1966) 816.

[17] P.Langevin, J.Physique 4 (1905) 678.

[18] C.R.A.Catlow, Chem.Phys.Lett. 39 (1976) 39.

[19] C.R.A.Catlow, J.Corish, J.M.Quigley and P.W.M.Jacobs, J.Phys. Chem.Solids 41 (1980) 231.

[20] F.Bassari and F.G.Airoldi, Nuovo Cimento 11 (1954) 274.

[21] M.P.Tosi and F.G.Fumi, Nuovo Cimento 8 (1958) 504.

[22] M.Rubenstein and E.Banks, J.Electro Chem.Soc. 206 (1959) 404.

[23] E.Banks and P.Wagner, J.Chem.Phys. 44 (1966) 713.

[24] A.Kessler and J.E.Caffyn, J.Phys.C:Solid State Phys. 5 (1972) 1134.

[25] C.Ramasastry and K.S.Viswanatha Reddy, Proc.R.Soc.Lond.A. 335 (1973) 1.

[26] D.L.Kirk and R.M.Innes, J.Phys.C. 11 (1978) 1105.

[27] F.Cusso and F.Jaque, J.Phys.C:Solid State Phys. 15 (1982) 2875.

[28] C.R.A.Catlow, K.M.Diller and M.J.Norgett, J.Phys.C:Solid State Phys. 10 (1977) 1395.

[29] C.R.A.Catlow, M.J.Norgett and T.A.Gross, J.Phys.C:Solid State Phys. 10 (1977) 1627.

Chapter IX

THERMALLY STIMULATED POLARIZATION AND DEPOLARIZATION CURRENT STUDIES IN PURE AND DOPED $NaNO_3$ CRYSTALS

Abstract

Results of careful measurements of thermally stimulated polarization current (TSPC) and thermally stimulated depolarization current (TSDC) carried out in single crystals of pure and doped $NaNO_3$ crystals in the temperature range 80K to 350K are presented. Both TSPC and TSDC spectra show sharp peaks in doped $NaNO_3$ crystals in which the temperatures corresponding to the current maxima depend on the nature of the impurities added. The activation energies and pre-exponential factors for dipole relaxation process have been evaluated from the TSPC and TSDC results. The DSC spectrum obtained for pure $NaNO_3$ also supports the results obtained from the TSPC and TSDC measurements.

9.1 INTRODUCTION

Sodium nitrate crystallises in the rhombohedral subgroup of the trigonal system of space group $R\bar{3}c$ with two formula units of $NaNO_3$ per unit cell [1-3]. The nitrogen and sodium atoms lie on threefold axes and the three oxygen atoms of each nitrate group are arranged symmetrically about the nitrogen atoms in planes normal to the threefold axes as shown in figure 9.1a. Each oxygen atom lies on a twofold axis. Sodium nitrate has been extensively studied since the work of Kracek [4] who first noticed the appearance of a gradual phase transformation. Kracek et al. [5] observed marked changes in the intensities of the X-ray reflections from some of the planes on heating $NaNO_3$ above 488K. They attributed this to the rotation of the NO_3^- ions about the trigonal axis. The investigations of Katelaar and Strijk [6] also show that the transition is caused by internal rotation of the NO_3 groups in the crystal. They found that the probable mode of rotation is that about an axis through the N-atom and perpendicular to the plane of the NO_3 group. Later specific heat investigations [7] confirmed the existence of a characteristic lambda curve with transformation beginning in the vicinity of 423K and reaching the lambda point at T_c = 549K, just below the melting point at 584K. This phase transition was shown to be of order-disorder type. It is the dynamics of the phase

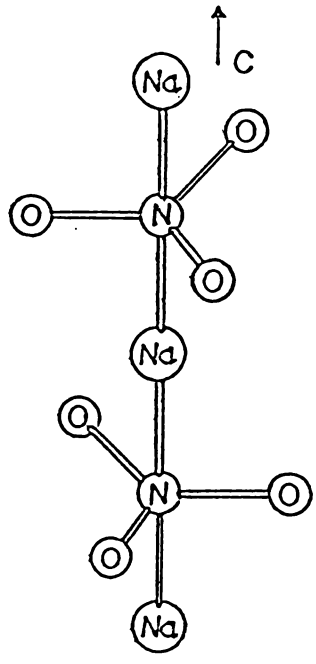

Figure 9.1a. Crystal structure of $NaNO_3$ crystal.

transition, i.e., the change from a complete order to complete disorder of the crystal structure, spread over a wide temperature range of nearly 100K, that generates most of the interest in sodium nitrate.

Terauchi and Yamada [8] by X-ray scattering,studied the phase transition of sodium nitrate crystal associated with the ordering of the orientation of NO_3^- ions. They have analysed the results on a microscopic basis and have concluded that the pair interactions between NO_3^- ions play an important role during this phase transition process.

In addition, the lattice dynamics of $NaNO_3$ has been investigated by neutron, Raman and infrared spectroscopy, mainly above room temperature in order to study the disorder phenomena related to the order-disorder phase transition. All the active lattice modes in sodium nitrate are known from the neutron scattering measurements of Logen et al. [9], Trevino et al. [10] and Lefebvre et al. [11]. Besides, the phonon dispersion curves of $NaNO_3$, Lefebvre et al. [11] have also studied the temperature behaviour of some lattice modes from room temperature upto 563K. The effect of heating, upon the frequencies and dampings of the Raman active lattice modes were studied from 300 to 573K [12-15]. It may be mentioned in this context that Lettieri et al. [16] using Raman spectro-

scopy have observed a soft lattice mode in the pressure induced ferroelectric phase above 45 kbar at room temperature.

The electrical conductivity, dielectric constant and loss of this material have been thoroughly investigated by Ramasastry and Murti [17] and Ramasastry and Syamasundara Rao [18] in the temperature range 300 to 480K, whereas the low temperature studies on this material are due to Badr and Kamel [19]. They have measured the resistivity and dielectric constant of $NaNO_3$ in the temperature range -30 to -80°C and obtained some anomalous change at -30°C in the ϵ vs T curve accompanied by a non-monotonous change in the resistivity plot. From the results they concluded that this anomalous change was due to the occurrence of a phase transition in the $NaNO_3$ crystals by the change in the nature of the vibrational mobility of the nitrate group which affects the temperature dependence of dielectric constant and resistivity. In this chapter we discuss the results obtained from TSPC and TSDC measurements made on single crystals of pure and doped $NaNO_3$ in the temperature range 80 to 350K. Detailed analysis of the TSPC and TSDC spectra have been made by studying their characteristics as a function of impurity concentration, poling field, poling temperature, poling time and heating rate.

9.2 EXPERIMENTAL DETAILS

Single crystals of pure and (Ba^{2+} and Sr^{2+}) doped $NaNO_3$ crystals were grown from melt using Bridgemann's technique in open pyrex glass tubes. Samples of typical sizes 6x6x1 mm^3 were prepared for TSPC and TSDC measurements after cleaving the grown samples along (100) faces. The thin film electrodes used were of evaporated aluminium (Difficulties were encountered with silver paint). The method of measurement of TSPC and TSDC and the experimental set up used have been already described in Chapter II. Thermally stimulated polarization current (TSPC) and thermally stimulated depolarization current (TSDC) were measured using Keithley model 617 Electrometer. The concentration of the impurities, in the specimens have been determined from the atomic absorption spectra obtained for the respective samples. The DSC spectrum of $NaNO_3$ was taken using a Perkin-Elmer instrument (Delta Series Model DSC 7) in the temperature range 120 to 300K with a heating rate of 10°C/m.

9.3 EXPERIMENTAL RESULTS

9.3.1 TSPC and TSDC measurements in $NaNO_3$ crystals

The TSPC measurements carried out in pure sodium nitrate by quenching the specimen to liquid nitrogen temperature and warming it with a biasing voltage of 200V (heating rate - 0.07K/sec) in the temperature range 80 to 350K give

a well defined current peak at 263K (denoted as B) as shown in figure 9.3a. The TSDC spectrum obtained by polarizing the specimen with a field of 2 KV/cm at 300K for a period of 2 minutes (heating rate 0.07K/sec) is shown in figure 9.3b. A sharp current peak is observed exactly at the same temperature where the TSPC peak is found to occur. The height of the TSPC peak is found to be large compared to that in the case of TSDC. It is also found that the height of the peaks increase slightly with the rate of heating.

9.3.2 TSPC measurements in doped $NaNO_3$ crystals

The TSPC spectra recorded for doped crystals for three different concentrations (250, 500 and 1000 ppm) of Ca^{2+} and Sr^{2+} impurities in the range 80 to 350K are shown in figures 9.3c and 9.3d. The spectra obtained for the two specimens by applying a biasing voltage of 200V (heating rate 0.07K/sec) show two distinct peaks of varying magnitudes. Let us denote these peaks as A and B in the increasing order of temperature. The temperature corresponding to the current maxima (T_m) for the peaks denoted by A are found to be 224.5K and 231K respectively for the Ca^{2+} and Sr^{2+} doped $NaNO_3$ crystals, whereas T_m for the peaks denoted by B is same as that for the current peak observed in the pure $NaNO_3$ crystals. Though the heights of the peaks A are found to increase in

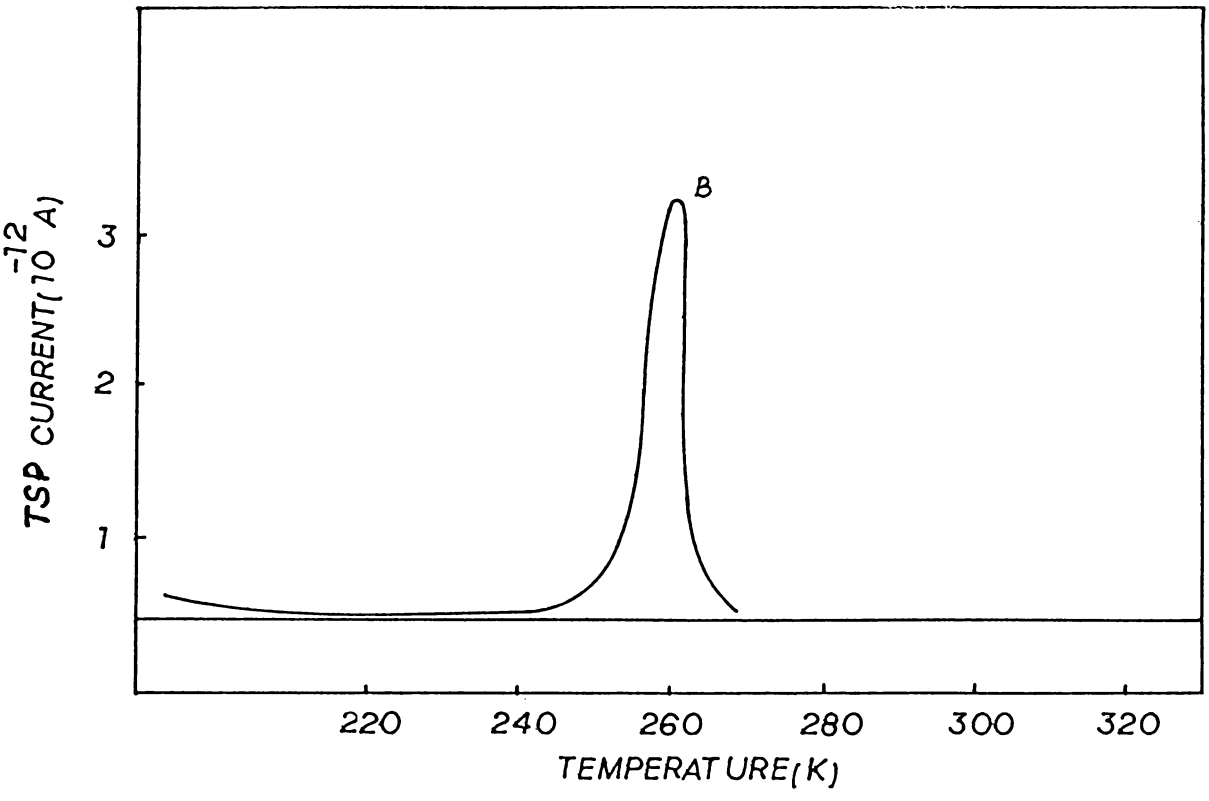

Figure 9.3a. TSPC spectrum of pure $NaNO_3$ crystal.

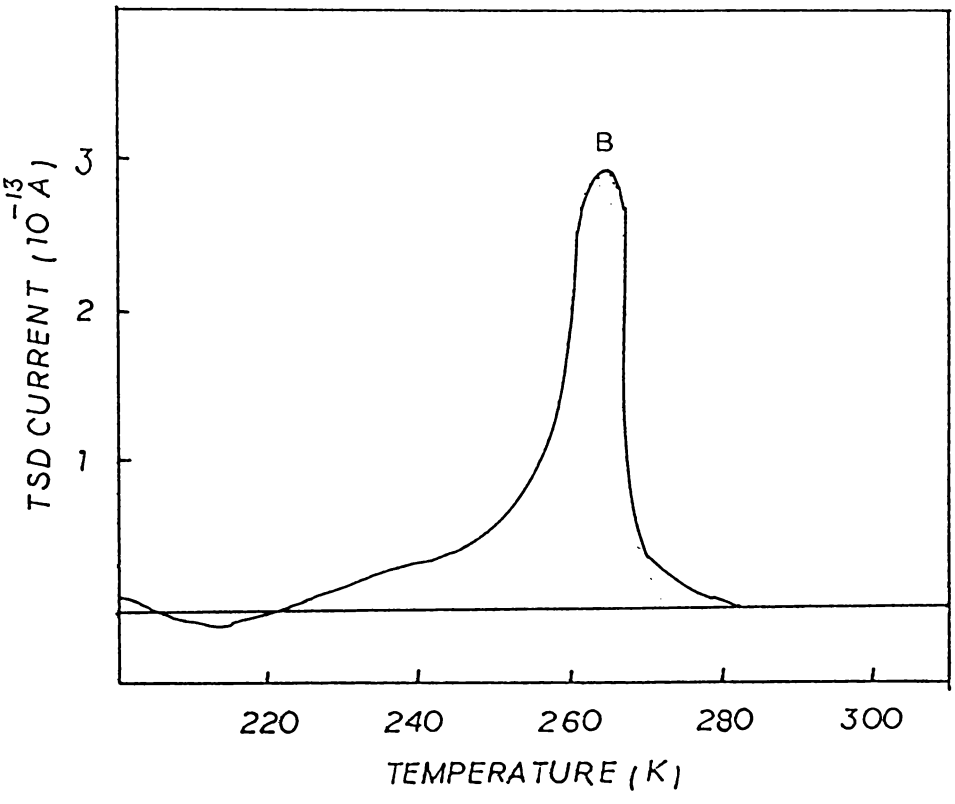

Figure 9.3b. TSDC spectrum of pure $NaNO_3$ crystal.

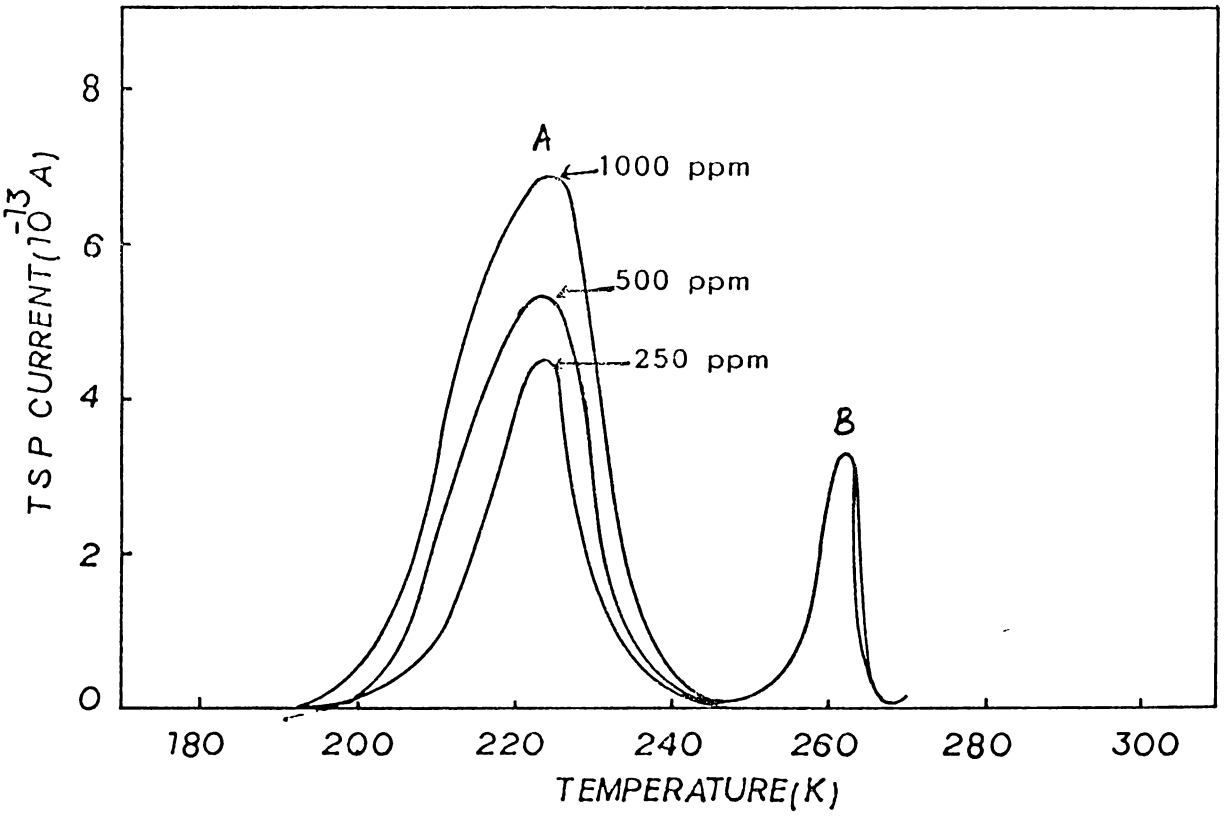

Figure 9.3c. TSPC spectra recorded for doped $NaNO_3$ crystals for various Ca^{2+} impurity concentrations.

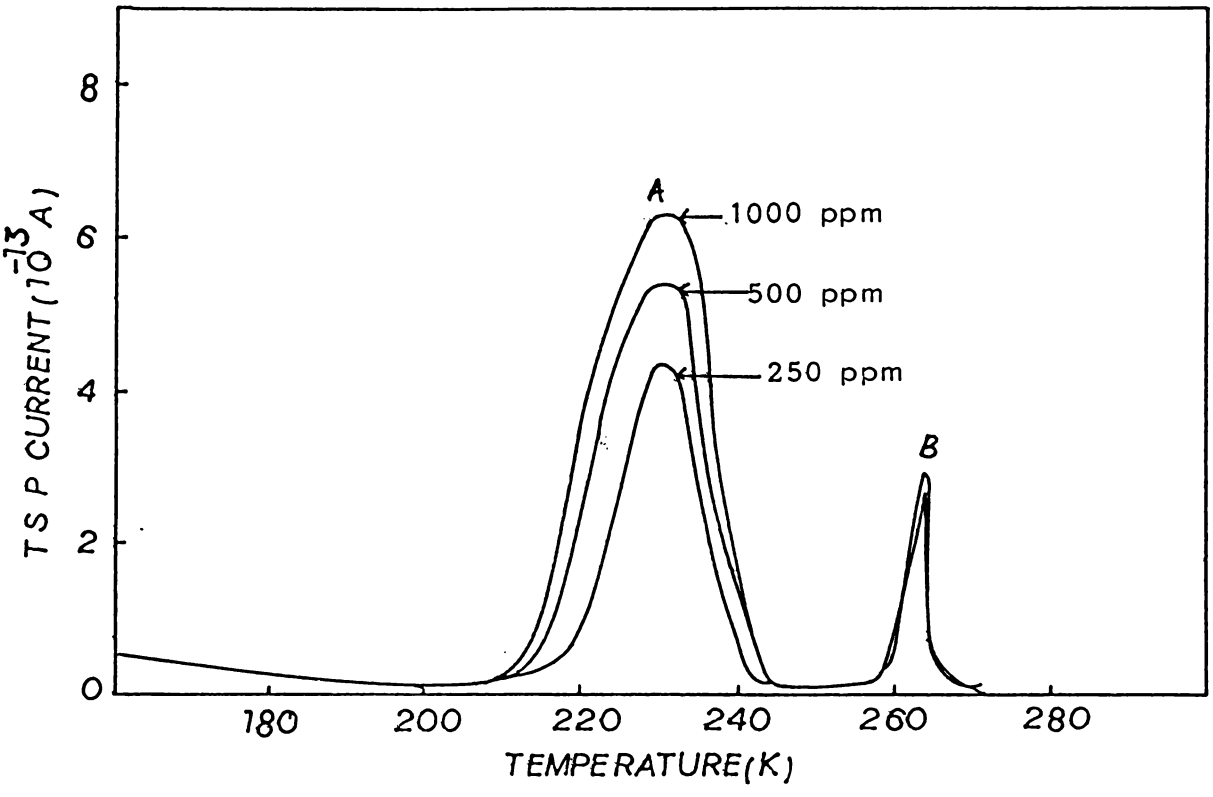

Figure 9.3d. TSPC spectra recorded for doped $NaNO_3$ crystals for various Sr^{2+} impurity concentrations.

proportion to the concentration of impurity ions, the magnitudes of the current peaks B are unaffected by this process. The shape of the current peaks also depends on doping concentration. The activation energies (E) and pre-exponential factors (τ_o) obtained by making use of the log I vs T^{-1} plots for the peaks A for both Ca^{2+} and Sr^{2+} doped specimens of $NaNO_3$ are shown in table 1.

Table 1

Values of various parameters obtained from TSPC spectra of doped $NaNO_3$ crystals

Sample	T_m(K)	E(eV)	τ_o(Sec)
$NaNO_3:Ca^{2+}$ 250 ppm	224.5	0.45	1.1×10^{-8}
$NaNO_3:Sr^{2+}$	231.0	0.49	2.78×10^{-9}

9.3.3 TSDC measurements in doped $NaNO_3$ crystals

The TSDC spectra recorded for doped $NaNO_3$ crystals for three different concentrations (250, 500 and 1000 ppm) of Ca^{2+} and Sr^{2+} impurities are shown in figures 9.3e and 9.3f. The spectra obtained by polarizing the specimen with

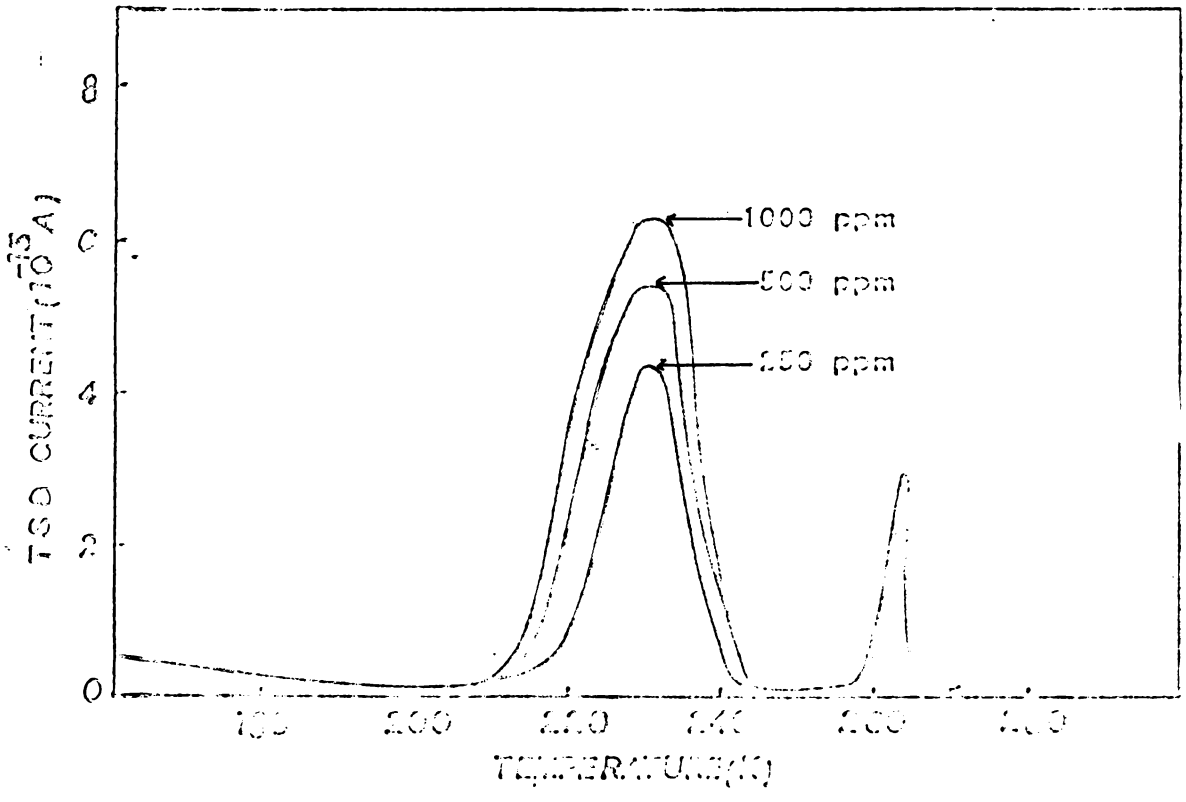

Figure 9.3e. TSDC spectra recorded for $NaNO_3$ crystals for various Ca^{2+} impurity concentrations.

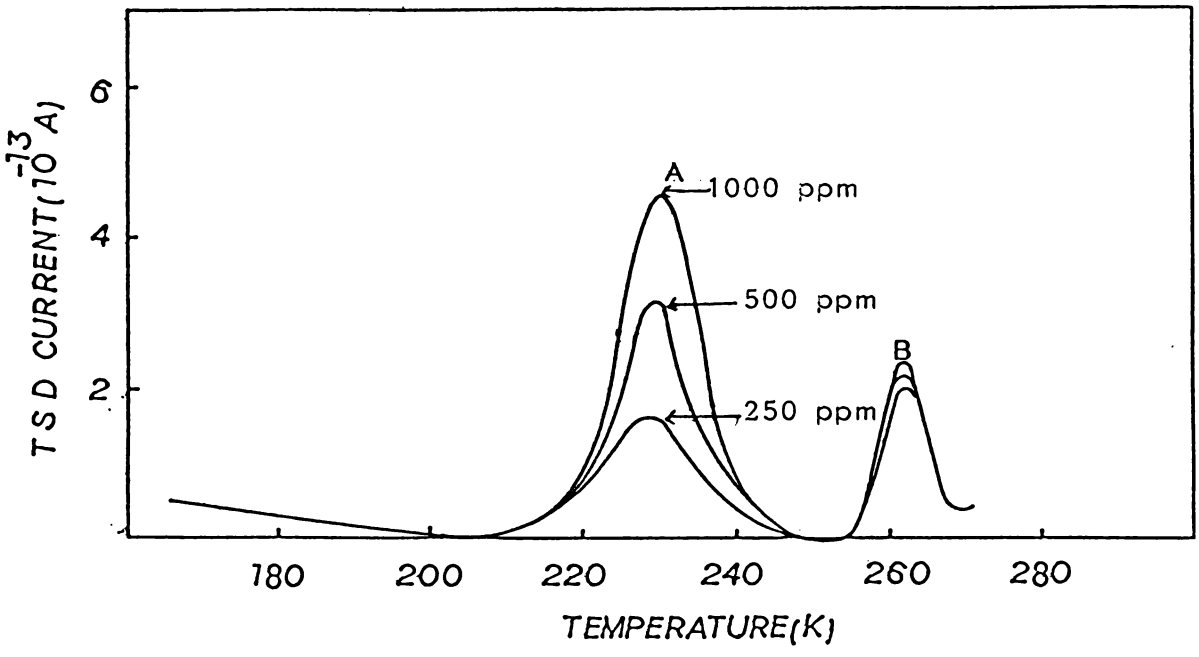

Figure 9.3f. TSDC spectra recorded for $NaNO_3$ crystals for various Sr^{2+} impurity concentrations.

a field of 2KV/cm for two minutes of 300K (heating rate 0.07K/sec) show two distinct current peaks. It is observed that the temperature corresponding to the current maxima for peaks A and B in both the specimens are found to be exactly the same as that obtained from TSPC measurements. The magnitudes of the TSPC peaks are found to be larger than that TSDC counterparts. It has been observed that the height and shape of the TSPC peaks A are strongly dependent on the concentration of the impurities while peaks B are found to be independent of the impurities present in the sample. The activation energies and pre-exponential factors evaluated by making use of the log I vs T^{-1} plots are shown in table 2.

Table 2

Values of various parameters obtained from TSDC spectra of doped $NaNO_3$ crystals

Sample	T_m(K)	E(eV)	τ_o (Sec)
$NaNO_3:Ca^{2+}$ (250 ppm)	224.5	0.46	6.5×10^{-9}
$NaNO_3:Sr^{2+}$ (250 ppm)	231.0	0.51	9.8×10^{-10}

9.3.4 Effect of poling field

The nature of variation of TSDC peaks A for Ca^{2+} doped (250 ppm) $NaNO_3$ as a function of poling field for fixed poling temperature and poling time is shown in figure 9.3g. The effect of poling field on the variation of TSDC peak A for Sr^{2+} doped (250 ppm) $NaNO_3$ crystals is shown in figure 9.3h. In both these specimens the height and shape of the TSDC spectra are found to vary with the increase in poling field. The height of the peaks shows linear relation with the field as shown in the inset of figures 9.3g and 9.3h. The height and shape of peaks B in Ca^{2+} and Sr^{2+} doped specimens are found to be unaffected by change in poling field. We have thus found that the role of biasing voltage in determining the nature of variation of the current peaks A in the TSPC spectra is the same as that of poling field in the TSDC spectra of the doped $NaNO_3$ crystals.

9.3.5 Effect of poling temperature

In order to study the effect of poling temperature on the nature of variation of the TSDC spectra, samples with fixed impurity concentration, poling field and poling time have been used. The effect of poling temperature on the nature of variation of peaks A in Ca^{2+} and Sr^{2+} doped specimens with impurity concentration 500 ppm, poling field 2KV/cm,

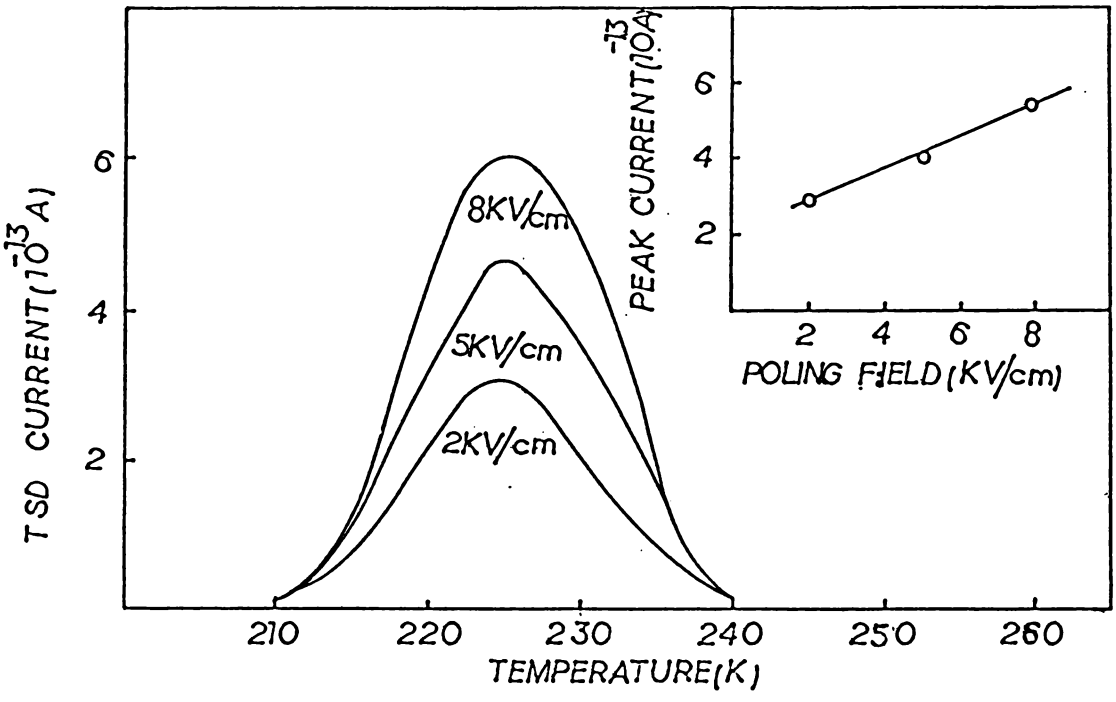

Figure 9.3g. Effect of poling field on the nature of variation of TSDC peak A in Ca^{2+} doped (250 ppm) $NaNO_3$ crystal. Inset shows the linear variation of the height of the current peak A.

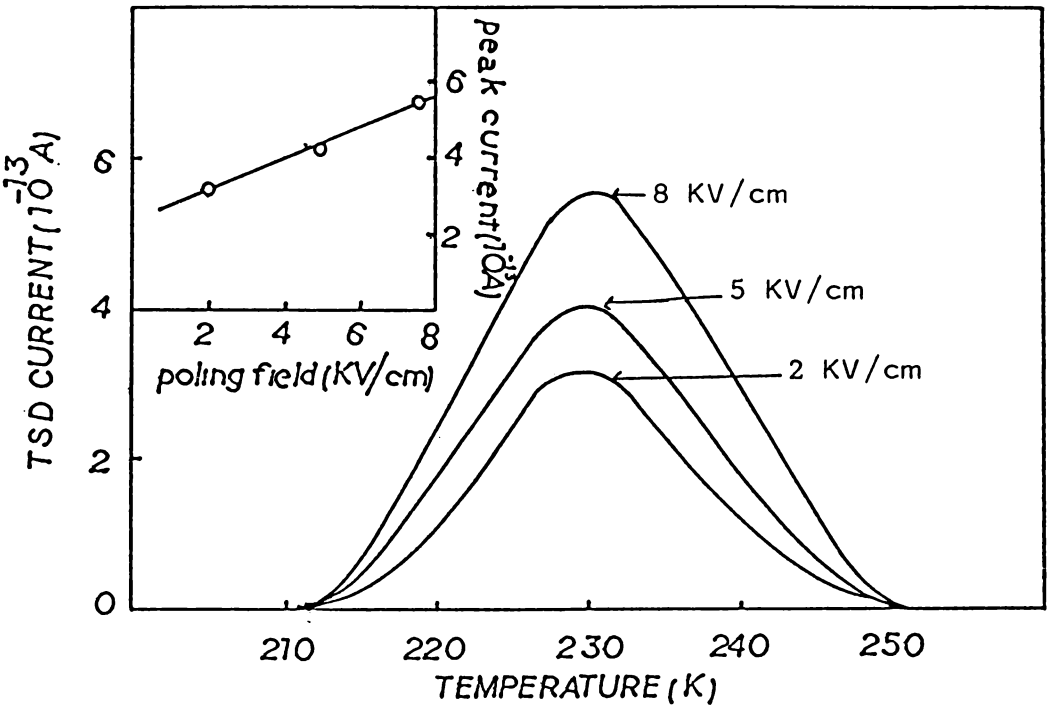

Figure 9.3h. Effect of poling field on the nature of variation of the TSDC peak A in Sr^{2+} doped (250 ppm) $NaNO_3$ crystal. Inset shows the linear variation of the peak height of the current peak A.

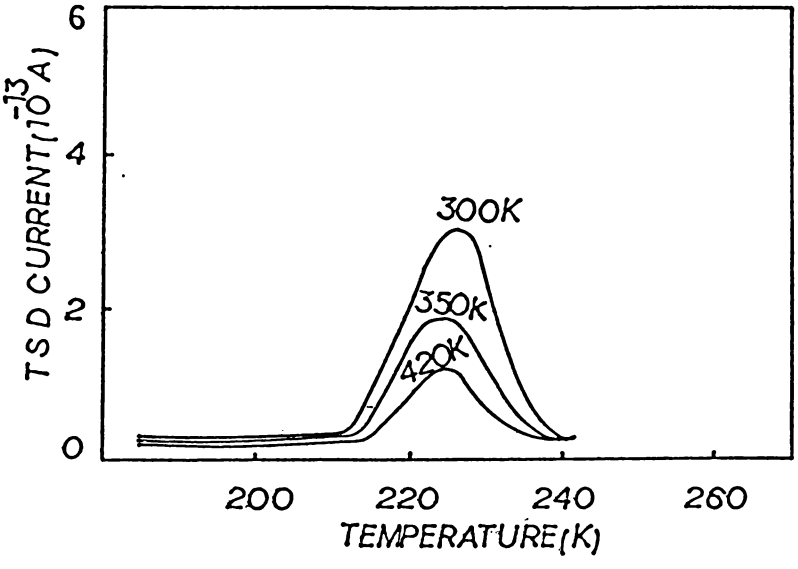

Figure 9.3i. Effect of poling temperature on the TSDC peak A in Ca^{2+} doped (500 ppm) $NaNO_3$ crystal.

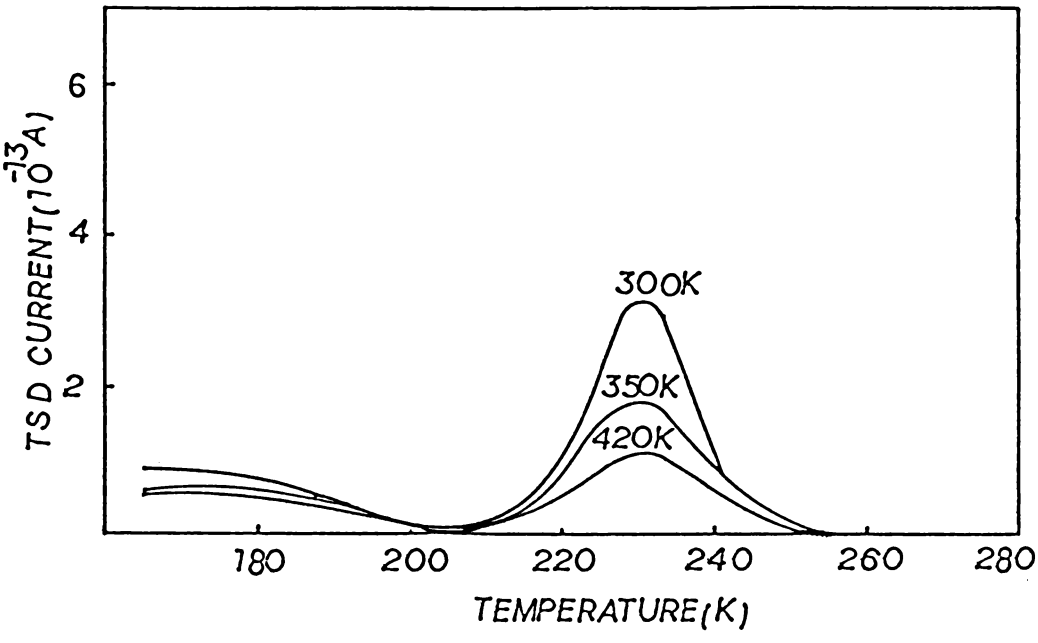

Figure 9.3j. Effect of poling temperature on the TSDC peak A in Sr^{2+} doped (500 ppm) $NaNO_3$ crystal.

and poling time 5 minutes is shown in figures 9.3i and 9.3j. Since, no appreciable variation in the B peaks has been observed, they have not been shown in the figure. It should be noted that the height of the peaks A in both the specimens is found to decrease with poling temperature. It should also be noted that the effect of poling temperature is more predominant in samples with higher impurity concentration.

9.3.6 Effect of poling time

In order to study the effect of poling time on the TSDC spectra of doped specimens of $NaNO_3$, we made TSDC measurements on samples containing a fixed amount of impurity ions by varying poling time, while keeping the poling field and temperature constant. Figure 9.3k shows the variation of the current maxima as a function of poling time ranging from 1-10 minutes for the peak A in Ca^{2+} doped (250 ppm) specimens, while figure 9.3l shows variation of the current maxima for the peak A in Sr^{2+} doped specimens for a fixed field of 2KV/cm and poling temperature 300K. It can be noted that the current maxima decrease slowly with increase in poling time. It is also observed that, the effect of poling time is more pronounced in samples with high impurity concentration and for higher poling temperature.

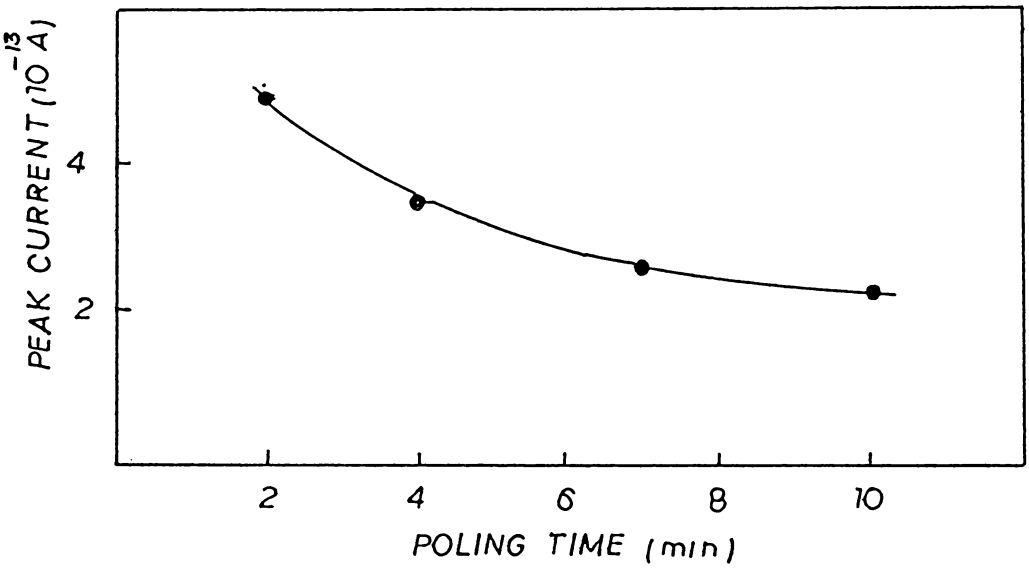

Figure 9.3k. Variation of the current maxima as a function of poling time for the peak A in Ca^{2+} doped (250 ppm) $NaNO_3$ crystal.

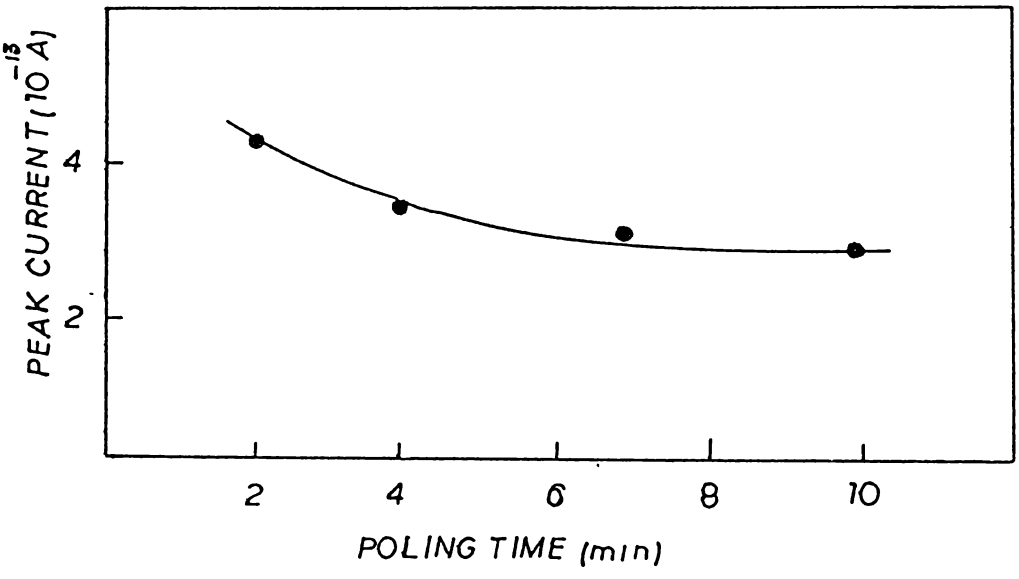

Figure 9.31. Variation of the current maxima as a function of poling time for peak A in Sr^{2+} doped (250 ppm) $NaNO_3$ crystal.

9.3.7 Effect of heating rate

For studying the effect of heating rate, we have carried out the TSPC and TSDC measurements in samples with fixed values for impurity concentration, poling temperature, poling field/biasing field and poling time. In this case the height of the current maxima is found to be increased with increase in heating rate without affecting the total integrated charges for each peak.

9.3.8 Results obtained from DSC studies

The differential scanning calorimetric studies carried out in powdered $NaNO_3$ in the temperature range 110K to 300K with a heating rate of 10°C/m is shown in figure 9.3m. A sharp peak with a maximum at 265K has been observed in the case of pure sodium nitrate crystal.

9.4 DISCUSSION

It is obvious from the TSPC and TSDC, the current peaks (B) observed in both pure and doped $NaNO_3$ crystals that this material undergoes a phase transition at 263K. As already mentioned $NaNO_3$ undergoes an anomalous change in its electrical properties as revealed in ϵ vs T curve and in the monotonous change in resistivity at -30°C. It

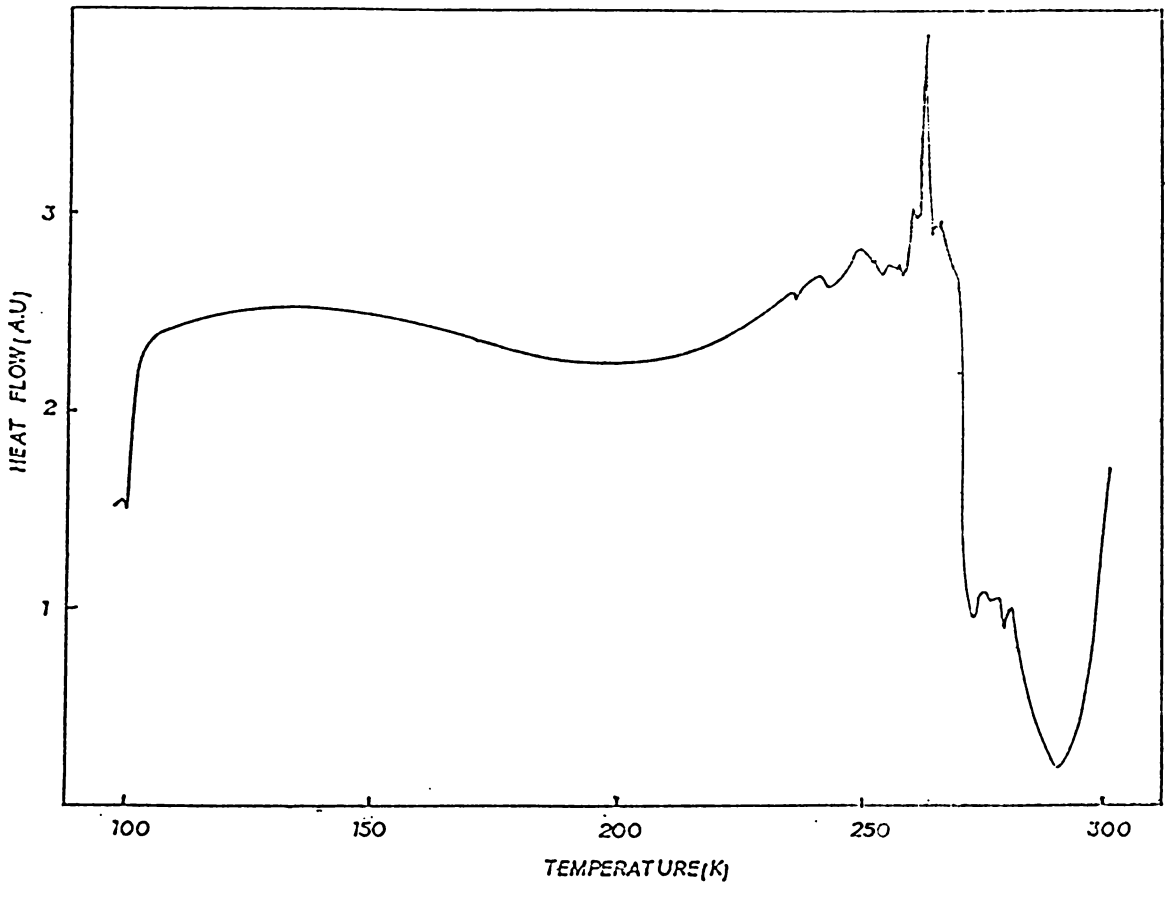

Figure 9.3m. DSC spectrum of pure $NaNO_3$ material.

is suggested that the pronounced increase in the value of a.c. conductivity reflects a co-operative change in the polarizability of the structural units in the unit cell [19]. Therefore it is advisable to look for common reason which might be related to the characters of the nitrate group that leads to some kind of modification of the crystal field as long as neither the basic crystal structure nor the valency of the positive ions can be the effective factor. A change in the torsional rigidity or clamping of the permanent dipoles associated with the nitrate group may apparently be excluded since it would be likely to affect also the value of the lattice parameter. Therefore it is highly probable that the freezing of the reorientational motion of the NO_3^- group about its threefold axis is responsible for the occurrence of this low temperature phase transition. Such successive blocking of the reorientational motion of the NO_3^- ions taking place while cooling the crystal might lead to the splitting of the vibrational bands and a considerable contraction of the line. Such splitting in the internal and external modes of vibrations was observed experimentally in IR and Raman spectroscopy for the nitrate crystals, specifically for $CsNO_3$ and $RbNO_3$ [20-23]. Thus the change in the character of the vibrational mobility of the nitrate group should thus result in occurrence of phase transition in this method.

Therefore, the results obtained here from TSPC and TSDC along with the results obtained from the DSC studies clearly establish that pure $NaNO_3$ undergoes a phase transition at 263K. Also, the impervious nature of peak A at 263K in TSDC and TSPC to various experimental conditions strongly support the above conclusions.

The origin of the lower temperature peaks observed below 263K in both Ca^{2+} and Sr^{2+} doped $NaNO_3$ crystals in the TSPC and TSDC measurements can be explained by considering the role of the substituted divalent impurity ions in the $NaNO_3$ lattice. It is well known that electrical conduction in ionic crystals like $NaNO_3$ is a defect controlled property and this defect concentration increases exponentially with rise in temperature. In the case of $NaNO_3$ crystal the well confirmed experimental result [17] is that the electrical conductivity is considerably lowered by the addition of Ba^{2+} to the lattice (Contrary results have been observed for SO_4^{2-} and Sr^{2+} doped $NaNO_3$ in which, it is found that conductivity increases with the substitution of these ions). To compensate the excess charge of the added divalent positive ion impurity (Z^{2+}), positive ion vacancies (V_p^-) or negative ion interstitials (X^-) may be created. If the mechanism of electrical conduction in this crystal is by the migration of either of these defects, the conductivity

must be enhanced. To account for the observed decrease in conductivity we should consider the effect of the above increase in number of negative carriers on the concentration of other defects such as negative ion vacancies (V_n^+) and positive ion interstitials (X^+). The concentration of positive ion vacancy [V_p^-], exists in equilibrium with the concentration of negative ion vacancy [V_n^+], and also with the concentration of positive ion interstitials [X^+]. Similarly, the concentration of negative ion interstitials [X^-] exists in equilibrium with that of negative ion vacancy [V_n^+]. These may be expressed by the following equations [24].

$$[V_p^-][V_n^+] = \exp(-g_S/kT) = x_S^2 \tag{9.1}$$

$$[V_p^-][X^+] = \exp(-g_F/kT) = x_F^2 \tag{9.2}$$

$$[X^-][V_n^+] = \exp(-g_{AF}/kT) = x_{AF}^2 \tag{9.3}$$

where S, F and AF stand for Schottky, Frenkel and Antifrenkel defects respectively, g for the free energy of formation of defects, and x for the concentration of either defects in pure crystal. It is understood from the expressions (9.1) to (9.3) that increase in [V_p^-] or [X^-] results in the decrease of [V_n^+] and/or [X^+]. That is, the addition of divalent positive ion impurities into the lattice has the

effect of decreasing the negative ion vacancies and/or positive ion interstitials. The conductivity will decrease if the process is mainly contributed by either anion vacancies or cation interstitials. Considerations based on both size and polarizability lead to the conclusion that nitrate ion should be less mobile. The nitrogen-oxygen bond is 1.2 Å with the oxygen having an ionic radius of 1.4 Å, whereas the ionic radius of Na^+ is 0.95 Å. Likewise, the polarizability of the nitrate ion is 3.4 to 4.0×10^{-24} cm^3 while that of the sodium ion is $0.41 \times 10^{-24} cm^3$ [25]. Hence on account of the larger size of the nitrate ion, interstitial anions are less likely to occur and positive ion vacancies may be assumed to produce charge compensation. Thus it is highly probable that the substitution of divalent cationic impurities viz., Ca^{2+} and Sr^{2+} in a $NaNO_3$ lattice produce positive ion vacancies. These positive ion vacancies along with the divalent cationic impurities produce impurity-vacancy (I-V) complexes and their reorientations give rise to current peaks in TSPC and TSDC measurements. Thus the origin of the current peaks observed in doped $NaNO_3$ crystals can only be due to the formation of I-V complexes in this material by the substitution of divalent cationic impurities. Again, the effect of various experimental parameters on the variation of TSPC and TSDC current peaks (A) fully establishes that the origin

of the current peaks (A) are due to the I-V complexes. The activation energy values and pre-exponential factors evaluated from both TSPC and TSDC are found to be approximately the same. From this it is clear that, the results obtained for both pure and doped specimens of $NaNO_3$ are not the artifact of the technique used but is due to the innate properties of these materials.

The observed difference in size of the current peak in TSDC method compared to that in the TSPC can be explained as follows. During the TSDC process the dc electric field not only polarizes the sample but also causes partial dissociation and hence it build up an ionic space charge in the materials (As noted in section 9.3.5 this effect is much more at higher poling temperatures). Thus the effective number of I-V complexes which reorient on heating process is now reduced and this gives a smaller magnitude for TSDC peak (A). A reduction of the internal field due to space charge effect can also contribute to this phenomenon [26,27].

9.5 CONCLUSIONS

The results obtained for pure and doped $NaNO_3$ single crystals from TSPC and TSDC measurements lead to the following conclusions:

1. Both TSPC and TSDC measurements show a single current peak (A) in pure crystals and two peaks (A and B) in doped specimens of $NaNO_3$.

2. The temperature corresponding to the current maximum for peaks (A) in both pure and doped specimens is found to be 263K, whereas the temperature corresponding to the current maximum for peaks (B) in doped specimens is found to be dependent on the nature of impurity added.

3. The current peak (A) observed in both pure and doped $NaNO_3$ crystals at 263K can be assigned as due to the occurrence of a phase transition in this material at this temperature, apparently due to reorientation of NO_3 ion in the crystal lattice.

4. The current peaks (B) observed in doped specimens of $NaNO_3$ are due to the reorientation of I-V dipoles formed by the substitution of divalent cationic impurities in the pure $NaNO_3$ crystals.

5. The observed decrease in size of the TSDC peaks compared to that in the TSPC peak may be due to the formation of space charges in the TSDC process.

6. The activation energy values and pre-exponential factors evaluated for peaks (A) are found to be same in both TSPC and TSDC measurements.

7. The DSC studies also support fully well the results obtained for $NaNO_3$ from TSPC and TSDC measurements.

9.6 REFERENCES

[1] R.W.G.Wyckoff, Phys.Rev. 16 (1920) 149.

[2] P.E.Tahvonen, Ann.Acad.Sci.Fenn Ser. A1 (1947) 42.

[3] R.L.Sass, R.Vidale and J.Donohue, Acta Cryst. 10 (1957) 567.

[4] F.C.Kracek, J.Am.Chem.Soc. 53 (1931) 2609.

[5] F.C.Kracke, E.Posnjak and S.B.Hendricks, J.Am.Chem.Soc. 53 (1931) 3339.

[6] J.A.A.Ketelaar and B.Strijk, Rec.Trav.Chem. 64 (1945) 174.

[7] V.C.Reinsborough and F.E.W.Wetmore, Aust .J.Chem. 20 (1967) 1.

[8] H.Terauchi and Y.J.Yamada, J.Phys.Soc.Japan, 33 (1972) 446.

[9] K.W.Logan, S.F.Trevino, R.C.Casella, W.M.Shaw, L.D. Muhlestein and R.D.Mical, "Phonons", M.A.Nusimovici (Ed.), Paris-Flammarion, 1971, p.104.

[10] S.F.Trevino, H.Prask and R.C.Casella, Phys.Rev.B. 10 (1974) 739.

[11] J.Lefebvre R.Currat, R.Fourret and M.More, J.Phys.C: Solid State Phys. 13 (1980) 4449.

[12] E.V.Chisler, W.C.Hamilton and B.Post, Acta Cryst. 23 (1967) 455.

[13] A.D.Prasad Rao, R.S.Katiyar and S.P.S.Porto, "Advances in Physics", J.P.Mathien (Ed.), London-Heyden, 1973, p.174.

[14] D.Y.Shen, S.S.Mitra, H.Prask and S.F.Trevino, Phys.Rev.B. **12** (1975) 4530.

[15] N.G.Neumann and H.Vogt, Phys.Status Solidi (b) **85** (1978) 179.

[16] T.R.Lettieri, E.M.Brody and W.A.Basset, Solid State Commun. **26** (1978) 235.

[17] C.Ramasastry and Y.V.G.S.Murti, Proc.Roy.Soc.Lond. A. **305** (1968) 441.

[18] C.Ramasastry and Y.Syamasundara Rao, J.Phys.C:Solid State Phys. **13** (1980) 887.

[19] Y.A.Badr and R.Kamel, Phys.Status Solidi (a) **53** (1979) K161.

[20] Y.A.Badr, S.V.Karpov and A.A.Shultin, Sov.Phys.Solid State **16** (1975) 8.

[21] M.H.Brooker, J.Chem.Phys. 59 (1973) 5828.

[22] S.V.Karpov and A.A.Shultin, Phys.Status Solidi **39** (1970) 33.

[23] Y.A.Badr and R.Kamel, Third European Crystallographic Meeting, Zurich, 1976.

[24] A.B.Lidiard, Handbuch der Physik **20** (1957) 246.

[25] J.R.Tessman, A.H.Kahn and W.Shockley, Phys.Rev. **92** (1953) 890.

[26] S.W.S.Mackeever and D.M.Hughes, J.Phys.D:Appl.Phys. **8** (1975) 1520.

[27] S.W.S.Mackeever and D.M.Hughes, J.Phys.C:Solid State Physics **14** (1981) 3547.

Chapter X

IONIC THERMOCURRENT STUDIES OF DOUBLY DOPED $NaNO_3$ CRYSTALS

Abstract

Ionic thermocurrent technique has been used to study the relaxation of Ca^{2+} and Ba^{2+} impurity complexes in $NaNO_3$ crystals. The ITC spectrum of doubly doped $NaNO_3$ gives two well defined peaks (A and B) at temperatures 223 and 252K. The peaks A and B are identified as due to the reorientation of Ca^{2+}-vacancy and Ba^{2+}-vacancy dipoles. The analysis of the peaks yields activation energy values of 0.46 and 0.53 eV and values for pre-exponential factors as 5.46×10^{-9} and 3.79×10^{-9} sec respectively for dipoles formed by Ca^{2+} and Ba^{2+} with vacancies.

10.1 INTRODUCTION

As demonstrated in earlier chapters, ionic thermocurrent measurement is a powerful technique for studying point defects and their interactions in ionic crystals when these defects are created by the substitution of divalent impurities leading to the formation of composite structures such as the impurity vacancy (I-V) complexes [1,2]. Since these structures may have a dipole moment, it is possible to probe these defects with an electric field using techniques like dielectric loss and isothermal charging and discharging current measurements. A variety of defects in ionic crystals [3] have been investigated using ionic thermocurrent technique. It is also well known that many physical properties of ionic crystals are extremely sensitive to the presence of divalent cations [4]. The dispersion state of the dopant and the manner in which these cations are incorporated in the host lattice are dependent upon the thermal history of samples [5]. The impurity ions and vacancies can be presented as individual defects independent of one another or they may form aggregates into dimers, trimers or higher order complexes [6-8]. The first attempt to study the effect of double doping technique was reported by Morigaki et al. [9] in alkali halides containing divalent paramagnetic and diamagnetic ions [10]. This technique was used primarily to avoid magnetic exchange and dipole-dipole interactions. Later this technique

has been extended to study aggregation of kinetics in doped alkali halides. A major advantage of this technique is that it can also be used to remove the aggregation of impurities. The mechanism behind this technique is to dope the pure material with a divalent cationic and a monovalent anionic impurity simultaneously. The first experimental study of this kind was performed by Yokozava and Kazumata [11] in NaCl doped with Mn^{2+} and F^- impurities. It is believed that Mn^{2+} vacancy complex is trapped and stabilised at F^- impurity to form cation impurity-vacancy-anion impurity complexes [represented by $(MV)_F$-]. Though the migration of $(MV)_F$- is not possible, only the rotation of MV dipole is possible. Thus the ITC study of such systems would ideally clarify the motion of bound vacancy in MV dipole associated with F^- impurity. As a result it is possible to control the properties of dipole polarization of impurity vacancy complexes by this technique. In the present chapter a detailed study of the ITC measurements in crystals obtained by simultaneous doping by two different divalent cation impurities have been reported. Results are presented for $NaNo_3$ crystals doped simultaneously with Ca^{2+} and Ba^{2+}. Such type of investigations have not been reported earlier in the literature for doubly doped non-cubic systems.

10.2 EXPERIMENTAL DETAILS

Single crystals of $NaNO_3$ doped with various amounts of $Ca(NO_3)_2$ and $Ba(NO_3)_2$ (ranging from 0.02 to 0.1 mole %) were grown from melt using Bridgman technique. No precipitation of impurities were observed during the growth process. Samples with their broad faces parallel to the growth axis coated with aluminium electrodes using vacuum evaporation technique were used for the ITC studies. The ITC measurements were carried out in a metallic chamber described in chapter II using the usual procedure. The current measurements were made using an electrometer (Keithley, model 617) and a heating rate of 0.07K/sec was maintained throughout the entire temperature range of study (80 to 300K).

10.3 RESULTS OF ITC MEASUREMENTS

The ionic thermocurrent spectrum obtained for doubly doped specimens of $NaNO_3$ containing 0.02 mole % Ca^{2+} and Ba^{2+} polarised at 300K with a fairly large field (3KV/cm) using a polarising time of 5 minutes is shown in figure 10.3a. The spectrum obtained shows two well defined current peaks (denoted as A and B in the increasing order of temperature) at temperatures 223 and 252K. It is observed that the magnitude of the current peak A is larger than that of the peak B. The current maxima for both these two peaks show linear relation with the

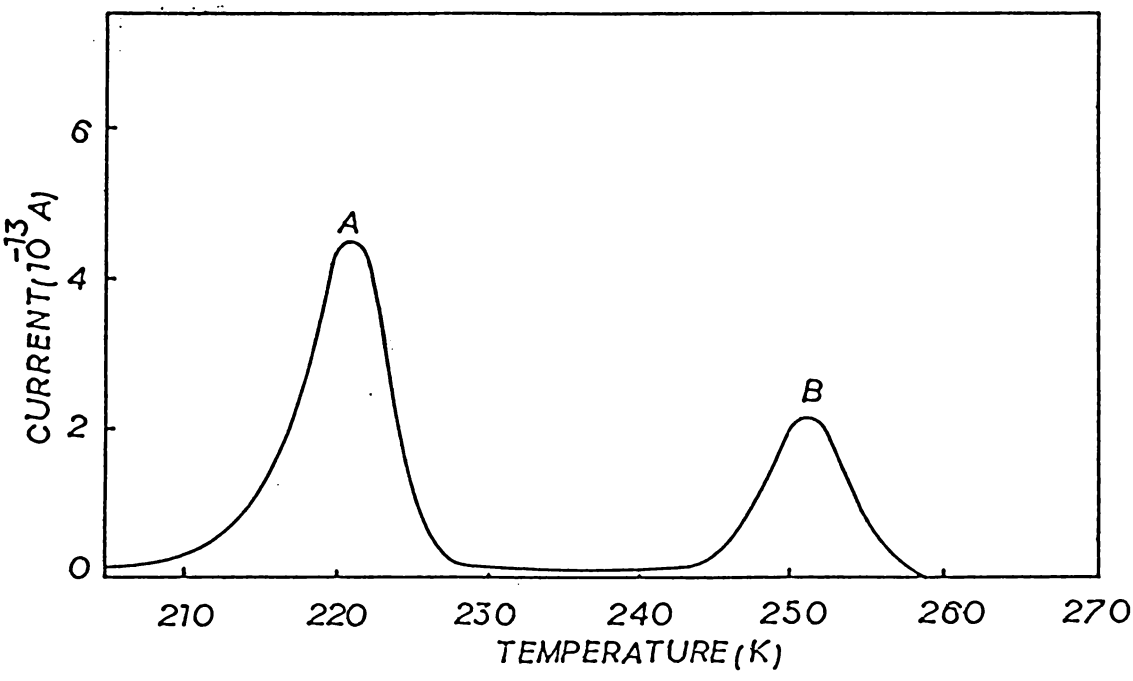

Figure 10.3a. ITC spectrum obtained for doubly doped (0.02 mole % Ca^{2+} and Ba^{2+}) $NaNO_3$ crystal.

applied field as shown in figure 10.3b. The variation of the height of the current peak A and B as a function of poling temperature is shown in figure 10.3c. It shows a smooth decrease in the height of the current maxima with the rise in poling temperature. Figure 10.3d shows the ITC spectrum obtained for 0.02 mole % Ca^{2+} and 0.05 mole % Ba^{2+} doped $NaNO_3$ crystals. The ITC spectrum obtained by polarising the specimen at 300K for 5 minutes with a field of 3 KV/cm indicates that only the peak B is enhanced when compared with those in figure 10.3a. In this case also, the height of the current peaks show linear variation with increase in poling field and a decrease with increasing poling temperature. It is also observed that for higher Ba^{2+} concentration only the size of the peak B is found to increase, whereas the magnitude of the current peak A remains almost the same. Figure 10.3e shows the nature of the variation of the ITC peaks A and B for a doubly doped $NaNO_3$ (0.02 mole % Ca^{2+} and 0.05 mole % Ba^{2+}) crystal annealed at 400K for one hour. It is observed that both these peaks are found to be almost suppressed.

On the other hand the increase in doping concentration of Ca^{2+} in $NaNO_3$ for fixed doping concentration of Ba^{2+} impurity causes changes only for the peak A. It is found that, the size of the peak A increases in proportion to the concentration

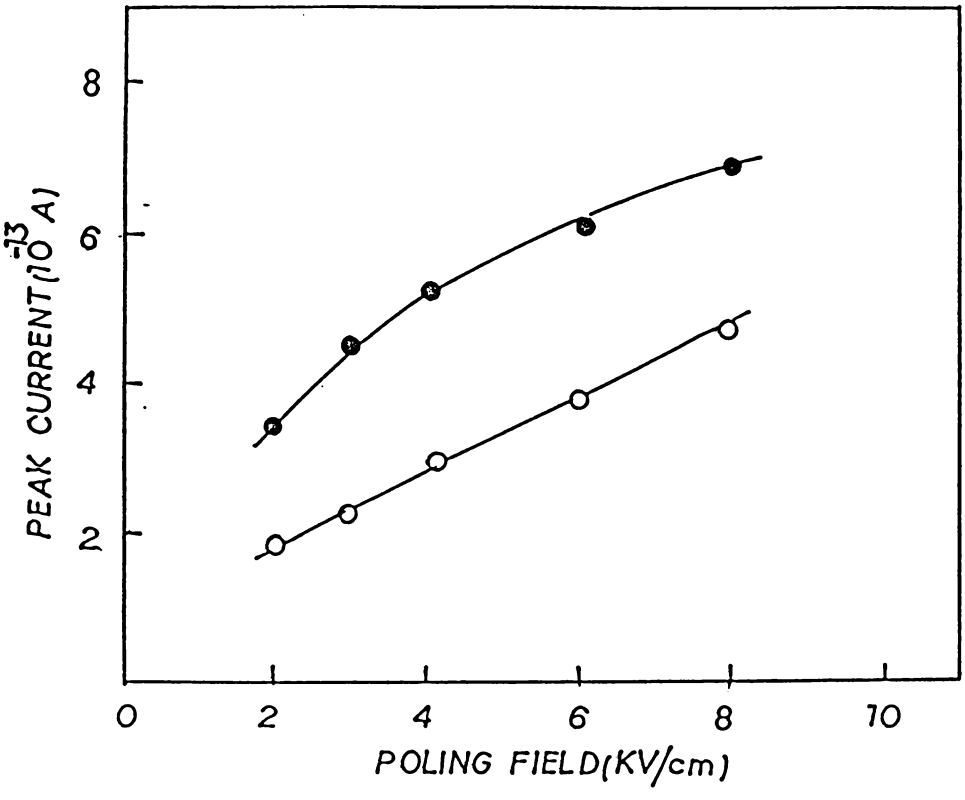

Figure 10.3b. Variation of peak height with poling field for (1)—●—●—●— peak A, (2)—○—○—○— peak B.

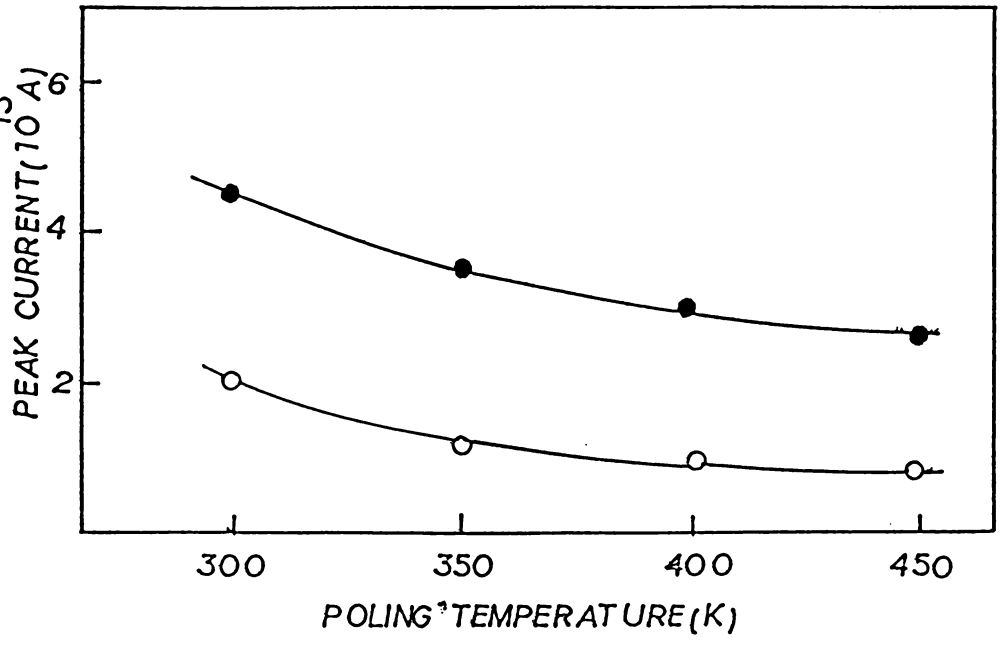

Figure 10.3c. Variation of peak height with poling temperature for (1)—●—●—● peak A, (2)—○—○—○— peak B. in a doubly doped $NaNO_3$ crystal.

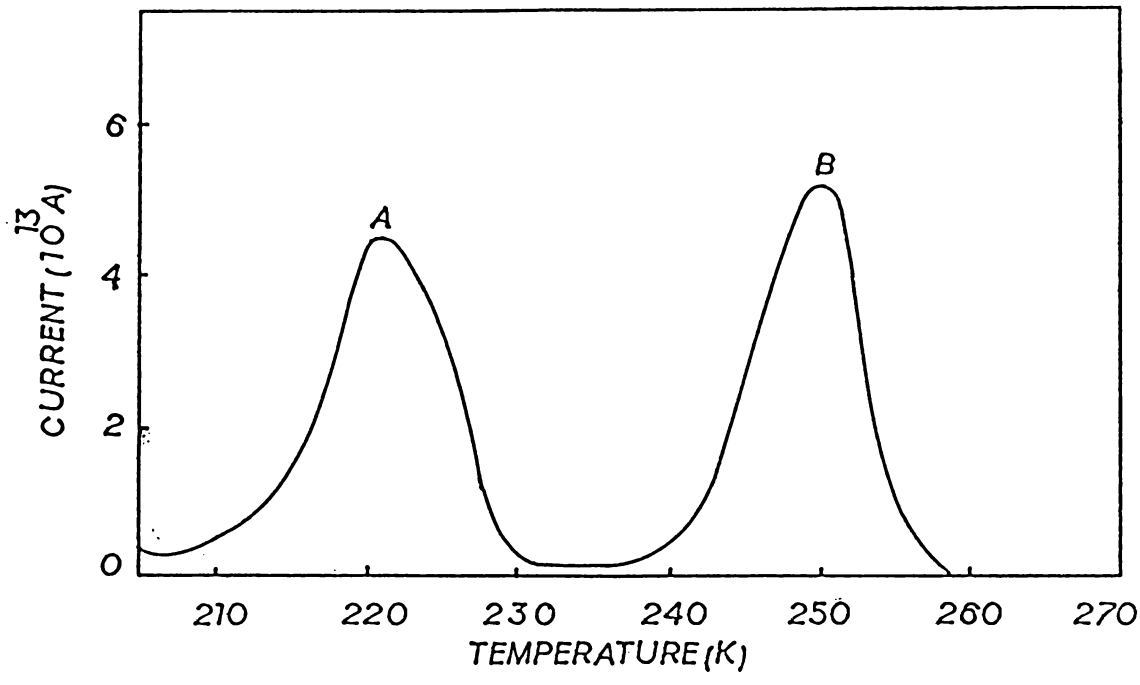

Figure 10.3d. ITC spectrum obtained for doubly doped (0.02 mole % Ca^{2+} and 0.05 mole % Ba^{2+}) $NaNO_3$ crystal.

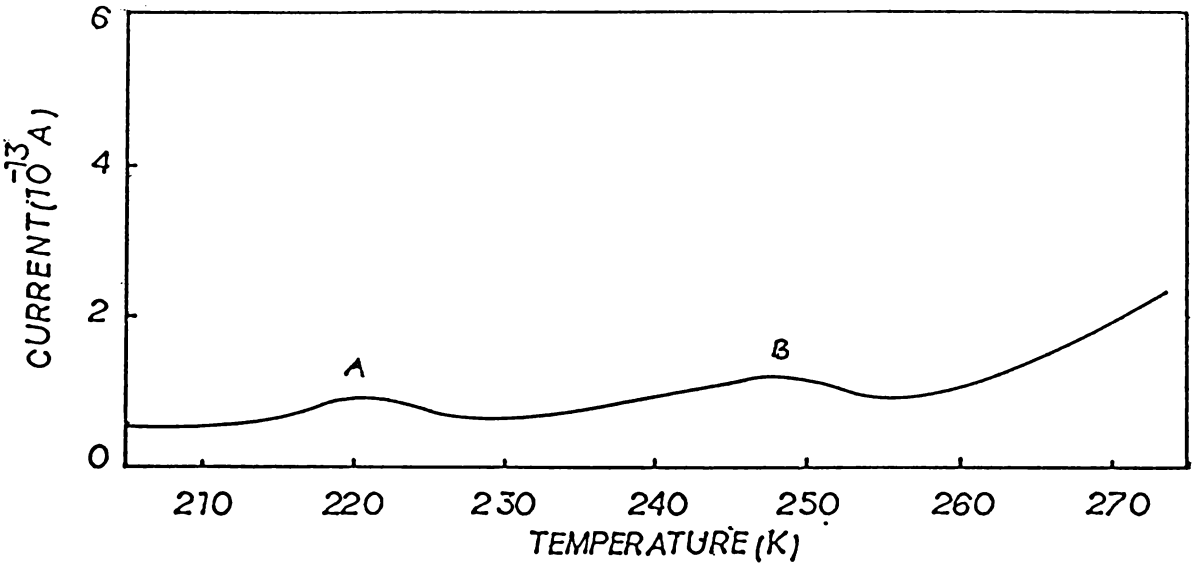

Figure 10.3e. Variation of ITC peaks A and B for a doubly doped (0.02 mole % Ca^{2+} and 0.05 mole % Ba^{2+}) $NaNO_3$ crystal annealed at 400K for one hour.

of Ca^{2+} impurities added. The activation energy values evaluated from the peaks A and B in $NaNO_3$ doped with 0.02 mole % Ca^{2+} and 0.05 mole % Ba^{2+} by making use of the initial rise method [12] are found to be 0.46 and 0.53 eV respectively. It is also observed that no appreciable change occurs in the activation energy values for the range of doping concentrations used here.

10.4 DISCUSSION

Although it is clear that the ITC peaks A and B shown in figure 10.3a obtained for doubly doped $NaNO_3$ crystals give the characteristics of the impurities incorporated in the material, a tentative explanation regarding the origin of each of these peaks can only be arrived at by considering the effect of various experimental parameters on the nature of variation of ITC peaks. To identify the species responsible for the ITC peaks, let us consider the effect of substitution of the two different cationic impurities on the $NaNO_3$ lattice. It is well known that substitution of covalent impurities in a lattice create vacancies or interstitials depending on the nature of impurities substituted and hence they form impurity-vacancy (I-V) dipoles in the specimen. Supposing that simultaneous substitution of two different cationic impurities in the same lattice is made, they form two different types of dipoles provided that the dipole-dipole

interaction is absent (or small). Depending on the size of the added divalent cationic impurities dipoles are formed at nearest neighbour and/or next nearest neighbour positions. Experimental results obtained here clearly show that the current peaks obtained for the doubly doped specimens of $NaNO_3$ are due to the formation of cation impurity-vacancy dipoles formed by the substitution of Ca^{2+} and Ba^{2+} impurity ions in the lattice. The amplitudes of these peaks preserved by a linear relation (shown in figure 10.3b) with the polarising field, clearly indicate the independent nature expected for the non-interacting dipoles. These conclusions are further supported by the results obtained for annealed samples. The observed suppression of ITC peaks with thermal annealing at higher temperature clearly shows that this process prohibits the formation of aggregate viz., Ca^{2+} vacancy and Ba^{2+} vacancy dipoles.

In order to identify the species responsible for the peaks A and B, we have extended the ITC studies on doubly doped crystals of $NaNO_3$ by changing the concentration of one of the species, while keeping the concentration of the other species fixed. It is observed that for higher concentration of Ba^{2+} impurities only the size of the peak B changed, which in turn unambiguously shows that the peak B can be attributed

to the I-V dipoles formed by Ba^{2+} ions in the $NaNO_3$ lattice. Hence one can indirectly confirm that the peak A should be due to the presence of Ca^{2+} impurities. This has been further verified by incorporating greater amount of Ca^{2+} impurities in the $NaNO_3$ lattice and in this case it is noted that only the peak A is found to be increased as expected. Thus it is clear that the two ITC peaks obtained for doubly doped $NaNO_3$ are associated with Ca^{2+}-vacancy and Ba^{2+}-vacancy reorientation. The activation energy for reorientation of these dipoles can be evaluated from the analysis of the ITC curve by making use of the equation,

$$kT_m^2 = bE\,\tau_o \exp\left(\frac{E}{kT_m}\right)$$

where b is the heating rate, τ_o is the reciprocal frequency factor [2].

The activation energy values obtained for the peaks at 223 and 252K are 0.46 and 0.53 eV with pre-exponential factors of 5.46×10^{-9} and $3.79 \times 10^{-9}\,sec^{-1}$ respectively. Thus in the present investigations simple and direct identification of the species responsible for the ITC peaks has become possible.

10.5 CONCLUSIONS

The ionic thermocurrent studies carried out in Ca^{2+} and Ba^{2+} doped sodium nitrate crystals in the temperature range 80-300K lead to the following conclusions.

1. The ITC studies carried out in doubly doped $NaNO_3$ crystal show two distinct current peaks, one at 223K and the other at 252K.

2. Both the peaks show linear dependence with the applied field.

3. The temperature corresponding to the current maximum for both the two peaks is found to be independent of poling field and poling temperature.

4. The current maximum of both the two peaks is found to be decreased with increase in poling temperature.

5. No ITC peaks are found in the annealed specimens of doubly doped $NaNO_3$ crystals.

6. The peak at 223K is attributed to the reorientation of Ca^{2+} vacancy dipoles and the peak at 252K can hence be due to the Ba^{2+} vacancy dipoles. This conclusion is further verified by concentration dependences of the peaks.

7. The activation energy values for Ca^{2+} and Ba^{2+} vacancy dipoles are found to be 0.46 and 0.53 eV and the values for pre-exponential factors are 5.46×10^{-9} and 3.79×10^{-9} sec.

8. Dipole-dipole interaction has no significant effect in this system.

10.6 REFERENCES

[1] J.H.Crawford,Jr., and L.M.Slifkkin, Ann.Rev.Materials Sci. 1 (1971) 139.

[2] C.Bucci and R.Fieschi, Phys.Rev.Lett. 12 (1964) 16.

[3] S.Radhakrishna and S.Haridoss, Crystal Lattice Defects. 7 (1978) 191.

[4] M.Hartmanova, M.Suizynska, I.Thurzo and H.Rezabkova, Czech.J.Phys.B 26 (1976) 1127.

[5] M.Hartmanova, Phys.Status Solidi (a). 7 (1971) 303.

[6] M.Ikeya, J.Phys.Soc.Japan 48 (1980) 1779.

[7] E.L.Kitts,Jr., M.Ikeya and J.H.Crawford. Jr., Phys.Rev.B 8 (1973) 5840.

[8] G.E.Mathews. Jr., and J.H.Crawford,Jr., Phys.Rev.B. 15 (1977) 55.

[9] K.Morigaki, M.Fujimoto and N.Itoh, J.Phys.Soc.Japan. 12 (1958) 694.

[10] M.Ikeya and J.M.Crawford,Jr., Phys.Status Solidi (a). 5 (1973) 643.

[11] Y.Yokozawa and Y.Kazumata, J.Phys.Soc.Japan. 16 (1961) 69.

[12] C.Bucci, R.Fieschi and R.G.Guidi, Phys.Rev. **148** (1966) 816.

[13] A.Kessler, J.Phys.C:Solid State Phys. **6** (1973) 1594.

[14] A.Kessler, J.Electrochem.Soc. **123** (1976) 1236.

[15] A.Kessler, J.Electrochem.Soc. **123** (1976) 1239.

[16] J.H.Crawford, Jr., J.Phys.Chem.Solids. **3** (1970) 399.

[17] D.M.G.Pinatti, S.C.Zilio and M.De Souza, Phys.Status Solidi (b). **94** (1979) 749.

[18] M.Siu Li and M.De Souza, Phys.Status Solidi (b). **92** (1979) 287.